COMPUTATIONAL STUDY OF THE STRUCTURE AND ELECTRONIC PROPERTIES OF Ag AND Au DOPED $(TiO_2)_n$ CLUSTERS (n = 2 - 6)

A THESIS SUBMITTED IN FULFILMENT

OF THE REQUIREMENTS FOR THE DEGREE OF

MASTER OF SCIENCE (CHEMISTRY)

OF

THE UNIVERSITY OF NAMIBIA

BY

ELIZETH AFONSO HUMBA

(201101614)

JULY 2020

Main Supervisor: Prof. Edet F. Archibong

(Department of Pharmaceutical Chemistry, University of Namibia)

Co-Supervisor: Dr. Likius Daniel

(Department of Chemistry, University of Namibia)

ABSTRACT

The titanium dioxide (TiO_2) clusters are aggregates of TiO_2 units that are intermediate in size between a molecule and the bulk material. It is known that molecular clusters exhibit unique properties as a function of size, composition, and atomic configuration. The goal of this study is to investigate variation in the structure and electronic properties of Ag and Au doped $(TiO_2)_n$ as the cluster size (n) increases. It is of interest to determine the size limit where the electronic properties of the doped clusters mimic that of the bulk material. And the need to shift the absorption wavelength of the $(TiO_2)_n$ clusters into the visible region of the electromagnetic spectrum has necessitated investigation into doping with the Au and Ag atoms.

The results reported in this thesis were obtained using mainly BPW91 variant of the Density Functional Theory (DFT) approximation. The 6-311+G (d) basis set, and the Stuttgart-Dresden (SDD) effective core potential were used to represent atomic orbitals. The structures of the most stable undoped and doped neutral cluster are similar for n = 6 only. In case of the anion, similar structures are observed for n = 3 and n = 6, while they are different for n = 2, 4 and 5. Vertical electron detachment energies (VEDE) are within 3.40 – 5.87 eV while adiabatic electron detachment energies (AEDE) and electron affinity (EA) vary from 1.92 to 6.52 eV. The values of these properties increase with the clusters size. The HOMO-LUMO (HL) gap was used as an approximation to the band gap, and it ranges between 0.33 - 3.59 eV and 0.19 - 3.27 eV for Ag and Au doped TiO_2 clusters, respectively. Singlet – singlet electronic transitions are predicted to occur at the visible region (400 – 800 nm) for n = 2, 5 and 6, in both doped systems. Major contributions to

the molecular orbitals are obtained from FMO. Molecular adsorption was the predominant type of interaction between water molecules and clusters. Binding energy values of -1.32 and -1.43 eV were obtained for the more reactive interaction of one water molecule with Ag and Au doped $(TiO_2)_n$ clusters (n = 2 - 6), respectively. With the exception of the HL gap of anionic Au doped $(TiO_2)_n$, the properties of the doped clusters investigated in this study did not converge to the bulk values, for n = 6 cluster length.

TABLE OF CONTENTS

LIST OF FIGURES

LIST OF TABLES

LIST OF CONFERENCE PROCEEDINGS

- University of Namibia - Royal Society-Department for International Development (RS-DFID) Africa Capacity Building Conference : 1st - 5th August 2017; Windhoek, Namibia

- University of Namibia - 5th Annual Science Research Conference: 15th - 16th November 2017; Windhoek, Namibia

- Kwame Nkrumah University of Science and Technology - Royal Society-Department for International Development (RS-DFID) Africa Capacity Building Conference : July 2018; Kumasi, Ghana

- University of Pretoria -Spring School: Solar Energy & Photosynthesis: 1st – 5th October 2018; Pretoria, South Africa

- University of Namibia- 6th Annual Science Research Conference: 14th – 15th November 2018; Windhoek, Namibia

ACRONYMS

a.u.: atomic unit

AEDE: Adiabatic Electron Detachment Energy

AEA: Adiabatic Electron Affinity

B3LYP: Becke, 3-parameter, Lee-Yang-Parr

BP86: Becke Perdew 86

BPW91: Becke Perdew-Wang 91

E_b: Binding energy

DFT: Density Functional Theory

FMO: Frontier molecular orbital

HOMO: Higher Occupied Molecular Orbital

LUMO: Lowest Occupied Molecular Orbital

MO: Molecular orbital

MP2: Second-Order Moller Plesset Perturbation Theory

NBO: Natural bond orbital

PBE: Perdew-Burke-Ernzerhof

PG: Point group

VEDE: Vertical Electron Detachment Energy

VEA: Vertical Electron Affinity

VIE: Vertical Ionization Potential

TDDFT: Time Dependence Density Functional Theory

SDD: Stuttgart-Dresden

ACKNOWLEDGMENT

I would like to thanks my family and friends, for supporting me with words of encouragements and prayers. My gratefulness to my supervisor Professor Edet F. Archibong, for such great supervision. I´ll always take you, as a father and a great friend. I thanks the National Commission on Research, Science and Technology (NCRST), for funding part of my studies and the Biochemistry and Chemistry department of University of Namibia (UNAM) for the facilities. The same way, I would like to thanks the Centre for High performance Computing (CHPC), South Africa, for the facilities provided to me. Last but not least I would like to thanks particularly Dr. Daniel, Dr. Uahengo, Ms. Thomas, Ms. Endjala, and Ms. Jacob for your friendship and help.

The Lord hath done great things for us; whereof I am glad, Psalm 126:3

DECLARATIONS

I, Elizeth Afonso Humba, declare hereby that this study is a true reflection of my own research, and that this work, or part thereof has not been submitted for a degree at any other institution.

Elizeth Afonso Humba		5th April 21
Name of Student	Signature	Date

CHAPTER 1. INTRODUCTION

1.1 Orientation of Study

Titanium oxide is an important semiconductor material, first discovered as a photocatalyst for water splitting by Fujishima and Honda in 1972. Titanium oxide (TiO_2), or 'titania', is an abundant white powdery solid in the bulk phase.

Since the discovery of Honda - Fujishima, research on various applications of titanium dioxide has attracted considerable attention. The interest in this very important oxide has been driven by some of its unique properties and numerous applications in science and technology.

TiO_2 has two stable crystalline structures: rutile and anatase. The former is about 2.6 kJ/mol more stable in ambient conditions. Anatase is stable when the particle diameter is between 2-14 nm, and due to its high refractive index, it has found important applications in antireflection coatings, narrow-band filters, and optical waveguides. Brookite is the third form of TiO_2. It is less stable when compared to rutile and anatase, and it is the least studied due to the difficulties of obtaining it in the pure phase. Brookite has been tested for environmental remediation, hydrogen formation, Li ion batteries and organic syntheses.

These three polymorphic forms of TiO_2 have the same chemistry but different structures and band gaps (E_g). The latter is 3.03 eV, 3.23 eV and 3.40 eV for rutile (tetragonal), anatase (tetragonal) and brookite (orthorhombic), respectively. These E_g values are considered to be large and they allow absorption of only approximately 5% of sunlight [1, 2, and 3]. Pure TiO_2 absorbs only in the ultraviolet portion of the solar spectrum.

TiO_2 possesses good properties such as:

- Thermal stability
- Chemical stability
- Non-toxicity and Non-corrosivity
- Low cost
- Good electrical conductivity
- Environmentally friendly and biocompatible.

TiO_2 has important applications in areas such as:

- Heterogeneous catalysis as a photocatalyst in water and air purification and in self-cleaning surfaces;
- Solar cells for the production of hydrogen and electrical energy, as gas sensor and in electrical devices;
- UV- proof pigments as white pigment, corrosion-protective coating, and as an optical coating;
- Earth sciences as antibacterial agent, gate insulator for MOSFETS, and as spacer material in magnetic spin-valve systems [4].

The main barrier of using titanium dioxide in many applications lies on the poor activation of TiO_2 by visible light due to large band gap and rapid recombination of photo-generated electron/hole. There are several reports with the main objective of modifying the band gap of different forms of TiO_2. Some of the techniques used in these studies include metal loading, metal ion doping, the use of composite semiconductor, anion doping and metal ion implantation.

Doping is the inclusion or substitution of a foreign atom into the TiO_2 semiconductor lattice in such a way as to induce new electronic states and new optical transitions not observed in the pure (undoped) material.

Suitable metal dopants include manganese (Mn), vanadium (V), chromium (Cr), iron (Fe), nickel (Ni), palladium (Pd), rhodium (Rh), tin (Sn), aluminum (Al), lead (Pb), platinum (Pt), cobalt (Co), copper (Cu), silver (Ag), and gold (Au).

Benefits of metal doping include:

- Excitation of electrons from defect state to the TiO_2 conduction band;
- Improved trapping of electrons to inhibit electron-hole recombination during irradiation;
- Band gap narrowing.

Wet methods used to dope TiO_2 include molecular precursor method (MPM), ion-assisted sputtering, plasma ion-implantation, chemical vapor deposition (CVD) and sol-gel method. Metal doped TiO_2 has been used in different fields such as:

- Medicine: for indoor airborne bacterial control ;
- Thin – films production: for gas sensor application and dye-sensitized solar cells;
- Degradation of nitrophenol in aqueous phase;
- Photocatalyst: for wastewater discoloring and hydrogen production.

Clusters are tiny bits of matter that serve as a bridge between gases and bulk phase materials. They are too small (few as 3 atoms) to be considered as liquids or solids and too large (about 20,000 atoms) to be considered as molecules.

Features of clusters include:

- Diverse geometry and bond connectivity;
- Modification of electronic structures and band gap;
- Greater effective surface area;
- Noticeable quantum–size effects.

Clusters exhibit dramatically different properties and reactivity as a function of their size, composition, and atomic configuration. They have discrete electronic states rather than bands (as in bulk phases). Various approaches have been developed for the study of their structures and properties and to track formation and growth of particles. Some of these approaches are the laser-induced breakdown spectroscopy (LIBS), the molecular beam mass spectrometry (MBMS), the electrical mobility measurements and negative ion photoelectron spectroscopy. Laser vaporization coupled with supersonic expansion can be used for clusters synthesis [5].

TiO_2 clusters are aggregates of TiO_2 molecules that are intermediate in size between the molecule and the bulk material. Some of the features of TiO_2 clusters have led to distinct improvement in photocatalytic activity. Numerous studies have also been documented for the study of undoped titanium oxide clusters experimentally and computationally.

Density functional theory (DFT) is at present the most popular and versatile computational technique used to study the geometrical structures and electronic properties of molecules, clusters, and bulk materials. DFT is based on quantum mechanical theory and uses

functional spatially dependent electron density. The densities are generated from basis sets which are mathematical functions used to represent atomic orbitals in electronic structure calculations. Using DFT, titanium dioxide has been widely studied in order to gain insight into the geometry, molecular reaction steps and electronic properties of these systems.

1.2 Statement of Problem

Titanium oxides have lower photocatalytic activity under visible light due in part to the large band gap (3.0 eV for rutile and 3.2 eV for anatase). This drawback has limited the use of TiO_2 in the visible region and subsequently in many applications.

Doping and variation of the particle size (as in clusters) are known to affect the band gap and could shift TiO_2 absorption to the visible and near infrared regions of the electromagnetic spectrum, thereby increasing the efficiency of the oxide and its applications in many areas including photocatalysis.

1.3 Objectives of the Study

The objectives can be summarized as follows:

- To computationally synthesize silver and gold doped TiO_2 clusters with different sizes and determine their electronic properties, including the band gaps, using DFT approximation;
- To investigate how the computed properties of the doped TiO_2 clusters vary with cluster size;
- To determine the size limit at which cluster properties will resemble those of the bulk material.

- To compare the computed structures and electronic properties of the doped and undoped TiO_2 clusters.

1.4 Significance of the Study

Clusters are known to possess unique properties which change with size. It will be of interest to know the limit at which doped TiO_2 clusters will possess the same properties as that of the bulk material. This research will contribute towards greater understanding of the role played by nanoparticle size and doping in enhancing the photocatalytic properties of TiO_2.

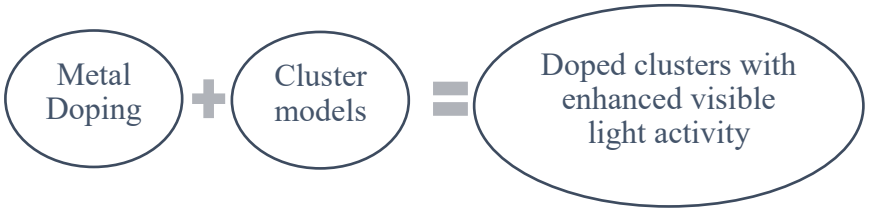

1.5 Limitation of the Study

The size of clusters limits the size of one particle basis sets that can be used for the calculations and it also imposes limitations on the number of cluster systems that can be computed within the period projected for the project.

1.6 Delimitation of the Study

The 6-311+G (d) basis set was used to represent the valence orbitals in this study.

CHAPTER 2. LITERATURE REVIEW

The semiconductor titanium dioxide has limited applications in solar energy conversion because it only absorbs approximately 5% of the solar light in the visible region. Therefore, different approaches have been used to extend the visible light activity of TiO_2. Doping has been one of the effective approaches used by researchers.

Zaleska [6] reported in a 2008 review that Oxonica Ltd. Developers, had doped TiO_2 with unequal proportions of one or more metal oxides namely zinc oxide, platinum oxide, magnesium oxide and/or aluminum oxide. These doped TiO_2 compounds were used for the degradation of impurities in the waste water**.**

Iron (Fe), manganese (Mn) and nickel (Ni) doped TiO_2 powders were synthesized using the sol–gel methods [7 and 16]. XRD of the prepared samples confirmed the anatase form with a trace amount of the rutile and/or brookite phases. Metallic Mn and Ni were detected after hydrogenation for 3h and 6h respectively, however metallic Fe remains doped within the TiO_2 lattice after hydrogenation [16]. Addition of 5% of Ni resulted in a shift from 342 nm to 350 nm in the electromagnetic spectrum [7].

According to Daniel et al [8], the introduction of Ag, even in small amounts can affect the properties of TiO_2-based thin films including crystal structure, morphology, and chemistry. Molecular Precursor Method (MPM) was used to synthesize the Ag doped TiO_2 thin films. Often in the bulk phase, the dopant can limit photo-carrier mobility by acting as a pinning center, with the defect state possessing very small dispersion [9]. Ni et al [10] called attention to the fact that a large quantity of metal particle deposition might reduce photon absorption of the TiO_2 and reduce its efficiency as electron-hole recombination

centers. Noble metals with suitable work function can help electron transfer, leading to higher photo-catalytic activity [6]. As the Fermi levels of these noble metals are lower than that of TiO_2, photo-excited electrons can be transferred from conduction band (CB) to metal particles deposited on the surface of TiO_2. Some extensive theoretical studies on doped bulk TiO_2 are given below.

Wang et al [11] used two unit cells in the anatase structure and substituted the Ti atom by a 3D transition metal atom [vanadium (V), chromium (Cr) manganese (Mn), cobalt (Co), nickel (Ni), copper (Cu) , and zinc (Zn)) or a 4D *tr*ansition metal atom (yttrium (Y), zirconium (Zr), niobium (Nb), molybdenum (Mo) , and silver (Ag)]. The E_g were determined as 2.84, 3.26, 3.35, 2.86, 2.80, 3.25, 3.20, 2.69, 3.15, 3.25, 3.33, 2.96, and 3.20 eV, respectively. In contrast Umebayashi and co-workers [12] used the same 3D metals, but in four unit cell of the rutile structure. They concluded that photoexcitation occur for V, Cr, Mn and Fe doped TiO_2 while Co, or Ni doped TiO_2 exhibit absorption spectra similar to pure TiO_2. The full-potential linearized-augmented plane-wave method (FP-LAPW) method based on DFT using WIEN2K code was used.

Guo and Du [13] performed calculations on a TiO_2 supercell containing 72 atoms ($Ti_{24}O_{48}$). The Cu, Ag and Au atoms were used to substitute Ti atom in TiO_2, resulting in $Ti_{23}CuO_{48}$, $Ti_{23}AgO_{48}$ and $Ti_{23}AuO_{48}$ stoichiometry. Cu and Ag doping enhanced the visible absorption in the range of 400-1000 nm and 500-1000 nm respectively. Au doping has also induced the visible light absorption enhancement but the absorption intensity is very low.

In another theoretical work, rutile was doped with more than one dopant atom. Wang and co-workers [39], doped rutile supercell with Niobium (Nb) atom, $Ti_{24-n}Nb_nO_{48}$, where n= 4, 8, 12, 16 and 20. This calculations were based on density functional theory (DFT),

performed within the generalized gradient approximation (GGA). The foregoing calculation used PBE0 and Dmol^3 codes while Wang and co-workers, used BPW91 and Vienna ab initio simulation package (VASP).

When the particle size is reduced, many interesting phenomena take place such as quantum-size effect. Two computational studies, in 2007 and 2016, equally concluded that model TiO_2 cluster structures have defect-free band structures, and exhibit strong quantum-size effect [1 and 14]. The latter study pointed that the band gap, rapidly approaches the bulk limit at n = 7 and remains constant up to n = 10. There are other published results on the growth behavior, stability, structural, electronic and magnetic properties of bare neutral $(TiO_2)_n$ clusters [2, 3 9, and 15].

Çakir and Gülseren [2] used transition metal vanadium (V), cobalt (Co) and platinum (Pt) to dope the bare cluster $(TiO_2)_{10.}$ As a result, band gap of 0.14, 0.45 and 1.65 eV for V, Co and Pt-doped $(TiO_2)_{10}$ respectively, was obtained compared to band gap of 3.51 eV of the bare $(TiO_2)_{10.}$ Cluster. V atom interacts more with the bare clusters followed by Pt and Co. Co and V atoms induce a magnetic moment.

Gold titanium oxide clusters ($AuTi_3O_n$) have been investigated by Hudson et al [32] using DFT. They concluded that the gold atom preferentially binds to titanium atoms over oxygen atoms, but does not significantly alter the cluster geometry. The EA values increase for n = 4 – 8 (Ti_3AuO_4 and Ti_3AuO_8). The SOMO and LUMO levels of Ti_3AuO_6 cluster are lower in energy than the SOMO and LUMO of the bare titanium oxide clusters.

Nighty nine (99) configurations of carbon (C), nitrogen (N) or sulfur (S) doped $(TiO_2)_n$ where n = 1 - 7, 10 and 13 were studied by Shevlin and co-workers [9]. The preferred dopant site depends upon the choice of dopant. S doped cluster has the lowest formation

energy, followed by N and then C doped cluster. They suggested cluster $(TiO_2)_6$, as the ideal size for the nonmetal doping.

Cao and co-workers [38] observed that nitrogen doping did not cause significant structural changes on cut out structures of $(TiO_2)_n$ where n = 10, 17, 21, 29. According to them, the red shift observed in experiments is due to the fact that N 2*p* states are located above the O 2*p* state.

Qu and Kroes [20] reported two proposed mechanism for of water photooxidation on the TiO_2 surface. The first one, is that the reaction starts by a nucleophilic attack of water molecule on surface-trapped hole, localized on a three-fold coordinated O atom at conner site. The second one involves surface trapped holes at bridging Ti-O-Ti sites. The two mechanism can be represented respectively by the two equations bellow:

$$[Ti_2\text{=O-Ti}]^+_s + H_2O \rightarrow [\text{Ti-O}^{\bullet}\ \text{HO-Ti}]_s + H^+$$

$$[\text{Ti-O-Ti}]^+_s + H_2O \rightarrow [\text{Ti-O}^{\bullet}\ \text{HO-Ti}]_s + H^+$$

The interaction of clusters with water molecule [2, 17, 18, 19, and 20], has been extensively studied. For example Chen and co-workers [18] used a novel Docking-HGA approach, by means of the tree growth-hybrid genetic algorithm–density functional theory (TG–HGA–DFT) and the B3LYP/DZVP2 method to predict the low energy structures of the $(TiO_2)_n(H_2O)_m$ ($n \leq 4$, $m \leq 2n$) and $(TiO_2)_8(H_2O)_m$ (m = 3,7,8) cluster – water complexes . The cluster condensation reaction energies, and infrared vibrational spectra were calculated for the obtained isomers.

Experiments have shown that water molecule is a) adsorbed molecularly at the (110) rutile surfaces and dissociative at defect sites such as oxygen vacancy, and b) adsorbed

dissociative on (001) anatase surface. The water molecule interacts with the titanium dioxide clusters through its O atoms and interatomic distance between O atom and Ti atom, is 2.17 ±0.02Å according to reference [2]. Previous theoretical calculations showed that for bare TiO_2 clusters, the dissociative adsorption is the dominant reaction for the first two water adsorption reactions for $(TiO_2)_n$ clusters where n = 1, 2 and 4, followed by molecular adsorption [18] and H-bonding [2]. The former is limited by the number of unsaturated Ti atoms.

Çakir and Gülseren [2] studied the interaction of bare clusters (n = 1 – 10) with a single and multiple water molecules. Three different adsorption modes were considered: molecular adsorption, dissociative adsorption and H-bonding. The structures where n = 3 and n = 4, have the most favorable adsorption site and a pronounced reduction in E_b than n = 10. They concluded that interaction strength between water and cluster depends on the cluster size.

CHAPTER 3. METHODOLOGY

All the calculations were performed using the BPW91 variant of the Density Functional Theory (DFT) method. Additional calculations were performed using B3LYP, M06L, PBEPBE and other functionals for calibration and comparison purposes. The 6-311+G (d) basis set was used for O and H and also to represent the valence orbitals of Ti, Ag, and Au. The Stuttgart-Dresden (SDD) effective core potential (ECP) was used to represent the inner orbitals of the heavy atoms. Ti atom was treated with 10-electron ECP while Ag and Au were treated with 28 and 60-electron ECP, respectively.

Gaussian 03 and Gaussian 09 Software packages [22 and 23] were used via the resources provided by the University of Namibia (UNAM) and the Centre for High Performance Computing (CHPC) South Africa. Gaussview [24] was used to draw the initial guess structures and to visualize the output files.

For pure $(TiO_2)_n$ clusters, initial structures consist of Ti_n atoms and O_{2n} atoms. For the doped systems one Ti atom is replaced by Ag and Au atom, respectively. Therefore, the stoichiometry of the Ag and Au doped systems are $Ti_{n-1}AgO_{2n}$ and $Ti_{n-1}AuO_{2n}$, respectively. For example when n = 2, bare $(TiO_2)_n$ consists of 2 atoms of titanium, and 4 atoms of oxygen while Ag doped $(TiO_2)_n$ consists of 1 atom of titanium, 4 atoms of oxygen and one atom of silver. The flowchart below illustrates the order of computation in this study:

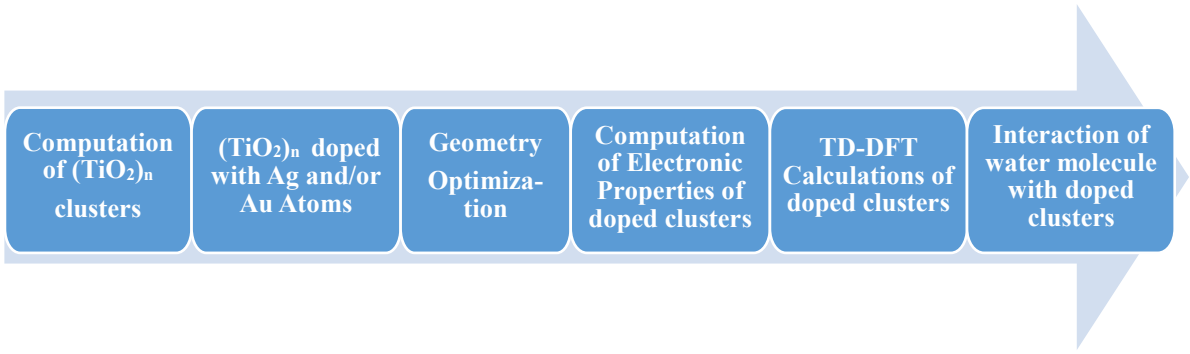

3.1 Doping Process

First, the initial structures of undoped $(TiO_2)_n$ considered in this study were identified through a comprehensive literature search. Special attention was given to the undoped $(TiO_2)_n$ clusters presented in the work of Weicham et al. [1]; Çakir and Gülseren [2]; Qu and Kroes [3]; Mingyang and Dixon [25]; and Archibong and St-Amant [26] for Al_2O_4 systems.

Then, geometry optimization was performed on the clusters. Only the singlet states of the neutral and doublet states of the anionic undoped $(TiO_2)_n$ clusters were fully optimized . The optimized structures were characterized by harmonic vibrational frequency analysis to ensure that all optimized structures were true minima (without any imaginary frequency, Nimag = 0) and not transition states (with only one imaginary frequency, Nimag = 1) or higher-order saddle points (with more than one imaginary frequency, Nimag > 1). The low-lying energy undoped structures obtained from n = 2 - 6 were compared with previous work [1, 2, 3, 15, 25, 27, and 28].

For the doped clusters, all unique (non-equivalent) Ti atoms in the optimized $(TiO_2)_n$ were substituted by Ag and Au atom, respectively. Subsequently, geometry optimization was performed for the Ag doped ($Ti_{n-1}AgO_{2n}$) and Au doped ($Ti_{n-1}AuO_{2n}$) neutral and anionic

species. The doublet and quartet states were optimized for the neutral species while for the anionic forms, the singlet and triplet states were optimized.

The spin-restricted formalism was employed for the singlet states (closed shell) of the anionic clusters while the spin-unrestricted algorithm was employed for the doublet, triplet and quartet (open shell) states. The computed stationary points of the doped clusters were also characterized as minima or saddle point via harmonic vibration frequency analysis.

3.2 Calculation of Electronic Properties

The electron affinity (EA), ionization potential (IP), adiabatic electron detachment energy (AEDE), and vertical electron detachment energy (VEDE) of the clusters were calculated as follows:

$$\text{EA} = E^{0}_{OPT} \text{ (ground state)} - E^{-}_{OPT} \text{ (ground state)} \quad (1)$$

$$\text{IP} = E^{+}_{OPT} \text{ (ground state)} - E^{0}_{OPT} \text{ (ground state)} \quad (2)$$

$$\text{AEDE} = E^{0}_{OPT} - E^{-}_{OPT} \quad (3)$$

$$\text{VEDE} = E^{0,-}_{SP} - E^{-}_{OPT} \quad (4)$$

In equations 1- 4, E^{0}_{OPT}, E^{+}_{OPT} E^{-}_{OPT} and $E^{0,-}_{SP}$ represent the energy of optimized neutral, energy of optimized cation, energy of optimized anion and single point energy of the neutral at anion geometry, respectively.

Optimized anionic clusters within 0.5 eV of the ground state structure were selected for VEDE calculations, and those within 0.3 eV were selected for Coupled-Cluster calculations involving Single and Double substitutions and perturbative inclusion of Triple excitations [CCSD (T)].

Chemical hardness is a measure of the chemical reactivity and stability of species and highlights the capacity of an atom to receive electrons. Chemical hardness together with chemical potential are useful concepts for understanding the behavior of chemical systems. The two quantities were calculated as follows:

$$\text{Chemical hardness} \quad \eta = \frac{IP-EA}{2} \qquad (5)$$

$$\text{Chemical potential} \quad \mu = \frac{IP+EA}{2} \qquad (6)$$

The HOMO-LUMO (HL) gap was calculated for the low-lying energy structures of both Ag and Au doped $(TiO_2)_n$ clusters. The HL was used to approximate the band gap and it was calculated as follows:

$$HL = LUMO - \text{HOMO} \qquad (7)$$

The molecular binding energies of the clusters were calculated as follows:

$$E_b \text{ (Ag cluster)} = \{E_T[(Ti_{n-1} Ag O_{2n})] + E(Ti^+)\} - \{E_T[(TiO_2)_n] + E_T[Ag^+]\} \quad (8)$$

$$E_b \text{ (Au cluster)} = \{E_T[(Ti_{n-1} Au O_{2n})] + E(Ti^+)\} - \{E_T[(TiO_2)_n] + E_T[Au^+]\} \quad (9)$$

E_b (Ag cluster) represents the binding energy of the Ag doped $(TiO_2)_n$ clusters, while E_b (Au cluster) is the binding energy of the Au doped $(TiO_2)_n$ clusters. $E_T[(Ti_{n-1} Ag O_{2n})]$ and $E_T[(Ti_{n-1} Au O_{2n})]$ are the total energies of Ag and Au doped $(TiO_2)_n$ clusters, respectively and $E_T[(TiO_2)_n]$ is the total energy of an undoped cluster. The $E_T[Ag^+]$, $E_T[Au^+]$ and $E_T[Ti^+]$ are the energies of Ag, Au and Ti cations, respectively. All the energies were calculated at the same level of theory.

3.3 TD-DFT Calculations

Time Dependent Density Functional Theory (TD-DFT) gives an exact solution of the Schrödinger equation [20]. It has been used successfully because of its outstanding accuracy and extensive application range. TD-DFT using BPW91 in conjunction with the 6-311+G (d) basis set and the SDD-ECP was employed to calculate the vertical excitation energies (single point TD-DFT calculations). Five lowest doublet and quartet excited states were computed for the lowest neutral Ag and Au doped $(TiO_2)_n$ clusters (n = 2 – 6). Five singlet and triplet excited states were computed for the lowest anionic structures for both Ag and Au doped systems. The computed oscillator strengths (*f*) are related to the intensities of the absorption band.

3.4 Interaction of Doped Cluster with Water Molecule

The clusters $(Ti_{n-1}MO_{2n})(H_2O)$ where M = Ag and Au, were constructed by attaching one H_2O molecule to the lowest energy $(Ti_{n-1}MO_{2n})$ clusters. The water complex was geometry optimized using BPW91.

Binding Energy (E_b) of the water complex was calculated as described in equation 10. In this equation the $E_T[Ti_{n-1}MO_{2n}]$ represents the energy of doped cluster, $E_T[H_2O]$ represents the energy of one molecule of H_2O, and the energy of doped cluster water complex is represented by $E_T[(Ti_{n-1}MO_{2n})(H_2O)]$.

$$E_b = E_T[(Ti_{n-1}MO_{2n})(H_2O)] - \{E_T[(Ti_{n-1}MO_{2n})] + E_T[H_2O]\} \quad (10)$$

One water molecule was attached at a distance of 2.0 ± 0.5 Å from the Ti atom, terminal Ti - O bond, O - O atoms, or dopant metals (Ag or Au), respectively. Figure 1 shows how the atoms in the structure were labeled and illustrates the attachment of a water molecule to the doped cluster.

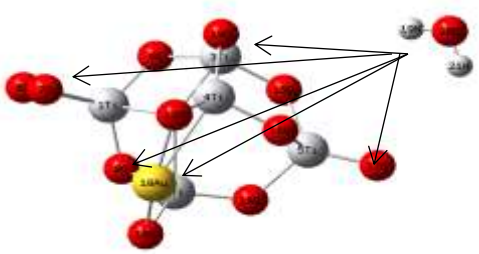

Figure 1: Example of attachment of one water molecule to one of the clusters. The Ti, O and Au atoms are represented by grey, red and yellow spheres.

3.5 Nomenclature

Since the structures reported in this work do not have unique system of naming, the following convention has been adopted throughout this thesis:

- The naming of the undoped structures (n-l-u) starts with an integer (n), which indicates the number of Ti atoms in the cluster, followed by the integer (l) which is used to label a specific isomer of system (n). Next is letter (u) which indicates undoped cluster. For example, in structure 2-1-u, the number "2" implies that the cluster consists of two Ti atoms; "1" signifies isomer 1 when n = 2 and "u" means undoped cluster.

- Naming of the doped structures (n-l-m-d) includes a third digit "m" which is the label (or position) of the substituted Ti atom in the undoped isomer (n-l-u), and a letter "d" which stands for a doped cluster. For example, in structure 2-1-1-d, the first digit "2" indicates a cluster with n = 2, the second digit "1" represents isomer 1 when n = 2, the third digit "1" specifies the label (or position) of the substituted Ti atom in undoped isomer (2-1) and letter "d" is for doped. Hence, this system of naming suggests that 2-1-1-d is a doped cluster derived from 2-1-u and the third

digit indicates that the Ti atom labeled “1” in (2-1-u) has been substituted with either Ag or Au.

The order of substitution was based on natural bond orbital (NBO) analysis [41] of the undoped (n-l-u) structures. Non-equivalent Ti atoms with high natural charges were the first to be substituted by Ag or Au atoms. For example in undoped structure 2-3-u, the two non-equivalent Ti atoms, 1Ti and 2Ti, have charges of 1.305 and 1.302, respectively. Doped cluster resulting from substituting 1Ti with Ag or Au was named 2-3-1-d and cluster obtained from substituting 2Ti was named as 2-3-2-d. Starting with the 2-3-u structure, Figure 2 shows the non-equivalent Ti atoms 2Ti and 1Ti and their respective natural charges, as well as the initial doped structures.

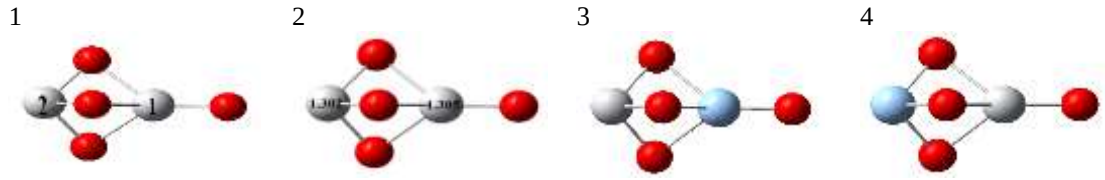

Figure 2: Steps involved in doping using the 2-3-u cluster as example. The Ti, O and Ag atoms, are indicated by gray, red and blue spheres, respectively.

The steps in Figure 2 involves

1. Identification of non-equivalent Ti atoms;

2. Determination of natural charges via NBO analysis;

3. Substitution of highest charge non-equivalent Ti atom by dopant atom;

4. Substitution continues until all non-equivalent Ti atom are substituted by the dopant atom.

If the optimized structure preserve initial configuration, the initial name is retained, otherwise the optimized structure is considered as a new doped structure and assigned a new name, using the convention explained above.

In some cases, letters A, B, and C are used to distinguish similar structures. These structures have the same geometrical configuration in space but different geometrical parameters. For example, 2-4-1-A-d, 2-4-1-B-d, and 2-4-1-C-d, are three stable structures with the same arrangement however their bond distances and bonds angles are different.

In this report, the gray, red, blue and yellow spheres represent the titanium, oxygen, silver and gold atoms, respectively. The bond lengths (R) are expressed in Angstrom units (Å) while the angles (θ) are in degrees (˚).

CHAPTER 4. RESULTS AND DISCUSSIONS

4.1 CALIBRATION TEST

In order to select a theoretical model for the calculations, calibration tests were performed. These calculations are needed in order to determine the reliability of the computational methods and to have confidence in the results obtained. Therefore, different levels of theory were tested to compute the geometry and electronic properties of ground state neutral and anionic forms of undoped $(TiO_2)_2$ clusters that is structure 2-1-u (C_{2h}), displayed in Figure 3.

Four different algorithms were tested: pure density functionals (BLYP, BP86, BPW91, and PBEPBE); hybrid functionals with Hartree-Fock (HF) exchange (B3LYP, B3P86, B3PW91); hybrid meta generalized gradient approximation (GGA) functional with the kinetic energy density gradient and no HF exchange (M06-L); and the second-order Moller-Plesset perturbation approximation (MP2). Three one-particle basis sets [6-311+G (d), 6-311+G (2d), and 6-311+G (2df)] were used for the valence orbitals and the effective core potential (ECP) [29] was employed for the inner atomic orbitals of Ti atom. The results of experimental and theoretical studies are available for neutral and anionic undoped $(TiO_2)_n$ clusters[2, 3, 5, 9, 12, 15, 21, 25, and 27]. These results are used for comparison purposes in the calibration study.

First, all the theoretical models employed in the calibration study predict the rhombic 2-1-u (C_{2h}), as shown in Figure 3, as the ground state structure of $(TiO_2)_2$ in perfect agreement with previous studies [2, 3, 9, 21, 25 and 27]. The bond distance between Ti and

bridge O atom, R (61), predicted by the methods range from 1.841 - 1.859 Å and the bond distance between Ti and terminal O atom, R (64), range from 1.623 - 1.648 Å.

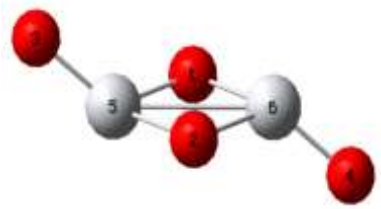

Figure 3: Structure of 2-1-u (C_{2h}). O atoms in red and Ti atoms in grey.

Table 1: Bond lengths [R (Å)] and bond angles [Θ (˚)] for the 2-1-u (C_{2h}) ground state structure of neutral $(TiO_2)_2$ and its anionic form using BPW91, BP86, B3LYP, MO6-L and MP2 methods.

	BPW91		BP86		B3LYP	MO6-L	MP2	
	Neutral	Anion	Neutral	Anion	Neutral	Neutral	Neutral	Anion
R(61)	1.845	1.868	1.845	1.868	1.841	1.844	1.859	1.869
R (64)	1.635	1.674	1.636	1.674	1.623	1.629	1.648	1.668
R(65)	2.716	2.710	2.716	2.709	2.717	2.716	2.713	2.705
Θ (162)	85.2	87.0	85.2	87.7	84.9	85.1	86.9	87.3
Θ (516)	94.8	93.0	94.8	92.9	95.1	94.8	93.7	92.7
Θ (356)	121.0	135.6	120.9	135.8	123.1	121.9	122.2	133.1

Angle of terminal O and two Ti atoms, Θ (356), is within 2.0˚ of each other, while angle formed by bridge O and two Ti atoms, Θ (516) is within 1.4˚. CCSD (T) results in reference [21] shows that R (61) and R (64) are 1.863 Å and 1.648 Å respectively.

In case of the anion, BPW91 and BLYP functionals predict a 2-1-u (C_{2h}:^2A_g) ground state geometry. The B3LYP hybrid functional with Hartree-Fock (HF) exchange, finds the structure as a transition state with one imaginary frequency of -203 cm^{-1} in agreement with reference 3 and 21. Efforts to obtain 2-1-u (C_{2h}:^2A_g) using M06-L failed as a result of symmetry breaking problems. The BPW91 functional suggests that 2-1-u (C_{2h}:^2A_g) and 2-2-u (C_{2v}:$^2A_1$) are nearly isoenergetic and within 1 kcal/mol of each other, while the more accurate CCSD (T) approximation predict 2-2-u (C_{2v}: $^2A_1$) as the ground state geometry of the anion, being 1.87 and 11.15 kcal/mol lower in energy than structures 2-1-u (C_{2h}: ^2A_g) and 2-3-u (C_{3v}: $^2A_1$), respectively, and in agreement with the results in reference 21.

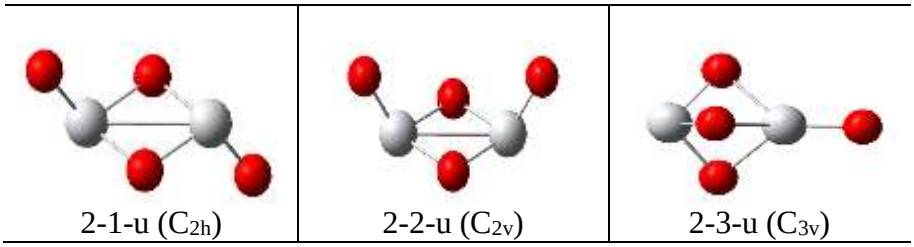

Figure 4: Undoped structures 2-1-u, 2-2-u and 2-3-u

Table 2: Relative energy (ΔE) in kcal/mol

	Structure	ΔE [a]	ΔE [b]	ΔE [c]
Ti_2O_4	2-1-u (C_{2h}:^1A_g)	0.00	0.00	0.00
	2-2-u (C_{2v}:$^1A_1$)	6.67	5.90	5.37
	2-3-u (C_{3v}:$^1A_1$)	15.64	17.59	15.37
$Ti_2O_4^-$	2-1-u (C_{2h}:^2A_g)	0.00	1.87	1.55
	2-2-u (C_{2v}:$^2A_1$)	0.92	0.00	0.00
	2-3-u (C_{3v}:$^2A_1$)	8.37	11.15	9.30

[a] BPW91, [b] CCSD (T)/BPW91, and [c] CCSD(T)/aD from reference [21]

The calculated R (61) and R (64) bond lengths of the anionic C_{2h} structure are 1.87 and 1.67 Å respectively, for all DFT methods. Similarly, CCSD (T)/aT results of reference [21] show that these bond lengths are within 0.20 Å of each other. A noticeable difference in bond angle is observed between the DFT approximations and MP2, where Θ (356) differs by as much as 2.4˚.

According to the experimental work of H-J Zhai and L-S Wang [15], structure 2-3-u (C_{3v} :$^2A_1$) in Figure 4 is responsible for the features obtained in the photoelectron spectroscopy of Ti_2O_4 anion. The computed VEDE and AEDE for the C_{3v} cluster in this study for all DFT methods and CCSD (T)/BPW91, are closer to the experimental values [15] and the CCSD (T) /BP86/aD results [21]. In case of 2-1-u (C_{2h}) structure, the BPW91 VEDE and AEDE are within 0.25 and 0.05 eV of the CCSD (T)/BP86/aD results [21], respectively, and within 0.30 and 0.37 eV from the experimental values in reference [15]. The computed CCSD (T)/BPW91 0.64 eV far from CCSD (T) /BP86/aD obtained in reference [21].

On the basis of Table 3, BPW91 was chosen as the functional for studying the systems considered in this work. First, the symmetry breaking problems of B3LYP and MP2 do not manifest in the BPW91 functional. Further, the geometric parameters and the electronic properties predicted by the BPW91 funtional agree very well with the prediction of the more accurate CCSD (T) approximation and experiments.

Table 3: VEDE (eV) and AEDE (eV) for 2-1-u (C_{2h}) and 2-3-u (C_{3v}) structures.

	2-1-u (C_{2h}:^2A_g)			
	VEDE	VEDE[b]	AEDE	AEDE[b]
B3LYP		2.26		1.87
BPW91	1.97		1.69	
PW91		2.04		1.78
BP86	2.13	2.11	1.84	1.85
CCSD(T)/BPW91	1.58		1.42	
CCSD(T)/BP86/aD		2.22		1.64
	2-3-u (C_{3v}:$^2A_1$)			
	VEDE	VEDE[b]	AEDE	AEDE[b]
B3LYP	2.52	2.45	2.07	2.20
BPW91	2.18		1.98	
PW91		2.19		2.01
BP86	2.31	2.24	2.11	2.07
CCSD(T)/BPW91	2.03		1.78	
CCSD(T)/BP86/aD		2.13		1.98
Exptl[c]	2.27±0.05		2.06±0.05	

[b] Theoretical results from reference [21], [c] Experimental results from reference [15]

4.2 FIXED NUCLEAR DOPPING (FND)

The cardinal objective of this research, as stated in section 1.3, is to investigate the variation in the properties of doped $(TiO_2)_n$ (n = 2 - 6) with cluster size. Initially, single point calculations were performed for the doped clusters using the BPW91 functional. These calculations are called fixed nuclear doping (FND) because the starting geometries were retained (unrelaxed and unoptimized) during the calculations.

For these set of calculations, only the most stable undoped structures for system n = 2 to n = 10 were doped by substituting one Ti atom with one Ag atom or Au atom, respectively. The number of doped clusters for each cluster group n are directly proportional to the number of non-equivalent Ti atoms in the structure. For example when n=5, the lowest energy cluster, 5-1-u (Figure 5) possesses four non-equivalent Ti atoms, therefore, four doped structures were generated.

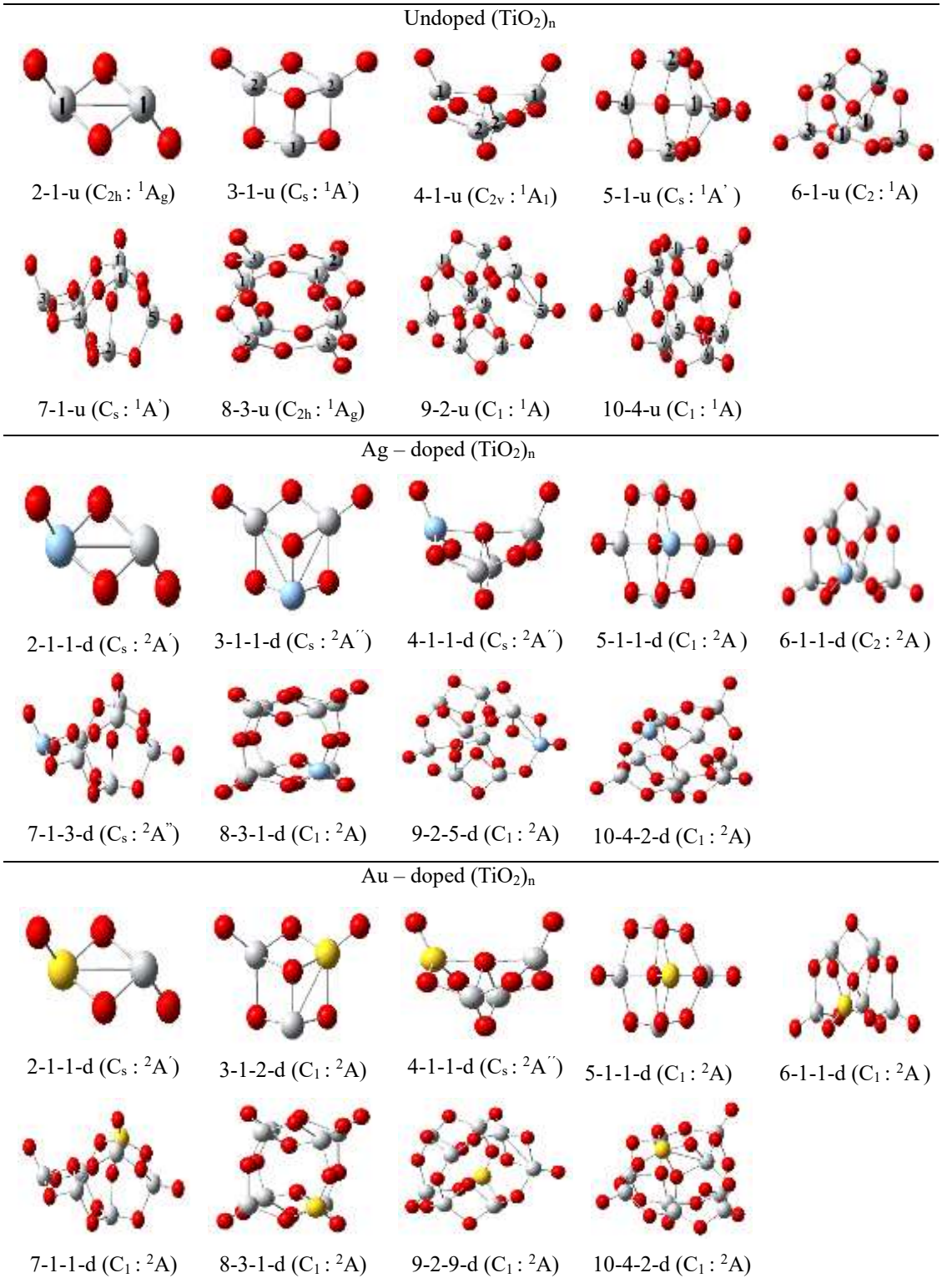

Figure 5: Lowest energy structures of undoped and Ag/Au FND, indicating their point group and electronic states, for n = 2 – 10 clusters.

The fixed nuclear doping calculations were performed to explore possible trend in the HL gap of the doped clusters and to compare the HL gap of doped clusters with the band gap in bulk TiO_2. Rutile is known to have a band gap of 3.0 eV and anatase 3.2 eV. According to Figure 6, the HL gap resulting from the FND are significantly lower than the band gap in bulk TiO_2. Figure 5 depicts the lowest energy undoped and FND clusters for n = 2 - 10 and the variation of the HL gap with cluster size (for n = 2 - 10) is shown in Figure 6.

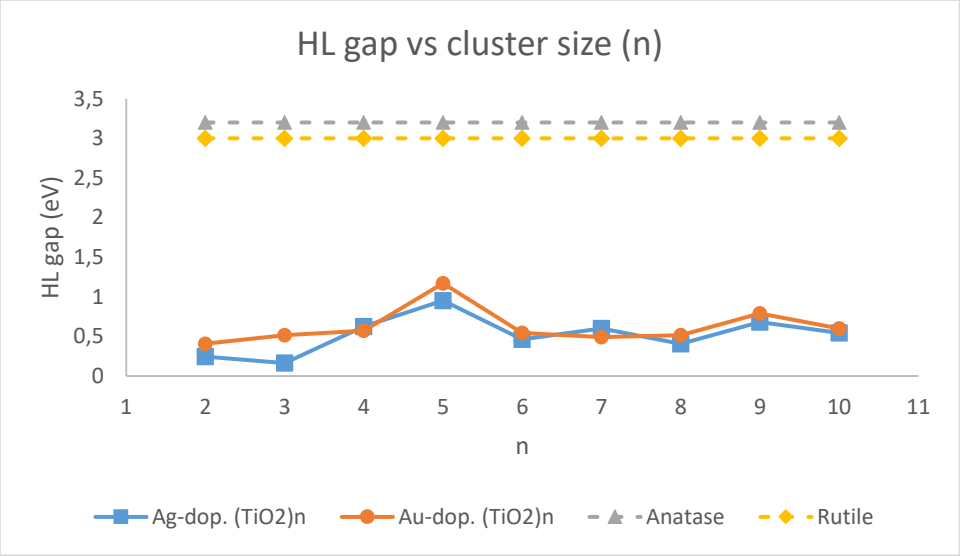

Figure 6: HL gap for FND of Ag and Au doping $(TiO_2)_n$ clusters (n = 2 - 10)

The fixed nuclear doping calculations were performed to explore possible trend in the HL gap of the doped clusters and to compare the HL gap of doped clusters with the band gap in bulk TiO_2. Rutile is known to have a band gap of 3.0 eV and anatase 3.2 eV. According to Figure 6, the HL gap resulting from the FND are significantly lower than the band gap in bulk TiO_2. Figure 5 depicts the lowest energy undoped and FND clusters for n = 2 - 10 and the variation of the HL gap with cluster size (for n = 2 - 10) is shown in Figure 6.

Figure 6, does not show any discernible trend in the HL gap of the Ag/Au FND clusters.

Generally, it seems the Ag doped clusters have lower HL gap compared to Au doped clusters. For both Ag and Au doped clusters, 5-1-1-d and 9-2-2-d, (n = 5 and n = 9) respectively, are the most stable (higher HL gap value), while Ag or Au dopant clusters with n = 4, 6 and 10 are likely to be the same. The plot exhibit oscillatory character from n = 5 to n = 10 in Ag doped system. Geometry optimization of the doped clusters is needed in order to obtain reliable results and the next section discusses geometry optimized (relaxed) Ag/Au doped TiO_2 clusters.

4.3 GEOMETRY AND PROPERTIES OF Ag DOPED $(TiO_2)_n$ CLUSTERS

Two common polymorphs of titanium dioxide are rutile and anatase. Rutile belongs to the space group P42/m n m (136) and anatase belongs to the space group I41/ a m d (141) [9, 11, and 14]. Each Ti atom in rutile is coordinated to six O atoms whereby four Ti-O bonds are shorter than the other two. Similarly in anatase, each Ti atom is coordinated to six O atom, and each oxygen atom is surrounded by three titanium atoms. Different Ti - O and Ti - Ti bond distances are found in the literature for rutile and anatase. The reported bond distances depend on the theoretical methods and levels employed in the studies. Table 4 lists experimental [30] and theoretical [31] results for Ti - Ti and Ti - O distances in the two common polymorphs of TiO_2. The results indicate that anatase has longer Ti - Ti and O - O bonds and shorter Ti - O than rutile.

Table 4: Bond length (Å) in rutile and anatase

	Rutile [a]	Rutile [b]	Anatase [b]
Ti-O	2.20	1.95	1.89
Ti-Ti	2.90	2.96	3.02
O-O	--	2.54	2.68

[a] Experimental bond distance from reference 30
[b] Theoretical bond distance from reference 31

In this work, the undoped clusters were obtained from the literature [1, 2, 3, 16, 25, and 27] and re-optimized. Subsequently, the optimized undoped clusters were doped using the procedures described in chapter 3. The following sections discuss the results for each doped cluster group starting from n = 2.

4.3.1 Geometry and Properties of Ag Doped $(TiO_2)_2$ Clusters, $TiAgO_4$

(a) Relative Energy of $TiAgO_4$ Clusters

Thirteen dopants sites were identified from the optimized undoped structures of $(TiO_2)_2$. Structure 2-4-1-B-d was found to be the lowest energy structure of the neutral and anionic $TiAgO_4$ clusters. The 2-4-1-B-d [C_{2v}:$^4A_2$] quartet is 56.38 eV higher in energy than the doublet 2-4-1-B-d [C_{2v}:$^2A_2$] structure. During geometry optimization, the neutral form of 2-5-1-d, and 2-10-1-d optimized to the lowest energy 2-4-1-B-d structure. The structures of 2-11-d (C_1:^{2}A) was 0.10 eV higher in energy than 2-4-1-B-d at BPW91 level. CCSD (T)// BPW91 results shows that 2-11-d lie much higher in energy than 2-4-1-B-d (0.21 eV).

In case of the anionic cluster, the relative energy ranges from 0.15 eV to 0.93 eV, as shown in Table 35 (Appendix 1.2). The anionic 2-4-1-B-d structure is predicted to be $^1A_1$ in C_{2v} symmetry. The 2-12-d (C_1:^{1}A) is at BPW91 and B3LYP levels 0.15 and 0.20 eV higher in energy than 2-4-1-B-d (C_{2v}: $^1A_1$), respectively. In the case of triplet, structures 2-4-1-B-d and 2-12-d optimized to structure 2-11-d (C_1: ^{3}A). The 2-11-d (C_1: ^{3}A).is 0.68 eV higher in energy than 2-4-1-B-d (C_{2v}: $^1A_1$).

(b) Geometrical Parameters of the Lowest Energy Structures of Energy $TiAgO_4$ Clusters

Optimized geometric parameters of the neutral and anionic $TiAgO_4$ are presented in Tables 5 and the structure is shown in Figure 7.

Table 5: Geometrical parameters for neutral and anionic 2-4-1-B-d structure. Bond length (R) and bond angle (Θ) were calculated at BPW91 level.

	R(61)	R(62)	R(65)	R(14)	R(53)	Θ (253)	Θ (164)	Θ (564)
Neutral	2.030	1.723	2.777	1.339	2.303	76.5	38.5	160.7
Anion	1.880	1.800	2.723	1.510	2.249	110.3	47.4	156.3

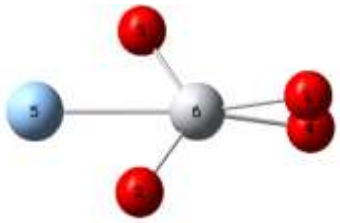

Figure 7: Doped 2-4-1-B-d structure of neutral and anionic $TiAgO_4$

In addition to the ground state $^2A_2$, the states $^2B_1$ and $^2B_2$ were obtained for 2-4-1-B-d at BPW91 level. Structures 2-4-1-B-d (C_{2v}: $^2B_1$) and 2-4-1-B-d (C_{2v}: $^2B_2$) are 0.85 eV and 1.21 eV higher than 2-4-1-B-d (C_{2v}: $^2A_2$).

Table 6: Geometrical parameters of neutral 2-4-1-B-d (C_{2v}). Bond length [R (Å)] and bond angle [Θ (˚)] were calculated at BPW91 level.

State	$^2A_2$	$^2B_1$	$^2B_2$	State	$^2A_2$	$^2B_1$	$^2B_2$
R(61)	2.030	1.829	2.042	Θ (263)	111.6	96.3	108.4
R(62)	1.723	1.836	1.722	Θ (164)	38.5	48.2	39.2
R(65)	2.777	2.855	2.831	Θ (564)	160.7	155.9	160.4
R(14)	1.339	1.494	1.369	Θ (253)	76.5	80.0	74.9
R(53)	2.303	2.127	2.297				

Neutral structures 2-4-1-A-d and 2-4-1-C-d, are very similar to neutral 2-4-1-B-d, as shown in Figure 8. They differ from 2-4-1-B-d in O - O bond length (1.00 Å, 1.30 Å respectively) and O-Ti-O bond angle (48˚, 62˚ respectively). These differences, show that the potential energy surfaces are made of very soft vibrational modes.

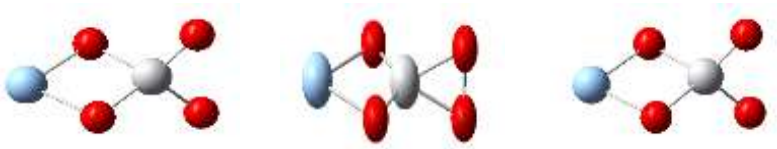

2-4-1-A-d (1.87) 2-4-1-B-d (0.00) 2-4-1-C-d (1.93)

Figure 8: Doped neutral 2-4-1-A-d, 2-4-1-B-d and 2-4-1-C-d. Relative energies (eV) are in parenthesis

(c) Vibrational Frequency of Lowest Energy Neutral and Anionic $TiAgO_4$ Clusters

The vibrational modes of neutral and anionic 2-4-1-B-d at the BPW91 and B3LYP levels are listed in Table 7 and 8, respectively. The ω1 (23 cm^{-1}) and ω12 (1121 cm^{-1}) vibration modes of 2-4-1-B-d (C_{2v}:$^2A_2$) lowest energy structure of $TiAgO_4$ are due to asymmetric vibrations of O-Ti-O atoms and bending of the O - O atoms, respectively. While ω3 (163 cm^{-1}) vibration mode corresponds to the asymmetric stretching of Ag dopant atom and Ti atom. The two highest peaks at 802 cm^{-1} (ω10) and 853 cm^{-1} (ω11) in the spectrum are due to degenerate bending of the O - O (connected to Ag atom) and the unique Ti atom. The IR spectrum for neutral 2-4-1-B-d (C_{2v}:$^2A_2$) cluster is shown in Figure 9.

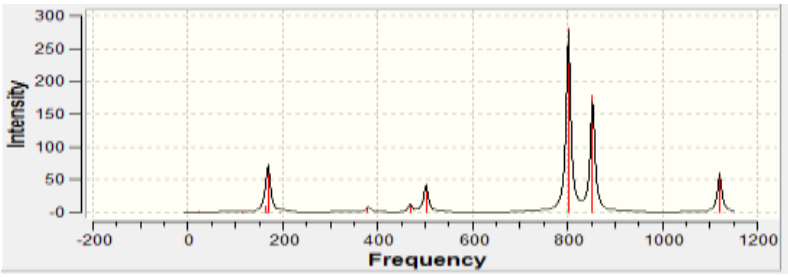

Figure 9: IR Spectrum for 2-4-1-B-d (C_{2v}:$^2A_2$) at BPW91/6-311+G (d)

Table 7: Vibrational modes and frequencies for 2-4-1-B-d (C_{2v}:$^2A_2$). Frequency (cm^{-1}) and IR intensity (km/mol) calculated at BPW91 and B3LYP level.

Modes	BPW91		B3LYP	
	Frequencies	IR intensity	Frequencies	IR intensity
ω12	1121	60	1181	44
ω11	853	178	911	253
ω10	802	280	849	366
ω9	502	43	523	69
ω8	468	11	480	9
ω7	379	8	389	12
ω6	196	0	195	0
ω5	169	71	184	83
ω4	168	1	175	1
ω3	163	9	167	12
ω2	114	0	114	0
ω1	23	2	26	1

Table 8: Vibrational modes and frequencies for 2-4-1-B-d (C_{2v}:$^1A_1$). Frequency (cm^{-1}) and IR intensity (km/mol) calculated at BPW91 and B3LYP level.

Modes	BPW91		B3LYP	
	Frequencies	IR intensity	Frequencies	IR intensity
ω12	823	283	847	313
ω11	747	290	787	327
ω10	679	280	719	357
ω9	581	20	604	34
ω8	580	40	594	39
ω7	410	20	424	30
ω6	242	0	253	0
ω5	212	55	229	66
ω4	182	13	186	16
ω3	165	0	178	0
ω2	149	0	169	0
ω1	49	0	57	0

Vibrational frequency calculations of anionic 2-4-1-B-d (C_{2v}:$^1A_1$), resulted in asymmetric stretching, degenerate bend of bridging O-O and Ti atom, and the symmetric stretch of O-O atoms of the ω12, ω11 and ω10 modes, respectively. These vibrations occurred from 679 cm^{-1} to 823 cm^{-1} (intensity of 280-289 km/mole). Symmetric stretching between Ag and Ti atom was found at a frequency of 182 cm^{-1} with intensity of 13 km/mole.

(d) HL Gap of Lowest Lying $TiAgO_4$ Clusters

The HOMO of 2-4-1-B-d (C_{2v}:$^2A_2$) is characterized by the overlap of the d and p atomic orbitals on Ag and p atomic orbital of adjacent O atom, respectively. The LUMO is mainly localized on Ag (s and p) bonding orbital. Figure 10 depicts the HOMO and LUMO of neutral and anionic 2-4-1-B-d cluster and corresponding HL gap for different functionals. Neutral 2-4-1-B-d hold a doublet (open shell) state, then two separate sets of singly occupied orbitals (α and β) were obtained. The α-HOMO/LUMO where used to calculate HL gap, as displayed in Table 9. The description of the HOMO of the anion is similar to that of the neutral molecule.

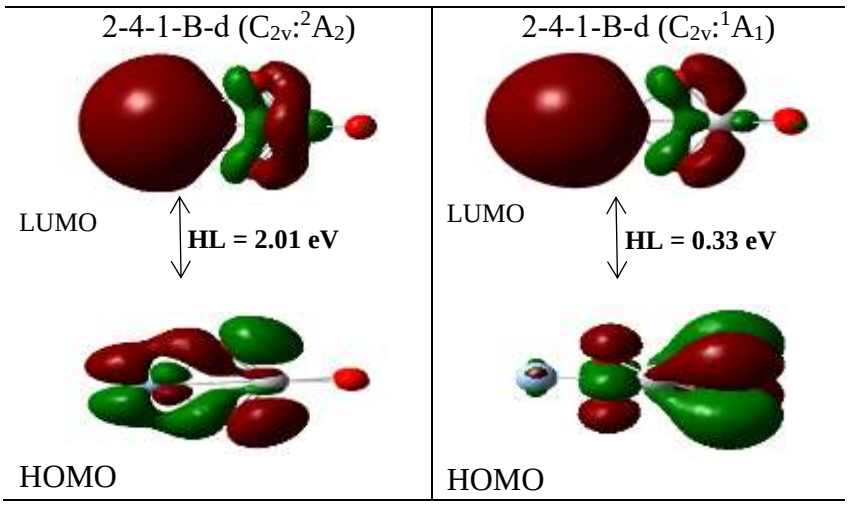

Figure 10: FMO of Ag doped clusters of neutral and anionic 2-4-1-B-d cluster.

There are similarities between LUMO of 2-4-1-B-d ($C_{2v:}$ $^2A_2$) and LUMO of 2-4-1-B-d (C_{2v}: $^1A_1$). For both orbitals, major contribution comes from (s) and (Pz) orbitals of the Ag atom with minor contribution from (s) orbitals on O - O atoms. The triplet state of the anion) 2-4-1-B-d (C_{2v}) is not stable, as it optimizes to structure 2-13-d ($C_{1:}$ ^3A) with HL gap of 1.44 eV. Table 9 provide the HL gap of low lying neutral and anionic 2-4-1-B-d (C_{2v}) cluster using different DFT functionals.

Table 9: Calculated α-HOMO (a.u.), α-LUMO (a.u.) and HL gap (eV) for neutral and anionic 2-4-1-B-d cluster

	2-4-1-B-d (C_{2v}:$^2A_2$)			2-4-1-B-d (C_{2v}:$^1A_1$)		
Method	α-HOMO	α-LUMO	HL	α -HOMO	α -LUMO	HL
B3P86	-0.285	-0.146	3.78	-0.069	0.004	1.99
BP86	-0.228	-0.156	1.96	-0.013	0.000	0.35
BPW91	-0.223	-0.149	2.01	-0.007	0.005	0.33
M06-L	-0.220	-0.126	2.56	-0.003	0.023	0.71
B3LYP	-0.266	-0.135	3.56	-0.053	0.014	1.82
B3PW91	-0.264	-0.125	3.78	-0.048	0.023	1.93
BLYP	-0.222	-0.157	1.77	-0.01	0.000	0.27
HF	-0.401	-0.018	10.42	-0.204	0.090	8.00
PBEPBE	-0.223	-0.153	1.90	-0.008	0.002	0.27
PBE1PBE	-0.272	-0.118	4.19	-0.055	0.028	2.26

(e) Electron Detachment Energy and Electron Affinity of $TiAgO_4$ Clusters

Detachment of an electron from the 32 (a2) HOMO of the 2-4-1-B-d (C_{2v}:$^1A_1$) anion yields the $^2A_2$ state of the neutral. Vertical electron detachment energy (VEDE) at BPW91, B3LYP, CCSD (T) //BPW91 and CCSD (T)//B3LYP levels are 3.38, 3.68, 3.28, and 3.90 eV, respectively, while adiabatic electron detachment energy (AEDE) values are 2.70, 2.76, 2.35 and 2.35 eV, respectively. Table 10 and 11 gives the summary of VEDE and AEDE using different functionals and the corresponding CCSD (T) results.

Electron affinity was calculated by subtracting the energy of optimized anion 2-4-1-B-d (C_{2v}: $^1A_1$) cluster from the optimized neutral 2-4-1-B-d (C_{2v}: $^2A_2$) cluster resulting in a value of 2.70 eV at BPW91.

Table 10: Calculated VEDE and AEDE at DFT and MP2

DFT	VEDE		AEDE
	$^2A_2$	$^2B_1$	$^2A_2$
B3P86	4.16	4.58	3.25
BP86	3.55	4.01	2.88
BPW91	3.38	3.86	2.70
M06-L	2.42	3.59	2.42
B3LYP	3.68	4.04	2.76
B3PW91	3.56	3.98	2.63
BLYP	3.42	3.83	2.75
MP2	57.55	59.43	56.66

Table 11: Calculated VEDE and AEDE at the CCSD (T)\\DFT and CCSD (T)\\MP2 levels

CCSD (T)\\	VEDE		AEDE
	$^2A_2$	$^2B_1$	$^2A_2$
B3P86	3.16	3.90	2.36
BP86	3.30	3.93	2.36
BPW91	3.28	3.94	2.35
M06-L	3.18	3.94	2.35
B3LYP	3.22	3.90	2.35
B3PW91	3.16	3.90	2.35
BLYP	3.35	3.93	2.35
MP2	3.29	3.91	2.35

(f) TD – DFT Calculations of Lowest Energy Neutral and Anionic $TiAgO_4$ Clusters

The result of TD-DFT calculations are plotted in Figure 11. The plot shows that the un-doped cluster 2-1-u (C_{2h}:^1A_g) does not absorb energy in the visible region, its λ_{max} being 355 nm. However, doping with Ag metal results in a bathochromic shift, and the $TiAgO_4$ cluster, 2-4-1-B-d (C_{2v}:$^2A_2$), absorbs at 1016 nm, (1.22 eV) due to excitation from HOMO - 1 to LUMO. This transition is spin allowed, doublet–doublet transition. The electronic excitation from HOMO to LUMO, Figure 10, although doublet-doublet, is forbidden (f=0.000) and occurs at 1754 nm (0.71 eV).

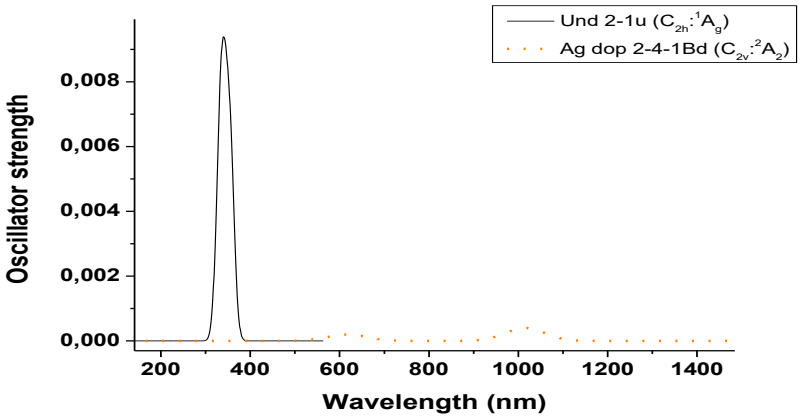

Figure 11: UV-Vis spectrum for neutral 2-1-u (C_{2h}:^1A_g) and 2-4-1-B-d (C_{2v}:$^2A_2$) at BPW91/6-311+ G (d)

The low energy transition for anionic 2-4-1-B-d (C_{2v}: $^1A_1$) structure is from HOMO to LUMO, Figure 10, at region of 3397 nm. This transition is spin allowed, i.e. singlet-singlet. The most intense spin allowed transition (f=0.0065) occurred at 748 nm (1.66 eV), and it was originated by the excitation from HOMO-2 to LUMO excitation. The HOMO-2 is a bonding orbital on the two pairs of O - O and Ti.

(g) Interaction of Water with the 2-4-1-B-d Cluster

One water molecule was attached close to 5Ag and 6Ti atoms (Figure 7), respectively, in 2-4-1-B-d. After geometry optimization, the two attachments end up dissociative adsorption of water with binding energy (E_b) of -1.00 eV. The weak interaction of the dissociated H atom with 2O of Ag doped cluster resulted in an asymmetric stretching at 883 cm^{-1} with very low intensity of 316 km/mol. According to reference 18, when dissociative adsorption of one water molecule occurred at the bare dimmer (Ti_2O_4), the new band near 3900 cm^{-1} is due to the OH stretch. This stretching vibration was observed at 3734 cm^{-1} in this study.

Figure 12: Dissociative adsorption of one water molecule on 2-4-1-B-d through 5Ag atom

4.3.2 Geometry and Properties of Ag Doped $(TiO_2)_3$ Clusters, Ti_2AgO_6

(a) Relative Energy of Ti_2AgO_6 Clusters

Table 12 lists the relative energies of the Ag doped $(TiO_2)_3$ clusters. Twelve doped clusters were successfully computed for neutral Ti_2AgO_6. In contrast to clusters where n = 2, Ag doped $(TiO_2)_3$ clusters have different lowest lying structure for neutral and anionic clusters. The lowest energy cluster for neutral Ti_2AgO_6 appears to be 3-8-d (C_1:^{2}A) depicted in Figure 13. From the results presented in Table 12, the five (5) low energy structures for neutral Ti_2AgO_6 are 3-1-1-d (C_s: ^{2}A$''$); 3-1-1-d (C_s: ^{4}A$''$); 3-2-1-d (C_s:^{2}A$''$); 3-9-d (C_s: ^{4}A$''$); 3-11-d (C_1: ^{2}A) and their relative energies are 1.22 eV, 1.10 eV, 1.49 eV. 1.73 eV and 0.44 eV, respectively. Structure 3-1-1-d (C_{2v}:$^3B_2$) was found to be the ground state for anionic Ti_2AgO_6 clusters. Table 12, shows other low energy structures for Ti_2AgO_6 anionic clusters, such as 3-1-1-d (C_{2v}: $^1A_1$), and 3-11-d (C_s: **^{1}A$'$**), with relative energies of 0.45 eV and 0.42 eV, respectively.

Table 12: Relative energy [ΔE (eV)] of Ti_2AgO_6 clusters

Structures	PG	Ti_2AgO_6		$Ti_2AgO_6^-$	
		State	ΔE	State	ΔE
3-1-1-d	C_{2v}			$^1A_1$	0.45
3-1-1-d	C_{2v}			$^3B_2$	*0.00*
3-1-2-d	C_s	$^2A''$	1.81		
3-1-2-d	C_s	$^4A''$	1.78		
3-2-1-d	C_s	$^2A''$	1.49	$^1A'$	1.32
3-2-1-d	C_s			$^3A''$	0.98
3-8-d	C_1	^2A	*0.00*	^1A	0.63
3-11-d	C_s			**$^1A'$**	0.42
3-11-d	C_1	^2A	0.44		

(b) Geometrical Parameters of the Lowest Energy Structures of Ti_2AgO_6 Clusters

The 3-8-d lowest energy of neutral Ti_2AgO_6, as shown in Figure 13, is characterized by a rhombic Ti_2O_2. Attached to the rhombic moiety are two O atoms and O – O unit (1.358 Å). There is a weak interaction between the dopant atom and the O atoms due to large interatomic distances. The 3-1-1-d (C_{2v}) structure is similar to the undoped 3-1-u (C_s) structure, i.e., the same arrangement of terminal Ti–O atom, Ti–Ti bond and Ti–O –Ti angle in doped structure differ from the undoped structure by about 0.11 Å and 5.5 ˚ respectively.

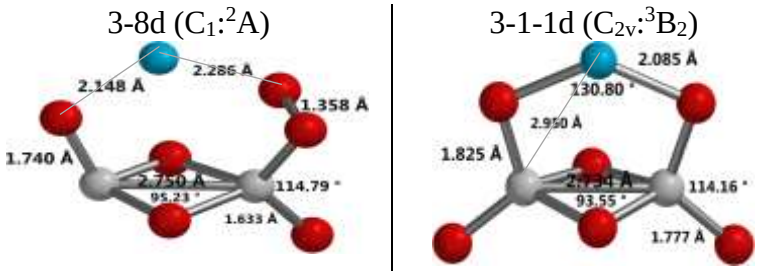

Figure 13: Geometrical parameters of neutral 3-8-d (C_1:^2A) and anionic 3-1-1-d (C_{2v}:$^3B_2$)

(c) Vibrational Frequency of Lowest Energy Neutral and Anionic Ti_2AgO_6 Clusters

Vibrational modes of lowest lying 3-8-d (C_1) and 3-1-1-d (C_{2v}) clusters are displayed in Table 13. According to reference 15, peaks at region of 770 cm^{-1} are useful to identify two-fold coordinated O atoms. In this case, the peak at approximately region of 770 cm^{-1} of structure 3-8-d (C_1:^{2}A) is assigned to symmetric stretching between Ti atom and two O atoms that are two-fold coordinated. This is the most pronounced peak. In Figure 14, the thin blue arrows, represents the displacement vectors for the vibrational modes.

Table 13: Vibrational modes and frequencies for lowest lying neutral and anionic Ti_2AgO_6 clusters. Frequency (cm^{-1}) and IR intensity (km/mol) were calculated at BPW91 level.

3-8-d (C_1:^{2}A)			3-1-1-d (C_{2v}:$^3B_2$)		
Modes	Frequencies	IR intensity	Modes	Frequencies	IR intensity
ω21	1057	44	ω21	714	39
ω20	994	241	ω20	676	3
ω19	830	55	ω19	667	46
ω18	771	317	ω18	600	159
ω17	719	157	ω17	587	82
ω16	583	184	ω16	544	0
ω15	460	30	ω15	447	0
ω14	418	27	ω14	430	0
ω13	404	28	ω13	407	1
ω12	350	3	ω12	388	1
ω11	344	6	ω11	369	2
ω10	299	2	ω10	280	1
ω9	270	1	ω9	243	7
ω8	242	2	ω8	224	0
ω7	189	11	ω7	181	4
ω6	171	2	ω6	164	30
ω5	154	9	ω5	155	2
ω4	12	2	ω4	130	0
ω3	113	2	ω3	129	6
ω2	75	6	ω2	101	4
ω1	63	3	ω1	75	1

For the Ag doped 3-1-1-d (C_{2v}:$^3B_1$) cluster, a band consisting of two peaks (ω17 and ω18) is observed in the region of 600 cm^{-1} due to bending of bridging O and terminal Ti - O

atoms. Vibrational mode ω21 at 714 cm^{-1} is due to symmetric stretching of O - O atoms through Ti atom.

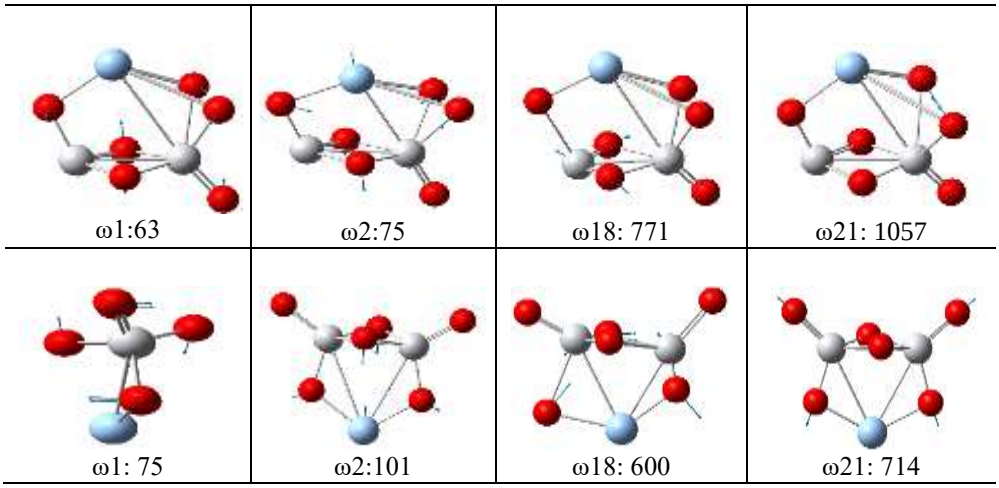

Figure 14: Displacement vector for vibration modes and frequencies (cm^{-1}) for up: neutral 3-8-d (C_1:^{2}A) and down: anionic 3-1-1-d (C_{2v}:$^3B_2$) clusters.

(d) HL Gap of Lowest Lying Energy Ti_2AgO_6 Clusters

HOMO and LUMO of most stable Ti_2AgO_6 species are displayed in Figure 15. The HOMO of most stable cluster for Ti_2AgO_6 is characterized by bonding between terminal O and bridging O, as well as the non-bonding (p) orbital of the O - O atoms. The extra electron will prefer the dopant atom Ag in case of reacting with other species.

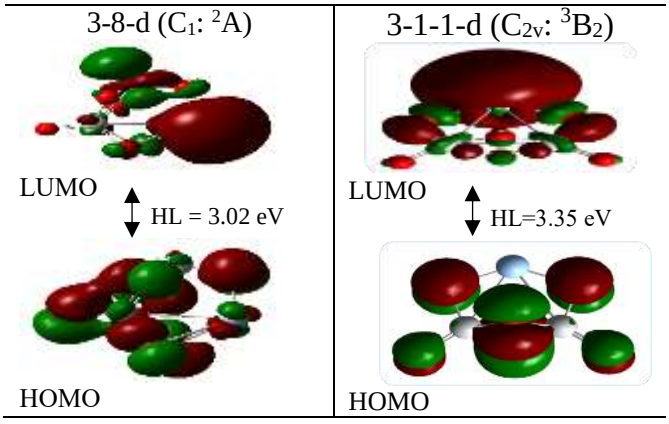

Figure 15: FMO of Ag-doped 3-8-d (C_1: ^{2}A) of neutral and 3-1-1-d (C_{2v}: $^3B_2$) of anion clusters at BPW91/6-311+G (d) level

The HL gap of most stable neutral Ti_2AgO_6 cluster is the same as Eg of rutile and approximately 1.00 eV larger than most stable neutral $TiAgO_4$ cluster.

No contribution to the HOMO of the anionic cluster 3-1-1-d (C_{2v}: $^3B_2$) from the dopant atom. Calculated HL gap was 3.35 eV, which is 0.15 eV above E_g of anatase.

(e) Electron Detachment Energy and Electron Affinity of Ti_2AgO_6 Clusters

The anion ground state is triplet form of 3-1-1-d (C_{2v}: $^3B_2$). The removal of one electron from HOMO is expected to yield a doublet ($^2A_2$) while removal of one electron from HOMO-2 yield a quartet state ($^4A_2$). Table 14 displays the detachment energies at BPW91, B3LYP, CCSD (T)//BPW91 and CCSD (T)//B3LYP levels. From Table 14, the results obtained using the B3LYP functional are in good agreement with the CCSD (T)//B3LYP results.

Table 14: VEDE for Ag doped 3-1-1-d (C_{2v}: $^3B_2$) at the BPW91, B3LYP, CCSD (T)//BPW91 and CCSD (T)//B3LYP

State	BPW91	B3LYP	CCSD (T)//BPW91	CCSD (T)//B3LYP
$^3B_2 \rightarrow {}^2A_1$	5.37	5.60	6.04	5.63
$^3B_2 \rightarrow {}^4A_1$	5.09	5.63	5.51	5.68

It was not possible to obtain the AEDE for cluster 3-1-1-d because its corresponding neutral structure was not stable. The AEDE for 3-1-2-d (C_s), 3-2-1-d (C_s), 3-2-2-d (C_{2h}), and 3-8-d (C_1) using BPW91 are 4.11, 4.72, 3.61 and 3.61 eV, respectively.

(f) TD – DFT Calculations of Lowest Energy Neutral and Anionic Ti_2AgO_6 Clusters

The UV-Vis spectrum for the doublet–doublet excitation excitations of 3-8-d (C_1:^2A), shows three peaks in the region of 877 - 1539 nm. The singlet-singlet excitations of the lowest lying neutral undoped structure [3-1-u (C_s: $^1A'$)] occurred at 430 - 605 nm and give

rise to two peaks. The low doublet–doublet excitation energy of 1539 nm (0.81 eV), is assigned to the weak transition from the HOMO to LUMO. The extra electron is not expected to be found at the silver atom, as it does not contribute to HOMO, as shown in Figure 15. The lowest lying energy anionic cluster, 3-1-1-d (C_{2v}:$^3B_2$), does not give any pronounced peaks.

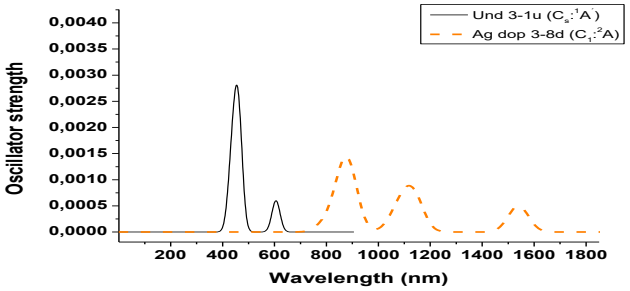

Figure 16: UV-Vis spectrum for neutral 3-1-u *(C_s: $^1A'$)* and neutral 3-8-d *(C_1:^2A)*

(g) Interaction of Water with the 3-8-d Cluster

The attachment of one water molecule to 3-8-d through 7Ti and 8Ti resulted in molecular adsorption interaction, while attachment through 9Ag resulted in H-bonding with 1O atom. The interaction of water with 9Ag and 8Ti atoms were predicted to be higher in energy than interaction with 7Ti atom. These interactions and respective binding energies are displayed in Figure 17.

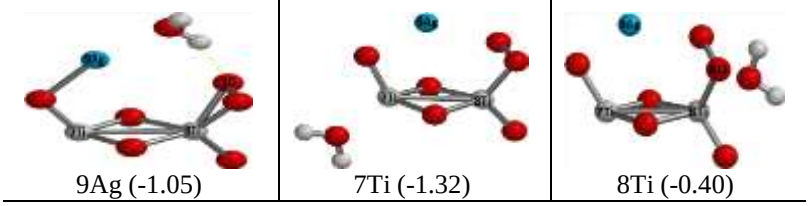

Figure 17: Geometries and E_b (eV) for the interaction of one water molecule with Ag doped 3-8-d cluster

The highest peak (476 km/mol) at 3328 cm^{-1} for the interaction through 9Ag, was due to the vibration of the bonded H and one of the oxygen atoms in O - O bond. Asymmetric stretching vibration of Ag dopant atom and other atoms occurred at 65 cm^{-1} with an intensity of 3 km/mole.

4.3.3 Geometry and Properties of Ag Doped $(TiO_2)_4$ Clusters, Ti_3AgO_8

(a) Relative Energy of Ti_3AgO_8 Clusters

Starting from the lower energy isomers of the undoped $(TiO_2)_4$ clusters, twenty six non-equivalent Ti atoms were considered for substitution by Ag atom. Some of the initially doped structures were not stable and optimized to other structures. The relative energy of the low-lying neutral Ti_3AgO_8 clusters range from 0.55 eV to 3.96 eV, while for the anionic Ti_3AgO_8 clusters, ranges from 0.21 eV to 3.91 eV, as shown in Tables 62 and 63 in Appendix 3.2.

The lowest energy clusters obtained were 4-21-d (C_1:^{2}A) and 4-9-1-d (C_s: $^3A^{"}$) for neutral and anionic, respectively. Cluster 4-21-d was derived from the unstable 4-10-3-d structure. Structure 4-9-1-d (C_s: $^2A^{"}$) which is the neutral form of 4-9-1-d (C_s: $^3A^{"}$) is 1.30 eV above the 4-21-d (C_1: ^{2}A) ground state structure of the neutral.

(b) Geometrical Parameters of the Lowest Energy Structures of Ti_3AgO_8 clusters

The lowest energy structure of neutral Ti_3AgO_8, 4-21-d (C_1: ^{2}A) is characterized by O - O bond length of 1.339 Å, a terminal Ti–O of 1.639 Å and a bridging Ag atom as shown in Figure 18. The most stable anionic cluster, 4-9-1-d (C_s: $^3A^{"}$) has three terminals Ti-O and a bridging Ag atom. Isomers 4-3-1-d (C_1: ^{3}A), 4-14-d (C_1:^{1}A), and 4-14-d (C_1: ^{3}A) of the anionic clusters are 0.21, 0.44, and 0.38 eV, respectively, higher in energy than

the 4-9-1-d (C_s: $^3A''$) lowest energy structure. The structures of the Ti_3AgO_8 clusters are displayed in Figure 90 and 91 (Appendix 3.2).

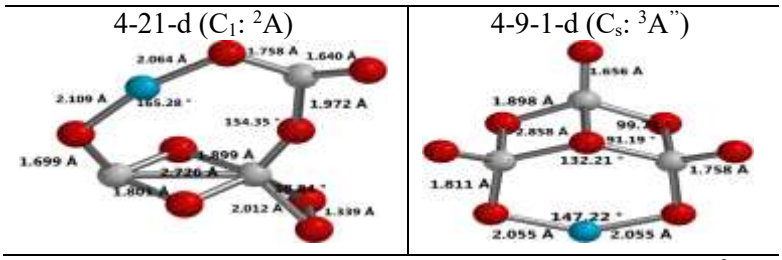

Figure 18: Geometrical parameters of neutral 4-21-d (C_1: ^2A) and anionic 4-9-1-d (C_s: $^3A''$)

It is noteworthy that structures that possess highly coordinated transition dopant metals and at least two terminal Ti-O bonds are high in energy and unfavorable [2, 9], e.g., structure 4-4-2-d, 4-5-2-d and 4-20-d.

(c) Vibrational Frequency of Lowest Energy Neutral and Anionic Ti_3AgO_8 clusters

Among the thirty vibration modes obtained for Ag doped 4-21-d (C_1: ^2A) cluster, only vibration at 59 cm^{-1} with intensity of 5.70 km/mol was assigned to the vibration of metal dopant atom as illustrated in Figure 19. The highest frequency was observed at 1101 cm^{-1} (ω30) as a result of asymmetric stretching of O - O atoms. In case of the anionic 4-9-1-d (C_s: $^3A''$) cluster, the highest vibration frequency occurs at 568 cm^{-1} and it is assigned to the bending vibration of the bridging O - O atoms. The three terminal Ti - O bonds vibrate simultaneously at 103.13 cm^{-1} with a very low intensity of 0.71 km/mol. Non-localized stretching of Ti - O bonds and Ag atom were observed at 82 cm^{-1}, with low intensity (7.61 km/mol).

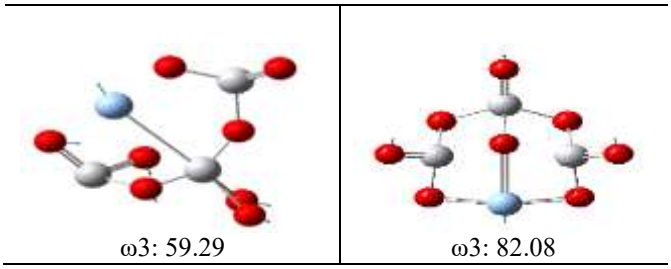

Figure 19: Displacement vector for vibration mode and frequencies (cm^{-1}) of neutral 4-21-d (C_1:^{2}A) and anionic 4-9-1-d (C_s: ^{3}A˝) clusters

(d) HL Gap of Lowest Lying Ti_3AgO_8 Clusters

Molecular orbitals of cluster 4-21-d (C_1:^{2}A) are spatially separated into α and β orbitals. The α-HOMO and α-LUMO were used to calculate the HL gap. The HL gap is 1.50 eV corresponding to half the band gap of rutile and lowest energy structure for Ti_2AgO_6, 3-8-d (C_1:^{2}A). For the anionic 4-9-1-d (C_s: ^{3}A˝), HL gap is 3.59 eV, that is 0.59 eV higher than band gap of rutile. Figure 20 shows FMO and corresponding HL gap for 4-21-d (C_1:^{2}A) and 4-9-1-d (C_s: ^{3}A˝).

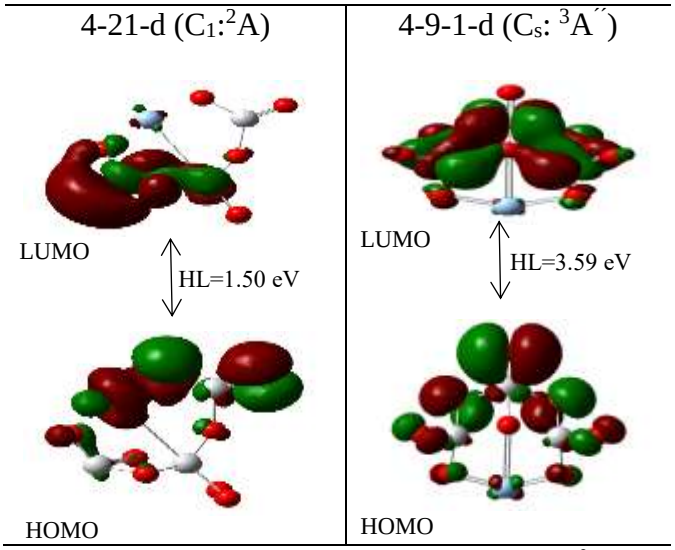

Figure 20: FMO of neutral Ag doped 4-21-d (C_1:^{2}A) and anionic 4-9-1-d (C_s: ^{3}A˝) clusters at BPW91/6-311+G (d) level

(e) Electron Detachment Energy and Electron Affinity of Ti_3AgO_8 Clusters

Calculated VEDE for cluster 4-9-1-d (C_s: $^3A''$) resulting in the $^2A'$ and $^4A'$ states, respectively, are 5.64 eV and 5.48 eV. Clusters 4-3-1-d (C_1: ^3A) and 4-14-d (C_1: ^1A , ^3A) are the only clusters within 0.5 eV of the 4-9-1-d (C_s: $^3A''$) ground state. Calculated VEDE for these clusters range from 5.26 - 5.44 eV, as shown in Table 65 (Appendix 3.2).

The lowest energy 4-21-d (C_1:^2A) neutral cluster and the lowest energy 4-9-1-d (C_s: $^3A''$) anionic clusters were used to calculate the electron affinity. Electron affinity of 4.56 eV was obtained for Ti_3AgO_8 by subtracting the energy of the two clusters.

(f) TD-DFT Calculations of Lowest Energy Neutral and Anionic Ti_3AgO_8 Clusters

A fatal error was encountered for the TD-BPW91 calculations of 4-21-d (C_1:^2A) for the Ti_3AgO_8 system. In case of the anionic cluster 4-9-1-d (C_s: $^3A''$), low excitation energy 8317 nm (0.15 eV) was obtained for the triplet-triplet excitation of one electron from HOMO to LUMO. The strong transition, with energy of 2533 nm (0.49 eV), occurred from HOMO to LUMO+1, Figure 21.

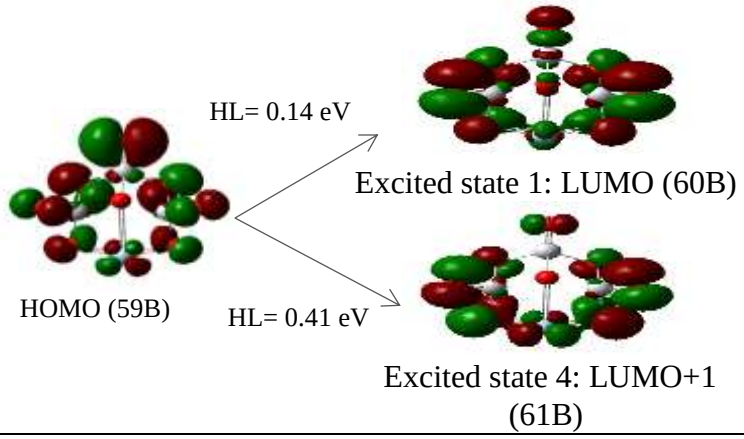

Figure 21: Singlet – singlet electronic transition in 4-9-1-d (C_s: $^3A''$)

(g) Interaction of Water with the 4-21-d Cluster

The Attachment of one water molecule close to 1Ti and 5Ti, resulted in the molecular adsorption of the water molecule to the 1Ti atom, with binding energy of -1.44 eV, as shown in Figure 22. The labelled structure in Figure 104 in Appendix 6 shows that 1Ti is three-fold coordinated atom (unsaturated), 5Ti is a four-fold coordinated atom (saturated), and 12Ag is two-fold coordinated atom (saturated). The fact that 1Ti is an unsaturated atom (tri-fold coordinated) without monovalent O atom, favored the molecular adsorption.

The initial attachment close to 9O resulted in H-bonding interaction, 1.04 eV higher in energy than molecular adsorption on 1Ti atom. The interactions of water molecule with cluster 4-21-d (C_1), is possible and it should be noted that a) water molecule prefers to interact with the tetracoordinated Ti atom (unsaturated) with no monovalent O atom and b) H-bonds are significantly weaker than the molecular adsorption mode.

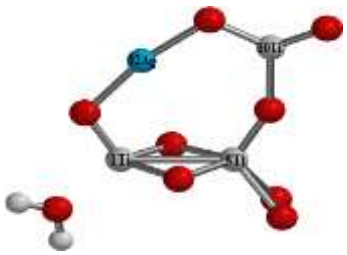

Figure 22: Molecular adsorption of one water molecule on 4-21-d through 1Ti atom

4.3.4 Geometry and Properties of Ag Doped $(TiO_2)_5$ Clusters, Ti_4AgO_{10}

(a) Relative Energy of Ti_4AgO_{10} Clusters

The Ti_4AgO_{10} is the largest system studied, due to the number of non-equivalent Ti sites to be doped. More than 40 structures were optimized successfully. Although the most stable undoped structure for Ti_4AgO_{10} is 5-1-u, structure 5-4-u is the one that gave rise to

most stable Ag doped structure, namely 5-4-1-d, for both neutral and anion clusters. This structure is depicted in Figure 23. The second low-lying cluster for neutral Ti_4AgO_{10} is 5-6-1-d (C_s: $^2A''$) which is 0.10 eV higher in energy than 5-4-1-d (C_1:^2A). The potential energy of anionic Ti_4AgO_{10} is congested, with about twenty structures found within 0.50 eV of the 5-4-1-d (C_1:^1A) ground state.

(b) Geometrical Parameters of the Lowest Energy Structures of Ti_4AgO_{10} Clusters

The lowest lying structures for neutral and anionic Ti_4AgO_{10} clusters are 5-4-1-d (C_1:^2A) and 5-4-1-d (C_1:^1A), respectively. Optimized geometric parameters of these structures are shown in Figure 23.

Structure 5-4-1-d (C_1:^2A) is characterized by a five-fold coordinated Ti atom, O-O bond length of 1.440 Å, and a terminal O-Ag bond length of 2.046 Å. Geometry parameters of neutral and anionic lowest lying energy of Ti_4AgO_{10} clusters differ by roughly ± 0.050 Å.

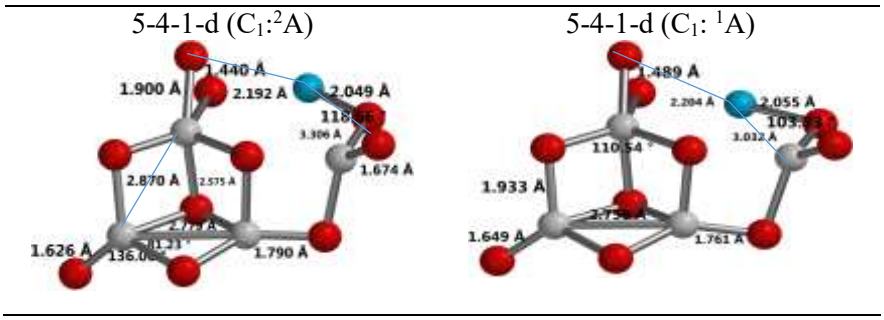

Figure 23: Geometrical parameters of 5-4-1-d (C_1:^2A) and 5-4-1-d (C_1: ^1A) cluster.

(c) Vibrational Frequency of Lowest Energy Neutral and Anionic Ti_5AgO_{10} Clusters

The number of vibrational modes calculated for ground state structure of doped $(TiO_2)_5$ is 39. Vibrations modes ω1 (40 cm^{-1}) and ω3 (70 cm^{-1}) are assigned to non-localized stretching of Ti - O bonds and Ag atom. The later occur at very frequency of 6 km/mol and is assigned to the asymmetric stretching (opposite direction) of Ag dopant atom and

undoped part of the cluster. Vibrational mode ω36, gives an intense peak of 1083 km/mol (803 cm^{-1}), that is assigned to asymmetric stretching of 11O and 2Ti atoms; and the degenerate bent of 13O - 3Ti - 8O atoms. Asymmetric stretching of 7O - 9O bond length of 1.49 Å and terminal 4Ti – 14O bond length of 1.62 Å, were observed at 888 cm^{-1} (162 km/mol) and 1023 cm^{-1} (307 km/mol), respectively, as shown in Figure 24. Labelled structure is in Figure 104 (Appendix 6).

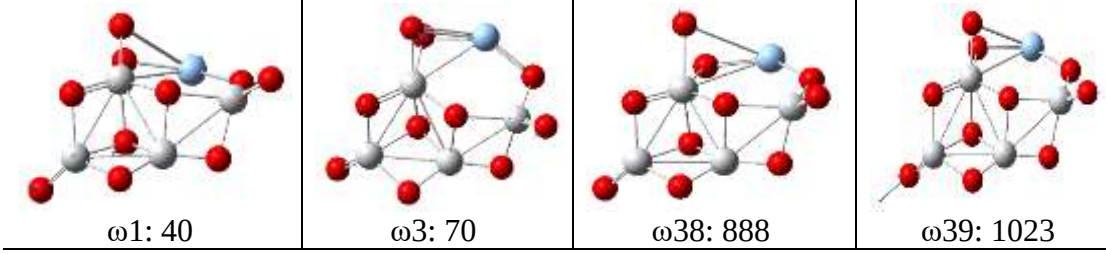

Figure 24: Displacement vector for vibration mode and frequencies (cm^{-1}) of neutral 5-4-1-d (C_1: ^2A) cluster

In case of the anion cluster, 5-4-1-d (C_1: ^1A), the two intense peaks in the spectrum are due to asymmetric stretching of one of bridging O atoms connected to terminal Ti atoms. Asymmetric stretching involving the two terminal Ti - O bonds are observed at 968 cm^{-1} (385 km/mol) and 986 cm^{-1} (311 km/mol). Vibrations modes ω2 (73 cm^{-1}) and ω3 (86 cm^{-1}) are assigned to non-localized stretching of Ti - O bonds and Ag atom.

(d) HL Gap of Lowest Lying Ti_4AgO_{10} Clusters

The HL gap of 5-4-1-d (C_1:^2A) lowest energy structure of neutral Ti_4AgO_{10} clusters, is 2.83 eV. The latter is approximately 0.05 eV lower than the HL gap of neutral 5-1-u (C_s: $^1A'$) lowest energy structure of the undoped cluster. HOMO is bonding and characterized by the overlap of orbitals in Ag, bridging O, tetracoordinated Ti and monovalent O atoms.

LUMO is characterized by overlap of atomic orbital of rhombus Ti_2O_2 with adjacent atoms. It receives no contributions from Ag dopant atom.

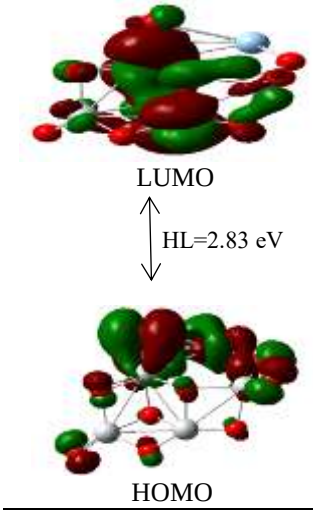

Figure 25: FMO of 5-4-1-d (C_1: ^{2}A) at BPW91/6-311+G (d) level

(e) Electron Detachment Energy and Electron Affinity of Ti_4AgO_{10} cluster

The 5-4-1-d (C_1:^{2}A) state of the neutral is obtained when one electron is detached from molecular orbital 74 (a) of the anion 5-4-1-d (C_1:^{1}A) ground state. The computed VEDE ($^1A \rightarrow {}^2A$) and AEDE ($^1A \rightarrow {}^2A$ and $^3A \rightarrow {}^4A$) are to 5.16, 4.83 and 5.02 eV, respectively, as shown in Table 80 - 82 in Appendix 4.2. The vertical electron detachment of 5-1-2-d (C_1: ^{3}A), 5-18-d (C_1: ^{3}A), 5-19-d (C_1: ^{3}A), and 5-21-d (C_1: ^{3}A) from the triplet state of the anion to the ground and first excited state of neutral, i.e.: doublet and quartet state, are in the range of 5.53 - 5.87 eV. These clusters have very similar geometries.

Electron affinity of 4.83 eV which also corresponds to the AEDE was calculated by subtracting the energy of 5-4-1-d (C_1:^{1}A) from the energy of neutral 5-4-1-d (C_1:^{2}A) cluster. Calculated EA is 4.83 eV.

(f) TD-DFT Calculations of Lowest Energy Neutral and Anionic Ti_4AgO_{10}

Maximum absorption for the 5-4-1-d (C_1:^{2}A) cluster is due to doublet-doublet transition from β-HOMO (73) to β-LUMO (74), with excitation energy of 1566 nm (0.79 eV). In case of the anion, lowest excitation energy 613 nm (2.02 eV) was obtained when an electron was excited from HOMO (74) to LUMO (75). The first ten excitation states for singlet-singlet and singlet-triplet of 5-4-1-d (C_1:^{1}A) cluster, occurred in the visible region (419 – 613 nm), but with very low intensity (0.0001 - 0.0032). The presence of Ag metal in 5-4-1-d (C_1:^{1}A) results in a hypsochromic shift, as shown in Figure 25.

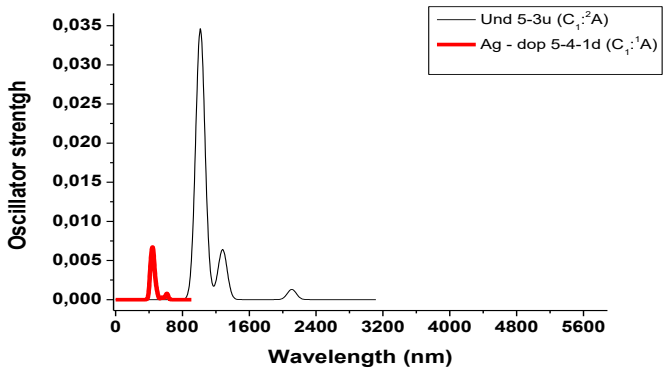

Figure 26: UV-Vis spectrum for anionic undoped 5-3-u (C_1:^{2}A) and Ag doped 5-4-1-d (C_1: ^{1}A) clusters

(g) Interaction of Water with the 5-4-1-d Cluster

Initially one water molecule was attached close to 4Ti atom, at a distance of 2.00 Å, Figure 27. After geometry optimization at BPW91/6-311+G (d) level, the water molecule was molecularly absorbed on 3Ti atom at a distance of 2.13 Å. That interaction gives the lowest energy for the water complex, [(Ti_4AgO_{10})(H_2O)].

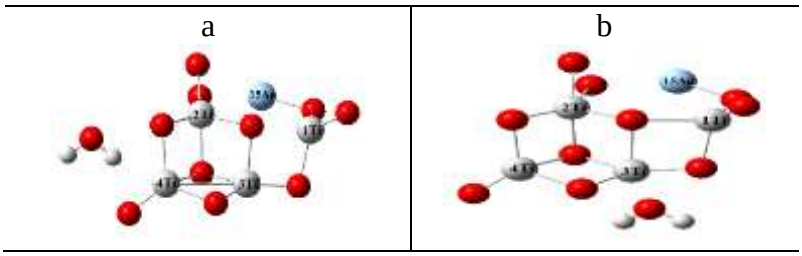

Figure 27: The 5-4-1-d water-complex: a) initial attachment and b) molecular adsorption of one water molecule in 5-4-1-d cluster through 4Ti atom.

Attachment of one water molecule to 3Ti and 6O atoms in structure 5-4-1-d (C_1) resulted in H-bonding with 6O atom, as shown in Figure 105 (Appendix 6.1). Although the two interactions occurred at the same atom, they have different orientation in space. A different H-bonding with 9O atom results from the attachment of one water molecule with one water molecule close to 15Ag.

4.3.5 Geometry and Properties of Ag doped $(TiO_2)_6$ Clusters, Ti_5AgO_{12}

(a) Relative Energy of Ti_5AgO_{12} Clusters

For the Ti_4AgO_{10} clusters, the computed lowest - energy structure is 6-1-2-d (C_1) for both neutral and negatively charged clusters. The second low-lying cluster for neutral Ti_5AgO_{12} is 6-1-1-d (C_1: ^{2}A) which is 1.57 eV higher in energy than 6-1-2-d (C_1:^{2}A). In case of the anionic cluster, the second low-lying cluster is 6-2-1-d (C_1: ^{1}A) which is 0.93 eV higher than 6-1-1-d (C_1: ^{1}A). The relative energy of the low-lying neutral clusters range from 1.57 eV to 4.19 eV, while for the anionic clusters, it ranges from 0.93 eV to 3.86 eV, as listed in Tables 90 and 91 (Appendix 5.2).

(b) Geometrical Parameters of the Lowest Energy Structures of Ti_5AgO_{12} Clusters

The lowest lying neutral Ti_5AgO_{12}, 6-1-2-d (C_1: ^2A), has four four-fold coordinated Ti atoms, a five-fold coordinated Ti atoms, a four-fold coordinated O atom, and O – O bond length of 1.332 Å. The lowest lying anionic Ti_5AgO_{12}, 6-1-2-d (C_1: ^1A), is characterized by five four-fold coordinated Ti atoms, a five-fold coordinated Ti atom a three-fold coordinated O atom, and O – O bond length of 1.478 Å, as shown in Figure 28. There is a weak interaction between the dopant atom and the O atoms due to large interatomic distances. The bond length between neutral and anionic lowest lying energy Ti_5AgO_{12} clusters differs by ±0.14Å.

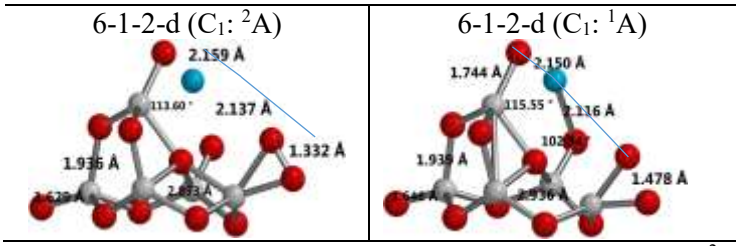

Figure 28: Geometrical parameters for neutral 6-1-2-d (C_1: ^2A) and anion 6-1-2-d (C_1: ^1A)

(c) Vibrational Frequency of Lowest Energy Neutral and Anionic Ti_5AgO_{12} Clusters

Cluster 6-1-2-d (C_1:^2A) presents a more congested IR spectrum. A weak vibration of Ag atom and bending (rock) of O - O atoms occur with low frequency of 45 cm^{-1}. The highest peaks at 876 cm^{-1} with intensity 761 km/mol, are assigned to the vibrations of bridging O atoms and terminal Ti - O atoms.

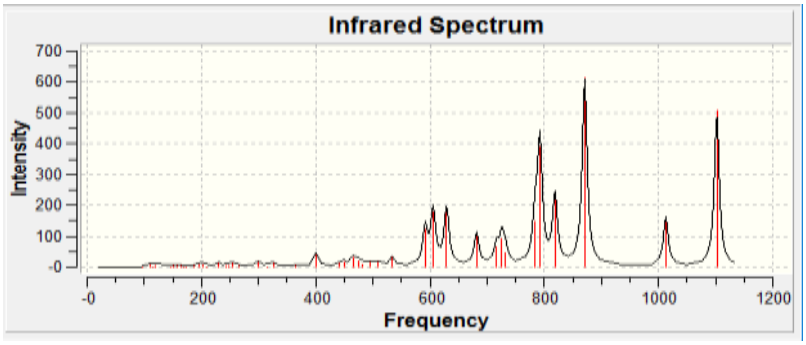

Figure 29: IR Spectrum for 6-1-2-d (C_1:^{2}A) at BPW91/6-311+G (d)

In case of 6-1-2-d (C_1:^{1}A) cluster, vibrations mode ω1 is attributed to rocking of O - O atoms and stretching of Ag dopant atom, while vibration mode ω3 is attributed to bent of O and Ag atoms, as shown in Figure 30. The vibration modes ω26 and ω27 are attributed to the vibration of the four-fold coordinated O atom and two terminal Ti-O moiety. These vibrations occurred around 394 cm^{-1} (4km/mol)) and 380 cm^{-1} (20 km/mol), respectively.

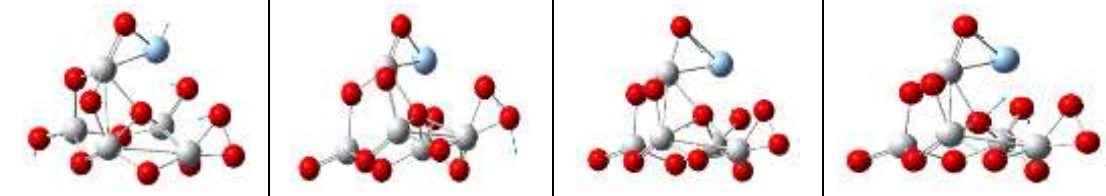

Figure 30: Displacement vector for vibration mode and frequencies (cm^{-1}) of neutral 6-1-2-d (C_1: ^{1}A) cluster

(d) HL Gap of Lowest Lying Ti_5AgO_{12} Cluster

Neutral 6-1-2-d (C_1:^{2}A) hold a doublet state (open shell) with two separate sets of singly occupied orbitals (α and β). The α-HOMO/LUMO where used to calculate HL gap, displayed in Figure 31. The HL gap for neutral Ti_5AgO_{12} cluster, 6-1-2-d (C_1:^{2}A) is 0.23 eV lower than band gap of rutile. Major contribution to HOMO of 6-1-2-d (C_1: ^{2}A), comes from bonding of terminal Ti (D) and O (Pz), and Ag (D) orbitals. The Ti atom from which

the O - O moiety is attached gives a higher contribution to the LUMO through the D orbital. HOMO of anionic Ti_5AgO_{12} ground state is characterized by the overlap of bridging O, Ti and the O - O orbitals, while LUMO is distributed throughout the entire cluster. HL gap of 6-1-2-d (C_1:^{1}A) is 2.12 eV, as observed in Figure 31.

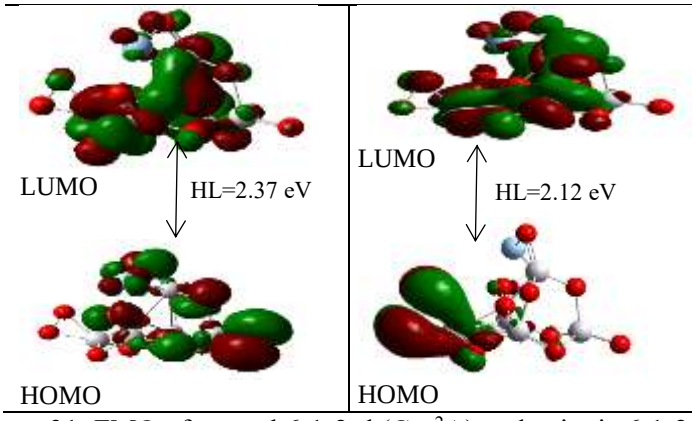

Figure 31: FMO of neutral 6-1-2-d (C_1: ^{2}A) and anionic 6-1-2-d (C_1: ^{1}A) at BPW91/6-311+G (d) level

(e) Electron Detachment Energy and Electron Affinity of Ti_5AgO_{12} clusters

Electron detachment from the HOMO (88) of the anionic cluster 6-1-2-d (C_1: ^{1}A) yields neutral 6-1-2-d (C_1: ^{2}A) cluster with VEDE of 5.27 eV. The nearest anionic cluster, 6-1-1-d (C_1: ^{3}A), is 0.94 eV energetically above the lowest lying energy 6-1-2-d (C_1: ^{1}A) cluster, as shown in Table 90 of Appendix 5.2. This restricted the VEDE calculation, only to 6-1-2-d (C_1: ^{1}A) cluster.

The AEDE (^{1}A→^{2}A) and (^{3}A →^{4}A) for lowest lying energy 6-1-2-d (C_1) cluster are 4.74 and 5.42 eV, respectively. The AEDE for Ti_5AgO_{12} ranges from 4.10 eV to 6.06 eV. A complete AEDE results for Ti_5AgO_{12} clusters are found in Table 93 of Appendix 5.2.

The EA of Ti_5AgO_{12} clusters was calculated by subtracting the energy of anionic lowest lying cluster, 6-1-2-d (C_1: ^1A), from the neutral lowest lying energy cluster, 6-1-2-d (C_1: ^2A), of Ti_5AgO_{12}. The computed EA for 6-1-2-d cluster is 4.74 eV.

(f) TD–DFT Calculations of Lowest Energy Neutral and Anionic Ti_5AgO_{12} Cluster

Doublet-Doublet excitation of 6-1-2-d (C_1:^2A) occurred at very low energy and far from visible region. Excitation energy range from 0.31 eV (3954 nm) to 0.64 eV (1933 nm). The former correspond to the lowest doublet-doublet excitations of 6-1-2-d (C_1:^2A), that cluster occurred from HOMO to LUMO with oscillator strength (f) of 0.0004.

The five (5) lowest singlet-singlet excitations for Ag doped 6-1-2-d (C_1:^1A) cluster occurred in the visible region from 454 – 560 nm. The excitation from the HOMO (88) to LUMO (89), Figure 32, gives rise to an intense peak at 560 nm (2.21 eV), for singlet-singlet transition. HOMO is classified as an antibonding molecular orbital while LUMO is characterized by bonding orbital between D and P orbitals of Ag and O - O atoms, respectively.

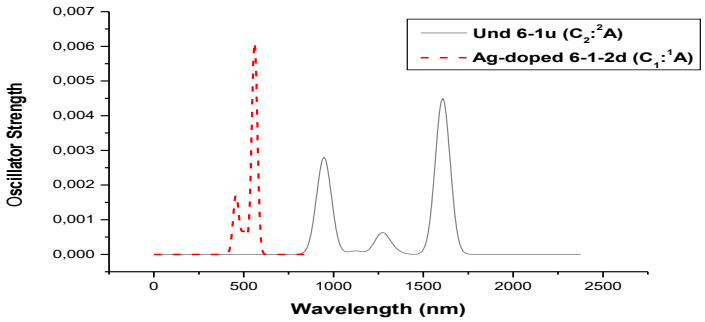

Figure 32: UV-Vis spectrum for anionic undoped 6-1-u (C_1:^1A) and Ag doped 6-1-2-d (C_1:^1A) clusters

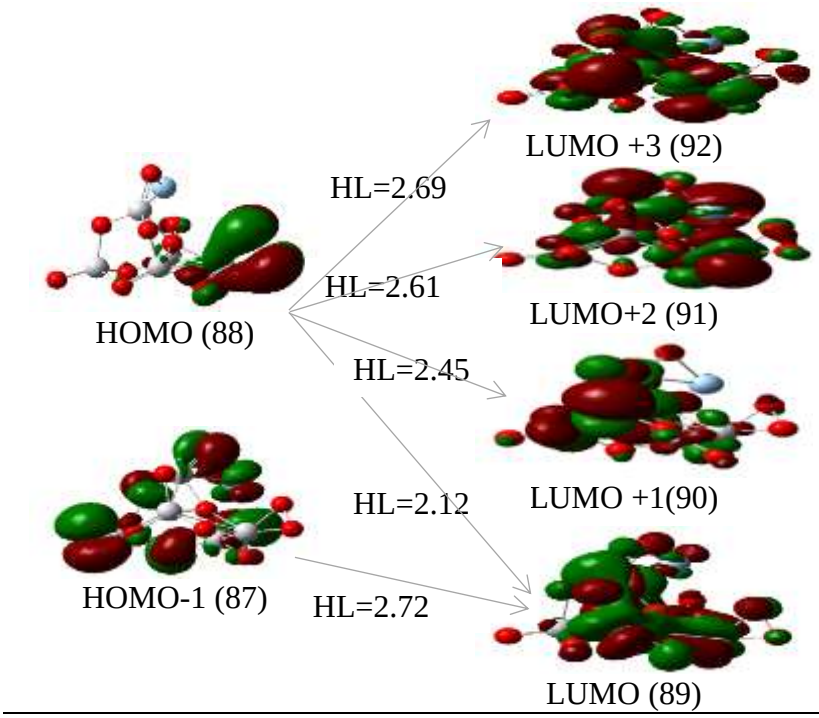

Figure 33: Singlet – singlet transition in 6-1-2-d (C_1:^{1}A) cluster

(g) Interaction of Water with the 6-1-2-d Cluster

The attachment of one water molecule close to 1Ti, 3Ti and 5Ti atoms, as shown in Figure 106 of Appendix 6.1, resulted in molecular adsorption on respective Ti atoms. Calculated E_b of these water-complexes of Ti_5AgO_{12} are -0.91 eV, -1.35 eV, and -0.38 eV, respectively, at BPW91/6-311+G (d).

The lowest energy product for the water interaction is obtained by the attachment of one water molecule to 6-1-2-d (C_1:^{2}A) close to atom 4Ti. The water molecule was molecularly absorbed on 4Ti atom, at a distance of 2.13 Å and E_b of -1.40 eV.

Attachment close to dopant atom 18Ag lead to the dissociation of the water molecule, as shown in Figure 106 of Appendix 6.1, where the H atom is interacting with 10O atom and OH interacts with 18Ag atom.

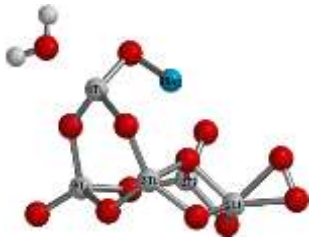

Figure 34: Molecular adsorption on cluster
6-1-2-d trough 4Ti atom

4.4 GEOMETRY AND PROPERTIES OF Au DOPED $(TiO_2)_n$ CLUSTERS

Starting from optimized Ag doped ($Ti_{n-1}AgO_{2n}$) clusters, the Ag atom was replaced by Au atom, and re-optimized. After geometry optimization, if the geometry is preserved, the Au doped $Ti_{n-1}AuO_{2n}$ clusters received the same name as corresponding Ag doped $Ti_{n-1}AgO_{2n}$ clusters, if not a new name is attributed to the new cluster. The doublet and quartet states were optimized for the neutral $Ti_{n-1}AuO_{2n}$ clusters, while for the anionic $Ti_{n-1}AuO_{2n}$ clusters, the singlet and triplet states were optimized.

4.4.1 Geometry and Properties of Au Doped $(TiO_2)_2$ Clusters, $TiAuO_4$

(a) Relative Energy of $TiAuO_4$ clusters

The 2-11-d clusters in Figure 35 was identified as the lowest lying energy structure for neutral and anionic forms of $TiAuO_4$ clusters at the BPW91/6-311+G (d) level. The two neutral clusters 2-11-d (C_1: ^2A) and 2-11-d (C_s: $^2A''$) are isoelectric, but more symmetrical C_s structure was consider as the lowest lying energy $TiAuO_4$ cluster. Relative energy of the neutral $TiAuO_4$ clusters with respect to the ground state structure ranges from 0.12 eV to 4.07 eV as listed in Tables 41 - 42 (Appendix 1.3). Structure 2-4-1-B-d (C_{2v}: $^2B_2$) which is the lowest lying neutral cluster for $TiAgO_4$, is 0.92 eV higher than 2-11-d (C_s: $^2A''$) of

$TiAuO_4$. Structure 2-13-d (C_1: ^2A) at BPW91 and CCSD (T) // BPW91 level is 0.12 eV and 0.14 eV, respectively, higher in energy than 2-11-d (C_s: $^2A''$) as shown in Table 15.

Table 15: Relative energy (eV) of lowest neutral and anionic $TiAuO_4$ clusters

		$TiAuO_4$			$TiAuO_4^-$		
Structure	PG	State	ΔE^a	ΔE^b	State	ΔE^a	ΔE^b
2-1-1-d	C_s	$^2A'$	0.93		$^1A'$	0.09	0.02
2-4-1-B-d	C_{2v}	$^2B_1$	0.92		$^1A_1$	0.28	0.07
2-11-d	C_1	^2A	0.00	0.00	^1A	0.00	0.20
2-11-d	C_1				^3A	0.34	0.26
2-11-d	C_s	$^2A''$	0.00	0.00			
2-13-d	C_1	^2A	0.12	0.14	^1A	0.13	
2-13-d	C_1				^3A	0.20	0.18
2-13-d	C_s				$^1A'$	0.12	0.00

[a] BPW91/6-311+G (d) and [b] CCSD (T) //BPW91/6-311+G (d)

From the results in Table 15, using the BPW91 functional, the potential energy surface of the anion appears to be flat with about five states competing for the ground electronic state. However, BPW91 seems to suggest 2-11-d (C_1: ^1A) as the ground state. The situation does not improve much at the CCSD (T) level with five states within 0.26 eV of each other. This highly correlated method, however, predicts a 2-13-d (C_s: $^1A'$) ground state with 2-1-1-d (C_s: $^1A'$) and 2-11-d (C_s: ^2A) just 0.02 eV and 0.07 eV, respectively above. It is reasonable to conclude that 2-1-1-d (C_s: $^1A'$), 2-11-d (C_s: ^2A) and 2-13-d (C_s: $^1A'$) states are nearly degenerate at the CCSD (T)//BPW91 level and any of these states could be the ground electronic state of $TiAuO_4$ if a larger basis set is used.

(b) Geometrical Parameters of the Lowest Energy Structures of $TiAuO_4$ Clusters

As discussed in the section 4.4.1 (a), the lowest energy neutral and anionic structures of $TiAuO_4$ is 2-11-d. This structure has a terminal O-Au bond length of 2.0 Å, a terminal Ti–O bond length of 1.676 Å and O – O bond length of 1.454 Å. Structure 2-13-d also

presented in Figure 35 has the same connectivity as structure 2-11-d, but the O - Au bond points in opposite direction. The geometrical parameters of anionic 2-11-d (C_1: ^1A) and 2-13-d (C_s: $^1A'$) are shown in Table 16.

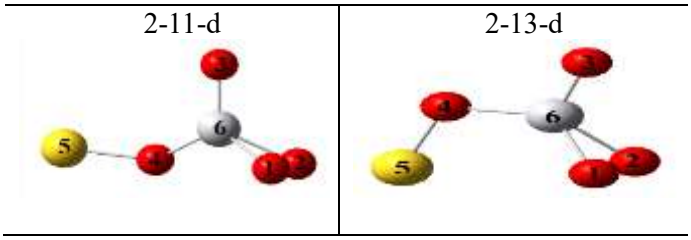

Figure 35: Geometry of doped 2-11-d and 2-13-d clusters at BPW91

Table 16: Geometrical parameters for anionic 2-11-d (C_1: ^1A) and 2-13-d (C_s: $^1A'$) obtained from the BPW91 functional. Bond length R [in (Å)] and bond angle Θ [in degrees].

	R(12)	R(16)	R(63)	R(64)	R(45)	Θ (162)	Θ (546)
2-11-d (C_1: ^1A)	1.454	1.918	1.676	1.851	2	44.5	137.6
2-13-d (C_s: $^1A'$)	1.509	1.881	1.682	1.930	1.978	47.3	111.3

(c) Vibrational Frequency of Lowest Energy Neutral and Anionic $TiAuO_4$ Clusters

Vibrational modes of neutral and anionic 2-11-d of $TiAuO_4$ clusters are listed in Table 17. These ω1 – ω7 vibrations are attributed mainly to asymmetric stretching of Ti and O atoms. None of the vibrations involve the Au dopant atom for both the neutral and anionic 2-11-d clusters.

Table 17: Vibrational modes and frequencies for neutral 2-11-d (C_1:^{2}A), anionic 2-11-d (C_1:^{1}A) and 2-13-d (C_s: ^{1}A´) clusters. Frequency (cm^{-1}) and IR intensity (km/mol) were calculated at BPW91 level.

Modes	2-11-d (C_1:^{2}A)	2-11-d (C_1:^{1}A)	2-13-d (C_s: ^{1}A´)
	Frequencies	Frequencies	Frequencies
ω12	1127	911	889
ω11	990	877	817
ω10	779	659	625
ω9	506	560	593
ω8	481	516	562
ω7	387	379	471
ω6	230	251	231
ω5	200	208	202
ω4	165	194	147
ω3	119	127	129
ω2	62	79	57
ω1	30	50	15

The ω10 (779 cm^{-1}) mode of neutral 2-11-d (C_1: ^{2}A) represent the asymmetric stretching of 4O - 6Ti while the ω11 (990 cm^{-1}) mode is due to symmetric stretching of terminal 3O - 6Ti. Labelled 2-11-d cluster is found in Figure 104 of Appendix 6.

In the case of anionic 2-11-d (C_1:^{1}A), mode ω11 is assigned to the bend of Ti and asymmetric stretching of O - O bonds at 877 cm^{-1} (426 km/mol) while vibration mode ω12 is assigned to symmetric stretching between Ti - O atoms at 911 cm^{-1} (240 km/mol). Vibrations modes ω10-11 of anionic 2-13-d (C_s: ^{1}A´) occur approximately at same frequency as 2-11-d (C_1:^{1}A). The high intense vibration mode ω10 (150 km/mol) is attributed to the vibration of bridging O atom and bend of Ti atom with O - O moiety, as shown in Figure 36. Vibration mode ω12 (889 km/mol) is assigned to asymmetric stretching between Ti-O atoms.

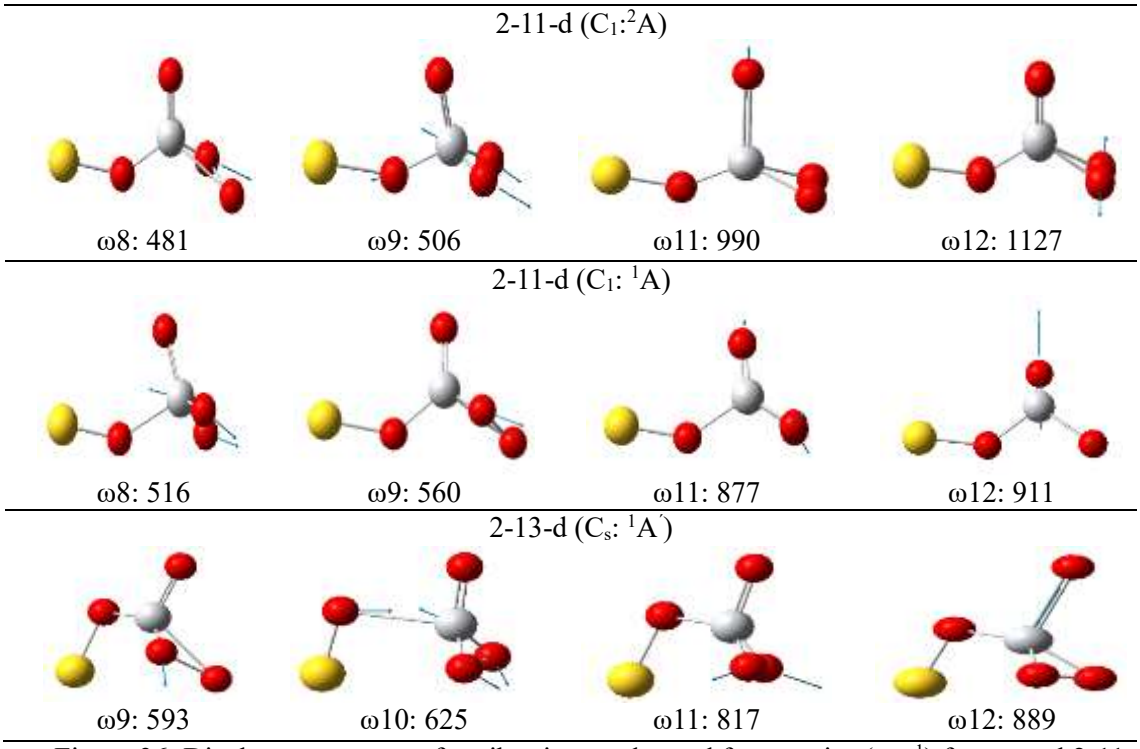

Figure 36: Displacement vector for vibration modes and frequencies (cm^{-1}) for neutral 2-11-d (C_1:^{2}A), anionic 2-11-d (C_1: ^{1}A) and 2-13-d (C_s: ^{1}A´) clusters.

(d) HL Gap of Lowest Lying $TiAuO_4$ Clusters

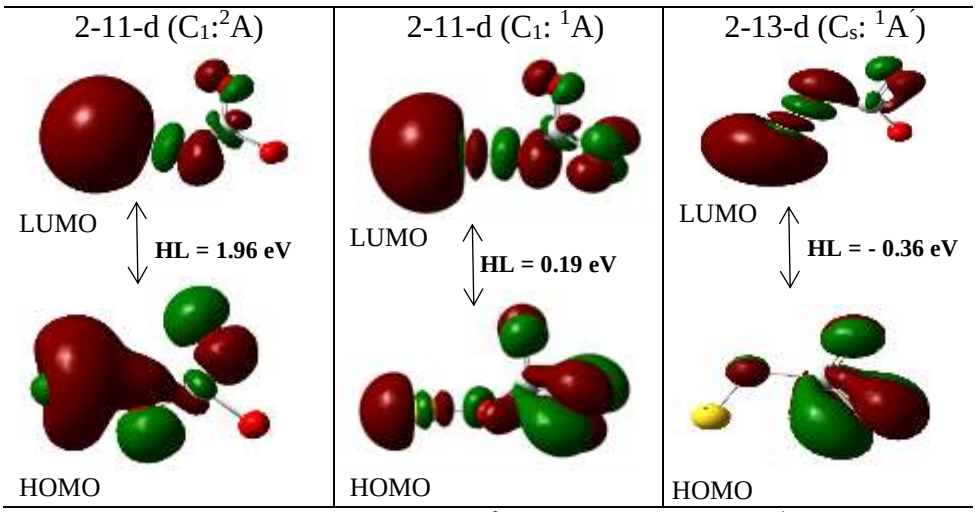

Figure 37: The FMO of neutral 2-11-d (C_1:^{2}A), anionic 2-11-d (C_1: ^{1}A) and 2-13-d (C_s: ^{1}A´) clusters at BPW91/6-311+G (d) level

The HL gap of neutral and anionic 2-11-d cluster are 1.96 eV and 0.19 eV, respectively,

as shown in Figure 37. The α-HOMO and α-LUMO were used to calculated HL gap for neutral 2-11-d (C_1:^{2}A), while αβ-HOMO and αβ-LUMO were used for anionic 2-11-d (C_1:^{1}A) cluster. In case of neutral 2-11-d (C_1:^{2}A) the HOMO is bonding with contributions from atomic orbitals on Au, bridging O and Ti atoms. The LUMO of neutral 2-11-d (C_1:^{2}A) is very similar to the anionic 2-11-d (C_1:^{1}A), except that it receives no contribution from the O-O moiety. A negative HL gap of -0.36 eV was obtained for 2-13-d (C_s: ^{1}A$'$) cluster at BPW91 functional, as shown in Figure 37. The situation changes when B3LYP functional is used and as result HL of 1.24 eV is obtained.

(e) Electron Detachment Energy and Electron Affinity of $TiAuO_4$ Clusters

The removal of the loosely electron from the singlet of 2-11-d (C_1: ^{1}A) yields a 2-11-d (C_1: ^{2}A) doublet state, with AEDE and VEDE of 2.99 eV and 3.40 eV, respectively. The calculated AEDE and VEDE at CCSD (T) //BPW91 for 2-11-d (C_1: ^{1}A) are 2.39 eV and 2.85 eV respectively, as shown in Tables 44 - 45 in Appendix 1.3. In case of anionic 2-13-d ($^1A' \rightarrow {}^2A''$) ground state calculated VEDE at BPW91 and CCSD (T)//BPW91 level are 3.66 eV and 3.71 eV respectively, as shown in tables 45 and 47 in Appendix 1.3.

The electron affinity (EA) was calculated by subtracting the energy of anion 2-11-d (C_1: ^{1}A) from neutral 2-11-d (C_1: ^{2}A) at BPW91/6-311+ G (d) level. The calculated EA for $TiAuO_4$ clusters is 2.99 eV.

(f) TD-DFT Calculations of Lowest Energy Neutral and Anionic $TiAuO_4$ Clusters

Maximum absorption for the neutral undoped 2-1-u (C_1:^{2}A) cluster is due to single-singlet transition from -HOMO-1 to LUMO, with excitation energy of 3.50 eV (355 nm). In case of neutral doped 2-11-d (C_1: ^{1}A) the unique allowed doublet-doublet excitation occurred at IR region (966 nm) but with low excitation energy of 1.28 eV and oscillator strength

of 0.0009 as shown in Figure 38.

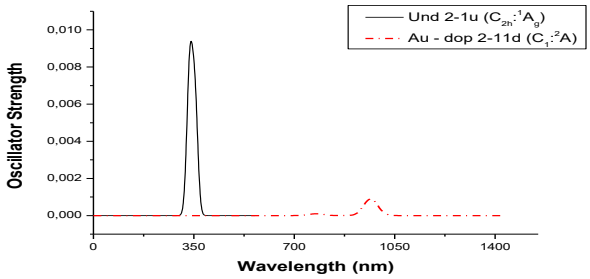

Figure 38: UV-Vis spectrum for neutral undoped 2-1-u (C_{2h}:^1A_g) and doped 2-11-d (C_1:^2A)

The doublet-doublet transition of anionic undoped 2-1-u (C_{2h}: ^2A_g) cluster, occurs from the HOMO to LUMO+4, whereas the singlet-singlet transition of anionic doped 2-11-d (C_1:^1A) cluster correspond to the transition between HOMO-2 to LUMO. The later give rise to the most intense peak at 662 nm in the 2-11-d (C_1:^1A) cluster. The low excitation of 0.67 eV (1842 nm) for doped 2-11-d (C_1:^1A) cluster is due to the singlet-singlet excitation from HOMO to LUMO.

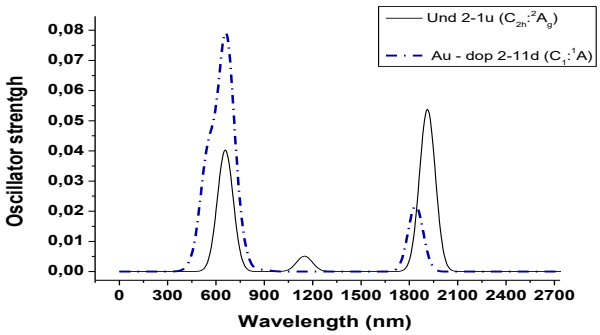

Figure 39: UV-Vis spectrum for anionic undoped 2-1-u (C_{2h}:^2A_g) and doped 2-11-d (C_1:^1A) clusters

The transitions of the anionic undoped 2-1-u (C_{2h}: ^2A_g) cluster, coincides with transitions of the doped 2-11-d (C_1:^1A) cluster in region around of 600 nm and 1950 nm, as shown in Figure 39.

(g) Interaction of Water with the 2-11-d Cluster

Molecular adsorption is the result of the attachment of one water molecule to 5Au atom at a distance of 2.0 Å. This is the only case where the attachment of water near to the dopant atom resulted in molecular adsorption instead of dissociative adsorption. Interatomic distance between Au dopant atom and O atom after geometry optimization is 2.16 Å. The attachment of H_2O to 6Ti resulted in molecular adsorption too. Calculated E_b for the attachment of H_2O to 5Au and 6Ti are -1.26 and -1.04 eV, respectively.

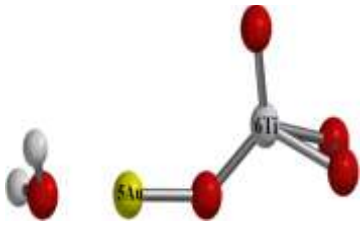

Figure 40: Molecular adsorption on 2-11-d through 5Au atom

4.4.2 Geometry and Properties of Au Doped $(TiO_2)_3$ Clusters, Ti_2AuO_6

(a) Relative Energy of Ti_2AuO_6 Clusters

Thirteen neutral and eleven anionic clusters were geometry optimized successfully for Ti_2AgO_6. The five low-lying energy structures of neutral Ti_2AgO_6 clusters are 3-8-d (C_s: $^2A''$), 3-11-A-d (C_1: ^2A), 3-2-1-d (C_s: $^2A''$), 3-10-d (C_s: $^2A''$) and 3-9-d (C_s: $^2A''$). These structures are 0.40 eV, 0.69 eV, 1.04 eV and 1.11 eV higher in energy than the ground state structure of neutral Ti_2AgO_6, structure 3-8-d (C_s: $^2A''$), respectively, as shown in Table 18.

Structure 3-1-1-d (C_{2v}: $^3B_2$) is the lowest lying anionic Ti_2AgO_6 clusters. The relative energy for the anionic clusters range from 0.19 – 2.96 eV. The triplet of structure 3-1-2-

d and the singlet of structure 3-6-1-d optimized to structure 3-10-d (C_s). Structure 3-10-d (C_s: $^1A'$) and 3-10-d (C_s: $^3A''$) are 0.98 eV and 0.19 eV higher in energy than the 3-1-1-d (C_{2v}: $^3B_2$) lowest energy cluster. The total energy and relative energy of neutral and anionic Ti_2AuO_6 clusters are shown in Table 55 and 56 (Appendix 2.3).

Table 18: Relative energy (eV) of neutral and anionic Ti_2AuO_6 clusters

Structure	PG	Ti_2AuO_6		$Ti_2AuO_6^-$	
		State	ΔE	State	ΔE
3-1-1-d	C_{2v}	$^2B_1$	1.14	$^1A_1$	0.20
3-1-1-d	C_{2v}			$^3B_2$	*0.00*
3-2-1-d	C_s	$^2A''$	0.69	$^1A'$	0.60
3-8-d	C_1	^2A	0.44	^1A	0.76
3-8-d	C_s	$^2A''$	*0.00*		
3-9-d	C_s			$^3A''$	0.88
3-10-d	C_s	$^2A''$	1.04	$^1A'$	0.98
3-10-d	C_s			$^3A''$	0.19
3-11-d	C_1	^2A	0.40	^1A	0.33

(b) Geometrical Parameters of the Lowest Energy Structures of Ti_2AuO_6 Clusters

The arrangement of atoms in ground state neutral and anionic Ti_2AuO_6 clusters are similar to those computed for corresponding Ti_2AgO_6 clusters, that is 3-8-d for the neutral species and 3-1-1-d for the anionic clusters. Geometric parameters of the lowest energy structure of Ti_2AuO_6 neutral and anionic clusters are shown in Figure 41.

3-8-d (C_s: $^2A''$) 3-1-1-d (C_{2v}: $^3B_2$)

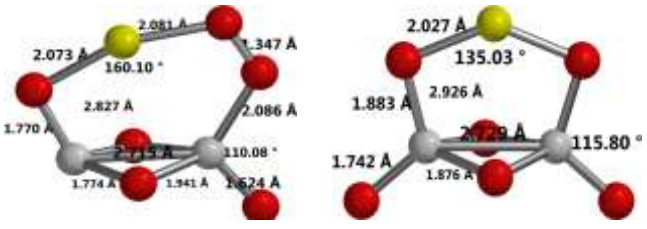

Figure 41: Geometric parameters for neutral 3-8-d (C_s: $^2A''$) and anionic 3-1-1-d (C_{2v}: $^3B_2$)

Neutral 3-1-1-d (C_s: $^4A''$), 3-2-2-d (C_{2h}: ^4A_g) and 3-10-d (C_s: $^4A''$) clusters are transition states (Nimag = 1). Structure 3-2-2-d (C_{2h}: ^4A_g), possesses a four-fold coordinated Au atom and terminal Ti–O bond length of 1.671 Å, whereas 3-10-d (C_s: $^4A''$) have two terminal Ti-O bonds, and loose O - Au - O bond. The 3-2-2-d and 3-10-d clusters are shown in Figure 88 in Appendix 2.3.

(c) Vibrational Frequency of Lowest Energy Neutral and Anionic Ti_2AuO_6 Clusters

The vibrational modes of lowest Energy neutral 3-8-d (C_s: $^2A''$) and anionic 3-1-1-d (C_{2v}:$^3B_2$) at the BPW91 level are listed below in Table 19.

Table 19: Vibrational modes and frequencies for lowest energy neutral and anionic Ti_2AuO_6 clusters. Frequency (cm^{-1}) and IR intensity (km/mol) were calculated at the BPW91 level.

3-8-d (C_s:$^2A''$)			3-1-1-d (C_{2v}:$^3B_2$)		
Modes	Frequencies	IR intensity	Modes	Frequencies	IR intensity
ω21	1038	118	ω21	717	2
ω20	1020	264	ω20	686	14
ω19	797	44	ω19	653	80
ω18	740	207	ω18	567	45
ω17	719	153	ω17	562	27
ω16	588	175	ω16	561	84
ω15	518	7	ω15	464	9
ω14	457	68	ω14	462	0
ω13	425	10	ω13	419	0
ω12	411	1	ω12	395	8
ω11	341	5	ω11	371	1
ω10	305	27	ω10	299	1
ω9	264	0	ω9	232	2
ω8	231	1	ω8	219	0
ω7	214	1	ω7	188	10
ω6	172	4	ω6	165	32
ω5	171	17	ω5	149	1
ω4	124	1	ω4	138	3
ω3	116	4	ω3	118	3
ω2	98	6	ω2	87	0
ω1	93	0	ω1	79	0

The stretching modes for three Ti - O - Ti bridges tetrahedrally coordinated to a terminal Ti-O moiety form a broad peak in the IR spectrum. It is noteworthy that the vibrations of Au doped $(TiO_2)_3$ are similar to Ag doped $(TiO_2)_3$ clusters, differing roughly by ± 10 cm^{-1}.

Two intense peak in neutral 3-8-d (C_s: $^2A''$) cluster due to the ω20 (264 km/mol) and ω18 (207 km/mol) modes are assigned to asymmetric stretching of terminal Ti - O bond and symmetric stretching of Ti - O bond adjacent to Au dopant atom, respectively. In case of 3-1-1-d (C_{2v}: $^3B_2$) of the anion, a broad peak is observed in the 561-567 cm^{-1} region due to overlap of the ω16-18 modes. These vibrations are assigned to rocking of O - Au - O and stretching of O atoms.

(d) HL Gap of the Lowest Lying Ti_2AuO_6 Clusters

The HL gap of lowest lying neutral Ti_2AuO_6 cluster, 3-8-d (C_s: $^2A''$), is 2.42 eV. The HOMO is characterized by an antibonding orbital involving the O - O moiety and overlap of Au (p) with adjacent O (p) orbitals, as shown in Figure 42.

Anionic Ti_2AuO_6 has 3-1-1-d (C_{2v}: $^3B_2$) ground state structure. The major contributions to its HOMO comes from Au (D orbital) and O (D and P orbitals), respectively. The LUMO is characterized by S, P and D orbitals on the Au atoms and overlap of D and P orbitals on Ti and bridging O atoms, as observed in Figures 42. HL gap of the lowest energy anionic 3-1-1-d (C_{2v}: $^3B_2$) cluster is 3.27 eV, that is 0.08 eV smaller than the gap computed for lowest energy, 3-1-1-d (C_{2v}: $^3B_2$) of Ti_2AgO_6, but 0.25 eV larger than Eg of anatase.

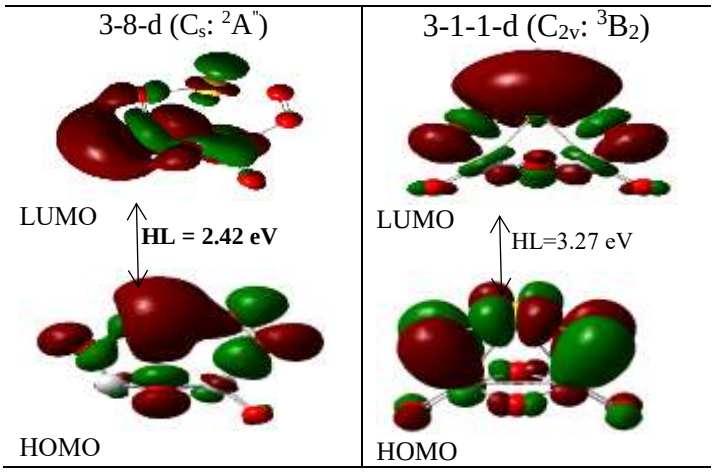

Figure 42: The FMO of neutral 3-8-d (C_s: $^2A''$) and anionic 3-1-1-d (C_{2v}: $^3B_2$) clusters at BPW91/6-311+G (d) level

(e) Electron Detachment Energy and Electron Affinity of Ti_2AuO_6 Clusters

Table 19 lists the vertical detachment energies for the ground state 3-1-1-d (C_{2v}) structure of anionic Ti_2AuO_6. The removal of one electron from the 3-1-1-d (C_{2v}: $^3B_2$) resulted in a doublet 3-1-1-d (C_{2v}:$^2A_1$) state. The quartet 3-1-1-d (C_{2v}:$^4A_1$) state was not obtained at BPW91 level, due to break of symmetry.

Table 20: VEDE for Au doped 3-1-1-d (C_{2v}: $^3B_2$) at the BPW91, B3LYP, CCSD (T)//BPW91 and CCSD (T)//B3LYP

	BPW91	B3LYP	CCSD (T) // BPW91	CCSD (T) // B3LYP
$^3B_2 \rightarrow {}^2A_1$	5.38	5.22	5.08	4.96
$^3B_2 \rightarrow {}^4A_1$	--	5.29	--	5.03

AEDE of lowest energy 3-1-1-d (C_{2v}) cluster is 5.18 eV and that of 3-8-d (C_1) 3.72 eV. Calculated AEDE of Ti_2AuO_6 clusters are found in Table 58 of Appendix 2.3. The EA was calculated by subtracting the energy of the 3-1-1-d (C_{2v}: $^3B_2$) anion from that of the neutral 3-8-d (C_s: $^2A''$). The calculated EA of Ti_2AuO_6 clusters is 4.04 eV.

(f) TD-DFT Calculations of Lowest Energy Neutral and Anionic Ti_2AuO_6 Clusters

UV-vis spectrum for the excitations of 3-8-d (C_1:^{2}A), resulted in two peaks at region of 624 nm and 711 nm, compared to 400-600 nm for the most stable neutral undoped structure, 3-1-u (C_s: ^{1}A´), as shown in Figure 43. The highest peak at 877 nm (1.41 eV) is due to transition from HOMO-3 (42B) to LUMO (46B). Anionic 3-1-1-d (C_{2v}:$^3B_2$) cluster, does not give any pronounced peak.

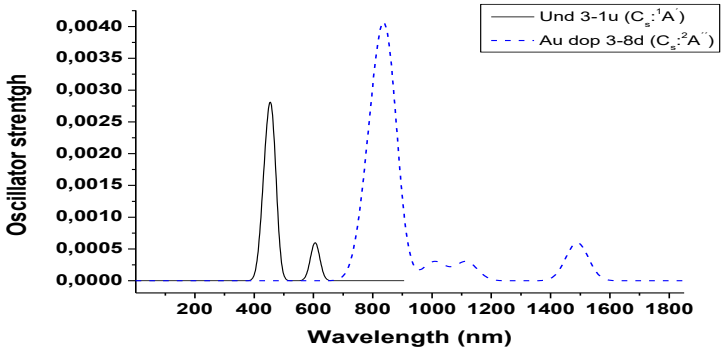

Figure 43: UV-Vis spectrum for neutral 3-1-u (C_s: ^{1}A´) and 3-8-d (C_1:^{2}A)

(g) Interaction of Water with the 3-8-d Cluster

One water molecule was molecularly adsorbed by 3-8-d (C_1:^{2}A) cluster, through 7Ti atom of the cluster. The E_b of 3-8-d (C_1:^{2}A) water-complex is -1.43 eV. The negative sign shows that the energy of the 3-8-d (C_1:^{2}A) water complex is less than sum of the energy of the doped 3-8-d (C_1:^{2}A) cluster and one water molecule. This E_b is the smallest within Au-doped $(TiO_2)_n(H_2O)$ clusters where n = 2 - 6.

9Au (-0.79)	7Ti (-1.43)	8Ti (-0.82)

Figure 44: Geometries and E_b (in eV) for the interaction of one water molecule with neutral Au-doped 3-8-d cluster

Dissociative adsorption through 9Au occurred, by the release in bond angle strain, between bond angle O-Au-O. Three-fold coordinated Ti atom favor the front side molecular adsorption of one H_2O molecule while four-fold coordinated (with a terminal Ti-O bond) favor side–side molecular adsorption of water molecule.

4.4.3 Geometry and Properties of Au doped $(TiO_2)_4$ Clusters, Ti_3AuO_8

(a) Relative Energy of Ti_3AuO_8 Cluster

Table 21 lists the relative energies of low-lying neutral and anionic Ti_3AuO_8 clusters. The 4-13-d (C_1: ^4A) structure is nearly isoenergetic with the 4-13-d (C_1: ^2A) structure using the BPW91 functional. However, at the more accurate CCSD (T) // BPW91 level, the 4-13-d (C_1: ^2A) structure appears to be the ground state of neutral Ti_3AuO_8, lying at 0.15 eV below 4-13-d (C_1: ^4A). The 4-21-d (C_1: ^2A) cluster, found as the ground state for Ti_3AgO_8 clusters, is 0.13 eV above ground state 4-13-d (C_1: ^2A) at the BPW91 level.

Table 21: Relative energy (eV) of neutral and anionic Ti_3AuO_8 clusters

Structure	PG	Ti_3AuO_8		$Ti_3AO_8^-$	
		State	ΔE	State	ΔE
4-5-1-d	C_s	$^2A'$	0.49		
4-9-1-B-d	C_s			$^1A'$	0.78
4-9-1-B-d	C_s			$^3A'$	0.63
4-13-d	C_1	^2A	0.00	^1A	0.87
4-13-d	C_1	^4A	0.00	^3A	0.00
4-21-d	C_1	^2A	0.13		
4-23-d	C_s	$^4A'$	0.75	$^3A''$	0.76

Cluster 4-13-d (C_1:^3A) was found as the ground state structure of anionic Ti_3AgO_8 clusters. Corresponding 4-13-d (C_1:^1A) singlet structure is 0.87 eV higher than 4-13-d (C_1:^3A). Other anionic Ti_3AuO_{12} clusters are at least 0.63 eV higher 4-13-d (C_1:^3A) in energy than the 4-13-d (C_1:^3A) most stable cluster. Relative energy of Ti_3AuO_{12} anionic clusters range from 0.63 eV to 2.99 eV above the ground state, as shown in Table 67-69 in Appendix 3.3.

(b) Geometric Parameters of the Lowest Energy Structures of Ti_3AuO_8 Clusters.

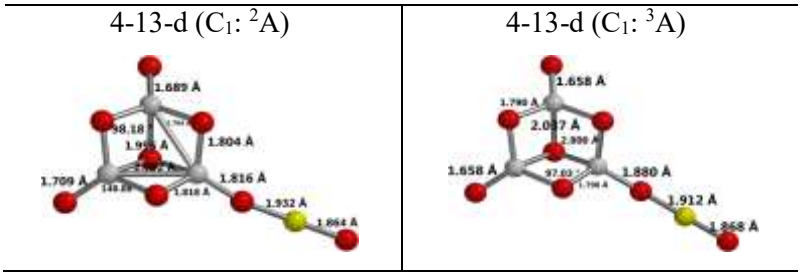

Figure 45: Geometric parameters for neutral 4-13-d (C_1: ^2A) and anionic 4-13-d (C_1: ^3A) clusters

The Ti_3AuO_8 clusters, have two-fold to three-fold coordinated Au atom and at least one terminal Ti-O bonds. Figures 92 - 93 in Appendix 3.3 display the geometry of obtained Ti_3AuO_{12}, clusters. The structure of 4-13-d (C_1) is characterized by two terminals Ti - O

bonds and a terminal Au - O bond.

(c) Vibrational Frequency of Lowest Energy Neutral and Anionic Ti_3AuO_8 Clusters

The vibrational mode at 671 cm^{-1} (5 km/mol), for neutral 4-13-d (C_1: ^2A), is assigned to the stretching of terminal Au - O with bond length of 1.86Å and the bridging O atom between the two terminal Ti - O bonds. The intense vibration around 730 cm^{-1} is assigned to the symmetric vibration of bridging the two bridging and three fold O atoms, while vibrations around 810 and 880 cm^{-1} are assigned to symmetric vibration of terminal O atoms and the O atom attached to Au atom.

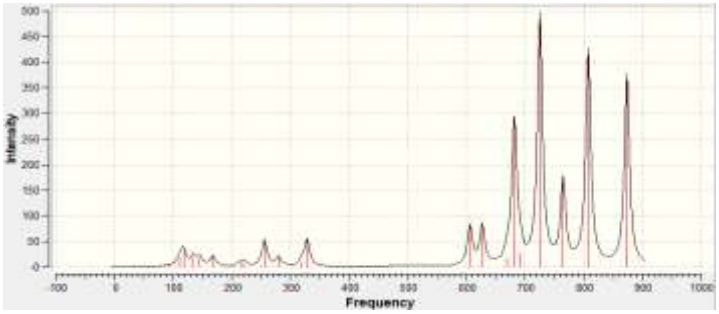

Figure 46: IR Spectrum for 4-13-d (C_1:^2A) at BPW91/6-311+G (d)

In case of the 4-13-d (C_1:^3A), Au - O participates in three vibrations in plane from 665 cm^{-1} to 720 cm^{-1}. The most intense peaks in the spectrum, as shown in Figure 47, was assigned to the degenerate bend of bridging O and Ti atom at 720 cm^{-1} and 728 cm^{-1}.

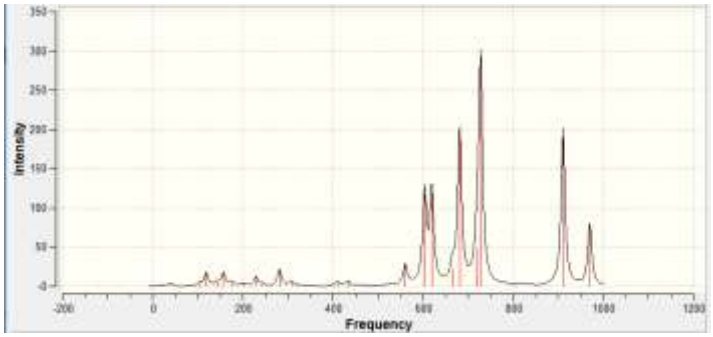

Figure 47: IR Spectrum for 4-13-d (C_1:^3A) at BPW91/6-311+G (d)

(d) HL Gap of Lowest Lying Ti_3AuO_8 isomers

HL gap of neutral 4-13-d (C_1: ^2A) and 4-13-d (C_1: ^4A) are 0.19 and 3.65 eV respectively, as shown in Figure 48. The HOMO of structure 4-13-d (C_1:^4A) is characterized by non-bonding orbital between Au and O atomic orbitals while LUMO is characterized by bonding interaction of Ti and bridging O atom. The Au atom does not contribute to the LUMO. HL gap of neutral 4-13-d (C_1: ^4A) is 0.63 eV higher than the E_g of bulk phase anatase. Figure 48, shows the FMO for the lowest lying neutral and anionic clusters of Ti_3AuO_8.

HL gap of anionic 4-13-d (C_1: ^3A) is 3.24 eV. Major contributions for HOMO come from O atoms of the undoped portion of the cluster. LUMO is bonding, with a very small contribution from the D orbital of Au and monovalent O atom.

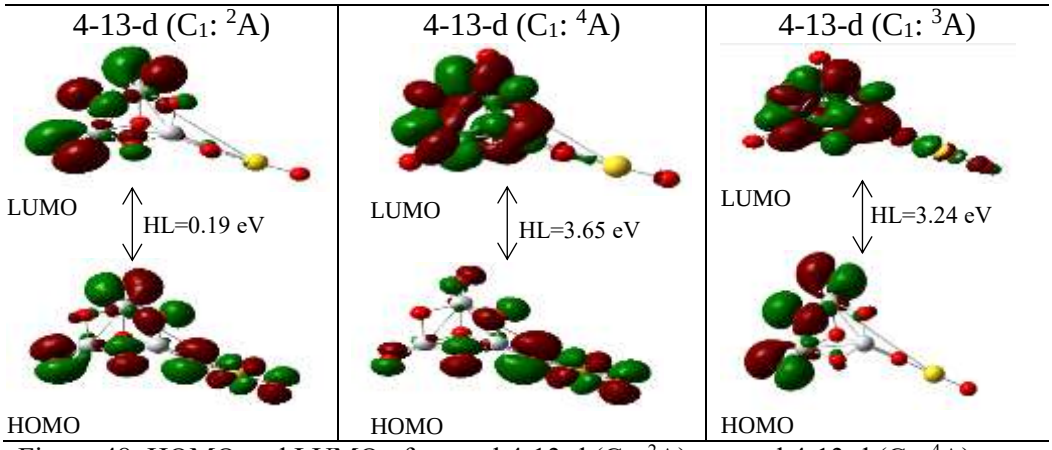

Figure 48: HOMO and LUMO of neutral 4-13-d (C_1: ^2A), neutral 4-13-d (C_1: ^4A) and anionic 4-13-d (C_1: ^3A) at BPW91/6-311+G (d) level

(e) Electron Detachment Energy and Electron Affinity of Ti_3AuO_8 Clusters

The triplet of 4-13-d (C_1: ^3A) have the electron configuration of (… $57a^2$, $58a^2$, $59a^2$, $60a^1$, $61a^1$). Detachment of one electron from MO $59a^2$ gives the 4-13-d (C_1: ^4A) quartet state, while the detachment of an electron from the $61a^1$ MO yields 4-13-d (C_1: ^2A). VEDE of

5.53 eV was computed for both ($^3A \rightarrow {}^4A$) and ($^3A \rightarrow {}^2A$) using BPW91 functional. The AEDE for ($^3A \rightarrow {}^4A$) and ($^3A \rightarrow {}^2A$) are 5.34 eV and 4.47, respectively. Calculated VEDE and AEDE for Ti_3AuO_8 clusters are tabulated in Table 71 and 72 of Appendix 3.3, respectively. Electron affinity was calculated by subtracting the energy of anionic 4-13-d (C_1:^3A) from the energy of neutral 4-13-d (C_1:^2A). The computed EA for Ti_3AuO_8 is 5.34 eV.

(f) TD - DFT Calculations of the Lowest Energy Neutral and Anionic Ti_3AuO_8 Cluster

The more intense (f = 0.0022) doublet-doublet transition for 4-13-d (C_1: ^2A), occurred at 2023 nm from HOMO-3 to LUMO with energy of 0.61 eV. Doublet-doublet transition from SOMO to LUMO occurred at the region of at 3562 nm with low energy of 0.35 eV and very low intensity of f=0.0006. Figure 49 shows the UV spectrum of undoped neutral 4-1-u cluster in addition to doped neutral 4-13-d (C_1: ^2A) cluster.

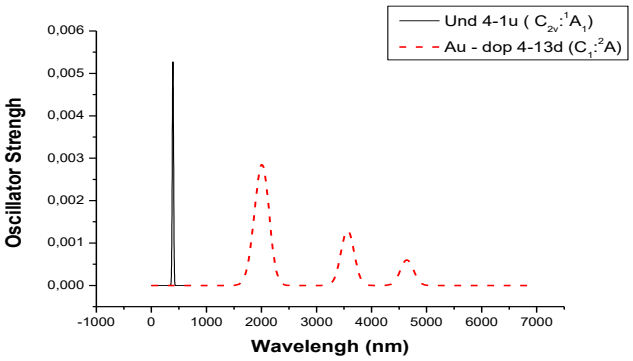

Figure 49: UV-Vis spectrum for anionic undoped 4-1-u (C_{2v}: $^1A_1$) and doped 4-13-d (C_1:^2A)

The lowest energy triplet-triplet excitation for 4-13-d (C_1:^3A) occurs at 9580 nm (0.13 eV) from HOMO to LUMO. These orbitals are shown in Figure 50. All triplet-triplet transitions in 4-13-d (C_1:^3A) occur with oscillator strength (f) of not more than 0.0007.

The electronic excitation spectrum of the doped 4-13-d (C_1:^{3}A) structure is different from that of undoped 4-2-u (C_{2v}:$^2A_1$) that have two pronounced peaks at 997 nm and 680 nm with oscillator strength (f) of 0.07 and 0.02, respectively, as shown in Figure 50.

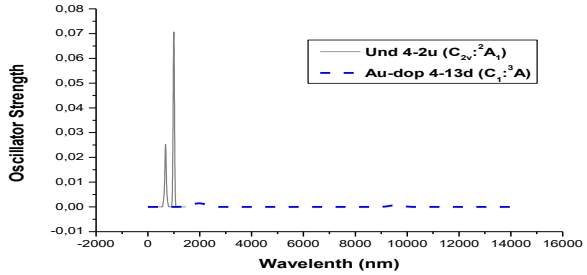

Figure 50: UV-Vis spectrum for anionic undoped 4-2-u (C_{2v}: $^2A_1$) and doped 4-13-d (C_1:^{3}A)

(g) Interaction of Water with the 4-13-d Cluster

Interaction of one water molecule with the 4-13-d (C_1: ^{2}A) cluster, results in the molecular adsorption of the water molecule through 2Ti atom, as shown in Figure 51. Calculated E_b is equal to -1.01 eV. The negative binding energy shows that the energy of the 4-13-d (C_1: ^{2}A) water-complex is less than sum of the energy of the doped 4-13-d (C_1: ^{2}A) cluster and one water molecule. The water molecule was adsorbed by the doped 4-13-d (C_1: ^{2}A) cluster.

The interaction of water molecule through 11O and 12Au atoms results in H bonding, whereby the H atom interacts with terminal Au - O bond and one of the bridging O atom, respectively, as shown in Figure 108 in Appendix 6.2. The H-bonding with Au - O bond gave a positive binding energy (E_b) of 0.14 eV. No dissociative adsorption was obtained for the interaction of water with the 4-13-d (C_1: ^{2}A) cluster.

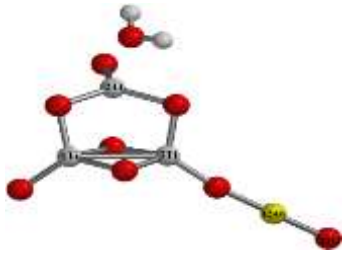

Figure 51: Molecular adsorption on 4-13-d (C_1: ^2A) through 2Ti atom.

4.4.4 Geometry and Properties of Au Doped $(TiO_2)_5$ Clusters, Ti_4AuO_{10}

(a) Relative Energy of Ti_4AuO_{10} Clusters

Table 22 lists the lowest lying neutral and anionic Ti_4AuO_{10} Clusters. Structure 5-6-1-d (C_s: $^2A''$) was found to be the lowest energy structure of neutral Ti_4AuO_{10} clusters. The 5-4-1-d (C_1: ^2A) structure, previously found as the ground state Ag doped $(TiO_2)_5$ cluster, is 0.46 eV above the 5-6-1-d (C_s: $^2A''$) ground state Au doped $(TiO_2)_5$ cluster. Based on the BPW91 calculations, all other structures are at least 0.90 eV above the lowest energy structure.

Table 22: Relative energy (eV) of neutral and anionic Ti_4AuO_{10} clusters

	PG	Ti_4AuO_{10}		$Ti_4AuO_{10}^-$	
Structure		State	ΔE	State	ΔE
5-2-2-d	C_1			^3A	0.29
5-3-1-d	C_1			^3A	0.33
5-4-1-d	C_1	^2A	0.46		
5-6-1-d	C_s	$^2A''$	*0.00*		
5-10-1-d	C_1	^4A	0.98		
5-18-d	C_1	^2A	0.91	^1A	0.30
5-18-d	C_1	^4A	0.79	^3A	*0.00*
5-21-d	C_1			^3A	0.29

For the anionic Ti_4AuO_{10} clusters, 5-18-d (C_1: ^3A) was found as the lowest energy structure. The five lowest-lying anionic clusters are 5-4-1-d (C_1:^1A), 5-2-2-d (C_1:^3A), 5-3-1-d

(C_1:^{3}A), 5-5-4-d (C_1:^{3}A), and 5-6-1-d (C_s: ^{1}A´). These clusters lie at 0.20 eV, 0.29 eV, 0.33 eV, 0.47 eV and 0.52 eV above the 5-18-d (C_1: ^{3}A) ground state structure. Full table relative energy are found in Table 84-86 of Appendix 4.3.

(b) Geometrical Parameters of the Lowest Energy Structures of Ti_4AuO_{10}

The 5-6-1-d (C_s: ^{2}A˝) cluster is characterized by O-O bond length of 1.322 Å, one terminal Ti - O bond and a bridging Au atom. Anionic 5-18-d (C_1: ^{3}A) ground state structure is characterized by three terminal Ti - O bonds and bridging Au atom, as shown in Figure 52. Most of Ti_4AuO_{10} clusters have either two-fold coordinated Au atom and three terminal Ti - O bonds or three-fold coordinated Au atom and two terminal Ti - O bonds.

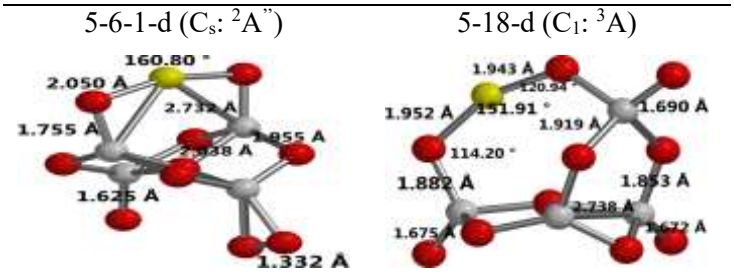

Figure 52: Geometric parameters for neutral 5-6-1-d (C_s: ^{2}A˝) and anionic 5-18-d (C_1: ^{3}A) lowest energy clusters.

(c) Vibrational Frequency of Lowest Energy Neutral and Anionic Ti_4AuO_{10} Clusters

The highest peak in the spectrum of neutral 5-6-1-d (C_s: ^{2}A˝) was assigned to the vibrations of bridging and the four-fold coordinated O atoms, as shown in Figure 53. Vibration involving the Au dopant atom was observed at 102 cm^{-1} (0.82 km/mol). The two peaks in spectrum of 5-6-1-d (C_s: ^{2}A˝), in Figure 53, at 1019 cm^{-1} (222 km/mol) and 1139 cm^{-1} (101 km/mol) describe the symmetric stretching of terminal Ti-O bond and asymmetric stretching of O - O, respectively.

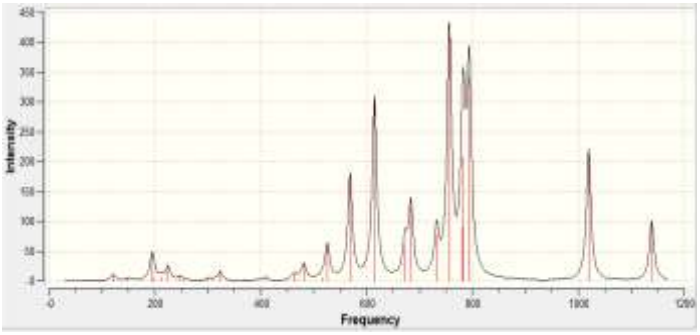

Figure 53: IR Spectrum for neutral 5-18-d (C_1:^{3}A) cluster at BPW91

Figure 54 shows the IR spectrum of the lowest lying anionic 5-18-d (C_1:^{3}A) cluster. The spectrum is characterized by three high peaks located at 595 cm^{-1} (200 km/mol) and 708 cm^{-1} (149 km/mol) which describe stretching of bridging O atoms and terminal Ti - O bonds. The peak at 926 cm^{-1} (87 km/mol) are attributed to the asymmetric stretching of terminal Ti-O bonds. No vibrational frequencies involve the Au dopant atoms, and the vibration that involve the O atoms attached to it are of very low intensity e.g., 2 km/mol (88 cm^{-1}) and 15 km/mol (608 cm^{-1}).

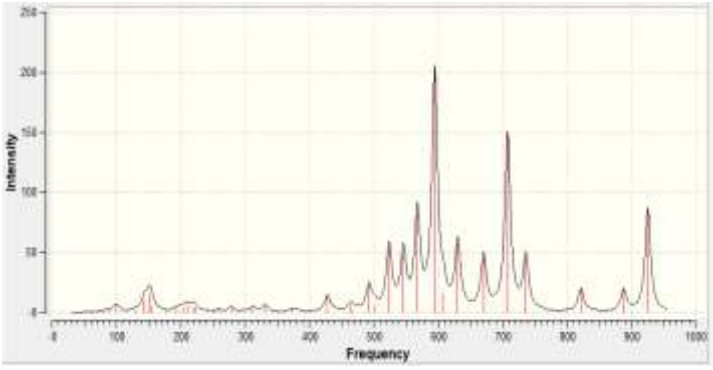

Figure 54: IR Spectrum for anionic 5-18-d (C_1:^{3}A) cluster at BPW91

(d) HL Gap of Lowest Lying Ti_4AuO_{10} Clusters

The HL gap of cluster 5-6-1-d (C_s: $^2A''$) is 2.69 eV. This value is small compared to lowest lying Ag doped $(TiO_2)_5$ cluster, 5-4-1-d (C_1: ^{2}A), of 2.83 eV. The HOMO is non-bonding

for Au (D) and O (P) orbitals. The LUMO is bonding with contributions from Au (D and P) and Ti (D) and O (P) orbitals.

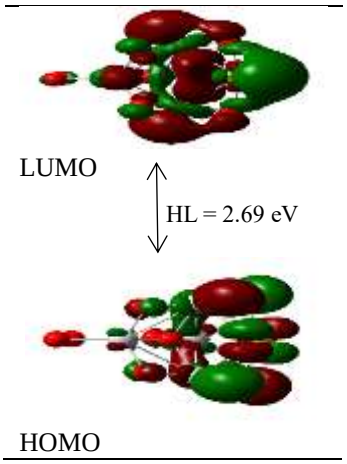

Figure 55: FMO of neutral 5-6-1-d (C_1: ^2A) cluster
at the BPW91/6-311+G (d) level

(e) Electron Detachment Energy and Electron Affinity of Ti_4AuO_{10} Clusters

The computed VEDE for the 5-18-d (C_1:^3A) ground state of the anionic clusters are 5.75 ($^3A\rightarrow^2A$) and 5.70 eV ($^3A\rightarrow^4A$), while the AEDE ($^1A\rightarrow^2A$ and $^3A\rightarrow^4A$) results are 5.39 and 5.57 eV respectively. Structures 5-2-2-d (C_1), 5-7-2-d (C_1) and 5-10-1-d (C_1) that are geometrically similar have the same VEDE of 5.81 eV for ($^3A\rightarrow^2A$) and 5.66 eV for ($^3A\rightarrow^4A$). These clusters have AEDE values in the range 3.38 ± 0.05 eV.

Electron affinity was calculated by subtracting the energy of anionic 5-18-d (C_1:^3A) from the energy of neutral 5-6-1-d (C_s: $^2A''$). The resultant EA for Ti_4AuO_{10} clusters is 4.78 eV.

(f) TD – DFT Calculations of Lowest Energy Neutral and Anionic Ti_4AuO_{10} Clusters

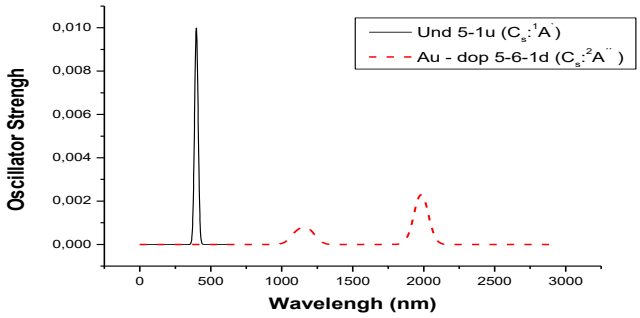

Figure 56: UV-Vis spectrum for neutral undoped 5-1-u (C_s: $^1A'$) and doped 5-6-1-d (C_1:$^2A''$)

Figure 56, shows the transition of undoped neutral 5-1-u and doped neutral 5-6-1-d (C_s: $^2A''$) ground state structures. Only one peak in region of 400 nm is observed in undoped 5-1-u cluster, due to transitions from HOMO-1 to LUMO (3.1 eV), HOMO to LUMO+1 (3.1 eV) and HOMO-2 to LUMO+1 (3.2 eV). For the neutral 5-6-1-d (C_s: $^2A''$) ground state structure, the first low energy transition occurs at 1982 nm (0.63 eV) from the HOMO to LUMO.

The first excitation for the anionic 5-18-d (C_1: ^3A) cluster, occurs at 9048 nm, (0.14 eV) from the HOMO to β-LUMO. The most intense peak of the anionic cluster involves excitation from HOMO to LUMO+1 at 3897 nm (0.32 eV). The LUMO+1 major contribution comes from orbitals on the Au atom and the monovalent O atoms. Figure 57 shows the transitions of anionic undoped 5-3-u cluster and doped 5-18-d (C_1:^3A).

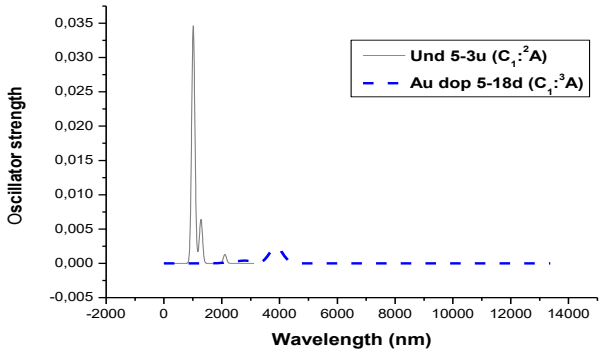

Figure 57: UV-Vis spectrum for anionic undoped 4-2-u (C_{2v}: $^2A_1$) and doped 4-13-d (C_1:^3A)

(g) Interaction of Water with 5-6-1-d Cluster

Interaction of one water molecule with the 5-6-1-d (C_s: $^2A''$) cluster, results in the molecular adsorption of one water molecule through 2Ti atom, as shown in Figure 58. As a result of this interaction, E_b of -1.22 eV was obtained.

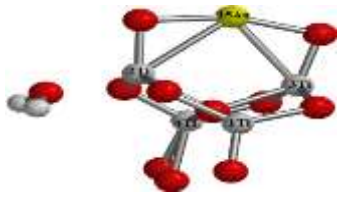

Figure 58: Molecular adsorption of one water molecule on cluster 5-6-1-d (C_s: $^2A''$) through 2Ti atom

E_b of 0.45 was obtained for the interaction of one water molecule through the 15Au atom. Positive E_b means that water molecule is not adsorbed by the 5-6-1-d (C_s: $^2A''$) cluster. Interatomic distance between the water molecule and 15Au is 2.12 Å. Table 108 in Appendix 6.2, shows the interaction of one water molecule with the 5-6-1-d (C_s: $^2A''$) cluster and corresponding E_b.

4.4.5 Geometry and Properties of Au doped (TiO2)6 Clusters, Ti5AuO12

(a) Relative Energy of Ti_5AuO_{12} Clusters

Clusters 6-1-2-d (C_1: ^2A) and 6-1-2-d (C_1: ^1A) were found to be the lowest lying structure, for neutral and anionic Ti_5AuO_{12} clusters, respectively as shown in Table 23. The results listed in Tables 95 and 96 in Appendix 5.3, show that none of the neutral clusters has relative energy below 0.50 eV. The nearest neutral low-lying structure, 6-1-1-d (C_1: ^2A), is 1.30 eV higher in energy than the ground state 6-1-2-d (C_1: ^2A) cluster. The relative energies for the neutral Ti_5AuO_{12} clusters range from 1.30 eV to 2.75 eV.

Table 23: Relative energy (eV) of neutral and anionic Ti_5AuO_{12} clusters

	PG	Ti_3AuO_8		$Ti_3AO_8^-$	
Structure		State	ΔE	State	ΔE
6-1-1-d	C_1	^2A	1.30		
6-1-1-d	C_1	^4A	1.43	^3A	0.95
6-1-2-d	C_1	^2A	*0.00*	^1A	*0.00*
6-1-3-d	C_1	^2A	1.52	^3A	0.78
6-2-1-d	C_1			^1A	0.85
6-4-1-d	C_1	^4A	1.44		
6-4-2-d	C_1			^1A	0.98

As listed in Table 23, the anionic Ti_5AuO_{12} clusters, 6-1-1-d (C_1: ^3A), 6-1-3-d (C_1: ^3A), 6-2-1-d (C_1: ^1A), 6-2-1-d (C_1: ^3A), 6-4-2-d (C_1: ^1A) are 0.95 eV, 0.78 eV, 0.85 eV, and 0.98 eV above the 6-1-2-d (C_1: ^1A) lowest energy cluster, respectively. The relative energies of the anionic Ti_5AuO_{12} clusters range from 0.78 eV to 1.98 eV. The complete table of Ti_5AuO_{12} relative energy is found in Tables 94 and 95 (Appendix 5.3).

(b) Geometrical Parameters of the Lowest Energy Structures of Ti_5AuO_{12} Clusters

Figure 59 displays the bond lengths and angles of the lowest energy structures for the

neutral and anionic Ti_5AuO_{12} clusters. The neutral 6-1-2-d (C_1:^{2}A) is characterized by O-O bond length of 1.336 Å, two-fold coordinated Au atom and four-fold O atom at the center of the cluster. Structure 6-1-2-d is the only structure that has a two-fold Au atom among the Ti_5AuO_{12} clusters. Other clusters, neutral and anionic, possess three-fold Au atom, e.g., 6-4-2-d (C_1: ^{2}A), 6-1-1-d (C_1: ^{3}A), 6-2-1-d (C_1: ^{1}A), and 6-2-1-d (C_1: ^{3}A) as shown in Figure 103 (Appendix 5.3). Bonds of anionic 6-1-2-d (C_1:^{1}A) are slightly longer than the bonds of neutral 6-1-2-d (C_1: ^{2}A), e.g., the O – O bond in anionic 6-1-2-d is 0.141 Å longer than in neutral 6-1-2-d.

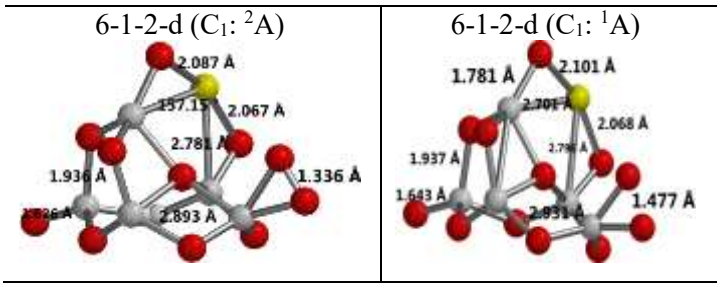

Figure 59: Geometric parameters for neutral 6-1-2-d (C_1: ^{2}A) and anionic 6-1-2-d (C_1: ^{1}A) clusters.

(c) Vibrational Frequency of Lowest Energy Neutral and Anionic Ti_5AuO_{12} Clusters

The IR spectrum of lowest lying neutral Ti_5AuO_{12} cluster, 6-1-2-d (C_1:^{2}A), depicted in Figure 60, can be summarized as follows:

- Delocalized stretching (50 - 820 cm^{-1});
- Stretching of three Ti - O - Ti bridges tetrahedral coordinated to a terminal Ti - O bonds (870 cm^{-1});
- Stretching of terminal Ti - O bond (1013 cm^{-1});
- Stretching of O - O atoms (1102 cm^{-1});

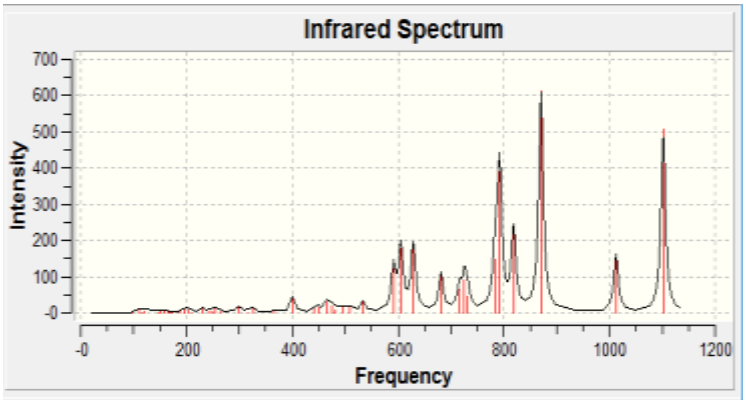

Figure 60: IR Spectrum for 6-1-2-d (C_1:^{2}A) at BPW91 level.

The IR spectrum of 6-1-2-d (C_1:^{1}A) lowest energy anionic Ti_5AuO_{12} cluster, can be summarized as:

- Delocalized stretching (46 - 785 cm^{-1});
- Stretching of three Ti - O - Ti bridges tetrahedrally coordinated to a terminal Ti - O bonds (848 cm^{-1});
- Stretching of O - O atoms (899 cm^{-1});
- Stretching of terminal Ti - O bond (988 cm^{-1});

The most intense peak of 960 km/mol (848 cm^{-1}) of the anionic 6-1-2-d (C_1:^{1}A) cluster is due to the stretching of three Ti - O - Ti bridges tetrahedral coordinated to a terminal Ti - O bonds.

(d) HL Gap of Lowest Lying Ti_5AuO_{12} Clusters

The HL gap of the 6-1-2-d (C_1: ^{2}A) ground state of neutral Ti_5AuO_{12} cluster, is 2.18 eV. The calculated HL of is 1.02 below the E_g of bulk anatase. HOMO of 6-1-2-d (C_1: ^{2}A) is anti-bonding with respect to orbitals on the Au atom and adjacent O atoms, as shown in Figure 61. HL gap of lowest energy anionic Ti_5AuO_{12} cluster 6-1-2-d (C_1: ^{1}A) is 2.09

eV, that is 1.11 eV below E_g of bulk anatase. The major contributions to the HOMO come from the orbitals on the 1Ti atom and O - O atoms attached to it. The LUMO involves orbitals that are delocalized over the entire molecule except to the monovalent O atom. The FMO and corresponding HL gap are shown in Figure 61. Labeled structures are in Table 104 (Appendix 6).

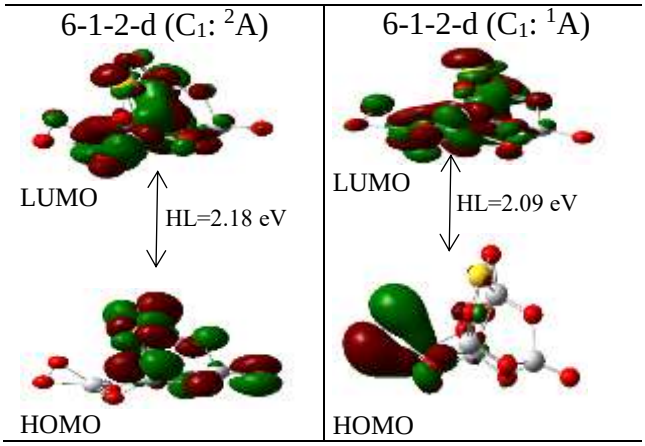

Figure 61: FMO of neutral 6-1-2-d (C_1: ^{2}A) and anionic 6-1-2-d (C_1: ^{1}A) at the BPW91/6-311+G (d) level.

(e) Electron Detachment Energy and Electron Affinity of Ti_5AuO_{12} Clusters

The 6-1-2-d (C_1: ^{1}A) ground state structure of the Ti_5AuO_{12} anion has the electron configuration of [… 85 $(a)^2$, 86 $(a)^2$, 87 $(a)^2$, 88 $(a)^2$]. Vertical detachment of one electron from molecular orbital 88 $(a)^2$ yields, 6-1-2-d (C_1: ^{2}A), with energy of 5.26 eV. The computed AEDE for the ($^1A \rightarrow {}^2A$) electronic transition is 4.86 eV. The electron affinity was calculated by subtracting the energy of 6-1-2-d (C_1: ^{1}A) ground state of the anion from the energy of 6-1-2-d (C_1: ^{2}A) ground state of the neutral. The EA of Ti_5AuO_{12} cluster is 4.86 eV, similar to the AEDE.

(f) TD – DFT Calculations of Lowest Energy Neutral and Anionic Ti_5AuO_{12} Clusters

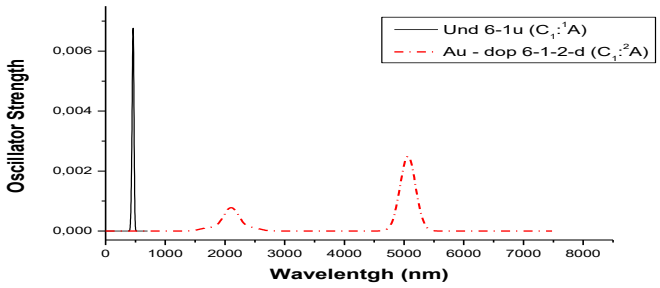

Figure 62: UV-Vis spectrum for neutral 6-1-u (C_1:^{1}A) and 6-1-2-d (C_1:^{2}A) clusters

Excitation of 6-1-2-d (C_1:^{2}A) cluster occur at region of 5063 nm, from orbital HOMO to LUMO with excitation energy of 0.244 eV and oscillator strength of 0.0025, as shown in Figure 62. A peak is observed for anion 6-1-u undoped ground state structure. In case of the 6-1-2-d (C_1:^{1}A) anionic cluster, the excitation from orbital HOMO to LUMO, gives the lowest excitation energy of 2.21 eV, in the region of 562 nm. Doping of the undoped cluster with Au metal to give 6-1-2-d (C_1:^{1}A) results in a hypsochromic shift (1.43 eV), as shown in Figure 63.

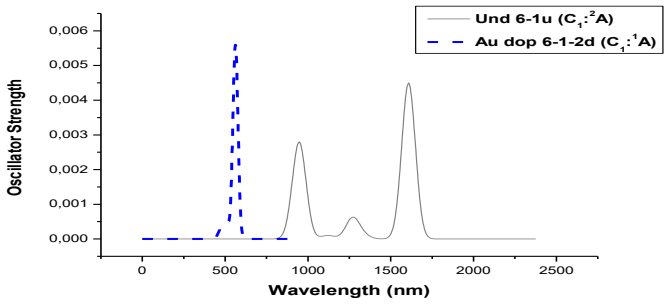

Figure 63: UV-Vis spectrum for anionic 6-1-u (C_1:^{2}A) and 6-1-2-d (C_1:^{1}A) clusters

(g) Interaction of Water with 6-1-2-d Cluster

The molecular adsorption of one water molecule through 3Ti atom was predicted to be the lowest energy of (Ti_5AuO_{12})(H_2O) complex, using the BPW91 functional, as shown in Figure 64. The binding energy of -1.23 eV indicate that neutral Ti_5AuO_{12} cluster, 6-1-2-d (C_1:^{2}A), interacts strongly with the water molecule. .

The attachment of one water molecule to 18Ag and 5Ti atoms resulted in dissociative adsorption and H-bonding interaction respectively. For the dissociative interaction, the H fragment is attached to 10O atom, while HO fragment is attached to 18Au atom with a distance of 2.10 Å. The H-bonding is described by a distance of 1.93 Å with the 17O atom. Dissociative interaction and H-bonding of 6-1-2-d (C_1: ^{2}A) are displayed in Figure 108 of Appendix 6.2

Figure 64: Molecular adsorption on cluster 6-1-2-d (C_1) through 3Ti atom.

4.5 VARIATION OF PROPERTIES WITH THE CLUSTER SIZE

The most stable structures for the undoped $(TiO_2)_n$, Ag doped $(TiO_2)_n$ and Au doped $(TiO_2)_n$ neutral and anionic clusters studied in this work are presented in Figure 65. The undoped $(TiO_2)_n$ has been previously been studied [1, 2, 3, 9, 15, 25, 27, and 28]. However, this study presents for the first time the variation of properties with size for the Ag doped $(TiO_2)_n$ and Au doped $(TiO_2)_n$ (n = 2 – 6) clusters.

Undoped $(TiO_2)_n$

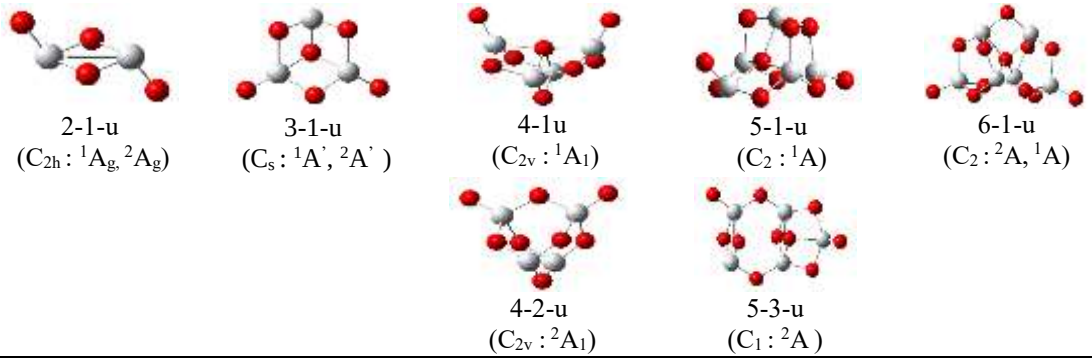

Ag – doped $(TiO_2)_n$

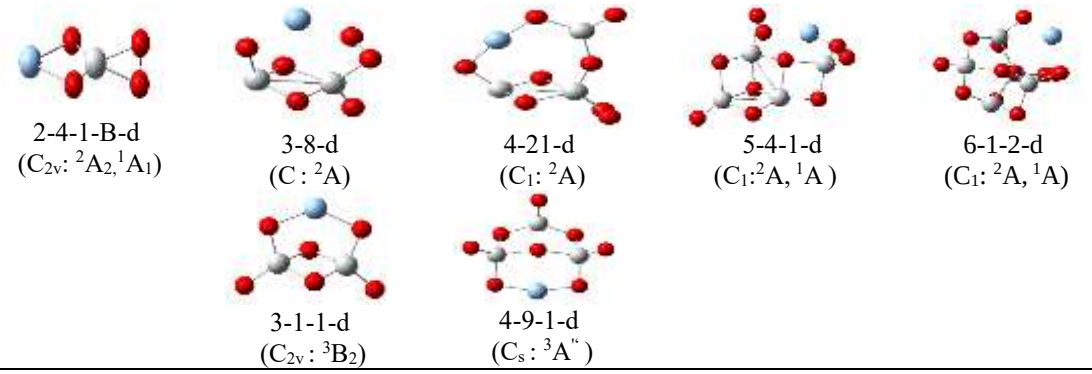

Au – doped $(TiO_2)_n$

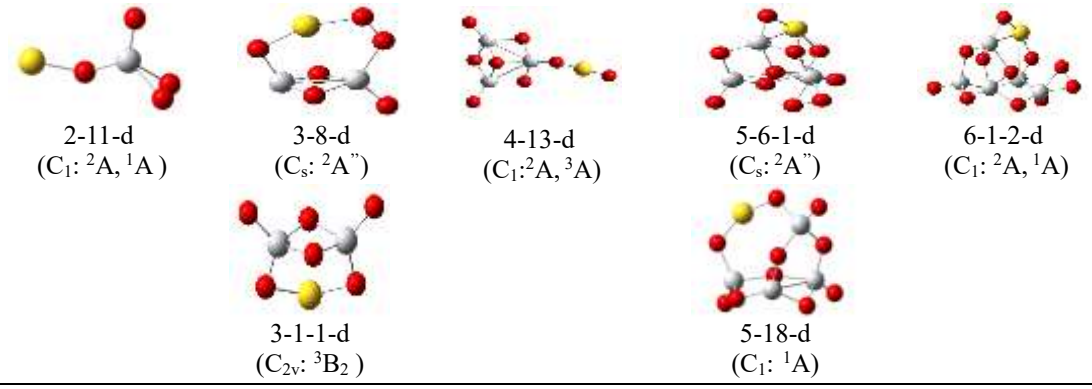

Figure 65: Lowest energy structures of undoped and Ag/Au doped $(TiO_2)_n$ clusters indicating their point groups and electronic states, for n = 2 – 6 clusters.

4.5.1 Variation of Binding Energy with Cluster Size (n)

The binding energies (E_b) of the lowest energy structures of Ag and Au-doped $(TiO_2)_n$ clusters (n = 2 – 6) were calculated as described in equations 8 and 9, respectively. The variation of binding energy with the cluster size (n) is shown in Figure 66. It is possible to observe that E_b for Ag-doped $(TiO_2)_n$ clusters, increase from n = 2 to n = 4 and slightly decreases from n = 4 to n = 6. In case of Au-doped $(TiO_2)_n$ clusters, E_b appears to increase monotonically except for n = 5 where there is a noticeable dip.

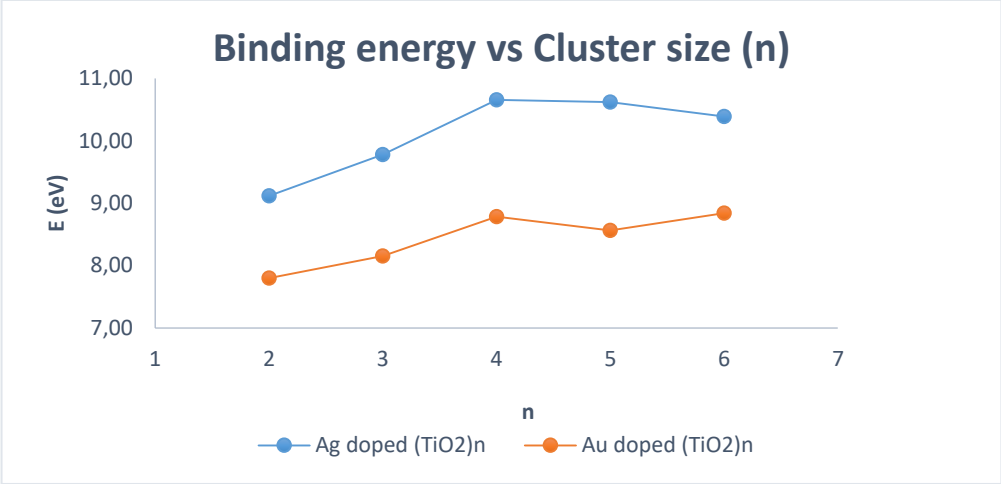

Figure 66: Binding energy for Ag and Au doped $(TiO_2)_n$ clusters

Hudson et al [32], attached one Au atom to the three-fold coordinated O atom in undoped 3-1-u cluster. Binding energy of - 0.75 eV was obtained for the $AuTi_3O_6$ (C_s: $^2A'$) clusters. They calculated the binding energy by subtracting the total energy of reactant from the energy of product as follow: $BE_{Au} = E_{(AuTi3O6)} - \{E_{(Ti3O6)} + E_{Au}\}$. The difference between this calculation and the one implemented here is that the energy of Ti cation was not added to the energy of the Au doped cluster, $AuTi_3O_6$.

4.5.2 Variation of HL Gap with Cluster Size (n)

Table 24 provides a summary of the HL gap of undoped and doped $(TiO_2)_n$ clusters computed with the BPW91 functional. It is well known that the rutile and anatase band gaps are 3.0 and 3.2 eV, respectively.

Table 24: HL gap of undoped, Ag and Au doped $(TiO_2)_n$ clusters were calculated using the BPW91 functional.

	Neutral			Anion		
n	Und.	Ag-dop.	Au-dop.	Und.	Ag-dop.	Au-dop.
2	3.32 [s]	2.01 [d]	1.96 [d]	0.33 [d]	0.33 [s]	0.19 [s]
3	2.04 [s]	3.02 [d]	2.42 [d]	1.22 [d]	3.35 [t]	3.27 [t]
4	3.02 [s]	1.50 [d]	0.19 [d]	0.98 [d]	3.59 [t]	3.24 [t]
5	2.88 [s]	2.83 [d]	2.69 [d]	0.57 [d]	2.01 [s]	3.26 [t]
6	2.64 [s]	2.37 [d]	2.18 [d]	0.65 [d]	2.18 [s]	2.09 [s]

[d] doublet, [q]quartet, [s]singlet, and [t]triplet.

Figure 67, appears to indicate an odd-even oscillation of the HL gap for the undoped, Ag and Au doped $(TiO_2)_n$ clusters, as a function of cluster size (n). The doped cluster Ti_3AuO_8, 4-13-d (C_1: ^2A), has a lower HL gap of 0.19 eV, which is 3.01 eV below E_g of anatase. This lower HL gap value originates the noticeable dip in the graph of HL gap of neutral Au doped $(TiO_2)_n$ clusters, as observed in Figure 67.

Qu [3, 20] observed the same odd-even oscillation for undoped $(TiO_2)_n$ clusters n = 2 - 9 [3] and n = 10 - 16 [20] respectively. In reference 9, undoped $(TiO_2)_n$ clusters of n = 2 – 5 and the S-doped $(TiO_2)_n$ clusters n = 2 - 13 presented the same feature. The same study state that the band gap of undoped clusters approaches the bulk limit at n = 7 and remains constant up to n = 10. HL gap is expected to decrease as the cluster size grows due to quantum sized effects [3 and 14]. However, in this work calculated HL gap oscillates with the clusters size.

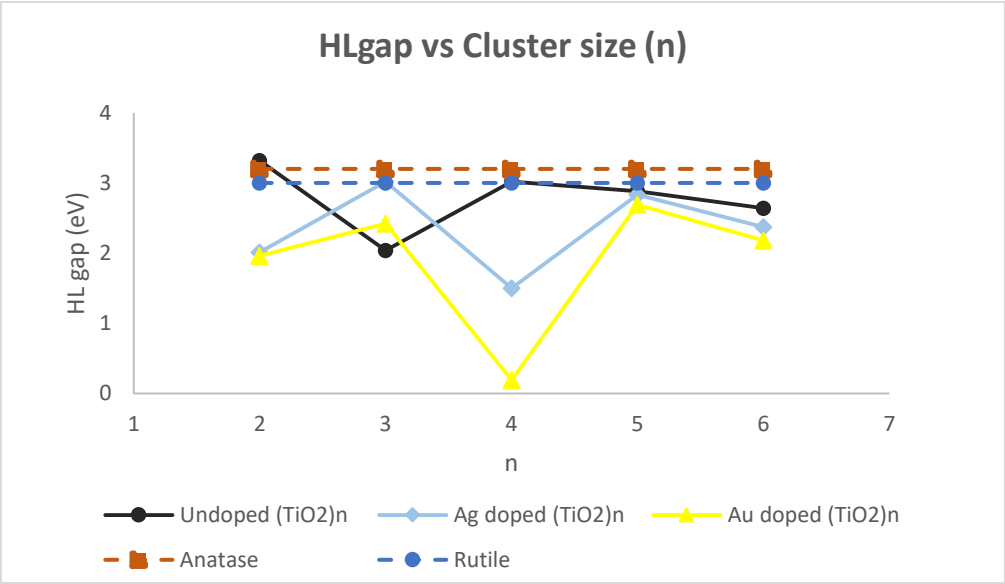

Figure 67: HL gap of neutral undoped, and Ag / Au doped $(TiO_2)_n$ clusters compared to the of the bulk material.

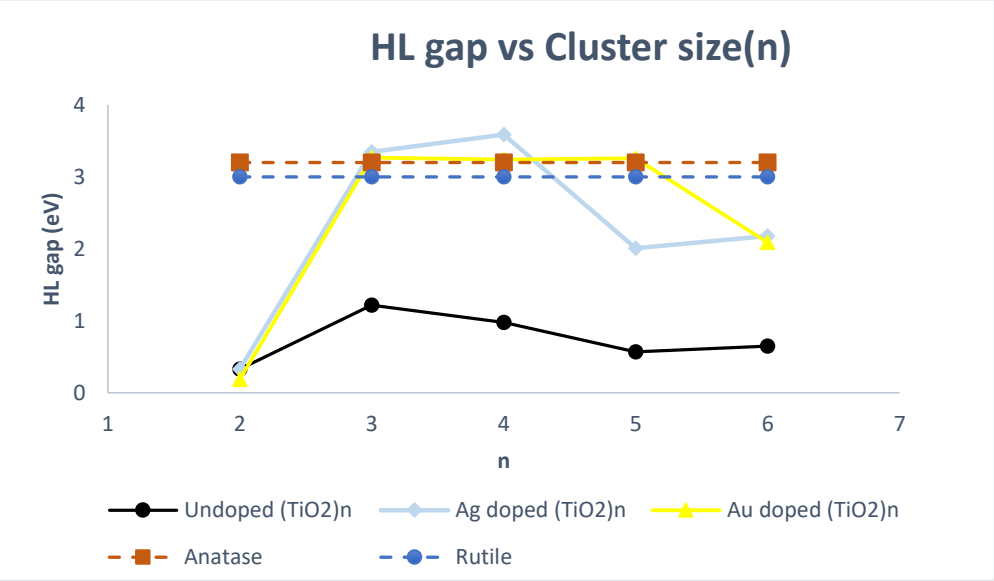

Figure 68: HL gap of anionic undoped, and Ag/Au doped $(TiO_2)_n$ clusters compared to the of the bulk material.

In the present work, Figure 68 shows that HL gap for Au doped $(TiO_2)_n$, anionic clusters became flat from n = 3 to n = 5, very close to that of anatase. No oven-odd oscillation or flatness are observed in the graph of Ag doped anionic clusters. The anionic Ag-doped

clusters, 3-1-1-d (C_{2v}: $^3B_2$) and 4-9-1-d (C_s: $^3A''$) are 0.15 and 0.39 eV above the E_g of anatase.

The measured HL gaps of Ag and Au doped $(TiO_2)_n$ clusters are plotted in Figures 69, in comparison with previous calculations of C, N and S doped $(TiO_2)_n$ clusters [9]. The HL gap of Ag and S doped $(TiO_2)_n$ clusters compete the highest places in the plot, while N doped $(TiO_2)_n$ clusters occupies the lower part of the plot as shown in Figure 69. Nevertheless, none of the doped clusters reached the band gap (E_g) of bulk TiO_2.

The HL gap of C, Au, Ag and S doped $(TiO_2)_n$ clusters for n = 2 and n = 6 are likely to be the same. The HOMO of this clusters is located at the dopant atom and/or one-fold oxygen. There is an overlap between the LUMO and HOMO states of those clusters that could represent an optically active transition.

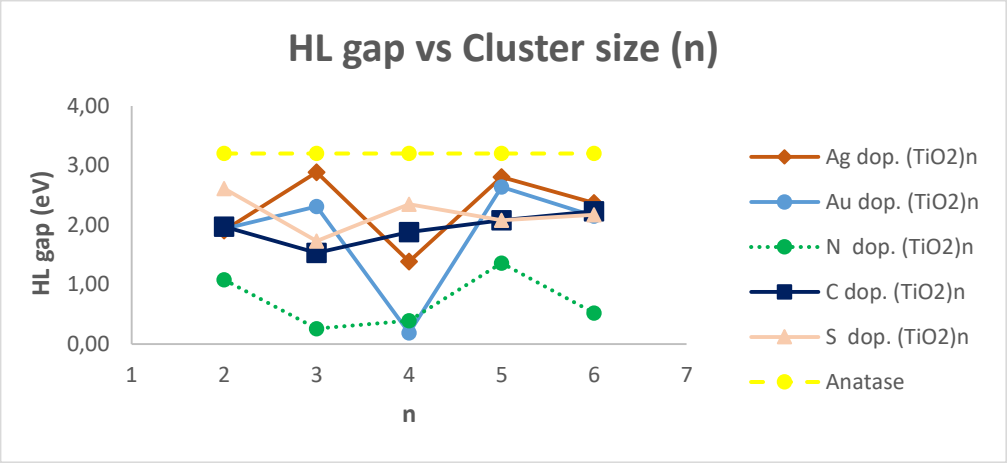

Figure 69: HL gap of undoped, Ag, Au, N, C and S doped clusters compared to bulk Anatase.

Mogal and co-wokers [42] affirmed that the band gap for TiO_2 thin films increase from 2.99 eV to 3.16 eV as the Ag content increases from 0.004 to 0. 0.015 mol. Another study, Peerakiatkhajorn [43] showed that the band gap energy values of Ag/TiO_2 thin films decrease from 2.84 eV to 2.65 eV when Ag contents increase from 0.01 mol to 0.2

mol. Table 24, in current study, shows that HL gap of Ag doped $(TiO_2)_n$ clusters decrease from 2.83 eV to 2.37 eV as cluster size increase from n = 5 to n = 6. The neutral Ag doped $(TiO_2)_3$ have HL gap of 3.02 eV, that is at least 0.14 eV lower compared to band gap of high concentrated Ag/TiO_2 thin film obtained in reference 42.

In case of Au/TiO_2 thin films, Mohite and co-workers [44], found that the band gap of Au/TiO_2 thin films, deposited at 1 - 4 % with Au content, decreases from 3.23 eV to 3.09 eV. Gültekin [45] used 10 – 50 % of Au content to synthesize Au/doped TiO_2 thin films and found band gap increasing from 3.75 eV to 3.89 eV. The HL gap of neutral Au-doped $(TiO_2)_n$ clusters obtained in the present work are below 2.6 eV.

4.5.3 Variation of Electron Detachment Energies with Cluster Size (n)

Figure 70 shows the trend in VEDE as the cluster size increases. The plot for the VEDE for Au doped $(TiO_2)_n$ clusters appears to be constant from n = 3 to n = 5 as observed in Figure 70. The same trend is observed for the HL gap of anionic clusters. The VEDE for Ag-doped $(TiO_2)_n$ clusters is slightly different from Au doped $(TiO_2)_n$ clusters, due to a decrease in the VEDE of cluster 5-4-1-d.

The VEDE of Ag doped $(TiO_2)_n$ cluster (n = 2 – 6), follow the same trend as undoped $(TiO_2)_n$ cluster of the same size. The Au doped $(TiO_2)_n$ cluster is likely to have the same trend as the undoped cluster in reference 15. However, the VEDE of the doped clusters are higher than the corresponding undoped clusters. They differ to about 2 eV.

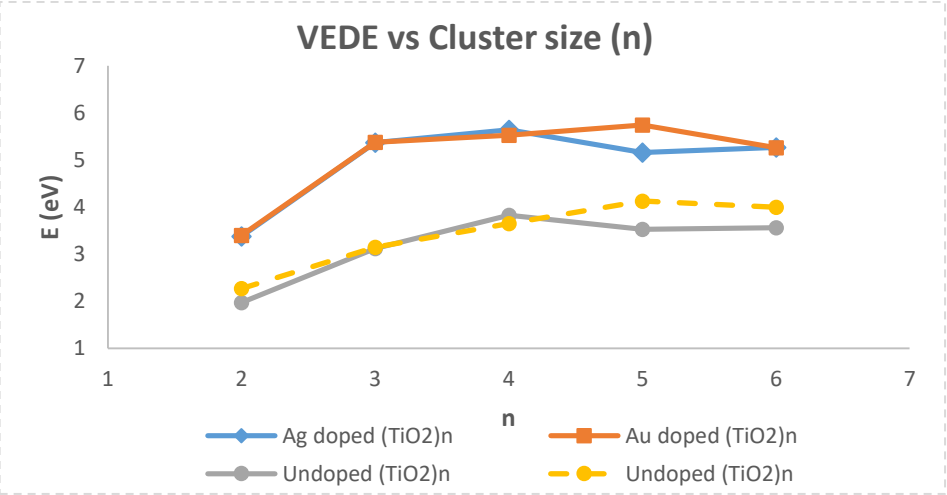

Figure 70: VEDE for Undoped, Ag and Au doped $(TiO_2)_n$ clusters. Theoretical results (dashed line) for undoped $(TiO_2)_n$ clusters, [15]

Next is the plot of AEDE against the cluster size. Figure 71, shows AEDE of undoped, Ag and Au- doped $(TiO_2)_n$ clusters increasing gradually from n = 2 to n = 4. There is a slight anomaly at cluster size n = 5. The results as depicted in Figure 71 also suggest that Ag and Au doped $(TiO_2)_n$ clusters, have nearly the same AEDE values from n = 2 - 4. The AEDE of the doped clusters are higher than the corresponding undoped clusters.

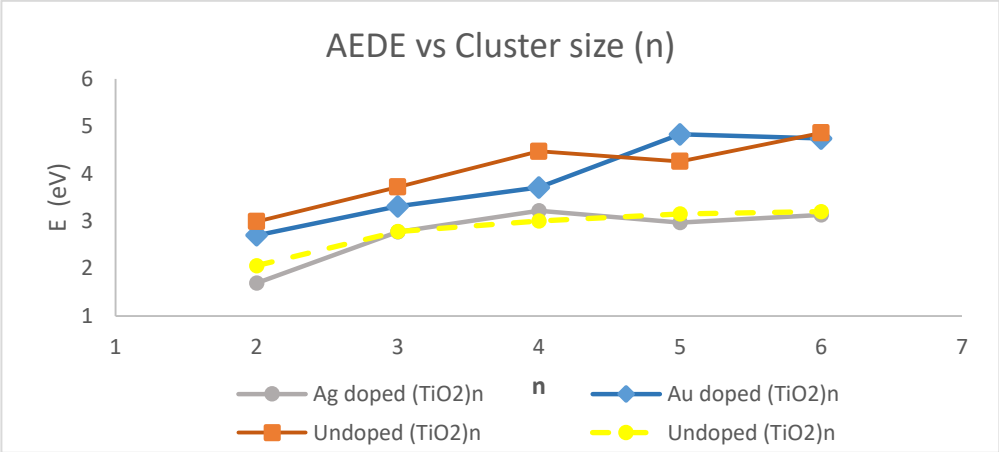

Figure 71: AEDE for Undoped, Ag and Au doped $(TiO_2)_n$ clusters. Theoretical results from ref. 15 are shown in dashed line.

4.5.4 Variation of Electron Affinity with Cluster Size (n)

According to Scanlon at el. [34], the theoretical and experimental electron affinity (EA) of rutile are 4.8 eV and 5.1 eV, respectively, while the corresponding values for anatase are 4.9 eV and 5.1 eV. Figures 72 and 73 show the vertical electron affinity (VEA) and adiabatic electron affinity (AEA), respectively, of undoped, Ag-doped, Au-doped $(TiO_2)_n$ clusters for n = 2 – 6 and bulk material anatase.

The AEA of Ag doped $(TiO_2)_n$ clusters increased gradually from n = 2 – 5, where it approach the theoretical AEA of rutile. In contrast, the Au doped $(TiO_2)_n$ increases from n = 2 - 4, where it overpass the experimental AEA of rutile and anatase by 0.24 eV, as observed in Figure 72. The AEA of Ag/Au doped $(TiO_2)_n$ cluster is higher than the AEA of corresponding undoped clusters.

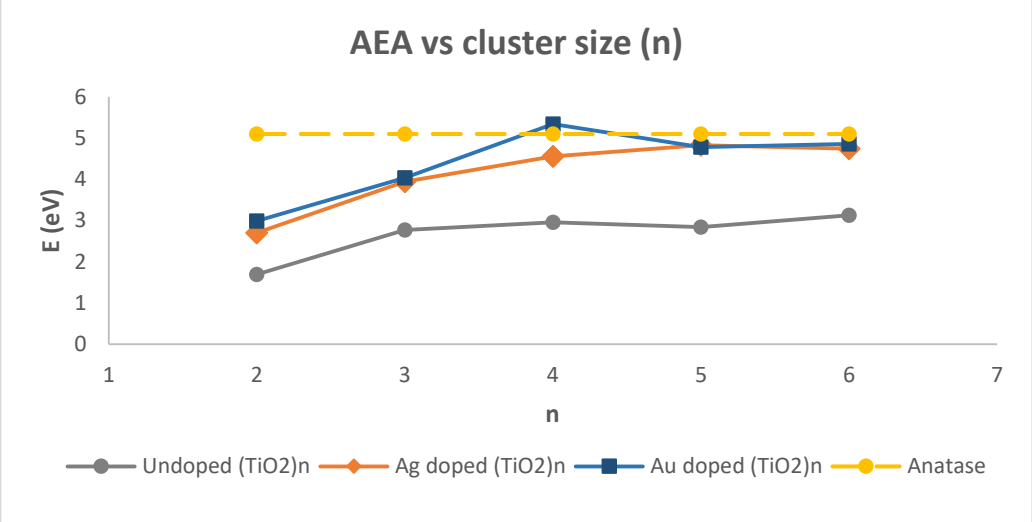

Figure 72: AEA (eV) of undoped, Ag and Au doped $(TiO_2)_n$ clusters at BPW91

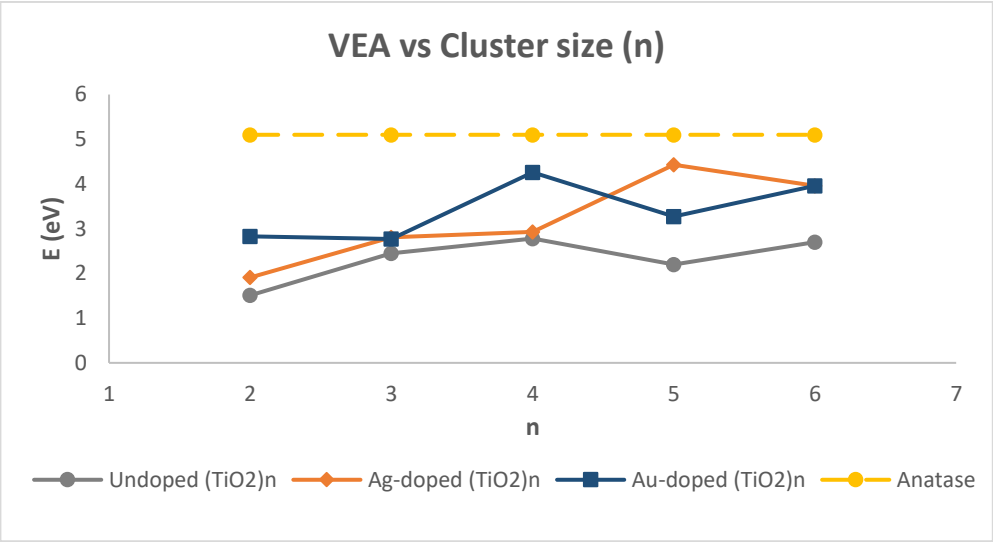

Figure 73: VEA (eV) of undoped, Ag and Au doped $(TiO_2)_n$ clusters at BPW91

The VEA of the Ag/Au doped $(TiO_2)_n$ clusters are higher compared to the corresponding undoped $(TiO_2)_n$ clusters, except for Au doped $(TiO_2)_4$ cluster, that is likely to be the same as the corresponding undoped cluster. The VEA Ag and Au doped $(TiO_2)_n$ cluster for n = 3 and n = 6 are likely to be the same. None of the three systems reached the VEA of bulk anatase, as observed in figure 73.

Table 99 in the appendix 7 lists the calculated AEA and VEA for undoped, Ag-doped and Au-doped $(TiO_2)_n$ clusters for n = 2 - 6, as well as the pair of lowest energy neutral and anionic clusters involved in the calculations. For the extension of our knowledge, no experimental or theoretical works were done for Ag and Au doped of $(TiO_2)_n$ clusters, then no comparison can be made.

4.5.5 Variation of Ionization Energy with Cluster Size (n)

The Koopmans' theorem [36] states that the ionization energy is the negative of the energy of the orbital from which the electron is ejected (HOMO). Then vertical ionization potentials (VIE) may be compared to the negative of the energy of the HOMO. Tables

25 and 26 present the VIE values, for undoped, Ag and Au doped $(TiO_2)_n$ clusters as well as the energy of -HOMO of α and β spatial orbitals of neutral Ag and Au doped $(TiO_2)_n$ clusters. The α and β spatial orbitals are for open shell systems, i.e. doublet, triplet and quartet while and αβ spatial orbitals are for closed shell system, i.e. singlet. The α, β and αβ spatial orbitals are indicated in Tables 25 and 26 by superscript a, b and c respectively. VIE was calculated, as indicated in equation 2, by subtracting the ground state energy of optimized neutral from single point energy of cation at the optimized geometry of ground state neutral.

Table 25: VIE and Negative HOMO of undoped and Ag doped $(TiO_2)_n$ clusters (eV).

N	Undoped $(TiO_2)_n$	Ag doped $(TiO_2)_n$		
	VIE	-HOMO [a]	-HOMO [b]	VIE
2	9.79	6.07	6.04	9.17
3	9.48	6.75	6.58	9.33
4	8.79	5.88	5.88	8.58
5	9.56	7.35	7.10	9.31
6	9.62	6.97	6.97	9.10

Negative HOMO[a] : α-HOMO and Negative HOMO[b]: β-HOMO

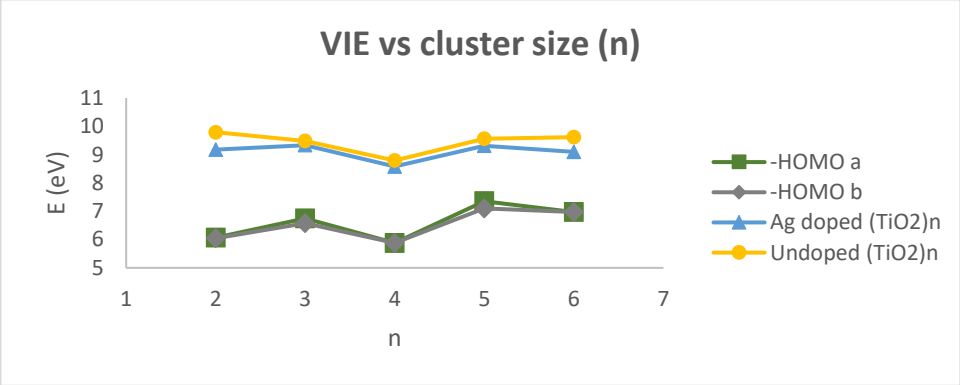

Figure 74: VIE of undoped and Ag doped $(TiO_2)_n$ clusters. -HOMO[a] (α-HOMO) and -HOMO[b] (β-HOMO) of Ag doped clusters $(TiO_2)_n$ clusters.

Negative of the energy of the HOMO and VIE of Ag doped clusters are within ±3.00 eV from each other. The energy between α-HOMO and β-HOMO do not differ by more than 0.25 eV from each other.

Table 26: VIE and Negative HOMO of undoped and Au doped $(TiO_2)_n$ clusters (eV).

	Undoped $(TiO_2)_n$	Au doped $(TiO_2)_n$		
n	VIE	-HOMO [a]	-HOMO [b]	VIE
2	9.79	6.91	6.86	9.65
3	9.48	6.75	6.56	9.49
4	8.79	7.81	7.81	9.91
5	9.56	6.91	6.91	9.30
6	9.62	6.94	6.91	9.10

Negative HOMO[a]: α-HOMO and Negative HOMO[b]: β-HOMO

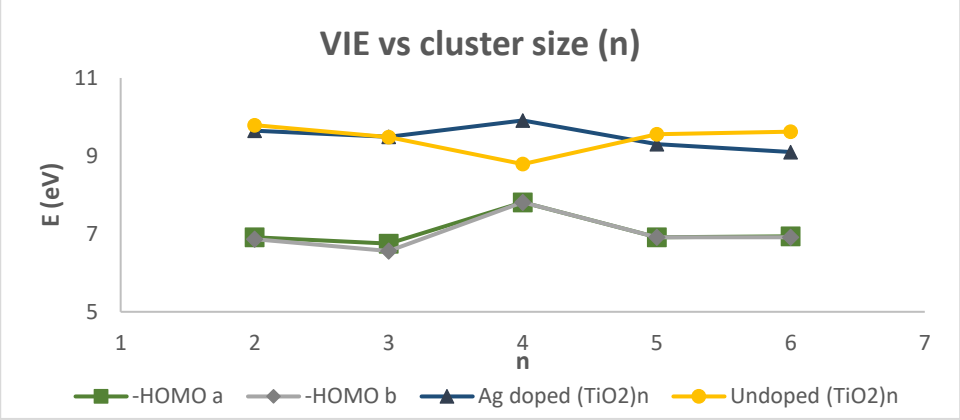

Figure 75: VIE of undoped and Au doped $(TiO_2)_n$ clusters. Negative HOMO[a] (α-HOMO) and Negative HOMO[b] (β-HOMO) of Au doped clusters $(TiO_2)_n$ clusters.

Vertical ionization potential for both Ag and Au doped $(TiO_2)_n$ clusters differ significantly from the negative of the energy of the HOMO within the Koopmans theorem. The difference between VIE and negative of the energy of the HOMO range from 0.98 eV to 2.9 eV. Although the magnitude is not the same, the VEA plot of Ag-doped $(TiO_2)_n$ clusters follow the same trend as negative of the energy of the HOMO.

As stated by Scanlon et al in reference 34, the ionization potential of rutile and anatase, were 7.83 eV and 8.30 eV respectively. Computed ionization potential of Ag and Au doped $(TiO_2)_n$ clusters obtained in this study are above those documented for rutile and anatase [34].

4.5.6 Variation of Chemical Hardness with Cluster Size (n)

The calculated chemical hardness and chemical potential are displayed in Tables 27 and 28. The chemical hardness and chemical potential were calculated using equations 5 and 6, respectively.

Table 27: Chemical hardness for undoped, Ag and Au doped $(TiO_2)_n$ clusters

n	Und.	Ag dop.	Au dop.
2	4.14	3.63	3.41
3	3.51	3.26	3.36
4	3.00	2.83	2.36
5	3.68	2.44	3.01
6	3.46	2.57	2.57

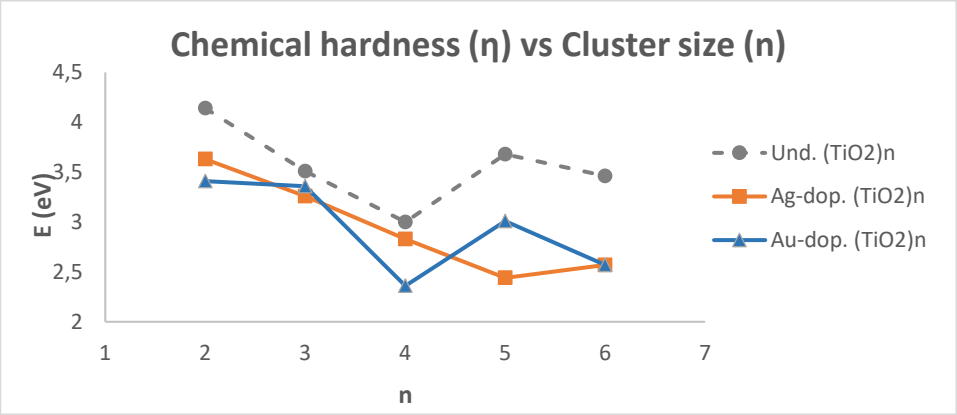

Figure 76: Chemical hardness for undoped, Ag and Au doped clusters.

Figure 76 shows that chemical hardness of Ag doped $(TiO_2)_n$ decreases from 3.63 eV to 2.44 eV as cluster size increases from n = 2 to n = 5. The higher hardness value for. The higher the hardness, more stable is the cluster and worse its reactivity, e.g., 2-4-1-B-d

and 2-11-d clusters are the most stable and less reactive clusters for Ag and Au doped $(TiO_2)_n$ systems respectively. The chemical hardness of the doped clusters is smaller than that of the undoped clusters, as shown in Figure 76.

Chemical potential of undoped $(TiO_2)_n$ clusters is likely to be the same for Ag doped $(TiO_2)_n$ clusters for n = 2 – 4. The chemical potential difference between undoped and Au doped $(TiO_2)_n$ clusters range from 0.17 eV to 1.78 eV. Figure 77 shows the even-odd oscillation for chemical potential of Ag and Au doped $(TiO_2)_n$ clusters until n = 6 where the two doped systems meet.

Table 28: Chemical potential for undoped, Ag and Au doped $(TiO_2)_n$ clusters.

	Und.	Ag dop.	Au dop.
2	5.65	5.54	6.24
3	5.96	6.07	6.13
4	5.78	5.76	7.56
5	5.88	6.87	6.28
6	6.16	6.53	6.53

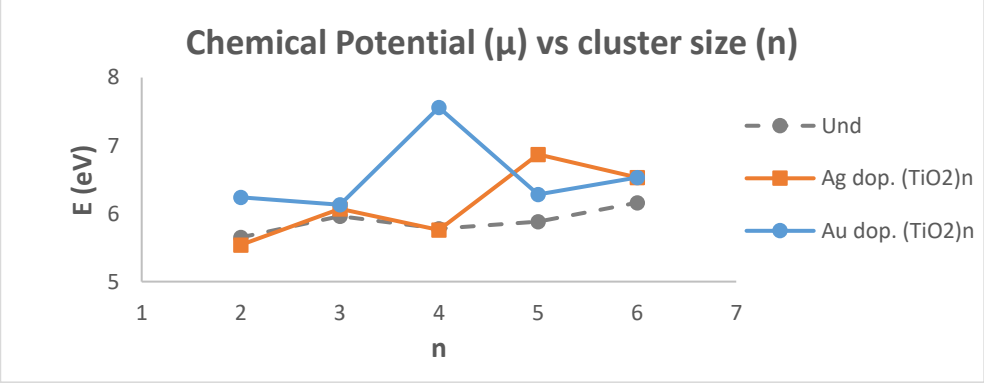

Figure 77: Chemical Potential for undoped, Ag and Au doped $(TiO_2)_n$ clusters

4.5.7 Variation of Lowest Excitation Energies with Cluster Size (n)

Zhao [40] synthesized the Ag and Au doped titanium dioxide nanoparticles. These nanoparticles absorbed over the visible region due to the metal content, e.g., Ag and Au/TiO_2 thin films showed peak around 600 nm.

Table 29: Lowest energy transition and their excitation energies for Ag doped $(TiO_2)_n$ clusters

Ag doped $(TiO_2)_n$					
N	Structure	E (eV)	*f*	Wavelength (nm)	Composition
2	2-4-1-B-d (C_{2v}:$^2A_2$)	0.7092	0	1754.52	98% (HOMO to LUMO)
3	3-8-d (C_1: ^{2}A)	0.8055	0.0005	1539.29	98% (HOMO to LUMO)
4	--				
5	5-4-1-d (C_1: ^{2}A)	0.7431	0.0210	1668.48	88.4% (HOMO-1 to LUMO)
6	6-1-2-d (C_1: ^{2}A)	0.3136	0.0004	3953.76	98%(HOMO to HOMO)
Ag doped $(TiO_2)_n^-$					
2	2-4-1-B-d (C_{2v}: $^1A_1$)	0.3651	0	3395.72	100% (HOMO to LUMO)
3	3-1-1-d (C_{2v}: $^3B_2$)	0.2500	0.0002	4958.67	96.2%(HOMO to LUMO)
4	4-9-1-d (C_S: $^3A''$)	0.1491	0.0001	8317.35	100%(HOMO to LUMO)
5	5-4-1-d (C_1:^{1}A)	2.0223	0.0009	613.09	99.6% (HOMO to LUMO)
6	6-1-2-d (C_1:^{1}A)	2.213	0.0061	560.26	96%(HOMO to LUMO)

Table 30: Lowest energy transition and their excitation energies for Au doped $(TiO_2)_n$ clusters

Au doped $(TiO_2)_n$					
n	Structure	E (eV)	*F*	Wavelength (nm)	Composition
2	2-11-d (C_1: ^{2}A)	1.2829	0.0009	966.43	94.1%(HOMO to LUMO)
3	3-8-d (C_s: $^2A'$)	0.8139	0.0000	1523.30	100%(HOMO to LUMO)
4	4-13-d (C_1:^{2}A)	0.2671	0.0006	4641.79	96% (HOMO-1 to LUMO)
5	5-6-1-d (C_s:$^2A'$)	0.6256	0.0023	1981.91	100% (HOMO to LUMO)
6	6-1-2-d (C_1:^{2}A)	0.2449	0.0025	5063.63	100% (HOMO to LUMO)
Au doped $(TiO_2)_n^-$					
2	2-11-d (C_1: ^{1}A)	0.674	0.0218	1838.69	71.7%(HOMO to LUMO)
3	3-1-1-d (C_{2v}: $^3B_2$)	0.1396	0.0000	8883.76	100%(HOMO to LUMO)
4	4-13-d (C_1:^{3}A)	0.1294	0.0007	9580.27	100%(HOMO to LUMO)
5	5-18-d (C_1:^{3}A)	0.137	0.0000	9048.24	92.8% (HOMO to LUMO)
6	6-1-2-d (C_1:^{1}A)	2.2059	0.0056	562.05	96.3% (HOMO to LUMO)

E (excitation energy) and *f* (oscillator strength)

According to Çakir and Gülseren [2], undoped TiO_2 clusters have electronic transitions from occupied states to unoccupied states, while for doped system (Co, V and Pt) different allowed transitions are observed [2]. Different allow transitions for Ag and Au doped $(TiO_2)_n$ clusters are observed in this study.

Tables 100 - 103 in appendix 8 and Figures 78–81, display the variation of lowest excitation energies and HL gap as cluster size (n) increases. Recall that α, β spatial orbital are for open shell systems, i.e.: doublet, triplet and quartet while and αβ spatial orbital is for closed shell systems, i.e.: singlet.

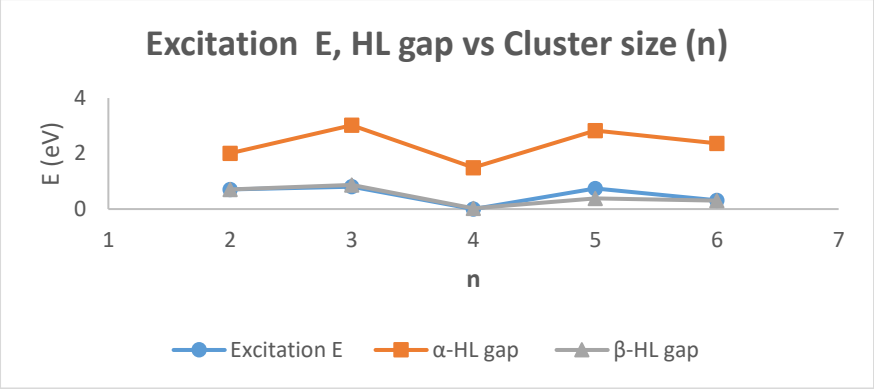

Figure 78: Excitation energy and HL gap for neutral Ag-doped $(TiO_2)_n$ clusters

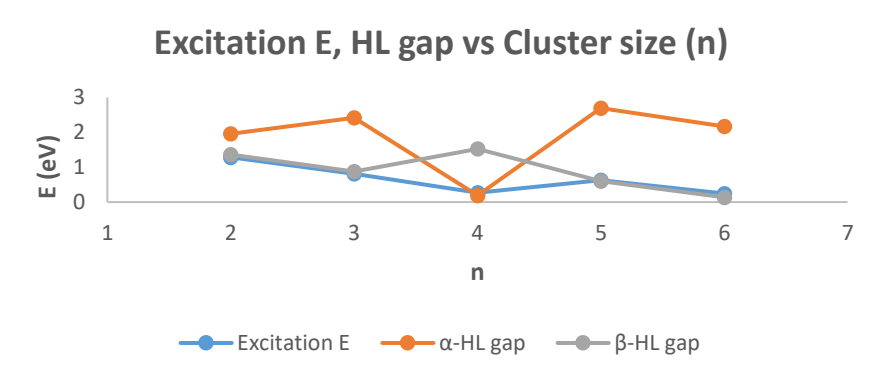

Figure 79: Excitation energy and HL gap for neutral Au-doped $(TiO_2)_n$ clusters

The excitation energies of the lowest doublet states is likely to be the same as the corresponding HL gap of neutral Ag doped $(TiO_2)_n$ clusters, except for n = 5. Although the lowest excitation energy for doublet-doublet transition is far from the α-HL gap in a range of 1.30 - 2.45 eV, the two lines follow almost the same trend, i.e.: even-odd oscillation. In case of neutral Au doped $(TiO_2)_n$ clusters, the excitation energies of the lowest doublet excited states is likely to be the same as the corresponding β-HL gap for neutral Au doped $(TiO_2)_n$ clusters, except for n = 4, but equal the α-HL gap of the cluster with the same size.

Next are the Figure 80 and 81, that show how the lowest excitation energy and HL gap vary as the cluster size increase from n = 2 to n = 6. The respective values are presented in Table 102 and 103 in Appendix 8. It should be noted that excitation energy as well as the HL gap are constant from n = 3 to n = 5 for Au doped $(TiO_2)_n$ clusters as shown in Figure 81.

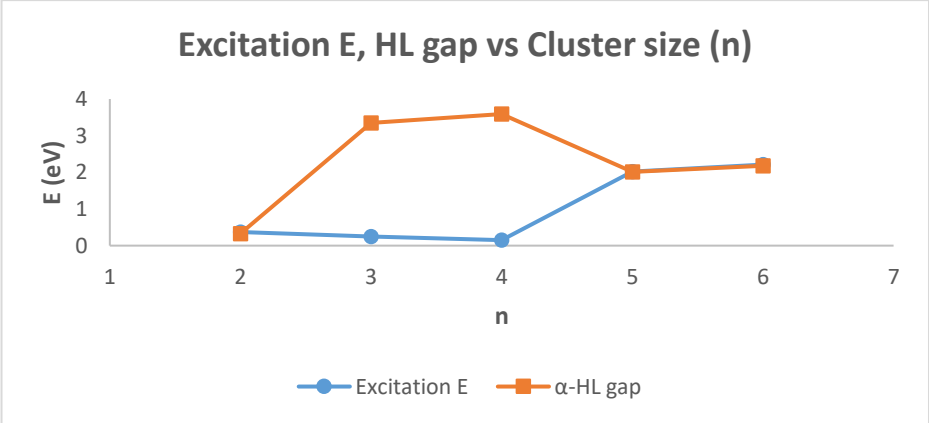

Figure 80: Excitation energy and HL gap for anionic Ag doped $(TiO_2)_n$ clusters

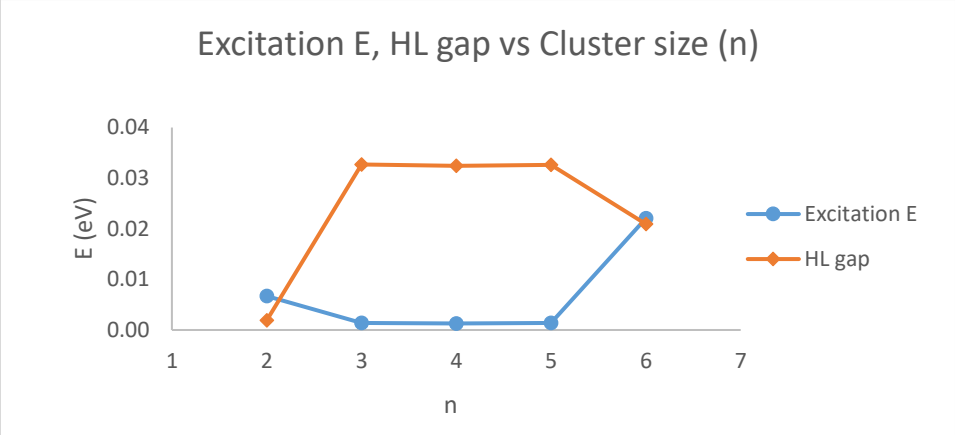

Figure 81: Excitation energy and HL gap for anionic Au doped $(TiO_2)_n$ clusters

4.5.8 Variation of Water Interaction with Cluster Size (n)

Water interaction with TiO_2 is a topic of great interest. TiO_2 is used in photocatalytic water splitting processes for the generation of hydrogen (H_2) and in heterogeneous catalysis for water and air purification [9 and 10]. The binding energy for the adsorption of water on rutile (100) surface which is 0.73 eV [2] as shown in Figure 82.

The strength of the interaction of water molecules with TiO_2 clusters to form complexes is influenced by the binding site and its surroundings [2 and 37]. In this work, the attachment of a H_2O molecule close to the dopant atom, except for Au-doping $(TiO_2)_2$, results either in H bonding or water dissociation adsorption. Au doped $(TiO_2)_n$ clusters are more compressed, their bond angles are broken prior to H_2O dissociation. For most of the Ag doped $(TiO_2)_n$ clusters, the Ag dopant atom is one-fold coordinated, thereby allowing H - bonding to be formed.

The binding energy (E_b) of a cluster is a useful measure of its stability and it was calculated using equation 8. The total energy of Ag/Au doped $(TiO_2)_n(H_2O)$ complexes is smaller than the sum of the energy Ag/Au doped $(TiO_2)_n$ clusters and energy of one water

molecule. Therefore, the E_b of molecular adsorption of water on Ag and Au doped $(TiO_2)_n(H_2O)$ complexes is larger in magnitude than the adsorption of H_2O molecule on the clean rutile surface, but has a negative sign ($E_b < 0$), that indicates that the reaction is exothermic. E_b values range from -1.44 eV to -1.00 eV.

The larger the E_b value, the larger the stability of the cluster. Binding energy of Au doped TiO_2 clusters water complexes, oscillates smoothly in an even-odd manner as the cluster size increases as shown in Figure 82. The molecular adsorption of water on Ag doped 4-21-d cluster and Au doped 3-8-d cluster have the lowest binding energy, so the less stable and more reactive Ag and Au doped $(TiO_2)_n$ water complexes, respectively.

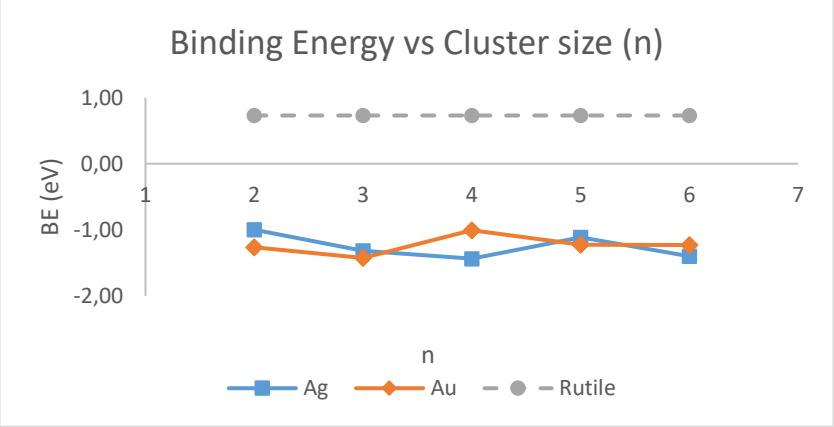

Figure 82: Binding energy of Ag, Au doped $(TiO_2)_n(H_2O)$ complexes

CHAPTER 5 CONCLUSION

A computational study of the geometry and electronic structure of Ag and Au doped $(TiO_2)_n$ clusters (n = 2 - 6) have been presented in this work. The research started with geometry optimization of well-known undoped clusters. However, the lowest energy structures reported in this thesis are not in agreement with few of the reports in the literature. The discrepancy observed could be due to different methods and basis sets applied in other studies, noting however, that the initial calibration study carried out in this work agree quite well with the results obtained using sophisticated theoretical approach. A summary of the similarities and contradictions between this work and those found in the literature for the undoped clusters is presented below in Table 31.

Table 31: Comparison of ground state geometries of undoped clusters as obtained in this study compared to the ones found in the literature.

n	References	
	Agreement	Disagreement
2	2, 3, 15, 25, 27	28
3	1, 2, 3, 25	27
4	2, 25, 27	1, 3
5	1, 2, 3	25, 27
6	1, 2, 3, 25	27

More than 200 doped structures were successfully optimized. The geometry, stability, and electronic properties of some of the doped clusters exhibit size dependence. Bond distances in the clusters vary from 1.33 Å to 2.80 Å. The O - O bonds are generally shorter than the M-Ti bonds where M stands for Ag or Au atom. The Au doped $(TiO_2)_n$ clusters are more compressed than the Ag doped $(TiO_2)_n$ clusters. The dopant atoms prefer to bind to oxygen atom rather than binding the Ti atoms. The order of stability of neutral and anionic species, differs among doped systems.

The introduction of Ag and Au dopants atoms to undoped $(TiO_2)_n$ clusters, reduced the IP to less than 0.62 eV, except for n = 4. Even then, those values are above the values reported for bulk rutile/anatase. The VEDE, AEA and E_b of doped clusters gradually increase as the cluster size increases. The AEA of cluster size with n = 5 and n = 6 mimic the EA value of the bulk material. The optical spectra of doped $(TiO_2)_n$ clusters occurred beyond the visible region, except for Ag doped 5-4-1-d (C_1:^{1}A), 6-1-2-d (C_1:^{1}A) clusters and Au doped 6-1-2-d (C_1:^{1}A) cluster, where lowest excitations occurred in the region between 560 - 613 nm.

The Ag and Au atoms give a considerable contribution to the HOMO of corresponding neutral doped $(TiO_2)_n$ clusters, in contrast to the anionic doped $(TiO_2)_n$ clusters. Dopants atoms, in most of the cases, give very low or no contribution to LUMO. The extra electron of the anion is strongly localized on oxygen atoms for both Ag and Au doped $(TiO_2)_n$ clusters.

Finally, it is noteworthy that in this study, the bulk values were not achieved for electronic properties such as the electron affinity, HL gap, chemical hardness and chemical potential for Ag and Au doped $(TiO_2)_n$ clusters (n = 2-6). Further, the results obtained in this research do not quantitatively give the magnitude of the band gap, when compared to Ag and Au doped TiO_2 synthesized experimentally, due to the well-known deficiency of the GGA method that was used in this study. However, the flatness obtained for the HL gap of anionic Au doped $(TiO_2)_n$ (n = 3-5) imitated the bulk material.

RECOMMENDATION

The electronic properties such as electron affinity, band gap and excitation energies of Ag and Au doped $(TiO_2)_n$ clusters (n = 2-6) did not converge to the bulk values in this study. Therefore, it is recommended that computational studies be carried out the Ag/Au doped TiO_2 clusters beyond the n = 6 limit. The time allocated for this research did not permit such extension.

It is also recommended here, that synthesis and characterization of the Ag and Au doped $(TiO_2)_n$ clusters be undertaken. Studies on the doped bulk material are available. More studies are required in the cluster synthesis and in the comparison of the cluster properties with the bulk material. And after that, with most appropriated engineering procedures, new devices may be designed, constructed and applied to the different promissory fields.

REFERENCES

[1] Weicham M, Xiaowei S, Fagiani M, Debnath S, Gewinner S, Neumark D. Gas phase vibrational spectroscopy of cold $(TiO_2)^-_n$ (n=3-8) cluster, Journal of Chemical Physics. 2016; 144. Available from: DOI: 10.1063/1.4942194

[2] Çakir D, Gülseren O. Ab initio study of neutral $(TiO_2)_n$ clusters and their interactions with water and transition metal atoms. Journal of Physics Condensed Matter, 2012, 144,124308-1. Available from: DOI: 10.1088/0953 8984/24/30/305301

[3] Qu Z, Kroes G. Theoretical Study of the electronic structure and stability of Titanium Dioxide clusters $(TiO_2)_n$ with n= 1 – 9. J. The Journal of Physical Chemistry B. 2006; 110 8998 -9007.

[4] Diebold U. Applications of TiO_2. Surface Science Reports. 2003; 48 (53- 229)

[5] Wu H, Wang L. Electronic Structure of Titanium Oxide Clusters: TiO_y. The Journal of Chemical Physics 107, 8221 (1997). Available from: DOI: 10.1063/1.475026

[6] Zaleska A. Doped-TiO_2: a review. DOI: 10.2174/187221208786306289

[7] Pranowo H, Kartini I. Physical Characterization of Ni (II) Doped TiO_2 Nanocrystal by Sol-gel process. Indonesia Journal of Chemistry. 2011; 11(135-139)

[8] Daniel L, Uahengo V, Determination of Optimal Heat Treatment Temperature for the Fabrication of Ag/TiO2 Composite Thin Films Using Molecular Precursor Method (MPM), International Journal of Current Research and Academic Review . 2015; 3 (2347-3215).

[9] Shevlin S, Woodley S. Electronic and Optical Properties of Doped and Undoped $(TiO_2)_n$ Nanoparticles. Journal of Physical Chemistry C. 2010; 114 (17333 – 17343).

[10] Ni M, Leung-Dennis K, Leung Y, Sumathy K. A Review and Recent Developments in Photocatalytic Water-Splitting Using TiO_2 for Hydrogen Production Renewable and Sustainable Energy. Rev. Sci. direct, Available from: DOI: 10.1016/j.rser.2005.01.009

[11] Wang Y, Zhang R, Li J, Lin S. First-principles Study on Transition Metal-doped Anatase TiO_2. Nanoscale Research Letter. 2014; 9 (46-AA).

[12] Umebayashi T, Yamaki T, Itoh H, Asai K. Analysis of Electronic Structures of 3d Transitions Metal-doped TiO_2 Based on Band Calculations, Journal of Physical Chemistry Solids. 2002; 63 (1909±1920). Available from: DOI: 10.1016/S0022-3697(02)00177-4

[13] Guo M, Du J. First Principle Study of Electronic Structures and Optical Properties of Cu, Ag and Au - doped Anatase $(TiO_2)_n$. Physica B: Condensed Matter. 2012; 407 (1003-1007)

[14] Auvinen S. Computational Modeling of the Properties of TiO_2 Nanoparticles. Dissertation. Lappeenranta University of Technology; 2013. DOI: 10024/94030/isbn9789522655455

[15] Zhai H, Wang L. Probing the Electronic Structure and Band Gap Evolution of Titanium Oxide Clusters $(TiO_2)_n^-$ (n = 1−10). Using Photoelectron Spectroscopy. Journal of the American Chemistry Society. 2007; 129 (3022-3026).

[16] Glaspell G. and Manivannan A. Sol–Gel Synthesis and Magnetic Studies of Titanium Dioxide Doped with 10% M (M=Fe, Mn and Ni). Journal of Cluster Science.16, 4 (2005; 16, 4. Available from: DOI: 10.1007/s10876-005-0023-z

[17] Weichman M, Debnath S, Kelly J, Gewinner S, Schöllkopf W, Neumark D, Asmis K. Dissociative Water Adsorption on Gas-Phase Titanium Dioxide Cluster Anions Probed with Infrared Photodissociation Spectroscopy. Topics in Catalysis; Available from: DOI: 10.1007/s11244-017-0863-4

[18] Chen M, Straatsma T, Dixon D. Molecular and Dissociative Adsorption of Water on $(TiO_2)_n$ Clusters, n = 1 to 4, Journal of Physical Chemistry *A*. Available from: DOI: 10.1021/acs.jpca.5b07697

[19] Berardo E, Hu H, Van Dam H, Shevlin S, Woodley S, Kowalski K, Zwijnenburg M. Describing Excited State Relaxation and Localization in $TiO_{110.}$ Journal of Chemistry Theory and Computation. Available from: DOI: 10.1021/ct500787x

[20] Qu Z, Kroes G. Theoretical Study of Stable, Defect-Free $(TiO_2)_n$ Nanoparticles with n= 10 – 16, Journal of Physical Chemistry B. 2007; 111 (16808-16817).

[21] Li S, Dixon D. Molecular Structures and Energies of the $(TiO_2)_n$ (n=1-4) Clusters and their anions. Journal of Physical Chemistry A. 2008; 112 (6646-6666). Available from: DOI: 10.1021/JP800170q

[22] Frisch M, Trucks G, Schlegel H, Scuseria G, Robb M, Cheeseman J, Vreven T, Pople J. Gaussian, Inc., Gaussian 03, Revision C.02, Wallingford CT, 2004. https://gaussian.com/g03citation/. (Accessed 9th August 2019)

[23] Frisch M, Trucks G, Schlegel H, Scuseria G, Robb M, Cheeseman J, Scalmani G, Fox D. Gaussian, inc et al. Gaussian 09, Revision A.02, Wallingford CT, 2016. https://gaussian.com/g09citation/. (Accessed 9th August 2019)

[24] Frisch A, Hratchian H, Dennington D, Keith T, Millam J. Gaussview. https://www.google.com/url?sa=t&rct=j&q=&esrc=s&source=web&cd=7&cad=rja&uact=8&ved=2ahUKEwj6n4u19vTjAhW0qHEKHU15AF8QFjAGegQIC-RAC&url=https%3A%2F%2Fwiki.crc.nd.edu%2Fw%2Fimages%2Fd%2Fd7%2FGaussview-5-ref.pdf&usg=AOvVaw2eqnXUn6X_ezQnSany7oYu (Accessed 9th August 2019)

[25] Chen M, Dixon D, Tree Growth – 0 for the Study of the Structure of Small $(TiO_2)_n$ Nanoclusters, for n = 2 - 13. Journal of Chemical Theory and Computation. Available from: DOI: 10.1021/ct400105c.

[26] Archibong E, Amant S. Molecular Structure of the AlO_2 Dimer, Al_2O_4. Journal of Physical Chemistry A 1998; 102, 34

[27] Hamad S, Catlow C, Woodley S, Lago S, Mejías J. Structure and Stability of Small TiO_2 Nanoparticles. Journal of Physical Chemistry. *B*, 2005, *109* (33), pp 15741–15748 DOI: 10.1021/jp0521914

[28] Albaret T, Finocchi F and Nogueira C Density Functional Study of stoichiometry and O-rich titanium oxygen clusters, Journal of Physical Chemistry 2000; 113 2238, Available from: DOI : 10.1063/1.482038

[29] Pritchard B, Altarawy D, Didier B, Gibson T, Windus T. A New Basis Set Exchange: An Open, Up-to-date Resource for the Molecular Sciences Community. J. Chem. Inf. Model. 2019, 59(11), 4814-4820, doi:10.1021/acs.jcim.9b00725.

[30] Kim J, Weichman M, Daniel M, Structural Isomers of Ti_2O_4 and Zr_2O_4 Anions Identified by Slow Photoelectron Velocity-Map Imaging Spectroscopy. Journal of the American Chemical Society. 2014; 136 (7159−7168). Available from: DOI: /10.1021/ja502713v|.

[31] Hagfeldt A, Bergstrom R, Siegbahn H, Lunell S. Structure and Stability of Small Titaium/Oxygen Cluster Studied by ab Initio Quantum Chemical Calculations, Journal of Physical Chemistry 1993; 97 (12725 – 12730)

[32] Hudson R, Falcinella A, Metha G. Molecular geometries and relative stability of titanium oxide and gold-titanium oxide clusters, Chemical Physics 2016;477 (8–18), Available from: DOI: 10.1016/j.chemphys.2016.08.006

[33] Woodley S, Hamad S, Mejías J, Catlow C. Properties of small TiO_2, ZrO_2 and HfO_2 nanoparticles. Journal of Materials Chemistry. (2006); 16, (1927-1933). Available from: DOI: 10.1039/b600662k

[34] Scanlon D, Dunnill C, Buckeridge J, Shevlin S. Band alignment of rutile and anatase TiO_2. Natural Materials. 2013 DOI: 10.1038/NMAT3697

[35] Chiodo L, Garcia-Lastra J, Mowbray D, Iacomino A, Rubio A. Tailoring electronic and optical properties of TiO_2: nanostructuring, doping and molecular-oxide interactions. World Scientific Review http://nano bio.ehu.es/files/articles/Chiodo__2010_586.pdf (Accessed from 14th May 2019)

[36] Tsuneda T, Song J, Suzuki S, On Koopmans' theorem in density functional theory. The Journal of Chemical Physics (2010) 133(17):174101. Available from: DOI: 10.1063/1.3491272.

[37] Lindan P, Harrison N. Mixed Dissociative and Molecular Adsorption of Water on the Rutile (110) Surface. The American Physical Society 0031-9007/98/80(4)/76

[38] Cao F, Tan K. Lin M. Zhang Q. A Density Functional Study of N-Doped TiO_2 Anatase Cluster. Chinese Journal of Structural Chemistry. 2009; 28, 8 (998-1002)

[39] Wang X, Wang F, Shang J, Zhou Y. Ab initio studies of Nb doping effect on the formation of oxygen vacancy in rutile TiO_2. J Physics and Chemistry of Solids. 2012; 73 (84–93)

[40] Zhao G, Kozuka H, Yoko T. Sol-gel preparation and photoelectrochemical properties of TiO_2 films containing Au and Ag metal particles, Thin Solid Films 277 (1996) 147, Available from: DOI: 10.1016/0040-6090(95)080066

[41] Weinhold F, Landis C and Glendening. What is NBO analysis and how is it useful. International Reviews in Physical Chemistry (2016) 35, 399-400. Available from: DOI: 10..1080/0144235X.2016.1192262

[42] Mogal S, Gandhi V, Mishra M, Tripathi S, Joshi P, Shah D. Single-Step Synthesis of Silver-Doped Titanium Dioxide: Influence of Silver on Structural, Textural, and Photocatalytic Properties. International Journal of Photoenergy. Available from: DOI:10.1155/2008/628713

[43] Peerakiatkhajorn P, Chawengkijwanich C, Onreabroy W, Chiarakorn S. Novel Photocatalytic Ag/TiO2 Thin Film on Polyvinyl Chloride for gaseous BTEX Treatment. Materials Science Forum. DOI:10.4028/www.scientific.net/MSF.712.133

[44] Mohite V, Mahadik M, Kumbhar S, Hunge Y, Kim J, Moholkar A, Rajpure K, Bhosale C. Photoelectrocatalytic degradation of benzoic acid using Au doped TiO2 thin

films. Available from: DOI: 10.1016/j.jphotobiol.2014.12.004

[45] Gültekin A, and Mehmetbey K. Effect of Au Nanoparticles Doping on the Properties of TiO_2 Thin Films. Available from: DOI: org/10.5755/j01.ms.20.1.3709.

APPENDIX

1 Cluster size n = 2

1.1 Ti_2O_4

Table 32: Total energy (E_T, a.u.) relative Energy (ΔE, eV), adiabatic electron detachment energy (AEDE, eV) for neutral and anionic Ti_2O_4 clusters at BPW91/6-311+G (d). PG: Point group

Structure	PG	Ti_2O_4			$Ti_2O_4^-$			
		State	E_T	ΔE	State	E_T	ΔE	AEDE
2-1-u	C_{2h}	^1A_g	-418.0060	0.00	^2A_g	-418.0680	0.00	1.69
2-2-u	C_{2v}	$^1A_1$	-417.9955	0.29	$^2A_1$	-418.0667	0.04	1.94
2-3-u	C_{3v}	$^1A_1$	-417.9810	0.68	$^2A_1$	-418.0538	0.39	1.98
2-4-u	C_{2v}	$^1A_1$	-417.9016	2.84	$^2A_1$	-418.0250	1.17	3.36
2-5-u	C_s	$^1A'$	-417.8300	4.79	$^2A''$	-417.8557	5.78	5.31
2-6-u	C_1	^1A	-417.8111	5.30	^1A	Optimizes to 2-4-u		5.82
2-7-u	C_2	^1A	-417.7237	7.68	^2B	-417.8051	7.13	2.22
2-8-u	C_1	^1A	Optimizes to 2-1-u					
2-9-u		Allocation failure for numerical quadrature						
2-10-u	D_{2h}	^1A_g (2)	-417.7895	5.89	^2A_g	Optimizes to 2-3-u		

Table 33: VEDE (eV) for $Ti_2O_4^-$ at BPW91/6-311+G (d).

Cluster	PG	State	VEDE
2-1-u	C_{2h}	$^1A_g \rightarrow {}^2A_g$	1.97
2-2-u	C_{2v}	$^1A_1 \rightarrow {}^2A_1$	2.22
2-3-u	C_{3v}	$^1A_1 \rightarrow {}^2A_1$	2.18

Table 34: HOMO (a.u.), LUMO (a.u.) and HL Gap (eV) for Neutral and Anionic $(TiO_2)_2$ Cluster.

DFT functional	Neutral			Anion		
	HOMO	LUMO	HL gap	HOMO	LUMO	HL gap
B3LYP	-0.3010	-0.118	5.01			
BPW91	-0.252	-0.130	3.32	0.006	0.018	0.33
BP86	-0.257	-0.135	3.32	0.001	0.013	0.33
B3P86	-0.321	-0.124	5.36			
PBE	-0.252	-0.134	3.21	0.006	0.018	0.33
MP2	-0.443	-0.029	11.27	-0.062	0.067	3.51
B3PW91	-0.300	-0.105	5.30			

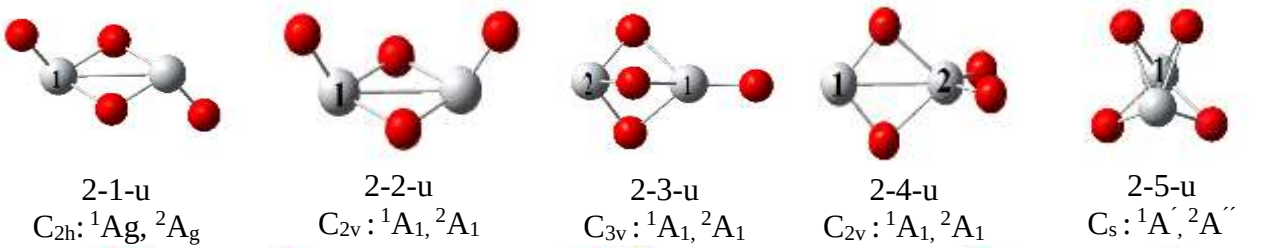

2-1-u C_{2h}: ^1Ag, ^2A_g | 2-2-u C_{2v} : $^1A_1$, $^2A_1$ | 2-3-u C_{3v} : $^1A_1$, $^2A_1$ | 2-4-u C_{2v} : $^1A_1$, $^2A_1$ | 2-5-u C_s : $^1A'$, $^2A''$

2-6-u C_1 : $^1A'$ | 2-7-u C_2 : ^1A, ^2B | 2-8-u | 2-9-u | 2-10-u D_{2h}: ^1Ag, ^2A_g

Figure 83: Structures of the $(TiO_2)_2$ clusters. Structure name, point group and state are displayed bellow each structure. The Ti and O atoms, are indicated by gray and red spheres respectively. Labels on Ti atom indicate the non-equivalent Ti atoms.

1.2 $TiAgO_4$

Table 35: Total energy (E_T, a.u.) and relative energy (ΔE, eV) for neutral and anionic $TiAgO_4$ at BPW91/6-311+G (d). Number of imaginary frequencies are in curved bracket. PG: Point group

Structure	PG	$TiAgO_4$			$TiAgO_4^-$		
		State	E_T	ΔE	State	E_T	ΔE
2-1-1-d	C_1	^2A	-506.3757	2.02	$^1A'$ (1)	-506.5151	0.93
		^4A	-506.3709	2.15	^3A	-506.5254	0.65
2-2-1-d		^2A	Optimizes to 2-1-1-d				
2-3-1-d		^2A	Convergence failure				
2-3-2-d		^2A	Optimizes to 2-4-1-A-d				
2-4-1-A-d	C_{2v}	$^2A_1$	-506.3810	1.87	$^1A_1$	Optimizes to 2-4-1-B-d	
2-4-1-B-d	C_{2v}	$^2A_2$	-506.4499	0.00	$^1A_1$	-506.5492	0.00
		$^4B_2$	-504.3778	56.38	^3A	Optimizes to 2-11-d	
2-4-1-C-d	C_{2v}	$^2A_1$	-506.3791	1.93	$^1A_1$	Optimizes to 2-4-1-B-d	
2-4-2-d		^2A	Optimizes to 2-1-1-d				
2-5-1-d		^2A	Optimizes to 2-4-1-B-d				
2-6-2-d	C_1	^2A	-506.4173	0.89	^1A	Originates 2-12-d	
2-7-1-d		^2A	Convergence failure				
2-10-1-d		^2A	Optimizes to 2-4-1-d				
2-11-d	C_1	^2A	-506.4463	0.10	^1A	-506.5395	0.26
		^4A	Optimizes to 2-4-1-B-d		^3A	-506.5241	0.68
2-11-d	C_s	$^2A''$	-506.4466	0.09	^1A	Optimizes to 2-4-1-B-d	
2-12-d	C_1	^2A	-506.3441	2.88	^1A	-506.5437	0.15
					^3A	Optimizes to 2-11-d	

Table 36: New structures of $TiAgO_4$

Doped Structure	Undoped Structure	Doped Position	Unstable
2-12-d	2-6-u	1	--

Table 37: Total energy (E_T, au) and relative Energy (ΔE, eV) for neutral and anionic $TiAgO_4$ clusters at CCSD (T) // BPW91/6-311+G (d). PG: Point group

Structure	PG	$TiAgO_4$			$TiAgO_4^-$		
		State	E_T	ΔE	State	E_T	ΔE
2-4-1-B-d	C_{2v}	$^2A_2$	-504.4476	0.00	$^1A_1$	-504.5341	0.00
2-11-d	C_1	^2A	-504.4398	0.21	^1A	-504.5084	0.70

Table 38: AEDE (eV) and VEDE (eV) for $TiAgO_4^-$ clusters at BPW91/6-311+G (d) and CCSD (T) // BPW91.

		BPW91		
Structure	PG	State	AEDE	
2-1-1-d	C_1	$^3A \rightarrow {}^4A$	4.20	
2-4-1-B-d	C_{2v}	$^1A_1 \rightarrow {}^2A_1$	2.70	
2-11-d	C_1	$^1A \rightarrow {}^2A$	2.54	
2-12-d	C_1	$^1A \rightarrow {}^2A$	5.43	
		CCSD(T)//BPW91		
Structure	PG	State	AEDE	VEDE
2-4-1-B-d	C_{2v}	$^1A_1 \rightarrow {}^2A_1$	2.35	3.28
2-11-d	C_1	$^1A \rightarrow {}^2A$	1.87	

Table 39: Total energy (E_T, a.u.) and relative Energy (ΔE, eV) for neutral and anionic $TiAgO_4$ structures at B3LYP/6-311+ G (d). PG: Point group

Structure	PG	$TiAgO_4$			$TiAgO_4^-$		
		State	E_T	ΔE	State	E_T	ΔE
2-1-1-d	C_1	^2A	-506.2733	2.56	^1A	-506.4114	1.56
2-4-1-B-b	C_{2v}	$^2A_2$	-506.3675	0.00	$^1A_1$	-506.4689	0.00
2-11-d	C_1	^2A	-506.3644	0.08	^1A	Optimizes to 2-4-1-B-d	
2-12-d	C_1	^2A	-506.2517	3.15	^1A	-506.4614	0.20

Table 40: Total energy (E_T, a.u.) calculated at different DFT functional and MP2 for neutral and anionic 2-4-1-B-b structure.

Method	(C_{2v} : $^2A_2$)	(C_{2v} : $^1A_1$)
BPW91 [a]	-506.4499	-506.5492
BPW91 [b]	-506.4619	-506.5596
BPW91 [c]	-506.4649	-506.5621
B3PW91 [a]	-506.2900	-506.3868
B3P86 [a]	-507.6072	-507.7265
BP86 [a]	-506.5035	-506.6094
B3LYP [a]	-506.3675	-506.4689
B3LYP [b]	-506.3801	-506.4800
B3LYP [c]	-506.3833	-506.4827
BLYP [a]	-506.2545	-506.3556
PBE1PBE [a]	-505.9462	-506.0393
M06-L [a]	-506.4137	-506.5027
MP2 [a]	-504.4298	-504.5121

[a] /6-311+G (d) [b] /6-311+G (2d) and [c] /6-311+G (2df)

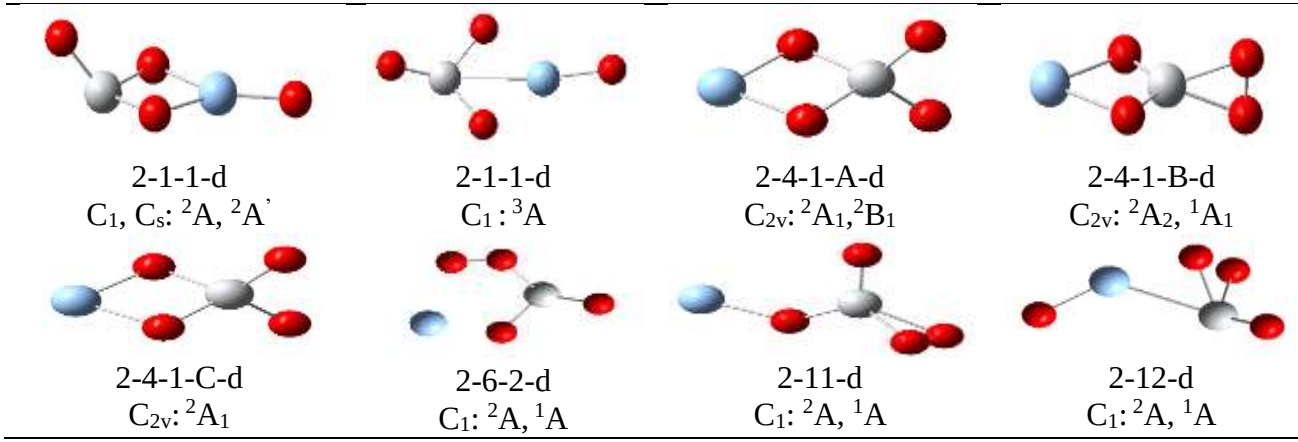

Figure 84: Structures of the $TiAgO_4$ clusters. Structure name, point group and state are displayed under each structure. The Ti, O, and Ag atoms are indicated by gray, red and blue spheres respectively.

1.3 $TiAuO_4$

Table 41: Total energy (E_T, au) and relative Energy (ΔE, eV) for neutral and anionic $TiAuO_4$ structures at BPW91/6-311+G (d). Number of imaginary frequencies are in curved bracket. PG: Point group

Isomer	PG	$TiAuO_4$			$TiAuO_4^-$		
		State	E_T	ΔE	State	E_T	ΔE
2-1-1-d	C_s	$^2A'$	-495.1945	0.93	$^1A'$	-495.3355	0.09
		^4A	Break of symmetry		^3A (1)	-495.3327	0.16
2-3-1-d		^2A	Convergence failure				
2-3-2-d		^2A	Convergence failure				
2-4-1-A-d	C_{2v}	$^2B_2$	-495.0791	4.07	$^1A_1$	-495.2944	1.21
		$^4A_1$	-495.1647	1.74	$^3A_2$	-495.2352	2.82
2-4-1-B-d	C_{2v}	$^2B_1$	-495.1950	0.92	$^1A_1$	-495.3285	0.28
		$^4B_2$	-495.1833	1.24	^3A	SCF convergence prob-lem	
2-11-d	C_1	^2A	-495.2287	0.00	^1A	-495.3387	**0.00**
2-11-d	C_1	^4A	-495.1710	1.57	^3A	-495.3262	0.34

Table 42: (Table 41 cont.) Total energy (E_T, a.u.) Point group (PG) and relative Energy (ΔE, eV) for neutral and anionic $TiAuO_4$ structures at BPW91/6-311+G (d). PG: Point group

Isomer	PG	$TiAuO_4$			$TiAuO_4^-$		
		State	E_T	ΔE	State	E_T	ΔE
2-11-d	C_s	$^2A''$	-495.2289	**0.00**	^1A	Breaks of symmetry	
2-12-d	C_1	^2A	-495.1605	1.86	^1A	FormBX had a problem	
		^4A	Optimizes to 2-14-d				
2-13-d	C_1	^2A	-495.2243	0.12	^1A	-495.3340	0.13
			-495.1744	1.48	^3A	-495.3313	0.20
2-13-d	C_s				$^1A'$	-495.3342	0.12
2-14-d	C_1	^2A	Error termination				
		^4A	-495.1009	3.48			

Table 43: New structures of $TiAgO_4$

Doped structure	Undoped Structure	Doped Position	Unstable
2-14-d	--	--	2-12-d (C_1:^4A)

Table 44: AEDE (eV) of $TiAuO_4^-$ clusters, calculated at BPW91/6-311+G (d) basis set and SDD effective core potential

Isomer	PG	State	AEDE	Isomer	PG	State	AEDE
2-1-1-d	C_s	$^2A'\rightarrow{}^1A'$	3.84	2-4-1-B-d	C_{2v}	$^2B_1\rightarrow{}^1A_1$	3.63
2-4-1-A-d	C_{2v}	$^2B_2\rightarrow{}^1A_1$	5.86	2-11-d	C_1	$^2A\rightarrow{}^1A$	2.99
2-4-1-A-d	C_{2v}	$^4A_1\rightarrow{}^3A_2$	1.92	2-11-d	C_1	$^4A\rightarrow{}^3A$	4.22

Table 45: VEDE (eV) for $TiAgO_4^-$ clusters at BPW91/6-311+G (d)

Structure	PG	State	VEDE	Structure	PG	State	VEDE
2-1-1-d	C_s	$^1A' \rightarrow {}^2A'$	4.07	2-13-d	C_s	$^1A' \rightarrow {}^2A''$	3.66
2-4-1-B-d	C_{2v}	$^1A_1 \rightarrow {}^2A_1$	5.83	2-13-d	C_s	$^3A' \rightarrow {}^2A'$	3.54
2-11-d	C_1	$^1A \rightarrow {}^2A$	3.40			$^3A' \rightarrow {}^4A'$	4.37
		$^3A \rightarrow {}^4A$	4.28				

Table 46: Total energy (E_T, a.u.) and relative Energy (ΔE, eV) for neutral and anionic $TiAgO_4$ clusters at CCSD (T) // BPW91/6-311+G (d)

Structure	PG	$TiAuO_4$			$TiAuO_4^-$		
		State	E_T	ΔE	State	E_T	ΔE
2-1-1-d	C_s				$^1A'$	-493.2702	0.02
2-4-1-B-d	C_{2v}				$^1A_1$	-493.2682	0.07
2-11-d	C_1	^2A	-493.1753	0.00	^1A	-493.2632	0.20
2-11-d	C_s	$^2A''$	-493.1754	0.00	^3A	-493.2613	0.26
2-13-d	C_s				$^1A'$	-493.2708	0.00
2-13-d	C_1	^2A	-493.1702	0.14	^3A	-493.2641	0.18

Table 47: AEDE (eV) and VEDE (eV) were calculated at CCSD (T) // BPW91/6-311+G (d) for neutral and anionic $TiAgO_4$ structures

Isomer	PG	State	VEDE	AEDE
2-1-1-d	C_s	$^1A' \rightarrow {}^2A'$	4.16	
2-4-1-B-d	C_{2v}	$^1A_1 \rightarrow {}^2A_2$	3.63	
2-11-d	C_1	$^1A \rightarrow {}^2A$	2.85	2.39
2-11-d	C_1	$^3A \rightarrow {}^2A$	2.57	
		$^3A \rightarrow {}^4A$	4.39	
2-13-d	C_s	$^1A' \rightarrow {}^2A''$	3.71	2.74
2-13-d	C_1	$^3A \rightarrow {}^2A$	3.20	
		$^3A \rightarrow {}^4A$	4.60	

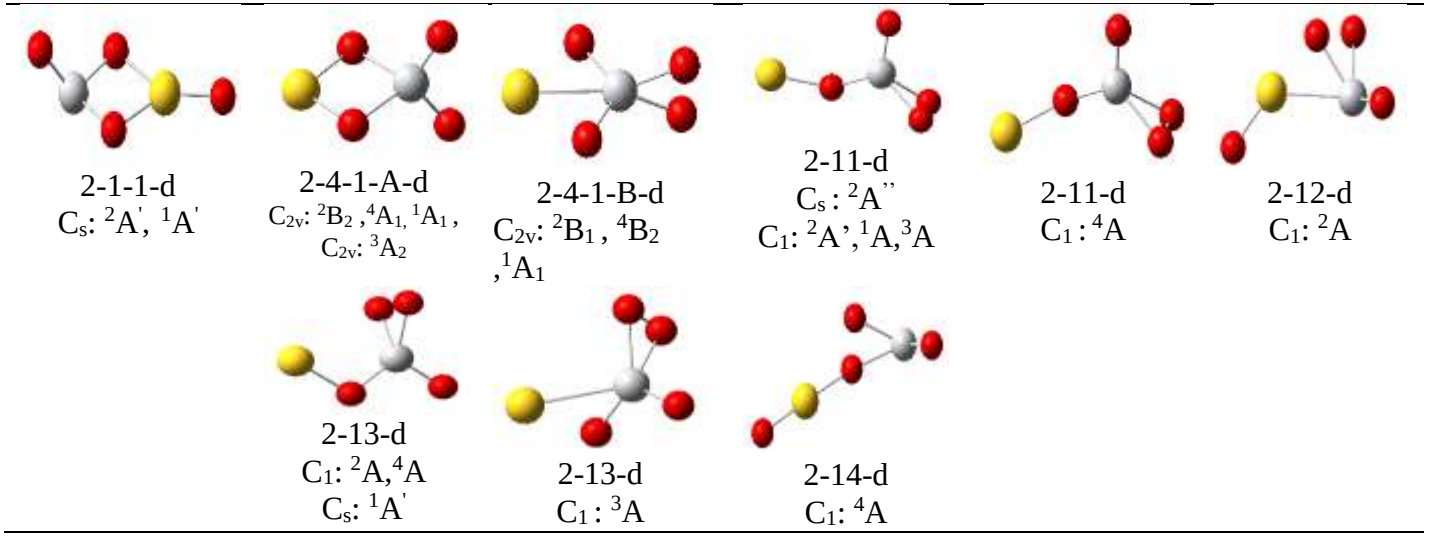

Figure 85: Structures of the $TiAuO_4$ clusters. Structure name, point group and state are displayed bellow each structure. The Ti, O, and Au atoms are indicated by gray, red and yellow spheres respectively.

2 Cluster size n = 3

2.1 Ti_3O_6

Table 48: Total energy (E_T, au) relative Energy (ΔE, eV), adiabatic electron detachment energy (AEDE, eV) for neutral and anionic Ti_3O_6 structures at BPW91/6-311+G (d) basis set. PG: Point group

Isomer	PG	Ti_3O_6			$Ti_3O_6^-$			AEDE
		State	E_T	ΔE	State	E_T	ΔE	
3-1-u	C_s	$^1A'$	-627.0908	***0.00***	$^2A'$	-627.1926	***0.00***	2.77
3-2-u	C_2	^1A	-627.0799	0.30	^2B	-627.1564	0.98	2.08
3-3-u	C_1	^1A	-627.0810	0.27	^2A	Optimized to 3-1-u		--
3-4-u	C_{2v}	$^1A_1$	-627.0622	0.78	$^2A_1$	-627.1352	1.56	1.98
3-5-u	C_s	$^1A'$	-627.0602	0.83	$^2A'$	-627.1399	1.43	2.17
3-6-u	C_s	$^1A'$	-627.0590	0.86	$^2A'$	-627.1457	1.28	2.36
3-7-u	C_s	$^1A'$	-626.9894	2.76	$^2A'$	-627.1003	2.51	3.02

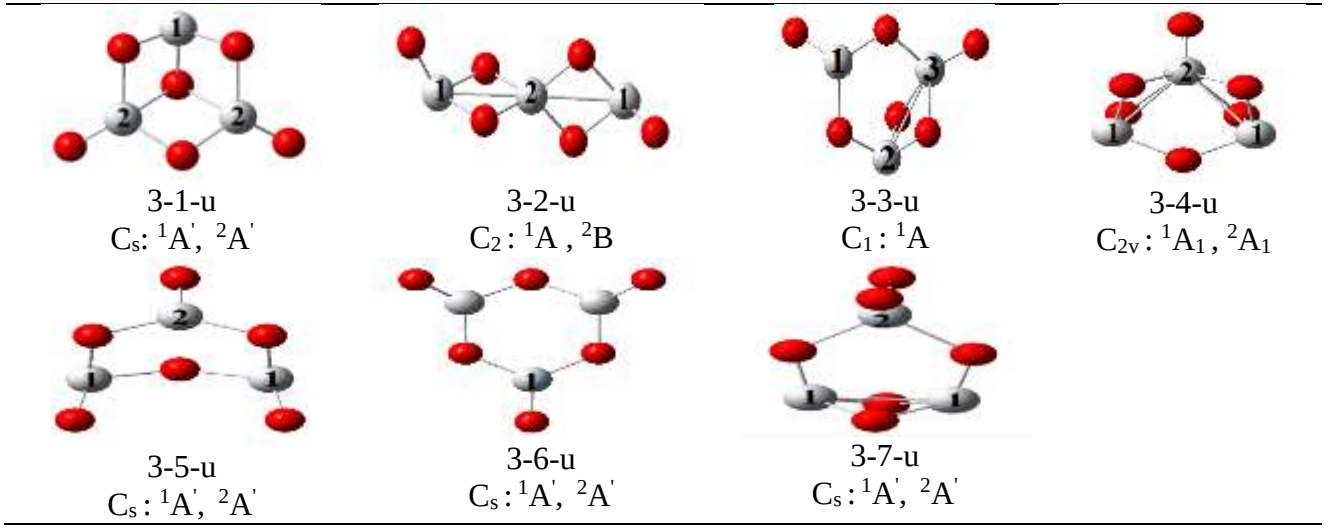

3-1-u
C_s: $^1A'$, $^2A'$

3-2-u
C_2 : ^1A , ^2B

3-3-u
C_1 : ^1A

3-4-u
C_{2v} : $^1A_1$, $^2A_1$

3-5-u
C_s : $^1A'$, $^2A'$

3-6-u
C_s : $^1A'$, $^2A'$

3-7-u
C_s : $^1A'$, $^2A'$

Figure 86: Structures of the Ti_3O_6 clusters. Structure name, point group and state are displayed bellow each structure. The Ti, and O atoms are indicated by gray, and red spheres respectively. Labels on Ti atom indicate the non-equivalent Ti atoms.

2.2 Ti_2AgO_6

Table 49: Total energy (E_T, a.u.) and relative Energy (ΔE, eV) for neutral and anionic Ti_2AgO_6 structures at BPW91/6-311+G (d). PG: Point group

Isomer	PG	Ti_2AgO_6			$Ti_2AgO_6^-$		
		State	E_T	ΔE	State	E_T	ΔE
3-1-1-d	C_s	$^2A''$	-715.4657	1.22			
3-1-1-d	C_s	$^4A''$	-715.4698	1.10			
3-1-1-d	C_{2v}				$^1A_1$	-715.6387	0.45
					$^3B_2$	-715.6553	***0.00***
3-1-1-d	C_1	^2A	-715.4657	1.22			
3-1-2-d	C_s	$^2A''$	-715.4440	1.81	$^1A'$	-715.5765	2.14
3-1-2-d	C_s	$^4A''$	-715.4450	1.78	$^3A'$	-715.5964	1.60
3-2-1-d	C_s	$^2A''$	-715.4556	1.49	$^1A'$	-715.6068	1.32
					$^3A''$	-715.6192	0.98

Table 50 (Table 49 cont.): Total energy (E_T, a.u.) and relative Energy (ΔE, eV) for neutral and anionic Ti_2AgO_6 clusters at BPW91/6-311+G (d). PG: Point group

Isomer	PG	Ti_2AgO_6			$Ti_2AgO_6^-$		
		State	E_T	ΔE	State	E_T	ΔE
3-2-2-d	C_{2h}	^2B_g	-715.4233	2.37	^1A_g	-715.5968	1.59
3-2-2-d	C_2				^3B	-715.5627	2.52
3-2-2-d	C_1				^3A	-715.5600	2.59
3-2-3-d		^2A	Optimizes to 3-1-2-d				
3-5-2-d	C_s	$^2A''$	-715.4088	2.77	^1A	No lower point found	
3-6-1-A-d	C_1	^2A	-715.4122	2.67			
3-6-1-B-d	C_1	^2A	-715.4053	2.86			
3-7-1-d	C_s	$^2A'$	-715.4237	2.36	$^1A'$	Error in termination	
3-7-2-d		^2A	Break of symmetry				

3-8-d	C_1	^2A	-715.5105	***0.00***	^1A	-715.6322	0.63
			-715.4321	2.13	^3A	-715.5627	
3-9-d	C_s	$^4A''$	-715.4468	1.73	$^3A''$	-715.6118	1.18
3-10-d	C_s				$^1A''$	Break of symmetry	
					$^3A''$	-715.6153	1.09
3-11-d	C_s				$^1A'$	-715.6397	0.42
3-11-d	C_1	^2A	-715.4944	0.44			
		^4A	-715.4216	2.42	^3A	-715.5797	2.06

Table 51: New structures of Ti_2AgO_6

Doped Structure	Undoped Structure	Doped Position	Unstable
3-8-d	3-4-u	1	--
3-9-d	--	--	3-8-d (C_1:^4A)
3-10-d	--	--	3-6-1-d (C_1:^3A)
3-11-A-d	3-7-u	1	--

Table 52: AEDE for $Ti_2AgO_6^-$ clusters at BPW91/6-311+G (d)

Isomer	PG	State	AED E	Isomer	PG	State	AED E
3-2-1-d	C_s	$^2A''\rightarrow{}^1A'$	4.11	3-8d	C_1	$^2A\rightarrow{}^1A$	3.31
3-2-2-d	C_{2h}	$^2B_g\rightarrow{}^1A_g$	4.72	3-1-2d	C_s	$^2A''\rightarrow{}^1A'$	3.61

Table 53: Total energy (E_T, au) and relative energy (ΔE, eV) for neutral and anionic Ti_2AgO_6 clusters at B3LYP/6-311+G (d). PG: Point group

Isomer	PG	Ti_2AgO_6			$Ti_2AgO_6^-$		
		State	E_T	ΔE	State	E_T	ΔE
3-1-1-d	C_s	$^2A''$	-715.3434	1.22			
3-1-1d	C_{2v}				$^1A_1$	-715.4912	1.33
					$^3B_2$	-715.5401	0.00
3-8-d	C_1	^2A	-715.3883	0.00	^1A	-715.5101	0.82
					^3A	-715.4639	2.07
3-11-d	C_1	^2A	-715.3703	0.49			
3-11-d	C_s				$^1A'$	-715.5207	0.53

Table 54: VEDE (eV) for $TiAgO_4^-$ clusters at BPW91/6-311+G (d), B3LYP/6-311+G (d), CCSD (T) // BPW91 and CCSD (T) // B3LYP

BPW91				B3LYP			
Isomer	PG	State	VED E	Isomer	PG	State	VED E
3-1-1-d	C_{2v}	$^1A_1 \rightarrow {}^2A_1$	4.89	3-1-1-d	C_{2v}	$^3B_2 \rightarrow {}^2A_1$	5.60
3-1-1-d	C_{2v}	$^3B_2 \rightarrow {}^2A_2$	5.37	3-1-1-d	C_{2v}	$^3B_2 \rightarrow {}^4A_1$	5.63
		$^3B_2 \rightarrow {}^4A_2$	5.09	3-11-d	C_s	$^1A' \rightarrow {}^2A''$	5.11
CCSD(T)//BPW91				CCSD(T)//B3LYP			
Isomer	PG	State	VED E	Isomer	PG	State	VED E
3-1-1-d	C_{2v}	$^3B_2 \rightarrow {}^2A_2$	6.04	3-1-1-d	C_{2v}	$^3B_2 \rightarrow {}^2A_2$	5.63
		$^3B_2 \rightarrow {}^4A_2$	5.51			$^3B_2 \rightarrow {}^4A_2$	5.68
3-11-d	C_s	$^1A' \rightarrow {}^2A'$	5.46				

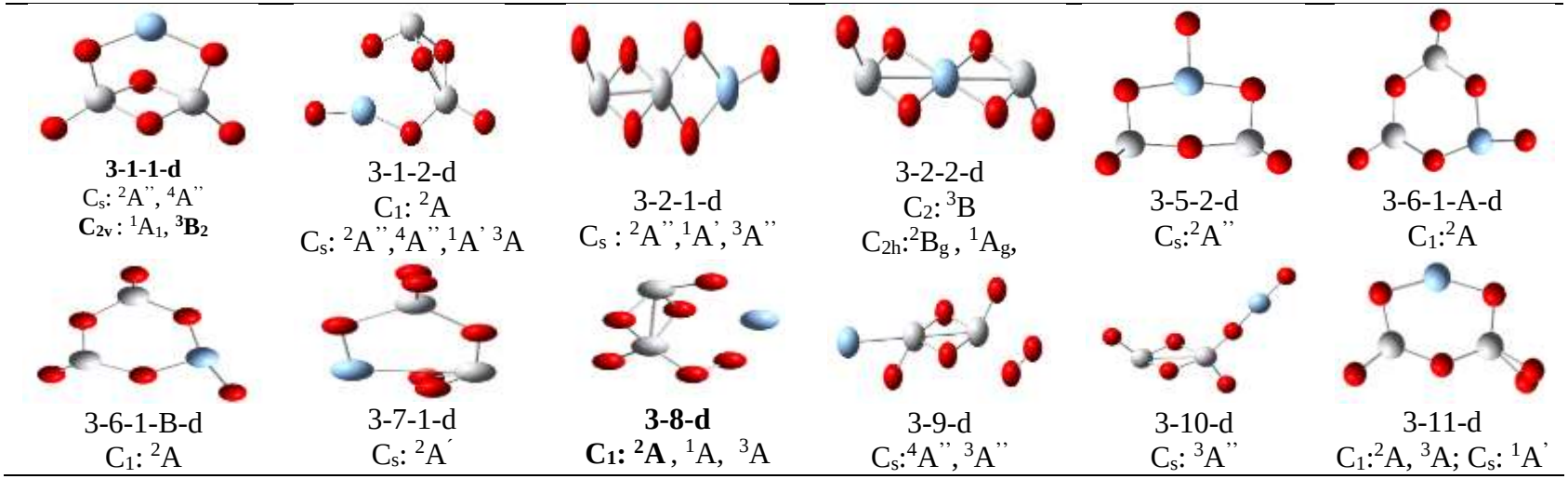

Figure 87: Structures of the Ti_2AgO_6 clusters. Structure name, point group and state are displayed bellow each structure. The Ti, O, Ag atoms are indicated by gray, red, and blue spheres respectively.

2.3 Ti_2AuO_6

Table 55: Total energy (E_T, a.u.) and relative energy (ΔE, eV) for neutral and anionic Ti_2AuO_6 clusters at BPW91/6-311+G (d). Number of imaginary frequencies are in curved bracket. PG: Point group

Isomer	PG	Ti_2AuO_6			$Ti_2AuO_6^-$		
		State	E_T	ΔE	State	E_T	ΔE
3-1-1-d	C_1	^2A	-704.2522	1.31			
3-1-1-d	C_s	$^4A''$ (1)	-704.2595	1.12			
3-1-1-d	C_{2v}	$^2B_1$	-704.2587	1.14	$^1A_1$	-704.4415	0.20
					$^3B_2$	-704.4489	***0.00***
3-1-2-d	C_s	$^2A''$	-704.2493	1.39	$^1A'$	-704.3911	1.57
		$^4A''$	-704.2546	1.25	^3A	Optimizes to 3-10-d	
3-2-1-d	C_s	$^2A''$	-704.2751	0.69	$^1A'$	-704.4267	0.60
		$^4A''$	-704.2598	1.11			

Table 56 (Table 55 cont.): Total energy (E_T, au) and relative Energy (ΔE, eV) for neutral and anionic Ti_2AuO_6 clusters at BPW91/6-311+G (d). Number of imaginary frequencies are in curved bracket. PG: Point group

Isomer		Ti_2AuO_6			$Ti_2AuO_6^-$		
		State	E_T	ΔE	State	E_T	ΔE
3-2-2-d	C_{2h}	^2B_g	-704.2329	1.84	^1A_g	-704.4069	1.14
		^4A_g (1)	-704.1734	3.46	^3B_g (2)	-704.3431	2.88
3-3-1-d		^2A	Convergence failure				
3-3-2-d		^2A	Optimizes to 3-1-1-d				
3-3-3-d		^2A	Optimizes to 3-1-2-d				
3-4-2-d		^2A	Optimizes to 3-6-1-B-d				
3-5-2-d	C_s	$^2A''$	-704.2207	2.17	$^1A''$	-704.3401	2.96
3-5-2-d	C_1	^4A	-704.2161	2.30			
3-6-1-d	C_1	^2A	-704.2355	1.77	^1A	Optimizes to 3-10-d	
		^4A	FormBX had a problem				
3-7-1-d		^2A	Give rise to 3-11-d				
3-7-2-d		^2A	Break of symmetry				
3-8-d	C_1	^2A	-704.2844	0.44	^1A	-704.4211	0.76
3-8-d	C_s	**$^2A''$**	-704.3005	***0.00***		Optimizes to 3-9-d	
		$^4A''$	-704.2333	1.83			
3-9-d	C_1				^1A	-704.3881	1.66
					^3A	-704.4095	1.07
3-9-d	C_s	$^2A''$	-704.2596	1.11	$^3A''$	-704.4165	0.88
3-10-d	C_s	$^2A''$	-704.2621	1.04	$^1A'$	-704.4128	0.98
3-10-d	C_s	$^4A''$ (1)	-704.2588	1.13	$^3A''$	-704.4418	0.19
3-11-d	C_1	^2A	-704.2857	0.40	^1A	-704.4367	0.33
		^4A	-704.2170	2.27	^3A	-704.3766	1.97

Table 57: Calculated AEDE (eV) of $Ti_2AuO_6^-$ at BPW91/6-311+G (d)

Isomer	PG	State	AEDE	Iso-mer	PG	State	AEDE
3-1-1-d	C_{2h}	$^2B_1 \rightarrow {}^1A_2$	4.97	3-6-1-d	C_1	$^1A \rightarrow {}^2A$	4.70
3-1-2-d	C_s	$^1A'' \rightarrow {}^2A'$	3.86	3-8-d	C_1	$^1A \rightarrow {}^2A$	3.72
3-2-1-d	C_s	$^1A'' \rightarrow {}^2A'$	4.13	3-10-d	C_s	$^2A'' \rightarrow {}^1A'$	4.10
3-2-2-d	C_{2h}	$^1B_g \rightarrow {}^2A_g$	4.73	3-11-d	C_1	$^2A \rightarrow {}^1A$	3.68
3-5-2-d	C_s	$^1A'' \rightarrow {}^2A''$	3.25				

Table 58: Total energy (E_T, a.u.) and relative Energy (ΔE, eV) at CCSD (T) // BPW91/6-311+G (d) for anionic Ti_2AuO_6 structures.

Isomer	PG	State	E_T	ΔE
3-1-1-d	C_{2v}	$^1A_1$	-701.5582	0.12
3-1-1-d	C_{2v}	$^3B_2$	-701.5625	0.00
3-10-d	C_s	$^3A''$	-701.5567	0.16

Table 59: Total energy (E_T, a.u.) and relative energy (ΔE, eV) for neutral and anionic Ti_2AuO_6 structures at B3LYP/6-311+G (d).

Isomer	PG	Ti_2AuO_6			$Ti_2AuO_6^-$		
		State	E_T	ΔE	State	E_T	ΔE
3-1-1-d	C_{2v}	$^2B_1$	-704.0739	1.71	$^3B_2$	-704.2869	*0.00*
3-8-d	C_s	$^2A''$	-704.1366	*0.00*	$^1A'$	-704.2610	0.70
3-10-d	C_s	$^2A''$	-704.0983	1.04	$^3A''$	-704.2760	0.30

Table 60: VEDE (eV) for $Ti_2AuO_6^-$ clusters at BPW91/6-311+G (d), B3LYP/6-311+G (d), CCSD (T) // BPW91 and CCSD (T) // B3LYP

BPW91				B3LYP			
Isomer	PG	State	VEDE	Isomer	PG	State	VEDE
3-1-1-d	C_{2v}	$^1A_1 \rightarrow {}^2B_1$	5.02	3-1-1-d	C_{2v}	$^3B_2 \rightarrow {}^2A_1$	5.22
3-1-1-d	C_{2v}	$^3B_2 \rightarrow {}^2A_1$	5.38				
3-10-d	C_s	$^3A" \rightarrow {}^2A"$	5.11	3-10-d	C_s	$^3A" \rightarrow {}^2A"$	5.56
		$^3A" \rightarrow {}^4A'$	5.29			$^3A" \rightarrow {}^4A"$	5.62
3-11-b	C_1	$^1A \rightarrow {}^2A$	4.50	3-11-d	C_1	$^1A \rightarrow {}^2A$	5.14
CCSD (T)//BPW91				CCSD (T)//B3LYP			
Isomer	PG	State	ΔE	Isomer	PG	State	VEDE
3-1-1-d	C_{2v}	$^3B_2 \rightarrow {}^2A_1$	5.08	3-1-1-d	C_{2v}	$^3B_2 \rightarrow {}^2A_1$	4.96
						$^3B_2 \rightarrow {}^4A_1$	5.03
3-10-d	C_s	$^3A" \rightarrow {}^2A"$	5.47	3-10-d	C_s	$^3A" \rightarrow {}^2A"$	5.59
		$^3A" \rightarrow {}^4A'$	5.68			$^3A' \rightarrow {}'^4A"$	5.68

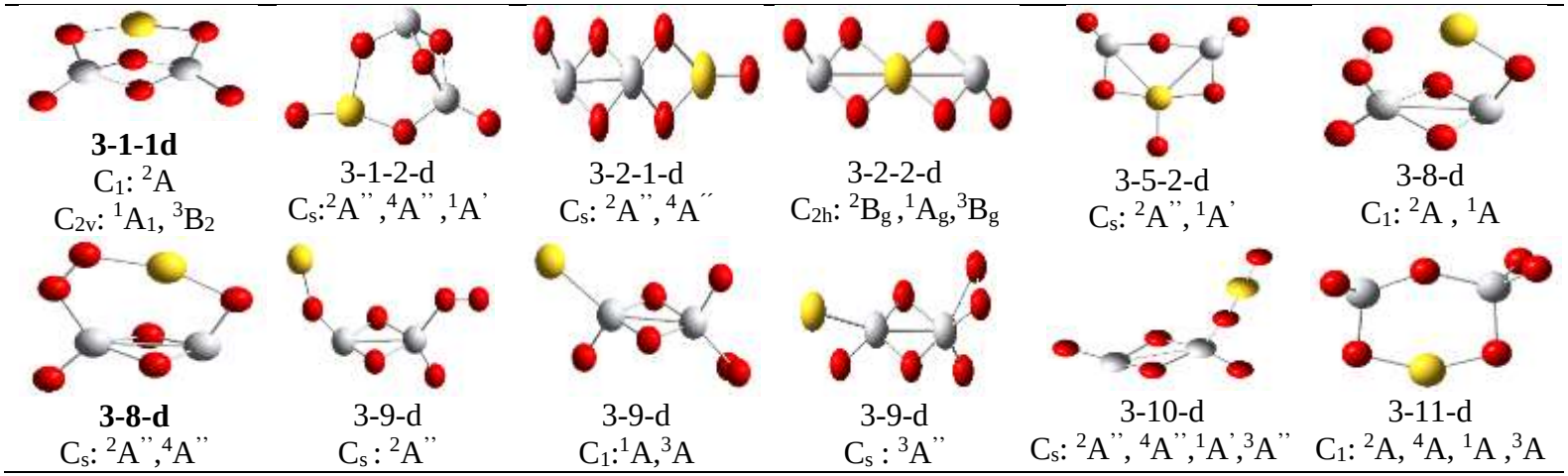

Figure 88: Structures of the Ti_2AuO_6 clusters. Structure name, point group and state are displayed under each structure. The Ti, O and Au atoms are indicated by gray, red, and yellow spheres respectively.

3 Cluster size n = 4

3.1 Ti_4O_8

Table 61: Total energy (E_T, au), relative Energy (ΔE, eV) and AEDE (eV) for neutral and anionic Ti_4O_8 clusters at BPW91/6-311+G (d).

Isomer	PG	Ti_4O_8			$Ti_4O_8^-$			AEDE
		State	E_T	ΔE	State	E_T	ΔE	
4-1-u	**C_{2v}**	$^1A_1$	-836.1849	***0.00***	$^2A_1$	-.836.2823	0.32	2.65
4-2-u	**C_{2v}**	$^1A_1$	-836.1756	0.25	$^2A_1$	-836.2939	***0.00***	3.22
4-3-u	C_{2h}	^1A_g	-836.1741	0.29	^2A_g	-836.2804	0.37	2.89
4-4-u	C_{2h}	^1A_g	-836.1725	0.34	^2A_g	-836.2663	0.75	2.55
4-5-u	C_{2h}	^1A_g	-836.1585	0.72	^2A_g	-836.2463	1.30	2.39
4-6-u	C_{2v}	$^1A_1$	-836.1526	0.88	$^2A_1$	-836.2614	0.89	2.96
4-7-u	C_1	^1A	-836.1514	0.91	^2A	-836.2609	0.90	2.98
4-8-u	T_d	$^1A_1$	-836.1304	1.48	$^2A_1$	-836.2649	0.79	3.66
4-9-u	C_s	$^1A'$	-836.1318	1.44	$^2A'$	-836.2459	1.31	3.11
4-10-u	C_s	$^1A'$	-836.0065	4.85	^1A	Optimizes to 4-9-u		--
4-11-u	D_{4h}	$^1A_{1g}$ (4)	-836.0675	3.19	$^2A_{1g}$ (5)	-836.1806	3.08	3.08
4-12-u	C_1	^1A	-836.1330	1.41	^2A	-836.2255	1.86	2.52

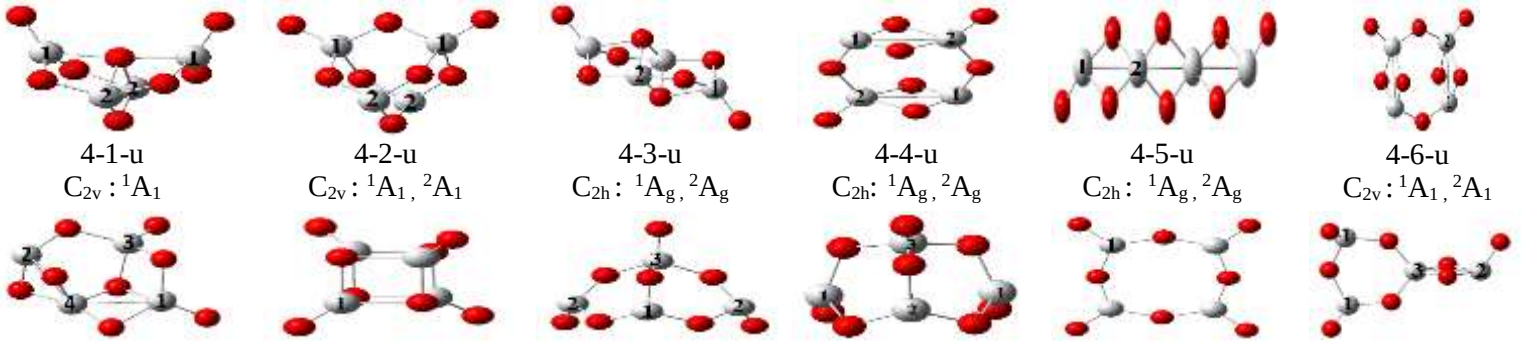

4-1-u C_{2v} : $^1A_1$ | 4-2-u C_{2v} : $^1A_1$, $^2A_1$ | 4-3-u C_{2h} : ^1A_g, ^2A_g | 4-4-u C_{2h}: ^1A_g, ^2A_g | 4-5-u C_{2h} : ^1A_g, ^2A_g | 4-6-u C_{2v} : $^1A_1$, $^2A_1$

4-7-u C_1 : ^1A, ^2A | 4-8-u Td: $^1A_1$; D_{2h}: $^2A_1$ | 4-9-u C_s : $^1A'$ $^2A'$ | 4-10-u C_s : $^1A'$ | 4-11-u D_{4h} : $^1A_{1g}$, $^2A_{1g}$ | 4-12-u C_1 : ^1A, ^2A

Figure 89: Structures of the Ti_3O_6 clusters. Structure name, point group and state are displayed bellow each structure. The Ti and O atoms are indicated by gray and red spheres respectively.

3.2 Ti_3AgO_8

Table 62: Total energy (E_T, au) and relative energy (ΔE, eV) for neutral and anionic Ti_2AgO_6 structures at BPW91/6-311+G (d). Number of imaginary frequencies are in curved bracket. PG: Point group

Cluster	PG	Ti_3AgO_8			$Ti_3AgO_8^-$		
		State	E_T	ΔE	State	E_T	ΔE
4-1-2-d	C_s	$^2A''$	-924.5244	1.30	$^1A'$	-924.7126	0.74
		$^4A''$	-924.5261	1.26	$^3A''$	-924.7185	0.58
4-2-1-d	C_1	^2A	-924.4985	2.01	^1A	Optimizes to cluster 4-9-2-d	
4-2-1-d	C_s	$^4A''$	-924.5019	1.92			
4-2-2-d	C_1	^2A	-924.5357	0.99	^1A	-924.7129	0.74
		$^4A''$	-924.5403	0.87	$^3A''$	-924.7202	0.54
4-3-1-d	C_s	$^2A''$	-924.5224	1.36			
		$^4A''$	-924.5217	1.38			
4-3-1-d	C_1				^1A	-924.7116	0.77
					^3A	-924.7321	0.21
4-4-1-d	C_1	^2A	-924.5247	1.29	^1A	-924.7016	1.04
		^4A	-924.5210	1.39	^3A	-924.6955	1.21
4-4-2-d	C_1	^2A	-924.4989	2.00	^1A	Give rise to cluster 4-19-d	
		^4A	-924.4791	2.54			
4-5-1-d	C_1	^2A	-924.5337	1.05	^1A	-924.6937	1.26
		^4A	-924.5233	1.33	^3A	-924.7076	0.88
4-5-2-d	C_1	^2A	-924.5023	1.90	^1A	-924.6866	1.45
		^4A	-924.4622	3.00	^3A	-924.6493	2.47
4-6-1-d	C_1	^2A	-924.5243	1.30	^1A	-924.6944	1.24
		^4A	-924.5203	1.42	^3A	-924.6965	1.18
4-7-1-d	C_1	^2A	-924.5282	1.20	^1A	-924.7141	0.70
		^4A	-924.5290	1.18	^3A	-924.7154	0.67
4-7-3-d	C_1	^2A	-924.4992	1.99	^1A	-924.6272	3.07
		^4A	-924.5008	1.95	^3A	-924.6937	1.26
4-7-2-d	C_1	^2A (1)	-924.5006	1.95	^1A	SCF convergence problems	
		^4A (1)	-924.5008	1.95			
4-7-4-d	C_1	^2A	-924.5250	1.29	^1A	-924.6996	1.10

Table 63 (Table 62 cont.): Total energy (E_T, au) and relative Energy (ΔE, eV) for neutral and anionic Ti_2AgO_6 clusters at BPW91/6-311+G (d). Number of imaginary frequencies are in curved bracket.

Cluster	PG	Ti_3AgO_8			$Ti_3AgO_8^-$		
		State	E_T	ΔE	State	E_T	ΔE
4-8-1-d		^2A	Convergence failure				
4-9-1-d	C_s	$^2A''$	-924.5244	1.30	$^1A'$	-924.7135	0.72
					$^3A'$	-924.7399	**0.00**
4-9-2-d	**C_1**	^2A	-924.4984	2.01	^1A	-924.6541	2.34
		^4A	-924.4999	1.97	^3A	FormBX had a problem	
4-10-1-d	C_1	^2A	Converged failure				
4-10-3-d	C_1	^2A	Originate 4-21-d				
4-12-1-d	C_1	^2A	-924.4872	2.31	^1A	-924.6644	2.04
		^4A	-924.4857	2.35	^3A	-924.7020	1.03
4-12-2-d	C_1	^2A (1)	-924.5066	1.79			
4-12-3-d	C_1	^2A	-924.4838	2.41	^1A	-924.6974	1.16
		^4A	-924.4269	3.96	^3A	-924.7155	0.66
4-13-d	C_1	^2A	-924.5200	1.42	^1A	-924.6797	1.64
		^4A	-924.5300	1.15	^3A	FormBX had a problem	
4-14-d	C_1	^2A	-924.5361	0.98	^1A	-924.7237	0.44
		^4A	-924.5357	0.99	^3A	-924.7260	0.38
4-14-d	C_2	^2B (1)	-924.5302	1.14			
4-15-d	C_1	^2A	-924.4859		^1A	Convergence failure	
				2.35			
		^4A	-924.4822	2.45			
4-17-d	C_1	^2A	-924.4504	3.32	^1A	-924.5962	3.91
		^4A	-924.4477	3.39	^3A	-924.6120	3.48
4-18-d	C_1	^2A	-924.5522	0.55	^1A	-924.6948	1.23
		^4A	Optimizes to 4-21-d		^3A	-924.6412	2.69
4-20-d	C_1	^2A	-924.4823	2.45	^1A	-924.6343	2.88
		^4A	-924.4832	2.42	^3A	-924.6522	2.39
4-21-d	C_1	^2A	-924.5723	***0.00***	^1A	-924.7087	0.85
		^4A	-924.5000	1.97	^3A	-924.7161	0.65
4-21-d	C_s				$^3A''$	-924.6703	1.90

Table 64: New structures of Ti_3AgO_8

Doped Structure	Undoped Structure	Doped Position	Expected to be /Unstable
4-13-d	4-1-u	1	--
4-14-d	4-3-u	2	--
4-15-d	4-6-u	2	--
4-16-d	4-7-u	2	--
4-17-d	4-9-u	3	--
4-18-d	4-10-u	3	--
4-20-d	--	--	4-4-2-d (C_1:^{1}A)
4-21-d	--	--	4-10-3-d (C_1:^{4}A)

Table 65: VEDE for $Ti_3AgO_8^-$ clusters at BPW91/6-311+G (d)

Cluster	PG	State	VEDE	Cluster	PG	State	VEDE
4-3-1-d	C_1	$^3A \rightarrow {}^2A$	5.44	4-14-d	C_1	$^1A \rightarrow {}^2A$	5.26
		$^3A \rightarrow {}^4A$	5.41	4-14-d	C_1	$^3A \, {}^2 \rightarrow A$	5.31
4-9-1-d	C_s	$^3A'' \rightarrow {}^2A'$	5.64			$^3A \rightarrow {}^4A$	5.34
		$^3A'' \rightarrow {}^4A'$	5.48				

Table 66: AEDE for $Ti_3AgO_8^-$ clusters at BPW91/6-311+G (d)

Isomer	PG	States	AEDE	Isomer	PG	States	AEDE	Isomer	PG	States	AEDE
4-1-2-d	C_s	$^1A' \rightarrow {}^2A''$	5.12	4-6-1-d	C_1	$^1A \rightarrow {}^2A$	4.63	4-13-d	C_1	$^1A \rightarrow {}^2A$	4.35
		$^3A' \rightarrow {}^4A'$	5.23			$^3A \rightarrow {}^4A$	4.79	4-14-d	C_1	$^1A \rightarrow {}^2A$	5.10
4-2-2-d	C_1	$^1A \rightarrow {}^2A$	4.82	4-7-1-d	C_1	$^1A \rightarrow {}^2A$	5.06			$^3A \rightarrow {}^4A$	5.18
4-2-2-d	C_s	$^1A' \rightarrow {}^2A''$	4.90			$^3A \rightarrow {}^4A$	5.07	4-17-d	C_1	$^1A \rightarrow {}^2A$	3.97
4-4-1-d	C_1	$^1A \rightarrow {}^2A$	4.81	4-7-1-d	C_1	$^1A \rightarrow {}^2A$	3.48			$^3A \rightarrow {}^4A$	4.47
		$^3A \rightarrow {}^4A$	4.75			$^3A \rightarrow {}^4A$	5.25	4-18-d	C_1	$^1A \rightarrow {}^2A$	3.94
4-5-1-d	C_1	$^1A \rightarrow {}^2A$	4.35	4-7-4-d	C_1	$^1A \rightarrow {}^2A$	4.75	4-20-d	C_1	$^1A \rightarrow {}^2A$	4.14
		$^3A \rightarrow {}^4A$	5.01	4-9-1-d	C_s	$^1A' \rightarrow {}^{2''}$	5.15			$^3A \rightarrow {}^4A$	5.57
4-5-2-d	C_1	$^1A \rightarrow {}^2A$	5.02	4-9-2-d	C_1	$^1A \rightarrow {}^2A$	4.24	4-21-d	C_1	$^1A \rightarrow {}^2A$	3.71
		$^3A \rightarrow {}^4A$	5.09							$^3A \rightarrow {}^4A$	5.88

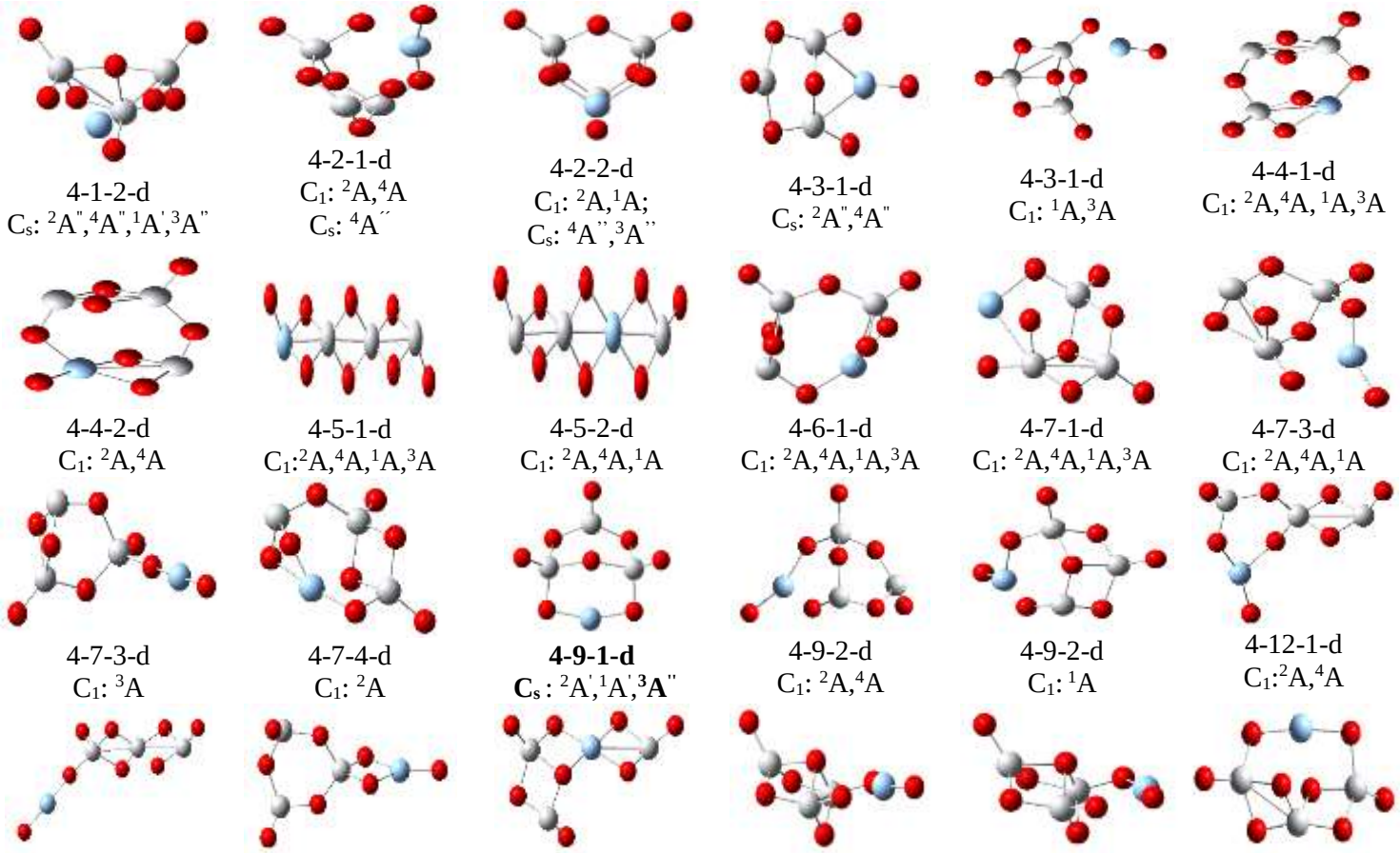

Figure 90: Structures of the Ti_3AgO_8 clusters. Structure name, point group and state are displayed bellow each structure. The Ti, O and Ag atoms are indicated by gray, red, and blue spheres respectively.

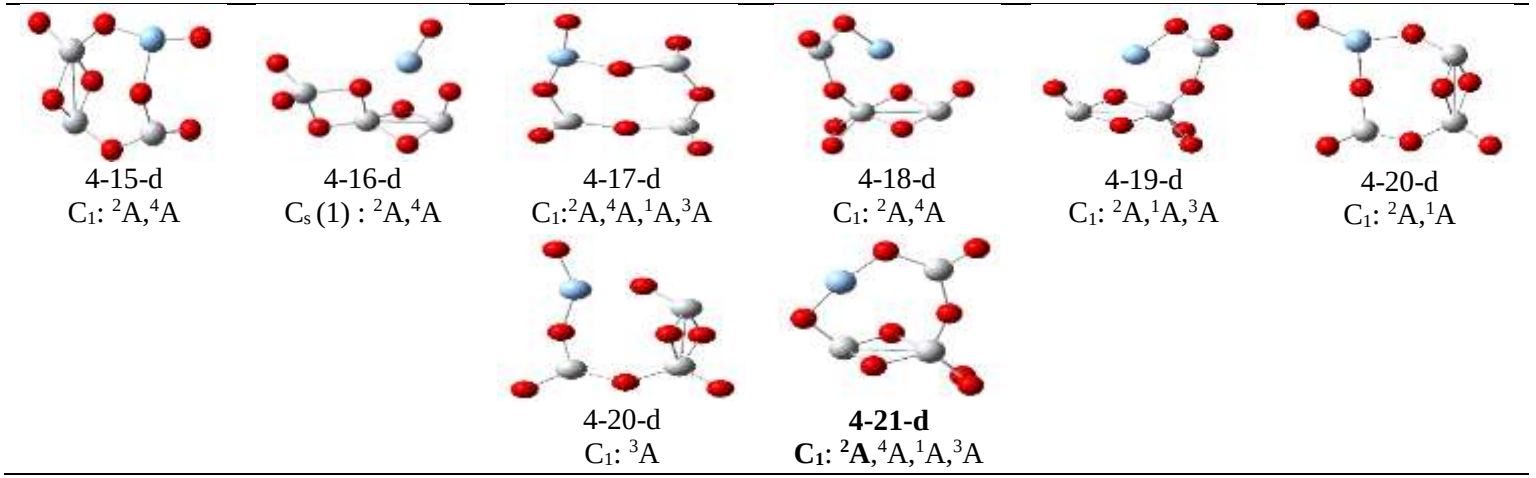

Figure 91 (Figure 90 cont.): Structures of the Ti_3AgO_8 clusters. Structure name, point group and state are displayed bellow each structure. The Ti, O, Ag atoms are indicated by gray, red, and blue spheres respectively.

3.3 Ti_3AuO_8

Table 67: Total energy (E_T, au) and relative energy (ΔE, eV) for neutral and anionic Ti_3AuO_8 clusters at BPW91/6-311+G (d). PG: Point group

Structure	PG	Ti_3AuO_8			$Ti_3AuO_8^-$		
		State	E_T	ΔE	State	E_T	ΔE
4-1-2-d	C_s	$^2A''$	-913.3119	1.62	$^1A'$	-913.5023	1.78
		$^4A''$	-913.3142	1.56	$^3A''$	-913.5033	1.75
4-2-2-d	C_1	^2A	-913.3262	1.23	^1A	-913.5054	1.69
		^4A	Convergence failure		^3A	-913.5059	1.68
4-3-1-d	C_s	$^2A''$	-913.3313	1.09	$^1A'$	-913.5062	1.67
		$^4A''$	-913.3436	0.75	^3A	No lower point found	
4-3-1-d	C_1	^2A	-913.3319	1.07		-913.5174	1.37
		^4A	-913.3280	1.18		-913.5191	1.32

Table 68 (Table 67 cont.): Total energy (E_T, au) and relative Energy (ΔE, eV) are calculated at BPW91/6-311+G (d) for neutral and anionic Ti_3AuO_8 structures. PG: Point group

		Ti_3AuO_8			$Ti_3AuO_8^-$		
Structure	PG	State	E_T	ΔE	State	E_T	ΔE
4-4-1-d	C_1	^2A	-913.3289	1.16			
		^4A	-913.3152	1.53			
4-4-1-d	C_s				$^1A'$	-913.5058	1.68
					$^3A''$	-913.4897	2.12
4-4-2-d	C_1	^{2a}	-913.3083	1.72	^1A	-913.4219	3.97
		^4A	-913.2915	2.17	^3A	Optimizes to 4-7-3-d	
4-5-1-d	C_s	$^2A'$	-913.3532	0.49	$^1A'$	-913.5135	1.47
			Originated 4-28-d		^3A	-913.5141	1.46
4-5-2-d	C_1	^2A	-913.3119	1.62	^1A	-913.4954	1.97
4-6-1-d	C_1	^2A	-913.3224	1.33	^1A	-913.4951	1.97
		^4A	-913.3195	1.41	^3A	Optimizes to 4-25d	
4-7-1-d	C_1	^2A	-913.3124	1.61	^1A	Convergence failure	
		^4A	-913.3168	1.49			
4-7-3-d	C_1	^2A	-913.3034	1.85	^1A	-913.4914	2.08
		^4A	-913.3371	0.93	^3A	-913.5197	1.31
4-7-2-d	C_1	^2A	-913.3076	1.74	^1A	FormBX problem	
		^4A	-913.2847	2.36			
4-7-4-d	C_1	^2A	-913.3225	1.33	^1A	-913.4976	1.91
4-9-1-A-d	C_s	$^2A''$	-913.3032	1.86	$^1A'$	-913.4997	1.85
		$^4A''$	Break of symmetry		$^3A'$	No lower point found	
4-9-1-B-d	C_s	$^2A'$	No lower point found		$^1A'$	-913.5389	0.78
					$^3A'$	-913.5446	0.63
4-9-2-d	C_1	^2A	-913.3107	1.65	^1A	-913.4698	2.66
4-12-1-d	C_1	^2A	-913.3051	1.80	^1A	-913.4578	2.99
		^4A	-913.2947	2.08	^3A	-913.4608	2.91
4-12-3-d	C_1	^2A	-913.2709	2.73	^1A	FormBX problem	
		^4A	-913.2765	2.58			

Table 69 (Table 67 cont.): Total energy (E_T, au) and relative Energy (ΔE, eV) for neutral and anionic

Ti_3AuO_8 clusters at BPW91/6-311+G (d). PG: Point group

Structure	PG	Ti_3AuO_8			$Ti_3AuO_8^-$		
		State	E_T	ΔE	State	E_T	ΔE
4-13-d	C_1	^2A	-913.3713	***0.00***	^1A	-913.5357	0.87
		^4A	-913.3714	***0.00***	^3A	-913.5677	***0.00***
4-14-d	C_1	^2A	-913.3272	1.20			
		^4A	Optimizes to 4-3-2-d				
4-14-d	C_2				^1A	-913.5106	1.55
					^3B	-913.5221	1.24
4-18-d	C_1	^2A	-913.3427	0.78	^1A	-913.4901	2.11
		^4A	-913.2549	3.17	^3A	Convergence failure	
4-19-d		^2A	Breaks of symmetry				
4-20-d	C_1	^2A	-913.2955	2.07	^1A	Optimizes to 4-3-1-d	
		^4A	Optimizes to 4-4-2-d				
4-21-d	C_1	^2A	-913.3668	0.13	^1A	-913.5082	1.62
		^4A	Convergence failure		^3A	-913.4701	2.66
4-22-d	C_1	^2A	-913.2945	2.09	^1A	FormBX had a problem	
4-23-d	C_1	^2A	-913.3434	0.76	^1A	-913.5108	1.55
4-23-d	C_s	$^4A'$	-913.3436	0.75	$^3A''$	-913.5398	0.76
4-24-d	C_1	^2A	-913.3353	0.98	^1A	-913.5124	1.50
		^4A	-913.2569	3.12	^3A	Optimizes to 4-9-1-d	
4-25-d	C_1	^2A	-913.3146	1.54	^1A	Convergence failure	
		^4A	-913.3195	1.41	^3A	-913.5047	1.71
4-26-d	C_1	^2A	-913.3267	1.22	^1A	-913.4814	2.35
		^4A	-913.3227	1.33	^3A	FormBX had a problem	
4-27-d	C_1	^2A	-913.3253	1.25	^1A	-913.5067	1.66
		^4A	-913.3279		^3A	-913.5208	1.28
4-28d	C_1	^2A	-913.2800	2.49	^1A	-913.4510	3.17
		^4A	-913.2633	2.94	^3A	Convergence failure	

Table 70: New structures of Ti_3AuO_8

Doped Structure	Undoped Structure	Doped Position	Expected to be /Unstable
4-9-1-B-d	--	--	4-24-d (C_s:$^3A'$)
4-22-d	4-9-u	3	--
4-23-d	4-8-u	1	--
4-24-d	4-10-u	1d	--
4-25-d	--	--	4-6-1-d (C_1:^3A)
4-28-d	--	--	4-5-1-d (C_1:^4A)
4-26-d	4-6-u	2	--
4-27-d	4-12-u	2	--

Table 71: VEDE for $Ti_3AuO_8^-$ clusters at BPW91/6-311+G (d)

Cluster	PG	State	VEDE
4-13-d	C_1	$^3A \rightarrow ^2A$	5.53
		$^3A \rightarrow ^4A$	5.53

Table 72: AEDE for $Ti_3AuO_8^-$ clusters at BPW91/6-311+G (d)

Cluster	PG	State	AEDE	Cluster	PG	State	AEDE
4-13-d	C_1	$^1A \rightarrow ^2A$	4.47	4-7-1d	C_1	$^1A \rightarrow ^2A$	5.13
		$^3A \rightarrow ^2A$	5.34	4-7-1d	C_1	$^3A \rightarrow ^4A$	5.12
		$^3A \rightarrow ^4A$	5.34	4-7-4d	C_1	$^1A \rightarrow ^2A$	4.77
4-1-2-d	C_s	$^1A' \rightarrow ^2A'$	5.18	4-9-1d	C_s	$^1A'' \rightarrow ^2A''$	5.35
		$^3A' \rightarrow ^4A''$	5.15	4-9-2d	C_1	$^1A \rightarrow ^2A$	4.33
4-2-2-d	C_1	$^1A \rightarrow ^2A$	4.88	4-18-d	C_1	$^1A \rightarrow ^2A$	4.01
4-3-1-d	C_s	$^1A' \rightarrow ^2A'$	4.76	4-23-d	C_1	$^1A \rightarrow ^2A$	4.55
4-4-2-d	C_1	$^1A \rightarrow ^2A$	3.09	4-23-d	C_s	$^3A' \rightarrow ^4A''$	5.34
		$^3A \rightarrow ^4A$	6.21	4-24-d	C_1	$^1A \rightarrow ^2A$	4.82
4-5-1-d	C_s	$^1A' \rightarrow ^2A'$	4.36	4-26-d	C_1	$^1A \rightarrow ^2A$	4.21
4-5-2-d	C_1	$^1A \rightarrow ^2A$	4.99	4-27-d	C_1	$^1A \rightarrow ^2A$	4.94
4-6-1-d	C_1	$^1A \rightarrow ^2A$	4.70	4-28-d	C_1	$^1A \rightarrow ^2A$	4.65

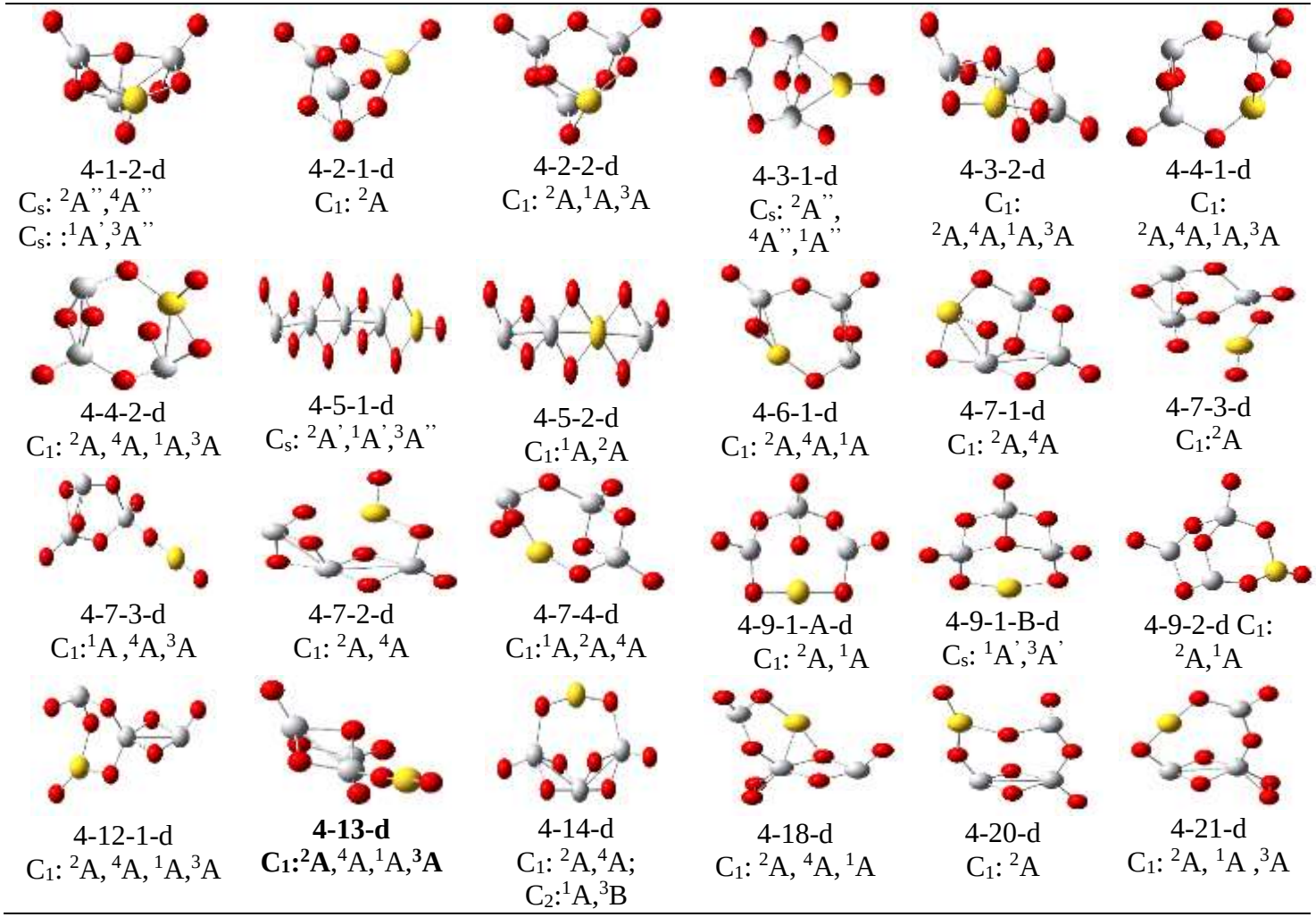

Figure 92: Structures of the Ti_3AuO_8 clusters. Structure name, point group and state are displayed bellow each structure. The Ti, O, Au atoms are indicated by gray, red, and yellow spheres respectively

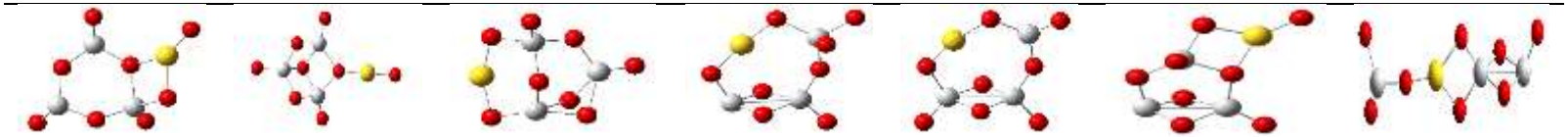

4-22-d C_1: ^2A | 4-23-d C_1:^2A,^1A C_s:$^4A'$,$^3A'$ | 4-24-d C_1: ^2A, ^4A | 4-25-d C_1: ^2A,^4A,^3A | 4-26-d C_1: ^2A,^4A,^1A | 4-27-d C_1: ^2A,^1A,^3A | 4-28-d C_1: ^2A,^1A,^3A

Figure 93 (Figure 92 cont.): Structures of the Ti_3AuO_8 clusters. Structure name, point group and state are displayed bellow each structure. The Ti, O, Au atoms are indicated by gray, red, and yellow spheres respectively.

4 Cluster size n = 5

4.1 Ti_5O_{10}

Table 73: Total energy (E_T, au) and relative energy (ΔE, eV) for neutral and anionic Ti_5O_{10} clusters at BPW91/6-311+G (d). Number of imaginary frequencies are in curved bracket.

Isomer	PG	Ti_5O_{10}			$Ti_5O_{10}^-$		
		State	E_T	ΔE	State	E_T	ΔE
5-1-u	C_s	$^1A'$	-1045.2762	***0.00***	$^2A'$	-1045.3773	0.09
5-2-u	C_s	$^1A'$	-1045.2714	0.13	$^2A'$	-1045.3744	0.17
5-3-u	C_1	^1A	-1045.2715	0.13	^2A	-1045.3808	***0.00***
5-4-u	C_1	^1A	-1045.2643	0.32	^2A	-1045.3754	0.15
5-5-u	C_1	^1A	-1045.2462	0.81	^2A	-1045.3665	0.39
5-6-u	C_s	$^1A'$	-1045.2535	0.62	$^2A'$	-1045.3690	0.32
5-7-u	C_1	^1A	-1045.2565	0.53	^2A	-1045.3629	0.49
5-8-u	C_{4v}	$^1A_1$ (2)	-1045.2667	0.26	$^2B_2$ (2)	-1045.3451	0.97
5-9-u	C_1	^1A	-1045.2582	0.49	^2A	-1045.3651	0.43
5-10-u	C_1	^1A	-1045.2669	0.25	^2A	-1045.3808	0.00
5-11-u		^1A	Break of symmetry				
5-12-u	C_1	^1A	-1045.2358	1.10	^2A	No lower point found	
5-13-u	C_{2v}	$^1A_1$	-1045.2153	1.66	$^2A_1$	-1045.3554	0.69

Table 74: Total energy (E_T, a.u.) and relative Energy (ΔE, eV) at B3P86/6-311+G (d).

Isomer	PG	Ti_5O_{10}		$Ti_5O_{10}^-$	
		State	E_T	State	E_T
5-11-u	C_{4v}	$^1A_1$	- 1047.7684	$^2B_1$ (2)	- 1047.8715

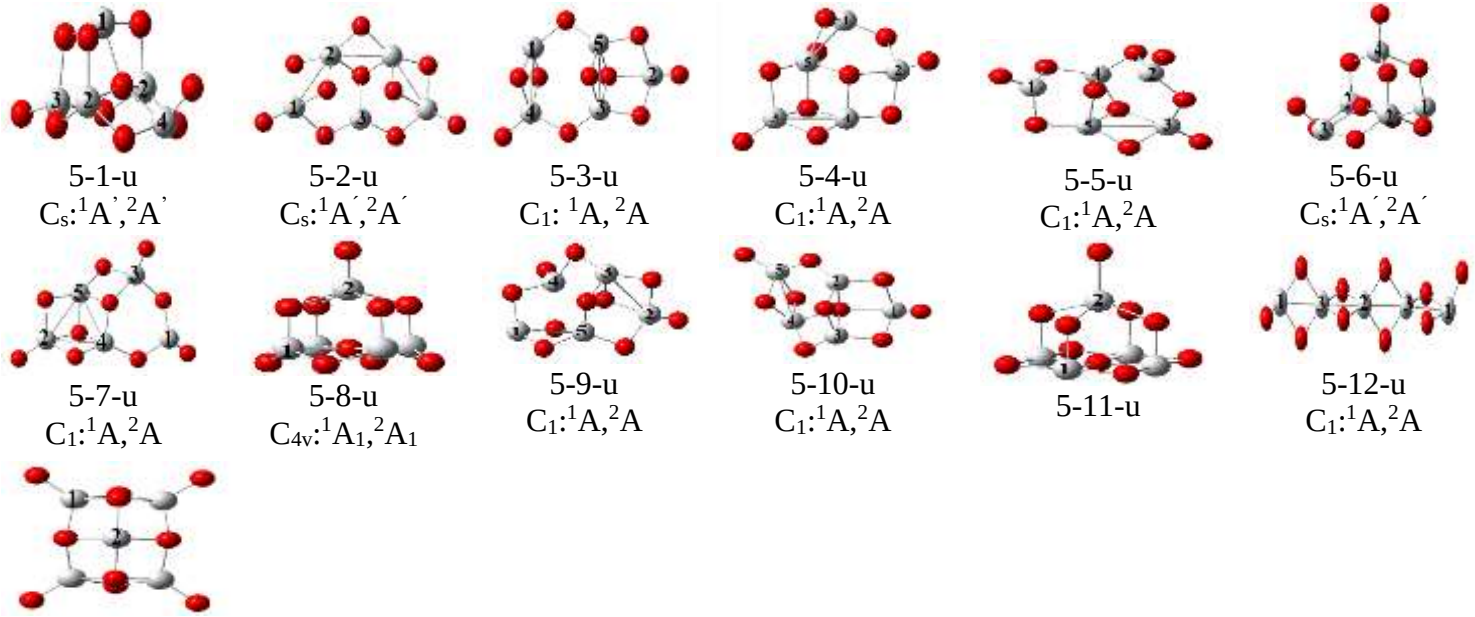

Figure 94: Structures of the Ti_5O_{10} clusters. Structure name, point group and state are displayed bellow each structure. The Ti and O atoms are indicated by gray and red spheres respectively.

4.2 Ti_4AgO_{10}

Table 75: Total energy (E_T, a.u.) and relative Energy (ΔE, eV) for neutral and anionic Ti_4AgO_{10} clusters at BPW91/6- 311+G (d).

Cluster	PG	Ti_4AgO_{10}			$Ti_4AgO_{10}^-$		
		State	E_T	ΔE	State	E_T	ΔE
5-1-1-d	C_s	$^2A'$	-1133.6132	1.41	$^1A'$	-1133.8129	0.80
		$^4A''$	-1133.6141	1.38	$^3A'$	Originated 5-21-d	
5-1-2-d	C_1	^2A	-1133.5909	2.01	^1A	-1133.8300	0.34
		^4A	-1133.5971	1.85	^3A	-1133.8394	0.08
5-1-3-d	C_s	$^2A''$	-1133.6193	1.24	^1A	Break of symmetry	
		^3A	No lower point found				
5-1-4-d		^1A	No lower point found				
5-2-1-d	C_1	^2A	-1133.6144	1.38	^1A	-1133.7864	1.52
		^4A	-1133.6152	1.35	^3A	-1133.8055	1.00
5-2-2-d	C_1	^2A	-1133.6306	0.93	^1A	-1133.8289	0.37
		^4A	-1133.6313	0.91	^3A	-1133.8314	0.30
5-2-3-d	C_s	$^2A'$	-1133.6047	1.64	$^1A'$	-1133.8006	1.14
		$^4A'$	-1133.5992	1.79	$^3A''$	-1133.8283	0.39
5-3-1-d	C_1	^2A	-1133.6318	0.90	^1A	-1133.8269	0.42
		^4A	-1133.6263	1.05	^3A	-1133.8243	0.49
5-3-2-d	C_1	^2A	-1133.6162	1.43	^1A	-1133.7760	1.81
		^4A	-1133.6124	1.43	^3A	-1133.7952	1.29
5-3-4-d	C_1	^2A	-1133.6019	1.72	^1A	Convergence failure	
		^4A	-1133.5852	2.17			
5-4-1-d	C_1	^2A	-1133.6649	***0.00***	^1A	-1133.8424	***0.00***
		^4A	-1133.5806	2.29	^3A	-1133.7653	2.10
5-4-2-d	C_1	^2A	-1133.6091	1.52	^1A	-1133.7463	2.62
		^4A	-1133.5939	1.93	^3A	-1133.7722	1.91
5-4-3-d	C_1	^2A	-1133.5940	1.93	^1A	-1133.7517	2.47
		^4A	Convergence failure		^3A	-1133.7751	1.83

Table 76 (Table 75 cont.): Total energy (E_T, au) and relative Energy (ΔE, eV) for neutral and anionic Ti_4AgO_{10} clusters at BPW91/6- 311+G (d).

Cluster	PG	Ti_4AgO_{10}			$Ti_4AgO_{10}^-$		
		State	E_T	ΔE	State	E_T	ΔE
5-4-4-d	C_1	^2A	-1133.6076	1.56	^1A	-1133.7865	1.52
		^4A	-1133.6064	1.59	^3A	-1133.7841	1.59
5-4-5-d	C_1	^2A	-1133.6022	1.71	^1A	-1133.7890	1.46
		^4A	-1133.5885	2.08	^3A	-1133.7780	1.75
5-5-1-d	C_1	^2A	-1133.6073	1.57	^1A	-1133.7857	1.54
		^4A	-1133.6071	1.57	^3A	-1133.8097	0.89
5-5-2-d	C_1	^2A	-1133.6068	1.58	^1A	-1133.7750	1.84
		^4A	-1133.6126	1.42	^3A	-1133.7981	1.21
5-5-3-d	C_1	^2A	-1133.6121	1.44	^1A	FormBX had a problem	
		^4A	-1133.6143	1.38			
5-5-4-d	C_1	^2A	-1133.6266	1.04	^1A	-1133.8172	0.69
		^4A	-1133.6267	1.04	^3A	-1133.8287	0.37
5-6-1-d	C_s	$^2A''$	-1133.6613	0.10	$^1A'$	-1133.8318	0.29
5-6-2-d	C_1	^2A	-1133.5891	2.06	^1A	-1133.7823	1.64
		^4A	-1133.5903	2.03	^3A	-1133.7736	1.87
5-6-3-d	C_s	^2A	-1133.6193	1.24	^1A	Breaks of symmetry	
		^4A	No lower point found				
5-6-4-d	C_s	$^2A''$	-1133.5892	2.06	^1A	-1133.7625	2.18
5-6-4-d	C_1	^4A	-1133.5765	2.41	^3A	FormBX had a problem	
5-7-1-d	C_1	^2A	-1133.6030	1.68	^1A	-1133.7738	1.87
		^4A	-1133.6056	1.61	^3A	-1133.7973	1.23
5-7-2-d	C_1	^2A	Optimizes to 5-10-2-d				
5-7-4-d	C_1	^2A	-1133.6143	1.38	^1A	-1133.8115	0.84
		^4A	-1133.6151	1.36	^3A	-1133.8149	0.75
5-8-1-d		^2A	No lower point found				
5-8-2-d	C_1	^2A	-1133.6079	1.55	$^1A'$	-1133.7990	1.18
5-8-2-d	C_s	$^4A''$	-1133.6102	1.49	$^3A''$	-1133.7996	1.17
5-9-1-d	C_1	^2A	-1133.6384	0.72	^1A	-1133.8125	0.81

Table 77 (Table 75 cont.): Total energy (E_T, a.u.) and relative Energy (ΔE, eV) for neutral and anionic Ti_4AgO_{10} clusters at BPW91/6- 311+G (d). Number of imaginary frequencies are in curved bracket.

Cluster	PG	Ti_4AgO_{10}			$Ti_4AgO_{10}^-$		
		State	E_T	ΔE	State	E_T	ΔE
		^4A	-1133.6316	0.91	^3A	-1133.8271	0.42
5-9-4-d		^2A	No lower point found				
5-9-3-d	C_1	^2A	-1133.5866	2.13	^1A	-1133.7619	2.19
		^4A	-1133.5853	2.17	^3A	-1133.7601	2.24
5-9-4-d		^2A	No lower point found				
5-9-5-d	C_1	^2A	-1133.5851	2.17	^1A	-1133.7727	1.90
		^4A	-1133.5848	2.18	^3A	FormBX had a problem	
5-10-1-d		^2A	Convergence failure				
5-10-2-d	C_1	^2A	-1133.5980	1.82	^1A	-1133.7916	1.38
		^4A	-1133.5930	1.96	^3A	-1133.7876	1.49
5-10-3-d	C_1	^2A	-1133.6098	1.50	^1A	-1133.7987	1.19
		^4A	-1133.6113	1.46	^3A	-1133.8107	0.86
5-10-4-d	C_1	^2A	-1133.6318	0.90	^1A	-1133.8269	0.42
		^4A	-1133.6263	1.05	^3A	-1133.8243	0.49
5-10-5-d	C_1	^2A	-1133.6056	1.61	^1A	-1133.7997	1.16
		^4A	-1133.5987	1.80	^3A	-1133.8189	0.64
5-12-1-d	C_s	$^2A''$	-1133.6113	1.46	$^1A'$	-1133.7771	1.78
		$^4A''$	-1133.6008	1.74	$^3A''$ (1)	-1133.7919	1.38
					^3A	-1133.7919	1.37
5-12-2-d	C_{2h}	^2B_g	-1133.5781	2.36	^1Ag	-1133.7754	1.82
5-12-2-d		^4A	Breaks of symmetry		^1A (1)	-1133.7266	3.15
					^3A	-1133.7267	3.15
5-12-3-d	C_s	$^2A''$	-1133.5793	2.33	$^1A'$	-1133.7722	1.91
5-12-3-d	C_1	^4A	-1133.5408	3.38	^3A	-1133.7348	2.93
5-13-2-d	C_1	^2A	-1133.6218	1.17	^1A	-1133.8225	0.54
		^4A	-1133.6230	1.14	^3A	-1133.8306	0.32

Table 78 (Table 75 cont.): Total energy (E_T, a.u.) and relative Energy (ΔE, eV) for neutral and anionic Ti_4AgO_{10} clusters at BPW91/6- 311+G (d). Number of imaginary frequencies are in curved bracket.

Cluster	PG	Ti_4AgO_{10}			$Ti_4AgO_{10}^-$		
		State	E_T	ΔE	State	E_T	ΔE
5-16-d	C_1	^2A	-1133.6153	1.35	^1A	-1133.7967	1.25
		^4A	-1133.6123	1.43	^3A	-1133.8299	0.34
5-17-d	C_s	^2A	-1133.6040	1.66	^1A	-1133.8311	0.31
5-17-d	C_1	^4A	-1133.6000	1.77	^3A	-1133.8336	0.24
					$^1A'$ (1)	-1133.8286	0.38
5-18-d	C_1	^2A	-1133.6372	0.75	^1A	-1133.8300	0.34
		^4A	-1133.6371	0.76	^3A	-1133.8395	0.08
5-19-d	C_1	^2A	-1133.5935	1.94	^1A	-1133.8238	0.51
		^4A	-1133.5978	1.83	^3A	-1133.8290	0.37
5-20-d	C_1	$^2A''$	-1133.6107	1.47	$^1A'$	-1133.7629	2.16
		$^4A''$	-1133.6124	1.43	$^3A''$ (1)	-1133.7865	1.52
5-21-d	C_1	^2A	-1133.6357	0.79	^1A	-1133.8259	0.45
		^4A	-1133.6356	0.80	^3A	-1133.8404	0.06
5-22-d	C_1	^2A	-1133.5924	1.97	^1A	-1133.7694	1.99
		^4A	-1133.5957	1.88	^3A	-1133.8028	1.08

Table 79: New structures of Ti_4AgO_{10}

Doped Structure	Undoped Structure	Doped Position	Expected to be /Un-stable
5-16-d	5-3-u	3	--
5-17-d	5-3-u	5	--
5-18-d	5-5-u	5	--
5-19-d	5-7-u	3	--
5-20-d	5-9-u	2	--
5-21-d	--	--	5-1-1-d (C_1:^3A)
5-22-d	5-13-u	1	--

Table 80: VEDE (eV) of $Ti_4AgO_{10}^-$ was calculated at BPW91/6-311+G (d) basis set and SDD effective core potential

Cluster	PG	State	VEDE	Cluster	PG	State	VEDE
5-1-2-d	C_1	$^3A \rightarrow {}^2A$	5.80	5-9-1-d	C_1	$^3A \rightarrow {}^2A$	5.53
		$^3A \rightarrow {}^4A$	5.65			$^3A \rightarrow {}^4A$	5.53
5-2-2-d	C_1	$^1A \rightarrow {}^2A$	5.57	5-16-d	C_1	$^3A \rightarrow {}^2A$	5.87
5-2-2-d	C_1	$^3A \rightarrow {}^2A$	5.64			$^3A \rightarrow {}^4A$	5.73
		$^3A \rightarrow {}^4A$	5.61	5-17-d	C_1	$^1A \rightarrow {}^2A$	5.58
5-2-3-d	C_s	$^3A'' \rightarrow {}^2A'$	5.56	5-17-d	C_1	$^3A \rightarrow {}^2A$	5.73
		$^3A'' \rightarrow {}^4A''$	5.57	5-17-d	C_1	$^3A \rightarrow {}^4A$	5.57
5-3-1-d	C_1	$^1A \rightarrow {}^2A$	5.57	5-18-d	C_1	$^1A \rightarrow {}^2A$	5.41
5-3-1-d	C_1	$^3A \rightarrow {}^2A$	5.60	5-18-d	C_1	$^3A \rightarrow {}^2A$	5.80
		$^3A \rightarrow {}^4A$	5.53			$^3A \rightarrow {}^4A$	5.65
5-4-1-d	C_1	$^1A \rightarrow {}^2A$	5.16	5-19-d	C_1	$^3A \rightarrow {}^2A$	5.80
5-5-4-d	C_1	$^3A \rightarrow {}^2A$	5.78			$^3A \rightarrow {}^4A$	5.67
		$^3A \rightarrow {}^4A$	5.69	5-21-d	C_1	$^1A \rightarrow {}^2A$	5.31
5-6-1-d	C_s	$^1A'' \rightarrow {}^2A'$	4.84	5-21-d	C_1	$^3A \rightarrow {}^2A$	5.70
						$^3A \rightarrow {}^4A$	5.66

Table 81: AEDE (eV) of $Ti_4AgO_{10}^-$ clusters at BPW91/6-311+G (d)

Cluster	PG	States	AEDE	Cluster	PG	States	AEDE	Cluster	PG	States	AEDE
5-1-1-d	C_s	$^1A' \rightarrow {}^2A''$	5.43	5-5-1-d	C_1	$^3A \rightarrow {}^4A$	5.51	5-10-3-d	C_1	$^1A \rightarrow {}^2A$	5.14
5-1-2-d	C_1	$^1A \rightarrow {}^2A$	6.51			$^3A \rightarrow {}^4A$	5.05			$^3A \rightarrow {}^4A$	5.43
		$^3A \rightarrow {}^4A$	6.59	5-5-2-d	C_1	$^1A \rightarrow {}^2A$	4.58	5-10-4-d	C_1	$^1A \rightarrow {}^2A$	5.31
5-2-2-d	C_1	$^1A \rightarrow {}^2A$	5.40	5-5-4-d	C_1	$^1A \rightarrow {}^2A$	5.19			$^3A \rightarrow {}^4A$	5.39
5-2-3-d	C_s	$^1A' \rightarrow {}^2A''$	5.33			$^3A \rightarrow {}^4A$	5.50	5-10-5-d	C_1	$^1A \rightarrow {}^2A$	5.28
		$^3A'' \rightarrow {}^4A''$	6.23	5-6-1-d	C_s	$^1A' \rightarrow {}^2A''$	4.64			$^3A \rightarrow {}^4A$	5.99
		$^3A \rightarrow {}^4A$	5.44	5-6-2-d	C_1	$^1A \rightarrow {}^2A$	5.26	5-12-1-d	C_s	$^1A' \rightarrow {}^1A'$	4.51
5-3-1-d	C_1	$^1A \rightarrow {}^2A$	5.31			$^3A \rightarrow {}^4A$	4.99	5-12-2-d	C_{2h}	$^2B_g \rightarrow {}^1A_g$	5.37
		$^3A \rightarrow {}^4A$	5.39	5-7-1-d	C_1	$^1A \rightarrow {}^2A$	4.65	5-12-3-d	C_s	$^2A'' \rightarrow {}^2A''$	5.25

Table 82 (Table 81 cont.): AEDE for $Ti_4AgO_{10}^-$ clusters at BPW91/6-311+G (d)

Cluster	PG	States	AEDE	Cluster	PG	States	AEDE	Cluster	PG	States	AEDE
5-3-2-d	C_1	$^1A\rightarrow^2A$	4.35	5-5-1-d	C_1	$^3A\rightarrow^4A$	5.22	5-12-3-d	C_1	$^3A\rightarrow^4A$	5.28
		$^3A\rightarrow^4A$	4.97	5-7-4-d	C_1	$^1A\rightarrow^2A$	5.37	5-16-d	C_1	$^1A\rightarrow^2A$	4.94
5-4-1-d	C_1	$^1A\rightarrow^2A$	4.83			$^3A\rightarrow^4A$	5.44			$^3A\rightarrow^4A$	5.92
		$^3A\rightarrow^4A$	5.02	5-8-2-d	C_s	$^3A''\rightarrow^4A''$	5.16	5-17-d	C_1	$^3A\rightarrow^4A$	6.36
5-4-2-d	C_1	$^1A\rightarrow^2A$	3.73	5-9-1-d	C_1	$^1A\rightarrow^2A$	4.74	5-18-d	C_1	$^1A\rightarrow^2A$	5.25
		$^3A\rightarrow^4A$	4.85	5-9-1-d	C_1	$^3A\rightarrow^4A$	5.32			$^3A\rightarrow^4A$	5.51
5-4-3-d	C_1	$^1A\rightarrow^2A$	4.29	5-9-3-d	C_1	$^1A\rightarrow^2A$	4.77	5-19-d	C_1	$^1A\rightarrow^2A$	6.27
5-4-4-d	C_1	$^1A\rightarrow^2A$	4.87	5-9-5-d	C_1	$^1A\rightarrow^2A$	5.10			$^3A\rightarrow^4A$	5.91
		$^3A\rightarrow^4A$	4.84	5-10-3-d	C_1	$^1A\rightarrow^2A$	5.09	5-21-d	C_1	$^1A\rightarrow^2A$	5.17
5-4-5-d	C_1	$^1A\rightarrow^2A$	5.08			$^3A\rightarrow^4A$	5.43			$^3A\rightarrow^4A$	5.57
		$^3A\rightarrow^4A$	5.16	5-10-2-d	C_1	$^1A\rightarrow^2A$	5.27				
5-5-1-d	C_1	$^1A\rightarrow^2A$	4.85			$^3A\rightarrow^4A$	5.30				

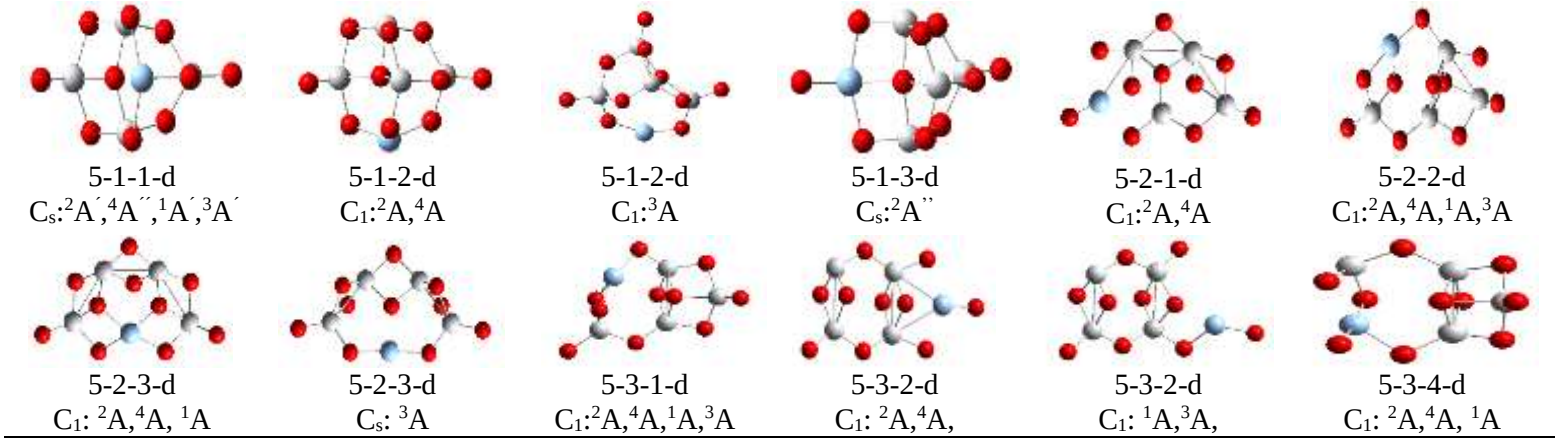

Figure 95: Structures of the Ti_4AgO_{10} clusters. Structure name, point group and state are displayed bellow each structure. The Ti, O and Ag atoms are indicated by gray, red and blue spheres respectively.

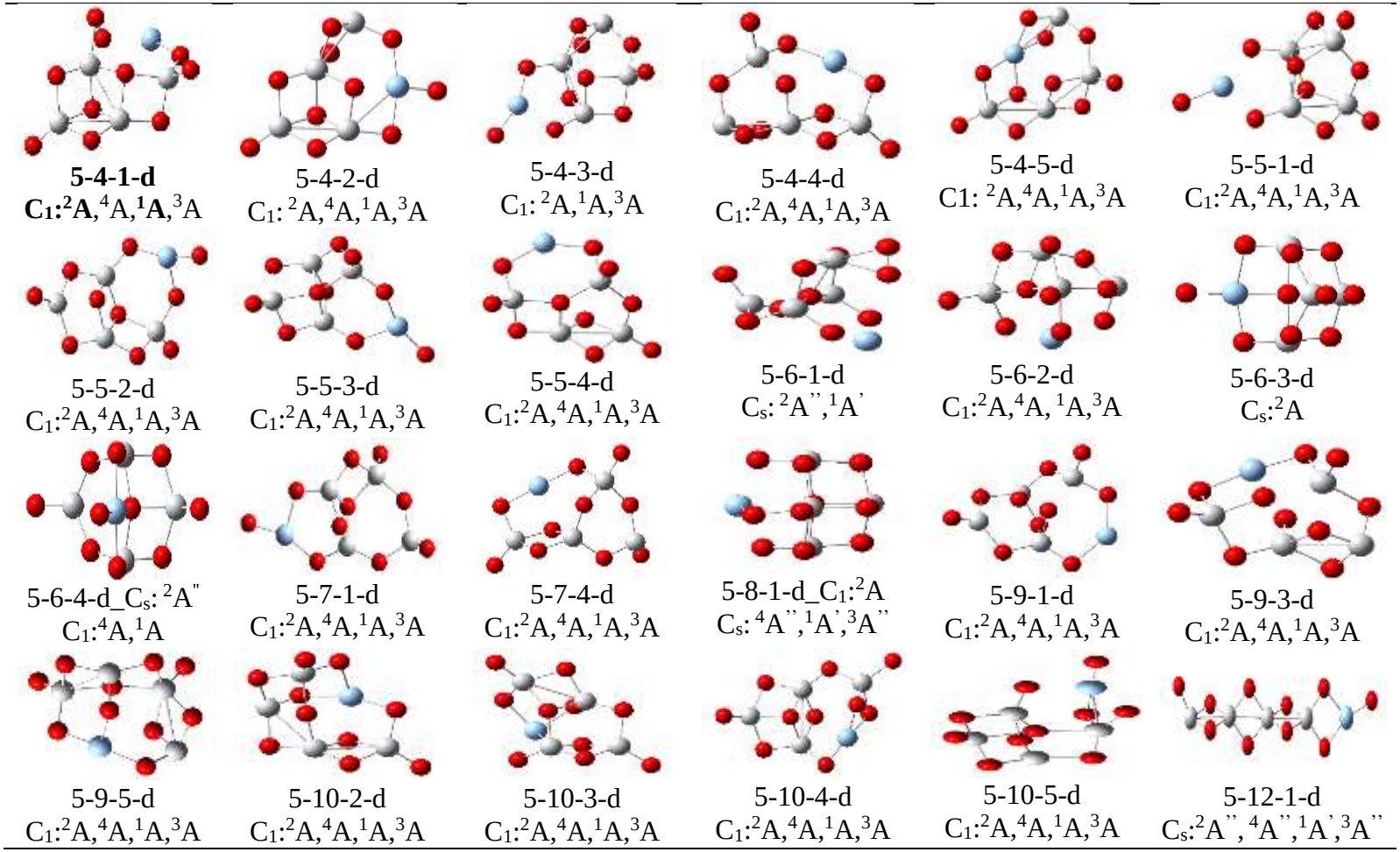

Figure 96 (Figure 95 cont.): Structures of the Ti_4AgO_{10} clusters. Structure name, point group and state are displayed bellow each structure. The Ti, O and Ag atoms are indicated by gray, red and blue spheres respectively.

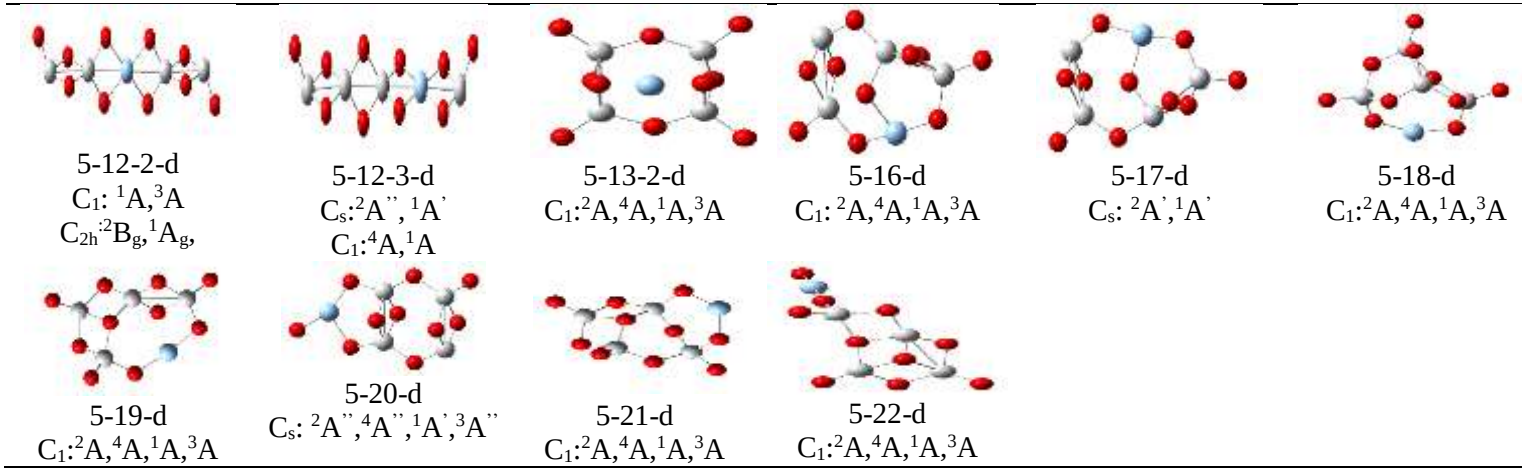

Figure 97 (Figure 95 cont.): Structures of the Ti_4AgO_{10} clusters. Structure name, point group and state are displayed bellow each structure. The Ti, O and Ag atoms are indicated by gray, red and blue spheres respectively.

4.3 Ti_4AuO_{10}

Table 83: Total energy (E_T, au) and relative Energy (ΔE, eV) for neutral and anionic Ti_4AuO_{10} clusters at BPW91/6- 311+G (d).PG: Point group

Structure	PG	Ti_4AuO_{10}			$Ti_4AuO_{10}^-$		
		State	E_T	ΔE	State	E_T	ΔE
5-1-1-d	C_s	$^2A''$	-1122.4126	1.59	$^1A'$	-1122.6040	1.16
		^4A	FormXB had a prob-lem		$^3A'$	FormBX had a prob-lem	
5-1-2-d	C_1	^2A	-1122.3882	2.25	^1A	-1122.5664	2.19
		^4A	Converged failure		^3A	Converged failure	
5-1-3-d	C_s	$^2A''$	-1122.4301	1.11	^1A	No lower point found	
5-1-3-d	C_1	^4A	-1122.4200	1.39			
5-1-4-d	C_s	$^2A''$	-1122.3950	2.06	^1A	No lower point found	
		$^4A''$	-1122.3824	2.40			
5-2-3-d	C_s	$^2A''$	-1122.4114	1.62	$^1A'$	-1122.6021	1.21
		$^4A'$	-1122.3839	2.37	$^3A'$	-1122.6235	0.63

Table 84 (Table 83 cont.): Total energy (E_T, a.u.) and relative Energy (ΔE, eV) for neutral and anionic Ti_4AuO_{10} clusters at BPW91/6- 311+G (d).

Structure	PG	Ti_4AuO_{10}			$Ti_4AuO_{10}^-$		
		State	E_T	ΔE	State	E_T	ΔE
5-2-1-d	C_1	^2A	-1122.4212	1.35	^1A	Converged failure	
		^4A	-1122.4235	1.29			
5-2-2-d	C_1	^2A	-1122.4290	1.14	^1A	-1122.6250	0.59
			Convergence failure		^3A	-1122.6361	0.29
5-3-1-d	C_1	^2A	-1122.4317	1.07	^1A	-1122.6279	0.51
		^4A	-1122.4203	1.38	^3A	-1122.6345	0.33
5-3-2-d	C_1	^2A	-1122.4233	1.30	^1A	Converged failure	
5-3-2-d	C_s	$^2A''$	-1122.4189	1.42	$^1A'$	-1122.5704	2.08
5-3-2-d	C_s	$^4A''$		1.27	^3A	Converged	
			-1122.4244			failure	
5-3-4-d	C_1	^2A	-1122.4111	1.63	^1A	-1122.5778	1.88
		^4A	-1122.4003	1.92			
5-4-1-d	C_1	^2A	-1122.4542	0.46	^1A	-1122.6393	0.20
		^4A	-1122.3621	2.96	^3A	-1122.5602	2.36
5-4-2-d	C_1	^2A	-1122.4218	1.34	^1A	Converged failure	
		^4A	Converged failure				
5-4-3-d	C_1	^2A	-1122.4033	1.84	^1A	-1122.5600	2.36
					^3A	-1122.6248	0.60
5-4-4-d	C_1	^2A	-1122.4052	1.79	^1A	-1122.5826	1.74
		^4A	-1122.4000	1.93	^3A	-1122.5775	1.88
5-4-5-d	C_1	^2A	-1122.4036	1.83	^1A	-1122.5903	1.54
5-5-1-d		^2A	-1122.4106	1.64			
		^4A	-1122.4128	1.58			
5-5-2-d	C_1	^2A	-1122.4294	1.13	^1A	-1122.6053	1.13
					^3A	-1122.6094	1.02
5-5-2-d		^2A	FormBX had a problem				
5-5-4-d	C_1	^2A	-1122.4225	1.32	^1A	-1122.6238	0.62
		^4A	-1122.4248	1.26	^3A	-1122.6296	0.47

Table 85 (Table 83 cont.): Total energy (E_T, au) and relative Energy (ΔE, eV) for neutral and anionic Ti_4AuO_{10} clusters at BPW91/6- 311+G (d). PG: Point group

Structure		Ti_4AuO_{10}			$Ti_4AuO_{10}^-$		
	PG	State	E_T	ΔE	State	E_T	ΔE
5-6-1-d	C_s	$^2A''$	-1122.4709	***0.00***	$^1A'$	-1122.6275	0.52
		$^4A''$		2.17	^3A		
			-1122.3912			FormBX had a problem	
5-6-2-d	C_1	^2A	-1122.3829	2.40	^1A	-1122.5997	1.28
		^4A	-1122.3772	2.55	^3A	-1122.5945	1.42
5-6-3-d	C_s	$^2A''$	-1122.4301	1.11	^1A	No lower point found	
5-6-3-d	C_1	^4A	-1122.4200	1.39			
5-6-4-d	C_1	^2A	-1122.3983	1.98	^1A	Convergence failure	
		^4A	-1122.3752	2.60			
5-7-1-d	C_1	^2A	-1122.4121	1.60	^1A	Convergence failure	
		^4A	-1122.4137	1.56			
5-7-2-d	C_1	^2A	Optimizes to 5-10-4d				
5-7-4-d	C_1	^2A	-1122.4080	1.71	^1A	-1122.6094	1.02
		^4A	-1122.4109	1.64	^3A	-1122.6205	0.71
5-8-2-d	C_s	$^2A''$	-1122.4009	1.91	$^1A'$	-1122.5891	1.57
5-8-2-d	C_1	^4A	-1122.3906	2.19	$^3A''$	-1122.5871	1.62
5-9-1-d	C_1	^2A	-1122.4289	1.14	^1A	-1122.6074	1.07
		^4A	-1122.4179	1.44	^3A	Converged failure	
5-9-3-d	C_1	^2A	-1122.3829	2.40	^1A	Converged failure	
		^4A	-1122.3733	2.66			
5-9-4-d			No lower point found				
5-9-5-d	C_1	^2A	-1122.3836	2.38	^1A	-1122.5710	2.06
		^4A	-1122.3783	2.52	^3A	-1122.5659	2.20
5-10-1-d	C_1	^2A	-1122.4281	1.17	^1A	-1122.6151	0.86
		^4A	-1122.4348	0.98	^3A	-1122.6345	0.33
5-10-1-d	C_1	^2A	-1122.3995	1.94	^1A	-1122.5923	1.48
		^4A	-1122.3827	2.40	^3A	-1122.5756	1.93
5-10-3-d	C_1	^2A	-1122.4024	1.86	^1A	-1122.5906	1.53
		^4A	-1122.3972	2.00	^3A	-1122.3972	6.79

Table 86 (Table 83 cont.): Total energy (E_T, au) and relative Energy (ΔE, eV) for neutral and anionic Ti_4AuO_{10} clusters at BPW91/6- 311+G (d). PG: Point group

Structure	PG	Ti_4AuO_{10}			$Ti_4AuO_{10}^-$		
		State	E_T	ΔE	State	E_T	ΔE
5-10-4-d	C_1	^2A	-1122.4317	1.07	^1A	-1122.6279	0.51
		^4A	-1122.4203	1.38	^3A	-1122.6349	0.32
5-10-5-d	C_1	^2A	-1122.4124	1.59	^1A	Converged failure	
		^4A	-1122.4217	1.34			
5-12-1-d	C_s	$^2A''$	-1122.4308	1.09	^1A	No lower point found	
		^4A	Convergence failure				
5-12-2-d	C_1	^2B_g	-1122.3921	2.15	^1A_g	-1122.5830	1.73
			No lower point found		^3B_g	-1122.5237	3.35
5-12-2-d	C_1	^2A	No lower point found				
5-12-3-d		^2A	No lower point found				
5-13-2-d	C_1	^2A	Convergence failure				
5-16-d	C_1	^2A	-1122.4141	1.55	^1A	-1122.5959	1.38
		^4A	-1122.4064	1.76	^3A	-1122.5903	1.54
5-17-d	C_1	^2A (1)	-1122.4039	1.82			
5-18-d	C_1	^2A	-1122.4376	0.91	^1A	-1122.6358	0.30
		^4A	-1122.4418	0.79	**^3A**	-1122.6467	***0.00***
5-19-d	C_1	^2A	-1122.3914	2.16	^1A	Converged failure	
		^4A	-1122.3917	2.16			
5-21-d	C_1	^2A	-1122.4288	1.15	^1A	-1122.6234	0.64
		^4A	-1122.4311	1.08	^3A	-1122.6361	0.29
5-22-d	C_1	^2A	-1122.3231		^1A	-1122.5829	
		^4A	Convergence failure		^3A	FormBX had a problem	

Table 87: VEDE for $Ti_4AuO_{10}^-$ clusters at BPW91/6-311+G (d)

Structure	PG	State	VED E	Structure	PG	State	VEDE
5-2-2-d	C_1	$^3A\rightarrow{}^2A$	5.78	5-10-1-d	C_1	$^3A\rightarrow{}^2A$	5.81
		$^3A\rightarrow{}^4A$	5.67			$^3A\rightarrow{}^4A$	5.66
5-3-1-d	C_1	$^3A\rightarrow{}^2A$	5.81	5-18-d	C_1	$^1A\rightarrow{}^2A$	5.56
		$^3A\rightarrow{}^4A$	5.66	5-18-d	C_1	$^3A\rightarrow{}^2A$	5.75
5-4-1-d	C_1	$^1A\rightarrow{}^2A$	5.36			$^3A\rightarrow{}^4A$	5.70
5-5-4-d	C_1	$^3A\rightarrow{}^2A$	5.79	5-21-d	C_1	$^3A\rightarrow{}^2A$	5.79
		$^3A\rightarrow{}^4A$	5.75			$^3A\rightarrow{}^4A$	5.66

Table 88: AEDE for $Ti_4AuO_{10}^-$ clusters at BPW91/6-311+G (d)

Cluster	PG	States	AEDE	Cluster	PG	States	AED E	Cluster	PG	States	AED E
5-1-1-d	C_s	$^1A'\rightarrow{}^2A''$	5.21	5-4-1-d	C_1	$^1A\rightarrow{}^2A$	5.04	5-7-4-d	C_1	$^3A\rightarrow{}^2A$	5.48
5-1-2-d	C_1	$^1A\rightarrow{}^2A$	4.84			$^3A\rightarrow{}^4A$	5.39			$^3A\rightarrow{}^4A$	5.70
5-2-3-d	C_s	$^1A'\rightarrow{}^2A''$	5.19	5-4-3-d	C_1	$^1A\rightarrow{}^2A$	4.26	5-8-2-d	C_s	$^1A'\rightarrow{}^2A''$	5.12
		$^3A'\rightarrow{}^4A'$	6.52	5-4-4-d	C_1	$^1A\rightarrow{}^2A$	4.83	5-9-1-d	C_1	$^1A\rightarrow{}^2A$	4.86
5-2-2-d	C_1	$^1A\rightarrow{}^2A$	5.33			$^3A\rightarrow{}^4A$	4.83	5-9-5-d	C_1	$^3A\rightarrow{}^2A$	5.10
5-3-1-d	C_1	$^1A\rightarrow{}^2A$	5.34	5-4-5-d	C_1	$^1A\rightarrow{}^2A$	5.08			$^3A\rightarrow{}^4A$	5.11
		$^2A\rightarrow{}^4A$	5.83	5-5-2-d	C_1	$^1A\rightarrow{}^2A$	4.79	5-10-1-d	C_1	$^3A\rightarrow{}^2A$	5.09
5-3-2-d	C_s	$^1A'\rightarrow{}^2A``$	4.12	5-18-d	C_1	$^1A\rightarrow{}^2A$	5.39			$^3A\rightarrow{}^4A$	5.43
5-3-4-d	C_1	$^1A\rightarrow{}^2A$	4.54			$^3A\rightarrow{}^4A$	5.57	5-12-2-d	C_{2h}	$^1A_g\rightarrow{}^2B_g$	5.19
5-16-d	C_1	$^2A\rightarrow{}^1A$	4.95	5-18-d	C_1	$^1A\rightarrow{}^2A$	5.48	5-21-d	C_1	$^3A\rightarrow{}^2A$	5.29
		$^3A\rightarrow{}^4A$	5.00	5-6-1-d		$^3A\rightarrow{}^4A$	6.04			$^3A\rightarrow{}^4A$	5.58
				5-6-2-d	C_s	$^1A'\rightarrow{}^2A''$	4.26				

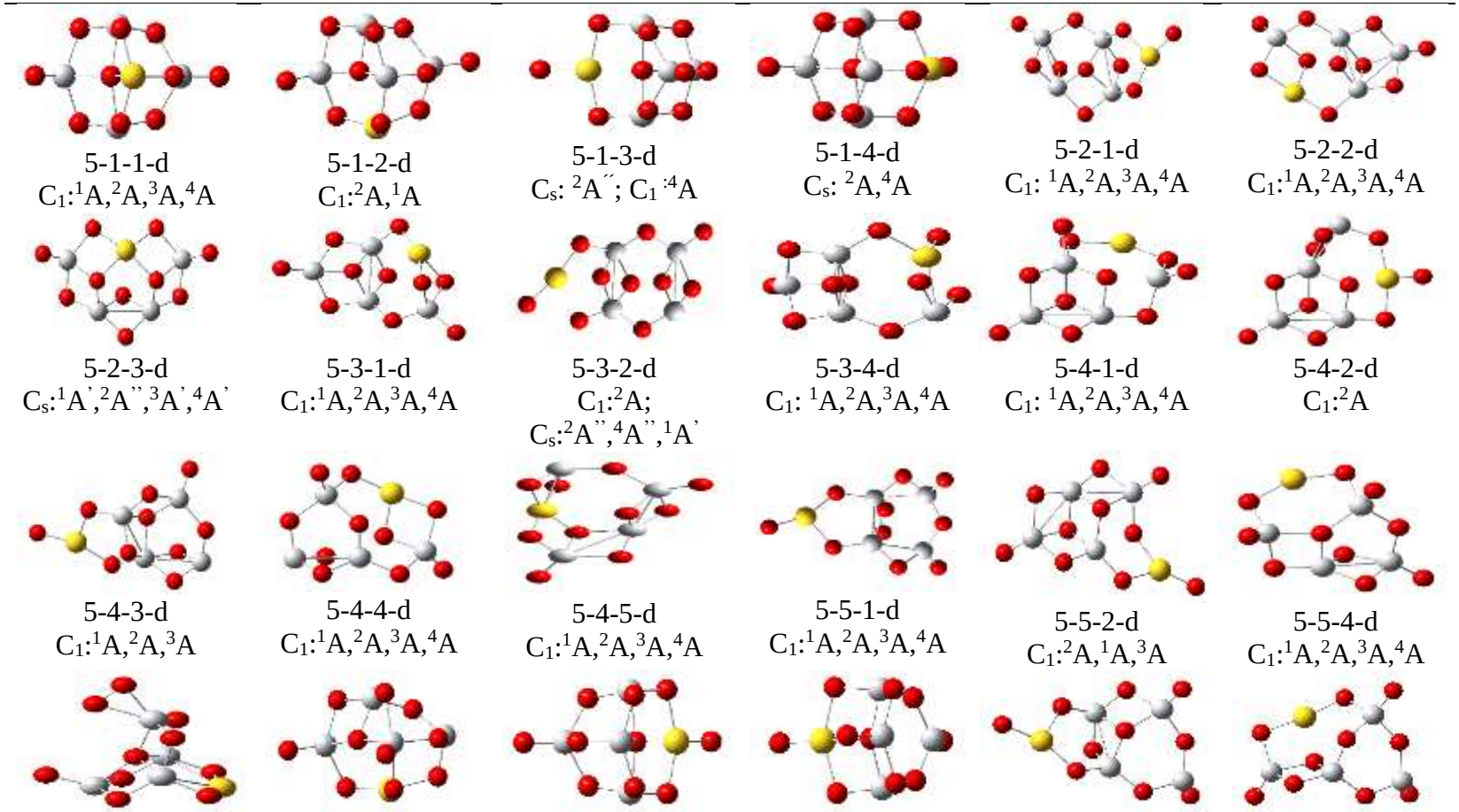

Figure 98: Structures of the Ti_4AuO_{10} clusters. Structure name, point group and state are displayed bellow each structure. The Ti, O and Au atoms are indicated by gray, red and yellow spheres respectively.

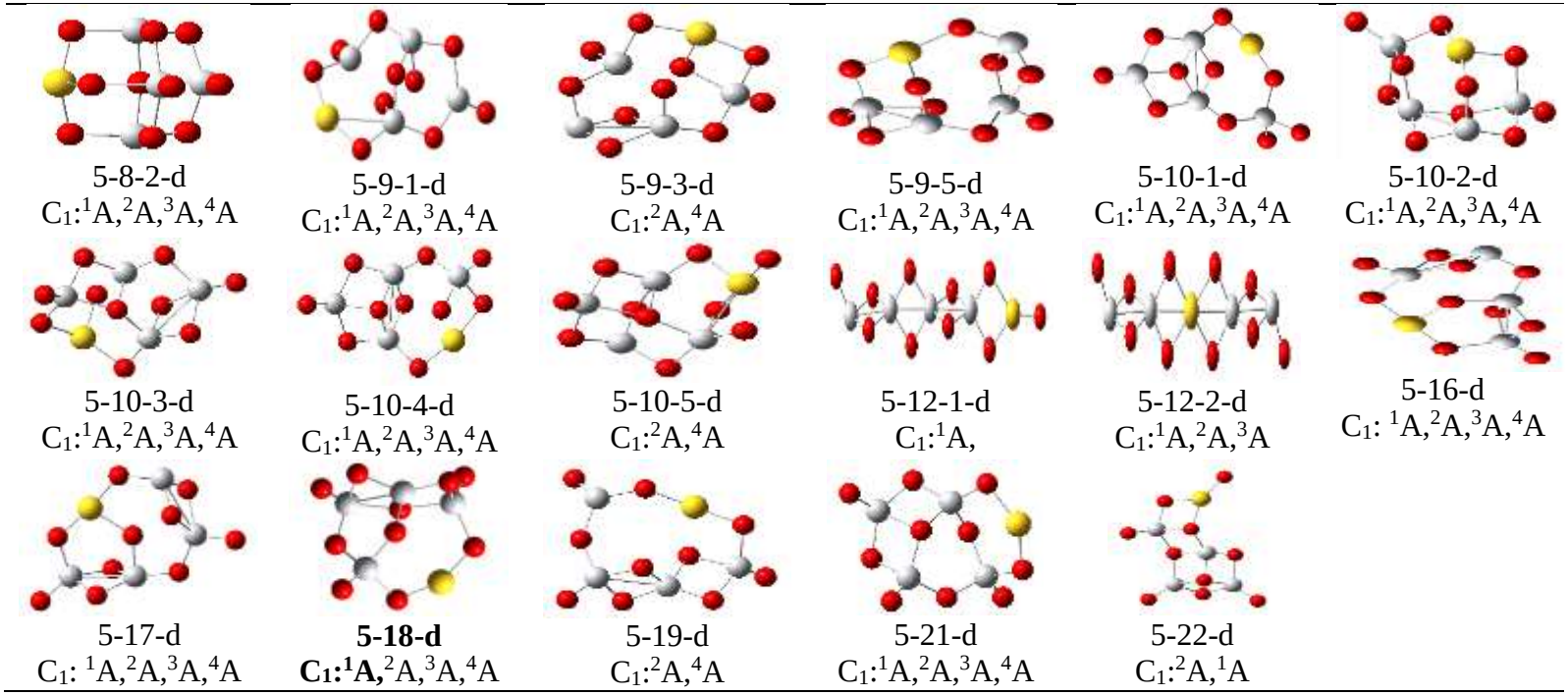

Figure 99 (Figure 98 cont.): Structures of the Ti_4AuO_{10} clusters. Structure name, point group and state are displayed bellow each structure. The Ti, O and Au atoms are indicated by gray, red and yellow spheres respectively.

5 Cluster size n = 6

5.1 Ti_6O_{12}

Table 89: Total energy (E_T, a.u.), relative Energy (ΔE, eV), AEDE for neutral and anionic Ti_6O_{12} clusters at BPW91/6- 311+G (d). PG: Point group

Structure	PG	Ti_6O_{12}			$Ti_6O_{12}^-$			
		State	E_T	ΔE	State	E_T	ΔE	AEDE
6-1-u	C_2	^1A	-1254.3995	**0.00**	^2A	-1254.5146	**0.00**	3.13
6-2-u	C_1	^1A	-1254.3754	0.66	^2A	-1254.5061	0.23	3.56
6-3-u	C_{2v}	$^1A_1$	-1254.3711	0.77	$^2A_1$	-1254.4961	0.50	3.40
6-4-u	C_{2v}	$^1A_1$	-1254.3790	0.56	$^2A_1$	-1254.4763	1.04	2.65
6-5-u	C_s	$^1A'$	-1254.3775	0.6	$^2A'$	-1254.4906	0.65	3.08
6-6-u	C_{2v}	$^1A_1$	-1254.3515	1.31	$^2B_1$	-1254.4574	1.56	2.88
6-7-u	C_{2v}	$^1A_1$	-1254.3495	1.36	$^2B_2$	-1254.4600	1.49	3.01

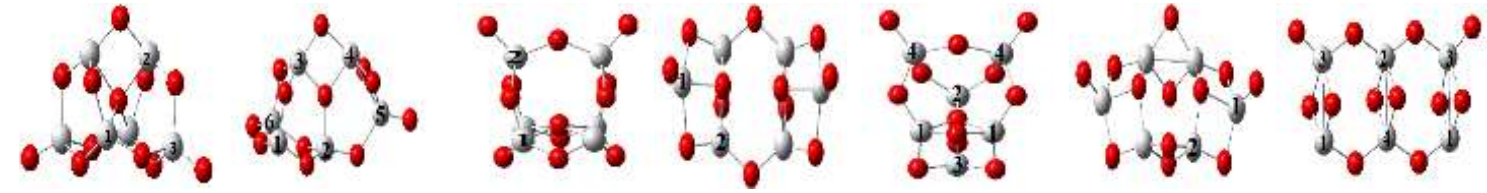

6-1-u C_2: ^1A,^2A | 6-2-u C_1: ^1A,^2A | 6-3-u C_{2v}:$^1A_1$, $^2A_1$ | 6-4-u C_{2v} : $^1A_1$$^2A_1$ | 6-5-u C_s : $^1A'$, $^1A'$ | 6-6-u C_{2v} : $^1A_1$, $^2B_1$ | 6-7-u C_{2v} : $^1A_1$, $^2B_2$

Figure 100: Structures of the Ti_6O_{12} clusters. Structure name, point group and state are displayed bellow each structure. The Ti and O atoms are indicated by gray and red spheres respectively.

5.2 Ti_5AgO_{12}

Table 90: Total energy (E_T, a.u.) and relative Energy (ΔE, eV) for neutral and anionic Ti_5AgO_{12} clusters at BPW91/6- 311+G (d).

Structure	PG	Ti_5AgO_{12}			$Ti_5AgO_{12}^-$		
		State	E_T	ΔE	State	E_T	ΔE
6-1-1-d	C_1	^2A	-1342.7391	1.57	^1A	-1342.9289	1.14
		^4A	-1342.7378	1.61	^3A	-1342.9365	0.94
6-1-2-d	C_1	**^2A**	-1342.7968	**0.00**	**^1A**	-1342.9709	**0.00**
		^4A	-1342.7124	2.30	^3A	-1342.9117	1.61
6-1-3-d	C_1	^2A	-1342.7045	2.51	^1A	-1342.8881	2.25
		^4A	-1342.7060	2.47	^3A	-1342.9121	1.60
6-2-1-d	C_1	^2A	-1342.7248	1.96	^1A	-1342.9366	0.93
		^4A	-1342.7242	1.97	^3A	-1342.9335	1.02
6-2-3-d	C_1	^2A	-1342.6985	2.67	^1A	-1342.8946	2.07
		^4A	-1342.6961	2.74	^3A	-1342.8892	2.22
6-2-2-d	C_1	^2A	-1342.6935	2.81	^1A	-1342.8818	2.42
		^4A	-1342.6918	2.86	^3A	-1342.9146	1.53
6-2-4-d	C_1	^2A	-1342.7125	2.29	^1A	-1342.8976	1.99
		^4A	-1342.7127	2.29	^3A	-1342.8965	2.02
6-2-5-d	C_1	^2A	-1342.7011	2.60	^1A	-1342.8517	3.24
		^4A	-1342.6953	2.76	^3A	FormBX had a problem	
6-2-6-d	C_1	^2A	-1342.6905	2.89	^1A	-1342.8691	2.77
		^4A	-1342.6879	2.96	^3A	-1342.8925	2.13
6-3-1-d	C_1	^2A	-1342.7328	1.74	^1A	-1342.9217	1.34
		^4A	-1342.7336	1.72	^3A	-1342.9304	1.10
6-3-2-d	C_s	$^2A''$	-1342.6936	2.81	^1A	-1342.8289	3.86
		$^4A''$	-1342.6946	2.78	^3A	-1342.8579	3.07
6-4-2-d	C_1	^2A	-1342.7224	2.03	^1A	-1342.9257	1.23
		^4A	-1342.7200	2.09	^3A	-1342.9256	1.23
6-4-1-d	C_s	$^2A''$	-1342.7241	1.98	^1A	-1342.8926	2.13
6-4-1-d	C_1	^4A	-1342.7180	2.15	^3A	-1342.9135	1.56

Table 91 (Table 90 cont.): Total energy (E_T, au) and relative energy (ΔE, eV)) for neutral and anionic Ti_5AgO_{12} clusters at BPW91/6- 311+G (d).

Structure	PG	Ti_5AgO_{12}			$Ti_5AgO_{12}^-$		
		State	E_T	ΔE	State	E_T	ΔE
6-5-1-d	C_1	^2A	-1342.7343	1.70	^1A	-1342.9235	1.29
		^4A	-1342.7355	1.67	^3A	-1342.9311	1.08
6-5-2-d	C_s	$^2A'$	-1342.7300	1.82	^1A	-1342.9089	1.69
		^4A	-1342.7289	1.85	$^1A'$ (1)	-1342.9088	1.69
					$^3A''$	-1342.9158	1.50
6-5-3-d	C_s	$^2A"$	-1342.7308	1.80	$^1A"$	No lower point found	
		$^4A"$	-1342.7316	1.77			
6-5-4-d	C_1	^2A	-1342.6989	2.66	^1A	Optimizes to 6-4-1-d	
		^4A	-1342.7012	2.60			
6-6-1-d	C_s	$^2A"$	-1342.7036	2.53	^1A	No lower point found	
		$^4A"$	-1342.6916	2.86			
6-6-2-d	C_1	^2A	-1342.6981	2.69	^1A	-1342.9026	1.86
		^4A	SCF convergence problem		^3A	-1342.8960	2.04
6-5-4-d	C_1	^2A	-1342.6989	2.66	^1A	Optimizes to 6-4-1-d	
		^4A	-1342.7012	2.60			
6-7-3-d	C_s	$^2A''$	-1342.6461	4.10	^1A	Break of symmetry	
		$^4A''$	-1342.6617	3.67			
6-7-1-d	C_1	^2A	-1342.7097	2.37	^1A	-1342.8954	2.05
		^4A	-1342.7036	2.53	^3A	-1342.8930	2.12
6-7-2-d	C_{2v}	$^2B_1$ (1)	-1342.6426	4.19			
		$^4A_2$	-1342.6447	4.14			
6-7-2-d	C_1				^1A	-1342.8311	3.8
6-7-4-d		^2A	No lower point found				

Table 92: VEDE (eV) for $Ti_5AuO_{12}^-$ clusters at BPW91/6-311+G (d)

Cluster	PG	State	VEDE
6-1-2-d	C_1	$^1A \rightarrow {}^2A$	5.27

Table 93: AEDE (eV) for $Ti_5AuO_{12}^-$ clusters at BPW91/6-311+G (d)

Structure	PG	State	AEDE	Structure	PG	State	AEDE	Structure	PG	State	AEDE
6-1-1-d	C_1	^2A-^1A	5.16	6-2-1-d	C_1	^2A-^1A	5.76	6-2-5-d	C_1	^2A-^1A	4.10
		^4A-^3A	5.41			^4A-^3A	5.69	6-3-1-d	C_1	^2A-^1A	5.14
6-1-2-d	C_1	^2A-^1A	4.74	6-2-3-d	C_1	^2A-^1A	5.34			^4A-^3A	5.35
		^4A-^3A	5.42			^4A-^3A	5.25	6-4-2-d	C_1	^2A-^1A	5.53
6-1-3-d	C_1	^2A-^1A	4.99	6-2-2-d	C_1	^2A-^1A	5.12			^4A-^3A	5.59
		^4A-^3A	5.61			^4A-^3A	6.06	6-5-1-d	C_1	^2A-^1A	5.15
6-2-1-d	C_1	^2A-^1A	4.86	6-2-4-d	C_1	^2A-^1A	5.04			^4A-^3A	5.32
		^4A-^3A	5.57			$^4A^3A$	5.00				

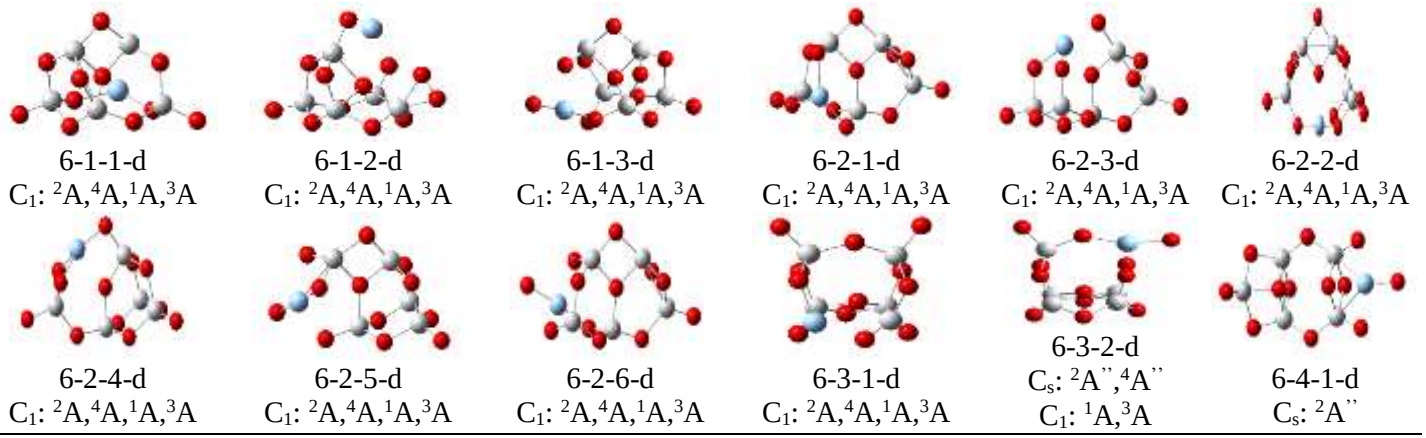

Figure 101: Structures of the Ti_5AgO_{12} clusters. Structure name, point group and state are displayed bellow each structure. The Ti, O and Ag atoms are indicated by gray, red and blue spheres respectively.

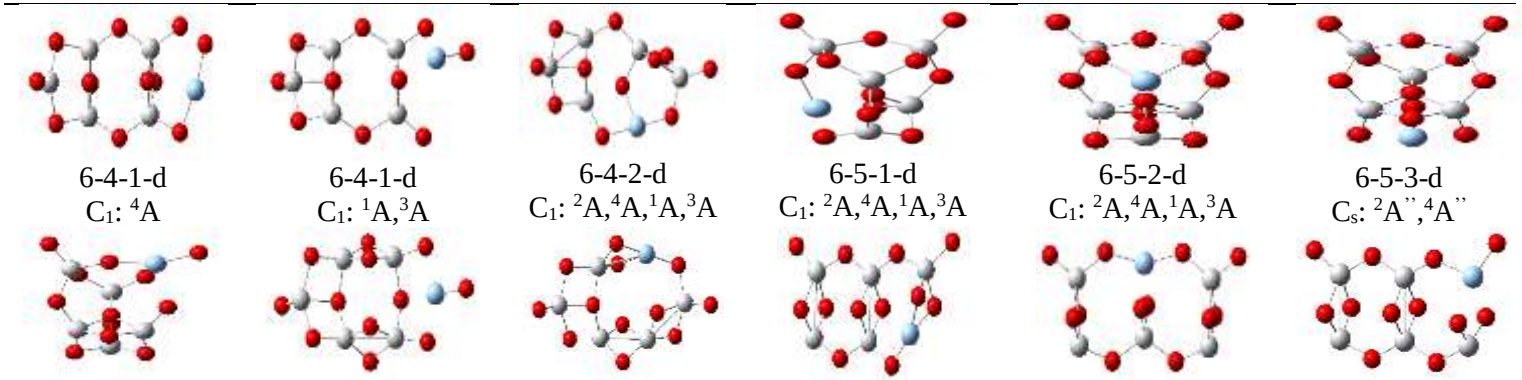

Figure 102 (Figure 101 cont.): Structures of the Ti_5AgO_{12} clusters. Structure name, point group and state are displayed bellow each structure. The Ti, O and Ag atoms are indicated by gray, red and blue spheres respectively.

5.3 Ti_5AuO_{12}

Table 94: Total energy (E_T, a.u.) and relative Energy (ΔE, eV) for neutral and anionic Ti_5AgO_{12} clusters at BPW91/6- 311+G (d). PG: Point group

Structure	PG	Ti_5AgO_{12}			$Ti_5AgO_{12}^-$		
		State	E_T	ΔE	State	E_T	ΔE
6-1-1-d	C_1	^2A	-1331.5361	1.30	^1A	-1331.7225	1.09
		^4A	-1331.5312	1.43	^3A	-1331.7275	0.95
6-1-2-d	C_1	^2A	-1331.5839	***0.00***	^1A	-1331.7625	***0.00***
		^4A	-1331.5092	2.03	^3A	-1331.6957	1.82
6-1-3-d	C_1	^2A	-1331.5280	1.52	^1A	-1331.7078	1.49
		^4A	-1331.5227	1.67	^3A	-1331.7339	0.78
6-2-1-d	C_1	^2A	-1331.5226	1.67	^1A	-1331.7313	0.85
		^4A	Convergence failure		^3A	-1331.7250	1.02
6-2-2-d	C_1	^2A	-1331.5265	1.56	^1A	-1331.6855	2.10
		^4A	-1331.4892	2.58	^3A	-1331.7168	1.24
6-2-3-d	C_1	^2A	-1331.4955	2.41	^1A	-1331.6897	1.98
		^4A	-1331.4829	2.75	^1A	FormBX had a problem	

Table 95 (Table 94 cont.): Total energy (E_T, au) and relative energy (ΔE, eV) for neutral and anionic Ti_5AgO_{10} clusters at BPW91/6- 311+G (d). PG: Point group

Structure	PG	Ti_5AgO_{12}			$Ti_5AgO_{12}^-$		
		State	E_T	ΔE	State	E_T	ΔE
6-2-4-d	C_1	^2A	-1331.5104	2.00	^1A	-1331.7137	1.33
		^4A	-1331.5011	2.25	^3A	-1331.7151	1.29
6-2-5-d	C_1	^2A	-1331.5071	2.09	^1A	Convergence failure	
		^4A	-1331.5132	1.92			
6-2-6-d	C_1	^2A	-1331.4948	2.42	^1A	-1331.7191	1.18
		^4A	-1331.4951	2.42	^3A	-1331.7250	1.02
6-3-1-d	C_1	^2A	-1331.5216	1.70	^1A	-1331.7088	1.46
		^4A	-1331.5241	1.63	^3A	-1331.7152	1.29
6-3-2-d	C_1	^2A	-1331.4919	2.50	^1A	Convergence failure	
		^4A	-1331.4988	2.32			
6-4-1-d	C_s	$^2A'$	-1331.5213	1.70	$^1A'$	Convergence failure	
6-4-1-d	C_1	^2A	-1331.5265	1.56	^1A	-1331.7091	1.46
		^4A	-1331.5310	1.44	^3A	FormBX had a problem	
6-4-2-d	C_1	^2A	-1331.5207	1.72	^1A	-1331.7264	0.98
		^4A	-1331.5141	1.90	^3A	-1331.7200	1.16
6-5-1-d	C_1	^2A	-1331.5188	1.77	^1A	-1331.7076	1.50
		^4A	-1331.5213	1.70	^3A	-1331.7118	1.38
6-5-2-d	C_1	^2A	-1331.5226	1.67	^1A	-1331.7022	1.64
		^4A	-1331.5136	1.91	^3A	-1331.6943	1.86
6-5-3-d	C_s	$^2A''$	-1331.5169	1.82	^1A	Break of symmetry	
		$^4A''$	-1331.5171	1.82			
6-7-1-d	C_s	^2A	-1331.5095	2.02	^1A	-1331.6956	1.82
		^4A	-1331.4982	2.33	^3A	-1331.7027	1.63
6-7-2-d		^2A	Break of symmetry				
6-7-4-d		^2A	No lower point found				
6-9-d	C_1	^2A	-1331.5106	1.99	^1A	Convergence failure	
		^4A	-1331.5005	2.27			

Table 96: New structures of Ti_5AuO_{12}

Doped Structure	Undoped Structure	Doped Position
6-9-d	6-7-u	3

Table 97: VEDE (eV) for $Ti_5AuO_{12}^-$ clusters at BPW91/6-311+G (d)

Cluster	PG	State	VEDE
6-1-2-d	C_1	$^1A \rightarrow ^2A$	5.26

Table 98: AEDE (eV) for $Ti_5AuO_{12}^-$ clusters at BPW91/6-311+G (d). PG: Point group

Structure	PG	State	AEDE	Struc-ture	PG	State	AEDE	Structure	PG	State	AEDE
6-1-1-d	C_1	$^1A \rightarrow ^2A$	5.07	6-2-6-d	C_1	$^3A \rightarrow ^4A$	6.26	6-4-2-d	C_1	$^1A \rightarrow ^2A$	5.60
		$^3A \rightarrow ^4A$	5.34	6-2-3-d	C_1	$^1A \rightarrow ^2A$	5.29			$^3A \rightarrow ^4A$	5.60
6-1-2-d	C_1	$^1A \rightarrow ^2A$	4.86			$^3A \rightarrow ^4A$	5.51	6-5-1-d	C_1	$^1A \rightarrow ^2A$	5.14
		$^3A \rightarrow ^4A$	5.07	6-2-4-d	C_1	$^1A \rightarrow ^2A$	5.57			$^3A \rightarrow ^4A$	5.18
6-1-3-d	C_1	$^1A \rightarrow ^2A$	4.89			$^3A \rightarrow ^4A$	5.65	6-5-2-d	C_1	$^1A \rightarrow ^2A$	4.89
		$^3A \rightarrow ^4A$	5.75	6-3-1-d	C_1	$^1A \rightarrow ^2A$	5.09			$^3A \rightarrow ^3A$	4.92
6-2-6-d	C_1	$^1A \rightarrow ^2A$	6.10			$^3A \rightarrow ^4A$	5.20				

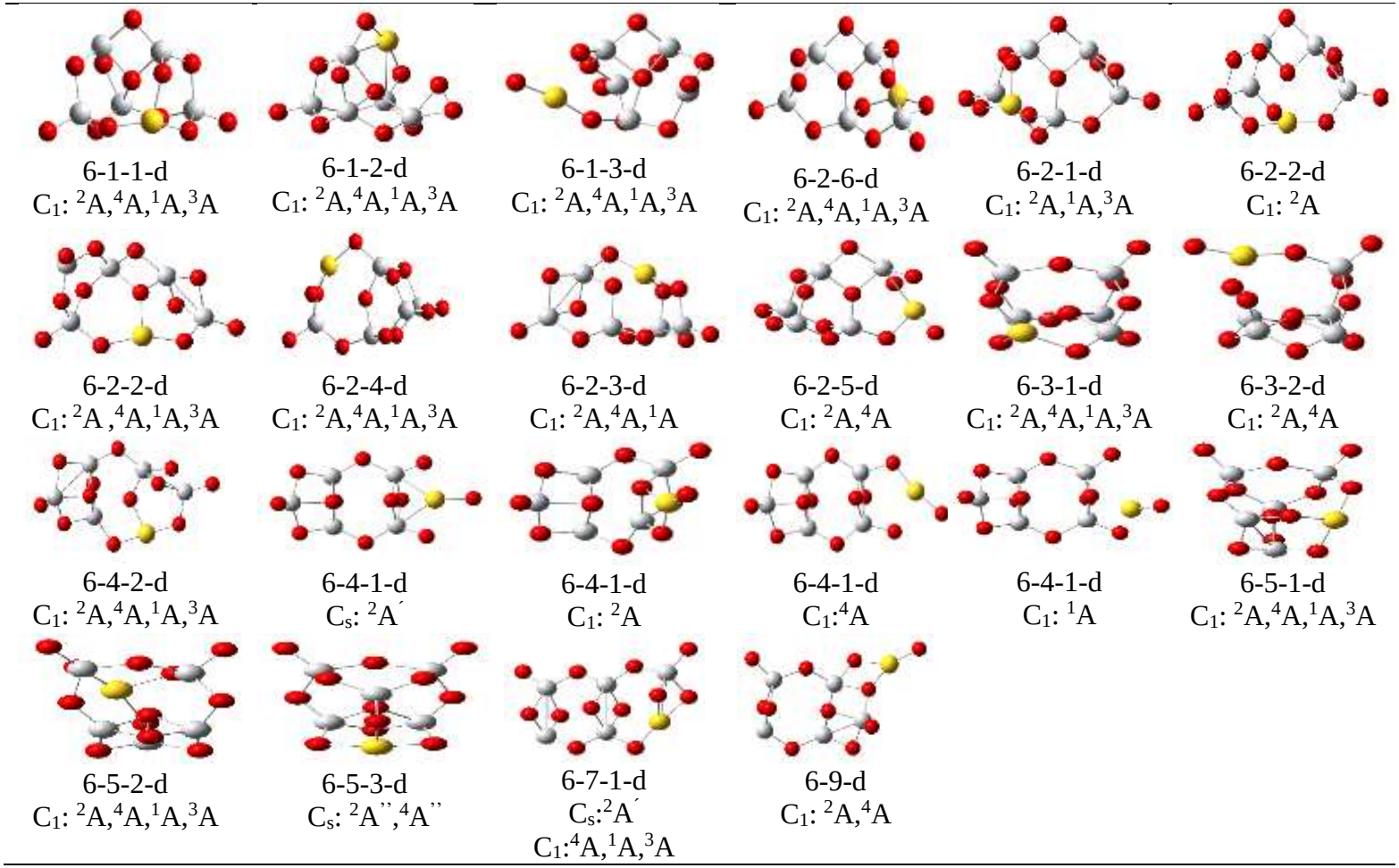

Figure 103: Structures of the Ti_5AuO_{12} clusters. Structure name, point group and state are displayed bellow each structure. The Ti, O and Au atoms are indicated by gray, red and yellow spheres respectively.

6 WATER INTERACTION

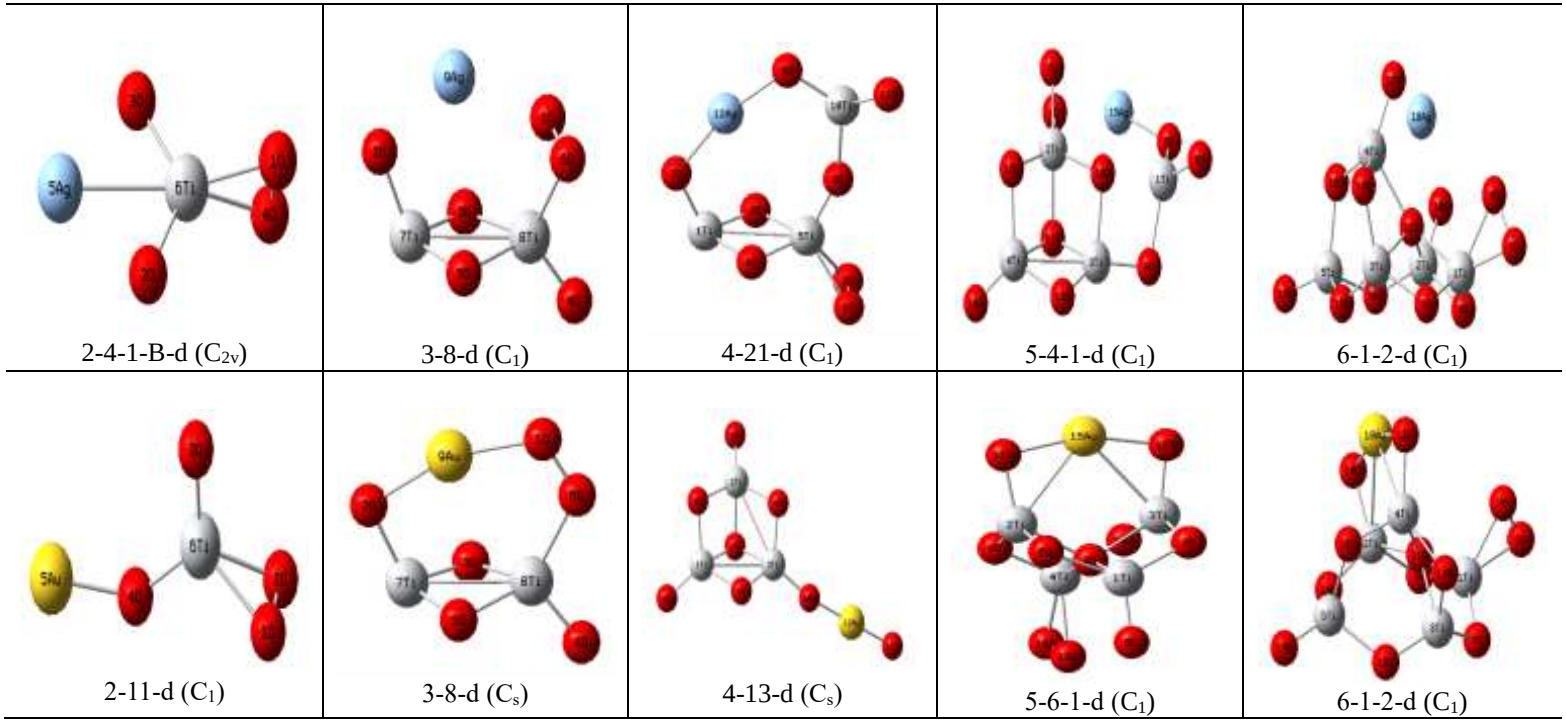

Figure 104: Points of attachment for the water interaction. Atoms were labelled using Gaussview program [24]. The Ti, O, Ag and Au atoms are indicated by gray, red, blue and yellow spheres respectively.

6.1 ($Ti_{n-1}AgO_{2n}$) (H_2O)

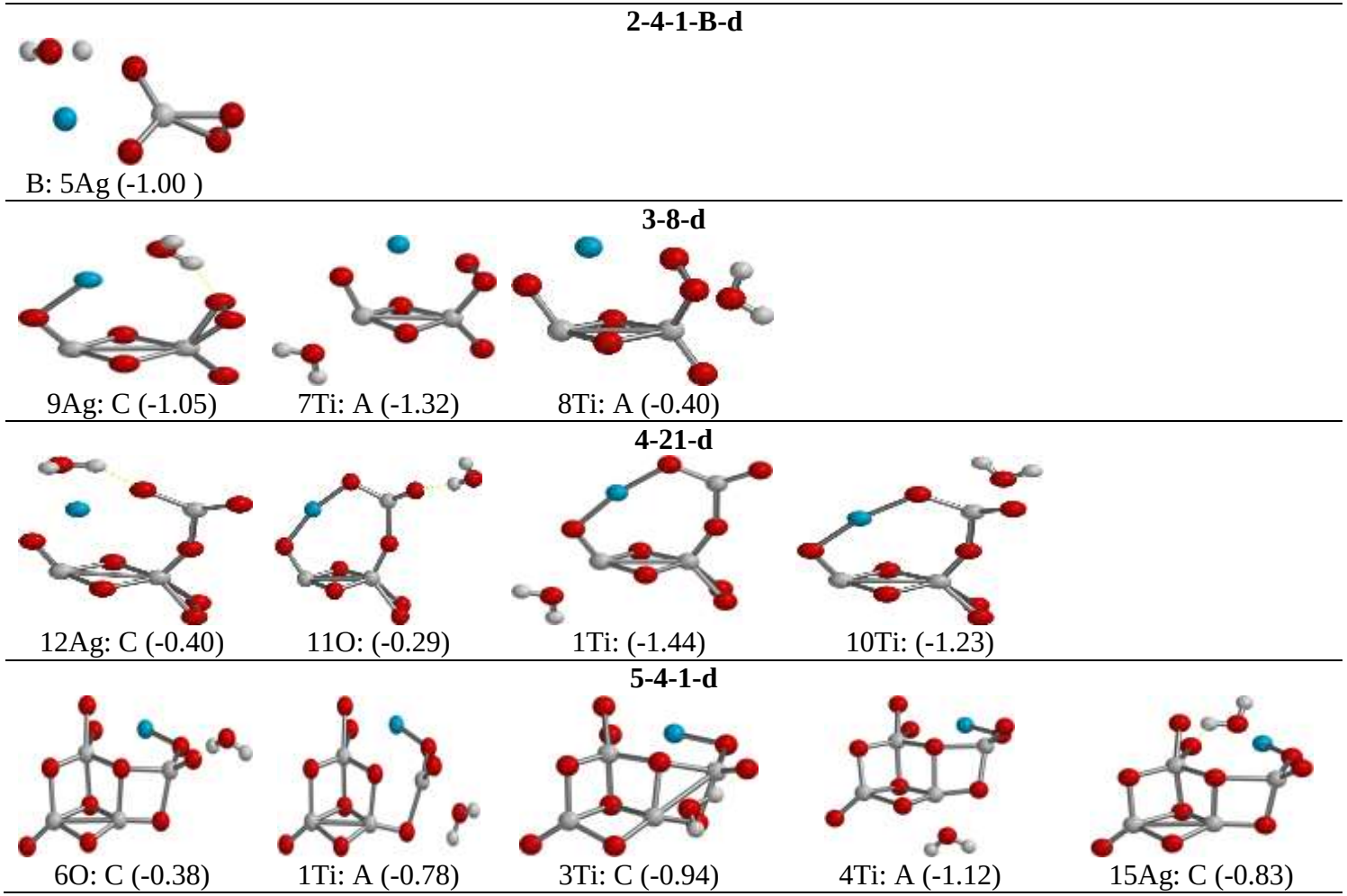

Figure 105: Interaction of one water molecule and lowest energy Ag doped $(TiO_2)_n$ (n = 2 - 6) clusters. Type of interaction A: Molecular adsorption; B: Dissociative adsorption; and C: H-Bonding. Point of interaction and E_b are below each structure.

6-1-2-d

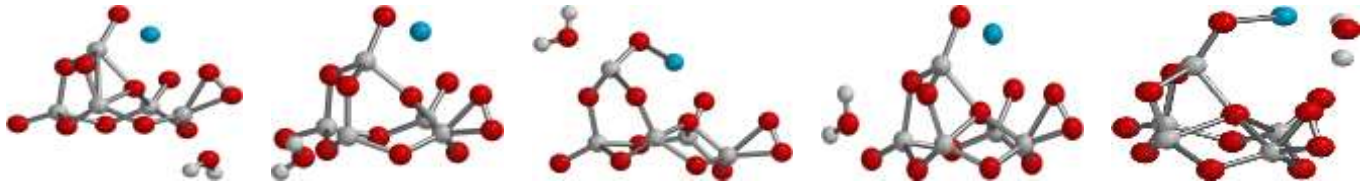

1Ti: A (-0.91) 3Ti: A (-1.35) 4Ti: A (-1.40) 5Ti: A(-0.38) 18Ag: C (-0.79)

Figure 106 (Figure 105 cont.): Interaction of one water molecule and lowest energy Ag-doped $(TiO_2)_n$ (n = 2 - 6) clusters. Type of interaction A: Molecular adsorption; B: Dissociative adsorption; and C: H-Bonding. Point of interaction and E_b are below each structure.

6.2 ($Ti_{n-1}AuO_{2n}$) (H_2O)

2-11-d

5Au: A (-1.26) 6Ti: A (1.04)

3-8-d

9Au: B (-0.79) 7Ti: B (-1.43) 8Ti: A (-0.82)

Figure 107: Interaction of one water molecule and lowest energy Au-doped $(TiO_2)_n$ (n = 2 - 6) clusters. Type of interaction A: Molecular adsorption; B: Dissociative adsorption; and C: H-Bonding. Point of interaction and E_b are below each structure.

4-13-d

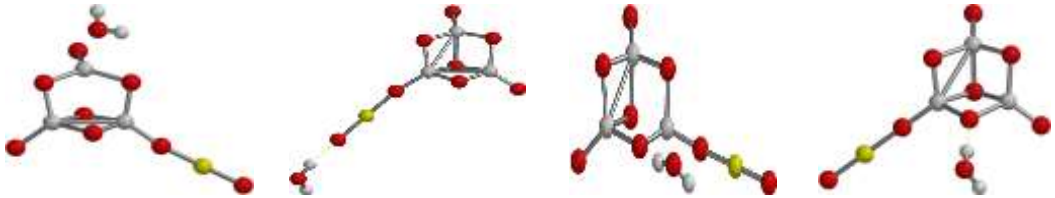

2Ti: A (-1.01) 11O: C (0.14) 3Ti: A (-0.83) 12Au: C (-0.20)

5-6-1-d

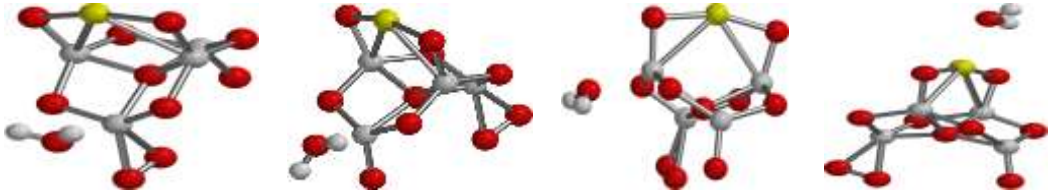

4Ti: A (-0.97) 1Ti: A (-1.14) 2Ti: A (-1.22) 15Au: A (0.45)

6-1-2-d

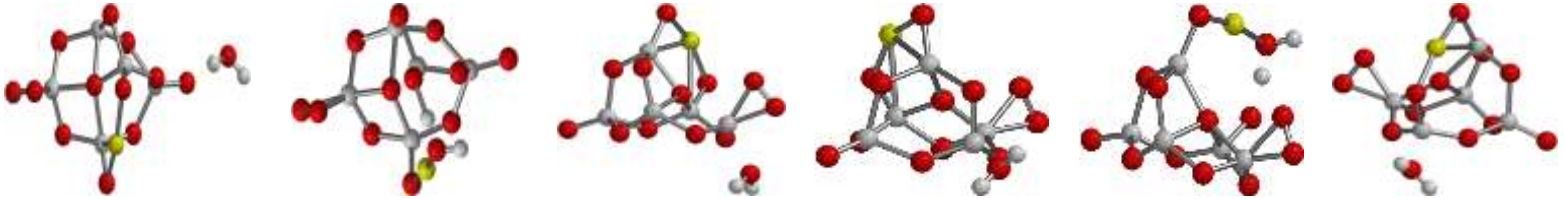

5Ti: C (-0.24) 4Ti: B (-0.82) 1Ti: A (-0.95) 3Ti: A (-1.23) 18Au: B (-0.81) 2Ti: A (-1.07)

Figure 108 (Figure 107 cont.): Interaction of one water molecule and lowest energy Au - doped $(TiO_2)_n$ (n = 2 - 6) clusters. Type of interaction A: Molecular adsorption; B: Dissociative adsorption; and C: H-Bonding. Point of interaction and E_b are below each structure.-

7 ELECTRON AFFINITY

Table 99: Electron affinity (eV) of undoped, Ag and Au doped $(TiO_2)_n$ clusters at BPW91 level

n	Clusters	AEA	VEA
	Undoped $(TiO_2)_n$		
2	2-1-u (C_{2h} : ^1A_g) ↔2-1-u (C_{2h} : ^2A_g)	1.69	1.51
3	3-1-u (C_s : $^1A'$) ↔ 3-1-u (C_s : $^2A'$)	2.77	2.45
4	4-1-u (C_{2v} : $^1A_1$) ↔ 4-2-u (C_{2v} : $^2A_1$)	2.96	2.78
5	5-1-u (C_s : $^1A'$) ↔ 5-3-u (C_1: ^2A)	2.84	2.20
6	6-1-u (C_2 : ^1A) ↔ 6-1-u (C_1 : ^2A)	3.13	2.70
	Ag doped $(TiO_2)_n$		
2	2-4-1-B-d (C_{2v}:$^2A_2$)↔ 2-4-1-B-d (C_{2v}:$^1A_1$)	2.70	1.91
3	3-8-d (C_1: ^2A) ↔ 3-1-1-d (C_{2v}: $^3B_2$)	3.94	2.81
4	4-21-d (C_1:^2A) ↔ 4-9-1-d (C_s :$^3A''$)	4.56	2.93
5	5-4-1-d (C_1: ^2A) ↔ 5-4-1-d (C_1: ^1A)	4.83	4.43
6	6-1-2-d (C_1 : ^2A) ↔ 6-1-2-d (C_1 : ^1A)	4.74	3.96
	Au doped $(TiO_2)_n$		
2	2-11-d (C_1: ^2A) ↔ 2-11-d (C_1: ^1A)	2.99	2.83
3	3-8-d (C_1: ^2A) ↔ 3-1-1-d (C_{2v} :$^3B_2$)	4.04	2.77
4	4-13-d (C_1:^2A) ↔ 4-13-d (C_1:^3A)	5.34	4.26
5	5-6-1-d (C_s : $^2A''$) ↔ 5-18-d (C_1 : ^3A)	4.78	3.27
6	6-1-2-d (C_1 : ^2A) ↔ 6-1-2-d (C_1 : ^1A)	4.86	3.96

8 EXCITATION ENERGY AND HL GAP

Table 100: Excitation energy (E, eV) and HOMO – LUMO (HL) gap (eV) for neutral Ag doped $(TiO_2)_n$ clusters

n	Structure	E	HL gap (α)	HL gap (β)
2	2-4-1-B-d (C_{2v}:$^2A_2$)	0.71	2.01	0.71
3	3-8-d (C_1: ^2A)	0.81	3.02	0.87
4	4-21-d (C_1: ^2A)	--	1.50	0.03
5	5-4-1-d (C_1:^2A)	0.74	2.83	0.38
6	6-1-2-d (C_1:^2A)	0.31	2.37	0.30

Table 101: Excitation energy (E, eV) and HOMO – LUMO (HL) gap (eV) for anionic Ag doped $(TiO_2)_n$ clusters

n	Structure	E	HL gap	HL gap
2	2-4-1-B-d (C_{2v}: $^1A_1$)	0.37	0.33[c]	
3	3-1-1-d (C_{2v}: $^3B_2$)	0.25	3.35[a]	0.27[b]
4	4-9-1-d (C_S: $^3A''$)	0.15	3.59[a]	0.14[b]
5	5-4-1-d (C_1:^1A)	2.02	2.01[c]	
6	6-1-2-d (C_1:^1A)	2.21	2.18[c]	

a: HL gap (α); b: HL gap (β); and c: HL gap (αβ);

Table 102: Excitation energy (E, eV) and HOMO – LUMO (HL) gap (eV) for neutral Au doped $(TiO_2)_n$ clusters

n	Structure	E	HL gap (α)	HL gap (β)
2	2-11-d (C_1: ^2A)	1.28	1.96	1.36
3	3-8-d (C_s: $^2A'$)	0.81	2.42	0.90
4	4-13-d (C_1:^2A)	0.43	3.65	0.30
5	5-6-1-d (C_s:$^2A'$)	0.63	2.69	0.60
6	6-1-2-d (C_1:^2A)	0.24	2.18	0.14

Table 103: Excitation energy (E) and HOMO – LUMO (HL) gap (eV) for anionic Au doped $(TiO_2)_n$ clusters

n	Structure	E	HL gap	HL gap
2	2-11-d (C_1: ^1A)	0.67	0.19[c]	
3	3-1-1-d (C_{2v}: $^3B_2$)	0.14	3.27[a]	0.16[b]
4	4-13-d (C_1:^3A)	0.13	3.24[a]	0.11[b]
5	5-18-d (C_1:^3A)	0.14	3.26[a]	0.14[b]
6	6-1-2-d (C_1:^1A)	2.21	2.09[c]	

a: HL gap (α); b: HL gap (β); and c: HL gap (αβ);